Static and Dynamic Imaging using Magnetic Field Gradients

静态与动态核磁成像

A thesis presented in partial fulfilment of
the requirements for the degree of
Master of Science
in Physics at
Massey University

by

Yang Xia

夏 阳

1988

Abstract

The theory and techniques of NMR imaging are described together with a detailed description of the Filtered Back Projection (FBP) technique used in an existing NMR imaging system.

The existing 'static' NMR imaging system has been modified to be capable of performing 'dynamic' NMR imaging experiments, as well as better 'static' NMR imaging experiments.

The potential of NMR microscopy in the imaging of both the static spin distribution $P(\mathbf{r}_0)$ and the dynamic spin correlation function $P(\mathbf{r}_0|\mathbf{r},t)$ has been investigated. Both homogeneous and inhomogeneous systems have been studied. Detailed theoretical analysis and experimental considerations of dynamic imaging experiments have been given.

A transverse resolution of 15 μm for a 1 mm slice thickness is obtained from a static imaging experiment of a phantom using the modified system. The rabbit trachea imaging experiment has revealed the asymmetrical collapse of tracheas under negative pressures, a collapse which had previously been considered as symmetrical process.

The Poiseuille flow experiment has involved the first simultaneous measurement of flow and diffusion at the microscopic level. Maps of two dimensional distribution functions of flow and diffusion are given by this experiment, highlighting this totally non-invasive dynamic imaging technique.

As an example of dynamic imaging, the wheat grain experiment has displayed the flow and diffusion maps within a single wheat grain *in vivo*.

Acknowledgments

First, I would like to thank my parents for their constant encouragement from the early years of my education by creating an environment conducive to study and thinking.

I wish to express my sincere gratitude to my supervisor, Professor Paul Callaghan, for providing continuing theoretical and technical guidance and careful instruction, for his great enthusiasm and patience while this manuscript has been written.

I would also like sincerely to thank the following people who have contributed to this work:

Dr Craig Eccles, now doing post-doctoral research at ETH, Switzerland, for his invaluable advice and great help during his time at Massey University.

The mechanical workshop staff for manufacturing parts of the gradient power supply.

The electronic workshop staff for providing technical assistance on a number of occasions.

Dr Rod Lambert of Physics and Biophysics Department and Dr Roger Pack of Physiology and Anatomy Department for their advice in the rabbit trachea experiment.

Dr Colin Jenner of the Waite Research Institute, Adelaide for his advice in the wheat grain experiment.

Dr Ian Brooking of the Plant Physiology Division of the DSIR for supplying the wheat samples used in the *in vivo* experiment.

Dr John Skipworth of Botany and Zoology Department for identifying the plant used in the static imaging experiment.

The academic, technical and clerical staff of Physics and Biophysics Department for their kindness and help.

Fellow post graduate students, Peter Daivis, James Conway, Peter Saunders and Mark Huirua for their friendship and support.

Massey University for providing financial support in the form of a Graduate Assistantship.

Finally I would like to express my deep appreciation of the unfailing encouragement and support given to me by my wife, Ping.

Contents

List of Figures

List of Tables

List of Symbols

a	RF coil radius	29
a_{mj}	Complex admixture amplitudes of a spin system	3
A	An operator representing an observable quantity	5
A	Signal amplitude	44
A	Cross sectional area	108
B_{eff}	Effective field in the rotating frame	7
$\mathbf{B}$	Magnetic field	6
B_0	Amplitude of the main magnetic field	3
$\mathbf{B}_0$	Main magnetic field, directed along the z axis	3
B_1	Amplitude of the transverse rf field $\mathbf{B}_1(\mathbf{t})$	7
$\mathbf{B}_1(\mathbf{t})$	RF field (in the transverse plane)	7
D	Self-diffusion coefficient	32
$\mathbf{D}$	Self-diffusion tensor	33
D_e	Extra broadening due to velocity spread	47
$E(m_j)$	Energy eigenvalues of a spin system	3
f	Spectrometer frequency	29
F	Noise figure of the spectrometer	16
F{ }	Fourier transform of the function in { }	23
$F_s\{\ \}$	sin transform of the function in { }	23
$F_c\{\ \}$	cos transform of the function in { }	23
g	Amplitude of PGSE gradient	32
$\mathbf{g}$	PGSE gradient in dynamic imaging	32
g_m	Maximum gradient employed in dynamic imaging	40
G	Amplitude of field gradient	32
$\mathbf{G}$	Field gradient	19
h(t)	Fourier transform of frequency domain function H(f)	38
H_I	Imaginary part of the discrete function H	42
H_R	Real part of the discrete function H	42
H(f)	Fourier transform of time domain function h(t)	38
$\mathcal{H}$	Hamiltonian operator	3
$\mathcal{H}_1(t)$	Perturbation term in Hamiltonian operator	7
i	$(-1)^{1/2}$	4
I	Function selected in dynamic imaging analysis program	91
Im[ ]	Imaginary part of a complex function in [ ]	36
j	Spin quantum number	3
$\mathbf{J}$	Spin angular momentum operator	3
k	Frequency domain (digital) variable	38
$\mathbf{k}$	Static reciprocal space vector	24
k_B	Boltzmann constant	5
K	Numerical factor in the calculation of S/N	16
l	Length of the pipe in Poiseuille sample system	119
L	Length of the conductor	16
m_j	Azimuthal quantum numbers	3
$\mathbf{M}$	Macroscopic magnetization vector	5
M_0	Magnitude of $\mathbf{M}$ in the equilibrium state	6
$M_\perp$	Transverse component of $\mathbf{M}$	9
n	Time domain (digital) variable	38
n_D	Maximum number of data images	36
n_1	A constant in the 'tube law'	109

N	Number of spins per unit volume	5
N	Total number of digits in time domain	38
N_h	Number of hydrogen nuclei per unit volume	16
N_p	Number of projections	29
N_{acc}	Number of accumulations per projection	25
p	Perimeter of the conductor	16
P	Transmural pressure difference	109
P_1	Constant asymptotic pressure	109
P_s	Self-correlation function of the nuclear spin	33
P^*	Filtered profile	25
Q	Quality factor of the coil	16
Q	Volume amount of fluid	120
$\mathbf{q}$	Dynamic reciprocal space vector	34
$\mathbf{r}$	Position vector	18
R	Attenuation factor	33
R	Radius of the pipe in dynamic imaging experiment	120
$Re[\ ]$	Real part of a complex function in [ ]	24
S	Fluid displacement vector	33
$S(t)$	FID signal	24
S^*	Complex conjugate of S	25
t_p	Duration of the pulse	9
t_{rep}	Repetition time of in experiments	25
T	Absolute temperature of a spin system	5
T	Time domain sampling interval	38
T	Sampling time in imaging experiments	96
T_c	Probe temperature	16
T_s	Sample temperature	16
T_1	Spin-lattice relaxation time	10
T_2	Spin-spin relaxation time	10
T_2^*	Transverse relaxation time	10
$Tr(\ )$	Trace of the operator in ( )	4
$U_E(t)$	Evolution operator	4
$U_{Rz}(\theta)$	Rotation operator	4
v	Velocity of fluid flow	33
V_c	Volume of the coil	16
V_s	Sample volume	16
w	Weight of the fluid	120
α	A variable in discrete Fourier transform	38
γ	Gyromagnetic ratio	3
δ	Duration of the PGSE pulse	32
η	Fraction of the coil volume occupied by the sample	16
η	Dynamic viscosity of the fluid	120
θ	Rotation angle of the magnetization vector	9
λ	Wave length	61
μ_0	Permeability of free space	16
$\boldsymbol{\mu}$	Magnetic moment vector	3
ν	Kinematic viscosity of the fluid	119
ξ	Complex FID signal	35

ρ	Density operator	4
ρ	Density of the fluid	119
ρ_I	Imaginary part of nuclear spin density	35
ρ_R	Real part of nuclear spin density	35
ρ_T	Resistivity of the conductor	16
$\rho(\mathbf{r})$	Nuclear spin density	24
σ	RF coil proximity factor	16
$\sigma(n)$	Noise function	127
τ	Short time interval	10
$\boldsymbol{\omega}$	Larmor precession frequency	7
$\boldsymbol{\omega}_0$	Larmor precession frequency due to $\mathbf{B}_0$	4
ω_1	Larmor precession frequency due to B_1	8
ω_{eff}	Precession frequency in the rotating frame	7
Δ	Separation of the PGSE pulses	32
ϕ	Projection angle in imaging experiment	24
$\vert j\ m_j\rangle$	Basis eigenket set of a spin system	3
$\vert\psi\rangle$	General quantum state of a spin j system	3
$\overline{\langle A\rangle}$	Ensemble average of the observable quantity A	4
$\overline{\vert a_{m_j}\vert^2}$	Normalized population in the eigenstate $\vert j\ m_j\rangle$	5
Δf	Bandwidth of the receiver	16
Δh	Height difference	120
Δv	Velocity spread between the adjacent pixels	47
Δx	Transverse resolution	29
ΔZ	Slice thickness	29
ΔE	Energy difference between the two adjacent states	7
ΔP	Pressure difference along the length of the pipe	119
$\Delta\phi$	Step angle in imaging experiment	25
∇B_0	Magnetic field gradient	19
∇P	Pressure gradient	119
$\hbar$	Planck's constant divided by 2π	3

Chapter 1 Introduction

1.1 Introduction

Nuclear Magnetic Resonance (NMR) Imaging is a non-invasive technique which gives the spatial distribution of the NMR signal intensity or other NMR parameters in a heterogeneous sample. The first experimental demonstration of the feasibility of macroscopic NMR imaging was given by Lauterbur in 1972 (1,2).

In conventional NMR it is usual to place the sample, which is homogeneous and small, in a very uniform magnetic field, so that the resonant frequency depends upon the external field modified slightly by the local environment. NMR spectra obtained in this way yield details of the local molecular environment.

By contrast, NMR Imaging concerns a sample which is heterogeneous, and usually not small. Furthermore, the sample is placed in a deliberately non-uniform magnetic field, which enables the hetero-structure of the sample to be derived and displayed.

Many different techniques have been described for NMR Imaging(3,4,5). Among these the Projection Reconstruction technique, originally from X-ray Tomography, is the most sensitive one(6).

The proton (^1H) is the most commonly used nucleus when doing imaging experiments, Hydrogen being the most abundant element in the living systems. ^1H is isotopically almost 100% abundant, and has the highest magnetic moment among stable nuclei, thus yielding optimum sensitivity. ^{19}F and ^{31}P nuclei are next in sensitivity and have some practical interest. Other nuclei are, in practice, difficult to image.

Traditionally NMR imaging reveals some stationary distribution functions of a nuclear spin system, for example, the spin density distribution. Such imaging is termed **'static' NMR imaging** in this thesis.

By incorporating the Pulse-Gradient-Spin-Echo (PGSE) technique, the NMR imaging can describe time-dependent functions. This technique is termed **'dynamic' NMR imaging**. Simultaneous imaging of flow and diffusion at the microscopic level can be performed using this new technique, which has been demonstrated by some imaging experiments in this work.

1.2 Organisation of the Thesis

This thesis is divided into 6 chapters.

Chapter 2 provides a description of NMR and NMR imaging. One of the most commonly used imaging techniques, **Filtered Back Projection (FBP),** is described in detail. The theory of dynamic imaging is discussed extensively in this chapter.

In Chapter 3 a brief description of an existing static NMR microscopic imaging system is given first, followed by some developments and modifications to this system which form part of the present work. These have improved this system and enabled the performance of the flow and diffusion imaging experiments.

The static imaging experimental results are presented in Chapter 4, while the dynamic results are in Chapter 5.

A brief summary and some comments about possible future work are given in Chapter 6.

Appendix A gives the complete software listings for the flow and diffusion imaging experiments. Appendix B gives the software listings for the simulating the uniformity of G_y field gradient.

Chapter 2 Theory of NMR Imaging

2.1 NMR Theory

NMR was discovered more than forty years ago and has become an important and active field linking Physics, Chemistry, Biology, Medicine and other subjects. The basic physics of NMR is well understood and described elsewhere(7,8,9). A brief review is given here as required for an understanding of NMR Imaging.

2.1.1 Nuclear Magnetism

A general state, $|\psi>$, of a spin system with a spin quantum number j, is described by the complex admixture amplitudes, a_{m_j}

$$|\psi> = \sum_{m_j} a_{m_j} |j\ m_j> \tag{2.1}$$

where $|j\ m_j>$ give the basis eigenket set, m_j are the usual azimuthal quantum numbers ranging from -j to j.

The energy eigenstates of the spin system are given by the Hamiltonian operator

$$\mathcal{H} = -\gamma B_0 J_z \tag{2.2}$$

where the constant γ is termed the gyromagnetic ratio and depends on the specific nucleus; the external magnetic field $\mathbf{B_0}$ is along the z axis; and J_z is the z component of the spin angular momentum operator $\mathbf{J}$.

From the equation

$$\mathcal{H}|\psi> = E(m_j)\,|\psi> \tag{2.3}$$

the energy eigenvalues $E(m_j)$ of this Hamiltonian operator can be derived as

$$E(m_j) = -m_j \gamma \hbar B_0 \tag{2.4}$$

where $\hbar$ is Planck's constant divided by 2π. (Note that semiclassically, $E = -\boldsymbol{\mu}\cdot\mathbf{B}$)

Equation (2.4) implies that a spin system with $j = 1/2$ has only two eigenstates (Figure 2.1), given by

$$E(\pm\tfrac{1}{2}) = \mp\tfrac{1}{2}\gamma\hbar B_0 \tag{2.5}$$

This case corresponds to the proton, the nucleus of interest in this work.

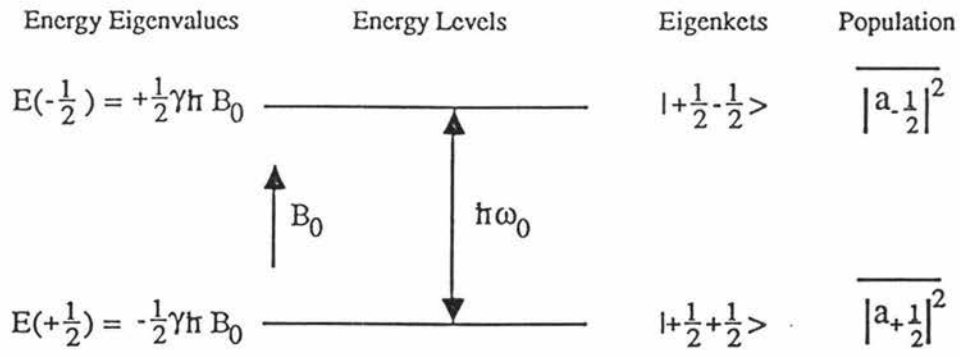

Figure 2.1 A Spin j = 1/2 System

If the Hamiltonian $\mathcal{H}$ is constant, the evolution of the spin system is given by

$$|\Psi(t)\rangle = \exp[-(i/\hbar)\mathcal{H}t]\,|\Psi(t_0)\rangle \tag{2.6}$$

where $i^2 = -1$.

Therefore the evolution operator,

$$U_E(t) = \exp[-(i/\hbar)\mathcal{H}t] \tag{2.7}$$

is just a rotation operator, namely

$$U_{R_z}(\theta) = \exp[(i/\hbar)\theta J_z] \tag{2.8}$$

This corresponds to rotation about the z axis with an angular frequency

$$\omega_0 = -\gamma B_0 \tag{2.9}$$

ω_0 is known as the **Larmor Precession Frequency.** The negative sign indicates the clockwise precession for the positive γ.

2.1.2 Macroscopic Magnetization

In fact we shall be dealing with nuclear ensembles, and will be interested in macroscopic ensemble average of the observable quantities. The following discussion is restricted to the $j = {}^1/_2$ system.

For such an average, it is useful to employ the density operator ρ with the property

$$\overline{\langle A\rangle} = \mathrm{Tr}(\rho A) \tag{2.10}$$

where $\overline{\langle A\rangle}$ is the ensemble average of the observable quantity represented by an operator A. ρ, in the chosen representation, is given by

$$\rho = \begin{pmatrix} \overline{|a_{1/2}|^2} & \overline{a^*_{1/2}a_{-1/2}} \\ \overline{a_{1/2}a^*_{-1/2}} & \overline{|a_{-1/2}|^2} \end{pmatrix} \tag{2.11}$$

with each element being an ensemble average. Note the diagonal elements represent the population in the corresponding eigenstates, and the off-diagonal elements are related to the çoherence between the states.

For spin $^1/_2$ particles, the nuclear magnetization vector M can be used to obtain ρ and so contains all information regarding the state of the ensemble. This magnetization is given by

$$M = \overline{\langle N\gamma J\rangle} \tag{2.12}$$

where N is the number of spins per unit volume, and the vector operator **J** refers to the separate cartesian components, i.e.,

$$M = N\gamma\{\ \overline{\langle J_x\rangle}i + \overline{\langle J_y\rangle}j + \overline{\langle J_z\rangle}k\ \} \tag{2.13}$$

In the absence of an external magnetic field, the magnetization vector should be zero due to the random directions of the magnetic dipoles of the nuclei.

If however a sample is in an external field, the normalized population $\overline{|am_j|^2}$ in the eigenstate $|jm_j\rangle$ under thermal equilibrium can be calculated by the Boltzmann Distribution

$$\overline{|am_j|^2} = \exp[-E(m_j)/k_BT]/\sum_{m_j} \exp[-E(m_j)/k_BT] \tag{2.14}$$

with k_B being the Boltzmann constant, T the absolute temperature of the spin system, and $E(m_j)$ given by Equation (2.4).

At room temperature, the population of the lower state $|^1/_2\ ^1/_2\rangle$ (along the field axis) is more than the higher state $|^1/_2\ -^1/_2\rangle$ (against the field axis). Although the difference is only a few ppm, we still can get a net equilibrium magnetization M which lies along the main field axis. A semiclassical description is shown in Figure 2.2.

Note this small magnetization of nuclei at room temperature is related to detection sensitivity and is a limitation in NMR imaging.

The transverse component of M is obviously zero due to the even distribution of the azimuthal phase angle of the precessing nuclei in the transverse plane.This corresponds to phase incoherence leading to zero value of the off-diagonal elements of ρ,

$$\overline{a^*_{1/2}a_{-1/2}} = \overline{a_{1/2}a^*_{-1/2}} = 0 \tag{2.15}$$

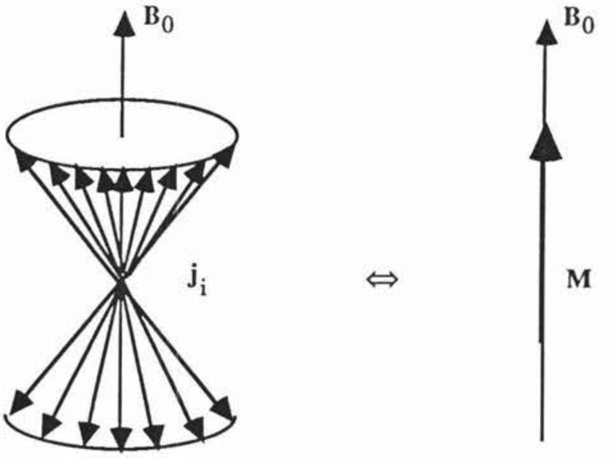

Figure 2.2 A Semiclassical Description of the Macroscopic Magnetization Vector

By considering Equations (2.2), (2.10), (2.11) and (2.12), the magnitude of the magnetization in the equilibrium state can be derived. At room temperature, the result is

$$M_0 = N(\gamma\hbar)^2[j(j+1)]B_0/3k_BT \tag{2.16}$$

The evolution of the magnetization in the presence of a magnetic field is obtained by considering the time dependence of the density matrix

$$d\rho/dt = (i/\hbar)[\rho\ ,\mathcal{H}] \tag{2.17}$$

where [ ] is the Poisson bracket.

Hence it may be shown

$$d\mathbf{M}/dt = \gamma(\ \mathbf{M}\times\mathbf{B}\ ) \tag{2.18}$$

or in the component form

$$dM_x/dt = \gamma\ (\ M_yB_z - M_zB_y\ ) \tag{2.19a}$$

$$dM_y/dt = \gamma\ (\ M_zB_x - M_xB_z\ ) \tag{2.19b}$$

$$dM_z/dt = \gamma\ (\ M_xB_y - M_yB_x\ ) \tag{2.19c}$$

Note this relationship describes a precessional motion about $\mathbf{B}_0$ at the Larmor frequency [Equation (2.9)].

We are interested in the behavior of such a macroscopic magnetization vector both as we rotate it by applying an external magnetic field and as it precesses and relaxes.

Due to Equation (2.5), the energy difference between the two adjacent states is

$$\Delta E = \langle {}^{1}/_{2}\ {-}^{1}/_{2}|\ \gamma B_0 J_z\ |{}^{1}/_{2}\ {-}^{1}/_{2}\rangle - \langle {}^{1}/_{2}\ {}^{1}/_{2}|\ \gamma B_0 J_z\ |{}^{1}/_{2}\ {}^{1}/_{2}\rangle$$

$$= \gamma \hbar B_0 \qquad (2.20)$$

Transitions between the two different energy states can be induced if there is a perturbation applied to the spin system. We can treat this perturbation by adding a time-dependent term

$$\mathcal{H}_1(t) = (-2\gamma B_1 \cos\omega_0 t) J_x \qquad (2.21)$$

to the Hamiltonian [Equation (2.2)]. This corresponds to a perturbation at a **resonant** frequency equal to the Larmor frequency ω_0.

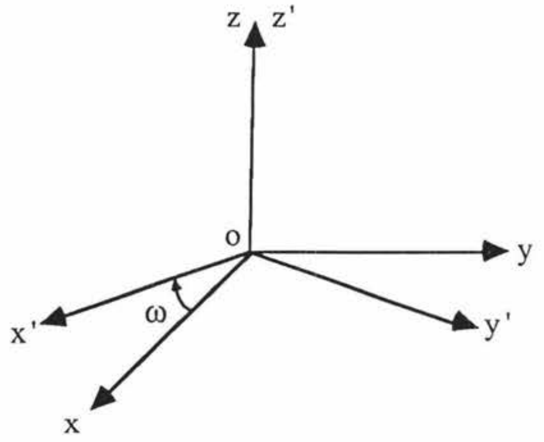

Figure 2.3
A Rotating Frame
($\gamma > 0$)

An alternative, but convenient description, is given by describing the system in a frame of reference rotating about $\mathbf{B}_0$ at ω (Figure 2.3). Consider the influence of a small linearly polarized radio frequency (**rf**) field $\mathbf{B}_1(t)$ oscillating in the transverse plane. This field is actually a superposition of two counter-rotating fields in the transverse plane

$$\mathbf{B}_1(t) = \mathbf{i}2B_1\cos\omega_0 t$$

$$= (\ \mathbf{i}B_1\cos\omega_0 t - \mathbf{j}B_1\sin\omega_0 t\ ) + (\ \mathbf{i}B_1\cos\omega_0 t + \mathbf{j}B_1\sin\omega_0 t\ ) \qquad (2.22)$$

with **i** and **j** are the unit vectors along x axis and y axis respectively.

In this rotating frame, the precession frequency of the magnetization will become

$$\omega_{eff} = \gamma B_{eff} = \gamma(\ B_0 - \omega/\gamma\ ) \qquad (2.23)$$

Since **M** is rotating at the Larmor frequency ω_0 about z axis in the laboratory frame, it will appear to be stationary in this rotating frame if ω is equal to ω_0. Therefore $\mathbf{B}_1(t)$ is the only non-zero field. The sign of γ determines which component of the $\mathbf{B}_1(t)$ affects the nuclei. For the case of the positive γ, the first term in Equation (2.22) will be effective. This component is therefore capable of interacting strongly with **M** despite its small size compared with $\mathbf{B}_0$. The other component which rotates at 2ω in the opposite direction will have negligible effect provided $B_1 << B_0$.

Combining Equations (2.19a-c) and the first term of Equation (2.22) yields the following equations for the motion of the magnetization in the magnetic fields

$$dM_x/dt = \gamma (M_yB_0 + M_zB_1\sin\omega_0t) \tag{2.24a}$$

$$dM_y/dt = \gamma (M_zB_1\cos\omega_0t - M_xB_0) \tag{2.24b}$$

$$dM_z/dt = \gamma (-M_xB_1\sin\omega_0t - M_yB_1\cos\omega_0t) \tag{2.24c}$$

By solving these equations we find, in the laboratory frame

$$M_x = M_0\sin\omega_1t\sin\omega_0t \tag{2.25a}$$

$$M_y = M_0\sin\omega_1t\cos\omega_0t \tag{2.25b}$$

$$M_z = M_0\cos\omega_1t \tag{2.25c}$$

Equations (2.25a-c) imply that on the application of a rf field which is rotating right at the Larmor frequency, the motion of magnetization can be decomposed into two precessional motions in the laboratory frame (Figure 2.4) – at ω_0 about B_0 and at ω_1 about B_1,

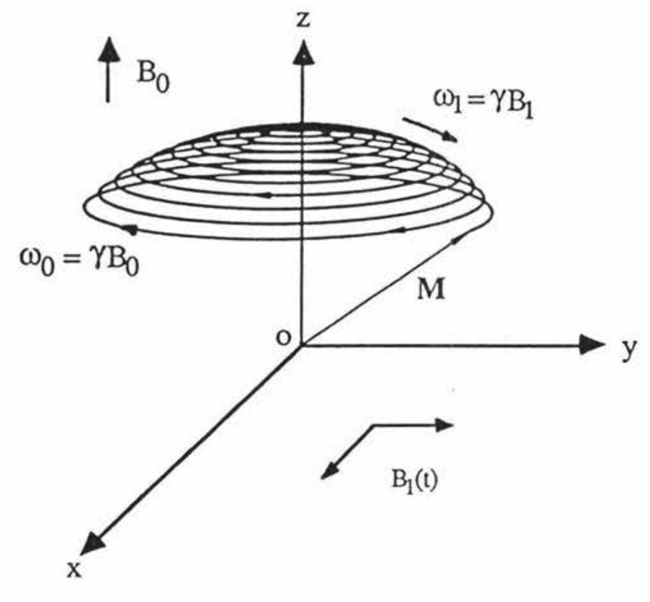

Figure 2.4

Motion of Magnetization in the Laboratory Frame or simply is one precession motion in the rotating frame (Figure 2.5) – at ω_1 about B_1.

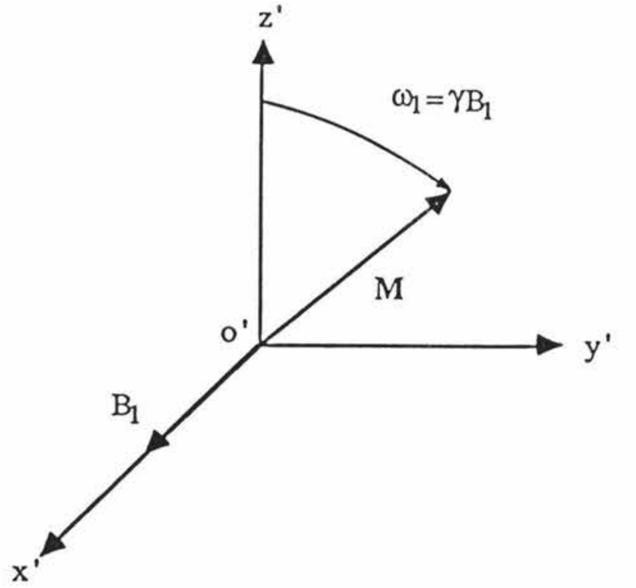

Figure 2.5

Motion of Magnetization in the Rotating Frame

By adjusting the intensity and/or duration of the rf field, we can rotate the magnetization **M** by any desired amount θ, given by

$$\theta = \gamma \int_0^{t_p} B_1(t)dt \tag{2.26}$$

with t_p is the duration of the pulse and $B_1(t)$ the rf field amplitude. Note the integral emphasizes that B_1 is not necessarily constant during the interval. A rotating field of the correct amplitude and duration required to tip **M** by 90 degree is called a 90° rf pulse, and similarly for any other angle.

We use a solenoidal coil, with its axis perpendicular to the static field $\mathbf{B}_0$, to apply $\mathbf{B}_1(t)$. The sample is inside the coil. The same rf coil is also used to detect the signal induced by **M** precessing in the transverse plane.

2.1.3 Relaxation Processes

In the equilibrium state, the magnetization of a nuclear spin system will be

$$|\mathbf{M}| = M_z = M_0 \tag{2.27}$$

and
$$M_\perp = 0 \tag{2.28}$$

Because the magnetization is stationary, no signal is detected.

A resonant rf pulse will induce non-zero $M_\perp$ and the precession of $M_\perp$ in the transverse plane containing the receiver coil will induce an oscillating EMF which can be detected by the spectrometer.

Following the disturbance from the equilibrium, the magnetization **M** will eventually return to its original position. This return to the thermal equilibrium is termed **relaxation**. We can write the rate of the change phenomenologically as

$$dM_z/dt = -(M_z-M_0)/T_1 \tag{2.29}$$

and

$$dM_\perp/dt = -M_\perp/T_2 \tag{2.30}$$

T_1 is known as the **spin-lattice relaxation time** or **longitudinal relaxation time**, it is the time required for the spin system to return to the thermal equilibrium with its surroundings after the excitation ends. The fluctuating magnetic fields of the nuclei making up the lattice (surroundings) must have appropriate frequency components to stimulate the transitions between energy levels. Consequently motion at the Larmor frequency is most efficient.

T_2 is called the **spin-spin relaxation time** or **transverse relaxation time** and corresponds to the "natural lifetime" of the free induction signal detected by the spectrometer. After the end of the excitation, the local fields associated with the magnetic properties of neighbouring nuclei will cause the precessing nuclei acquiring a range of slightly different precessional frequencies, therefore the free induction signal will dephase.

In practice there are other contributions, for example, the non-uniformity of the $\mathbf{B}_0$ (which is never perfect) across the sample, which will lead to the signal decaying faster than the "natural" rate. The actual decay time is given by T_2*.

For any system, it can be shown that

$$T_1 \geq T_2 \tag{2.31}$$

Note that the decay of the signal in the time domain leads to a spectral broadening. The two broadening examples given correspond respectively to **homogeneous** and **inhomogeneous** broadening. These are distinguished by the fact that the homogeneous broadening is inherently irreversible whereas the signal lost in the time domain due to the inhomogeneous broadening may be recovered using, for example, an appropriate rf pulse sequence. Homogeneous broadening arises from relaxation processes.

Another example of relaxation behaviour is that associated with diffusive motion of nuclei in the presence of a magnetic field gradient. The loss of phase coherence associated with such motion may be distinguished from the coherent phase shifts associated with flow. This distinction will be addressed subsequently (see Section 2.3).

We can use the spin-echo technique$^{(10)}$ to remove the effect of the $\mathbf{B}_0$ inhomogeneity. If at a time τ after the application of the 90 degree pulse we apply a 180 degree pulse, the direction of the dephasing magnetization will be reversed resulting in a refocused $\mathbf{M}_\perp$ at time 2τ. Any reduction in the amplitude of $\mathbf{M}_\perp$ will be due to T_2. There are two basic forms of the spin-echo technique, namely, $90|_{x'}$-τ-$180|_{y'}$ (Figure 2.6) and $90|_{x'}$-τ-$180|_{x'}$ (Figure 2.7). We will also find that the spin-echo technique plays an important role in NMR imaging.

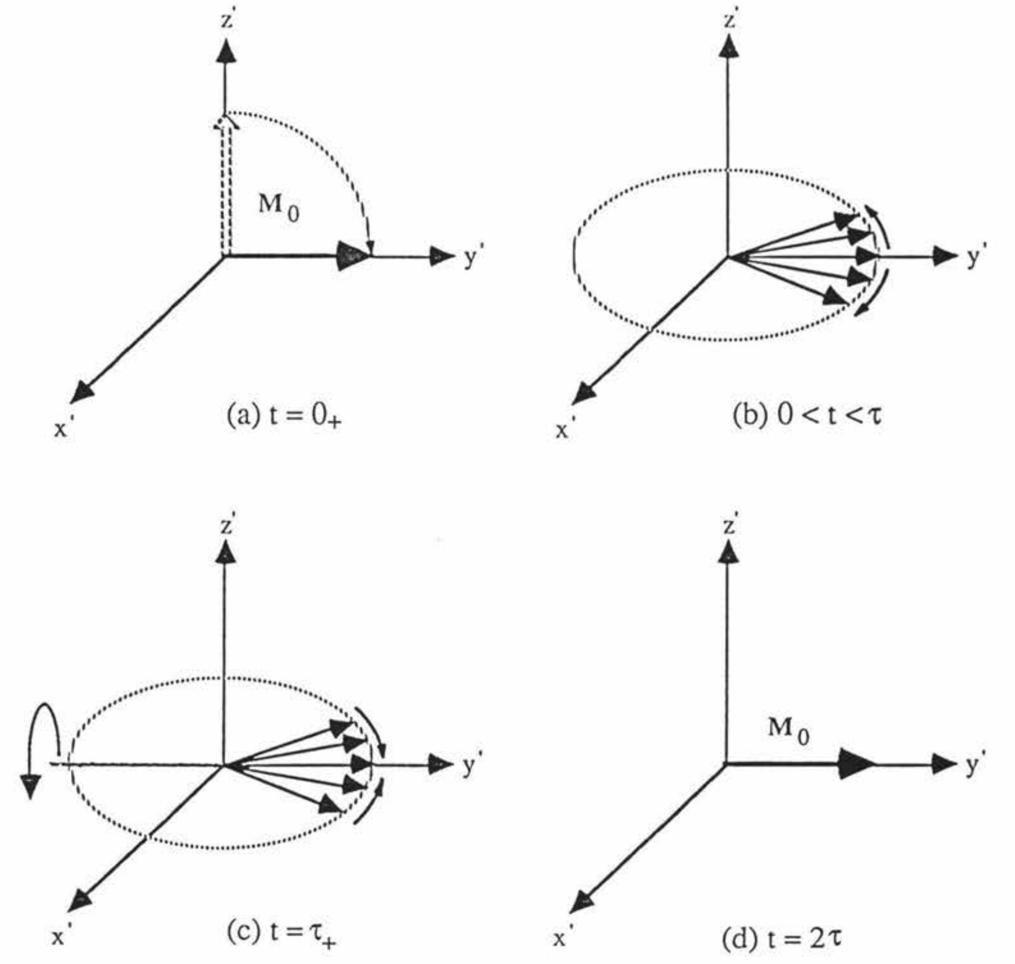

(a) $t = 0_+$

(b) $0 < t < \tau$

(c) $t = \tau_+$

(d) $t = 2\tau$

(e) Pulse Sequence and Nuclear Signal

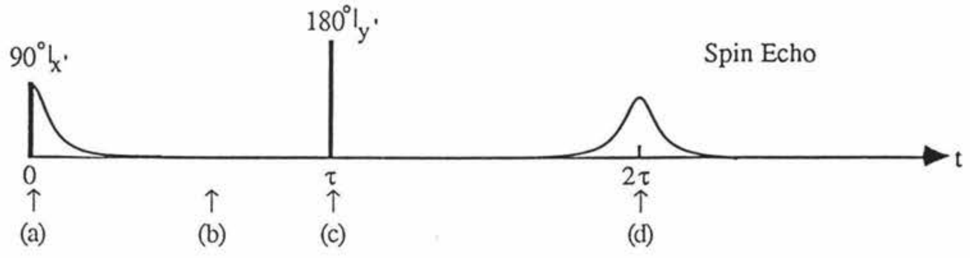

Figure 2.6 $90^\circ|_{x'} - \tau - 180^\circ|_{y'}$ Pulse Sequence and Spin Echo

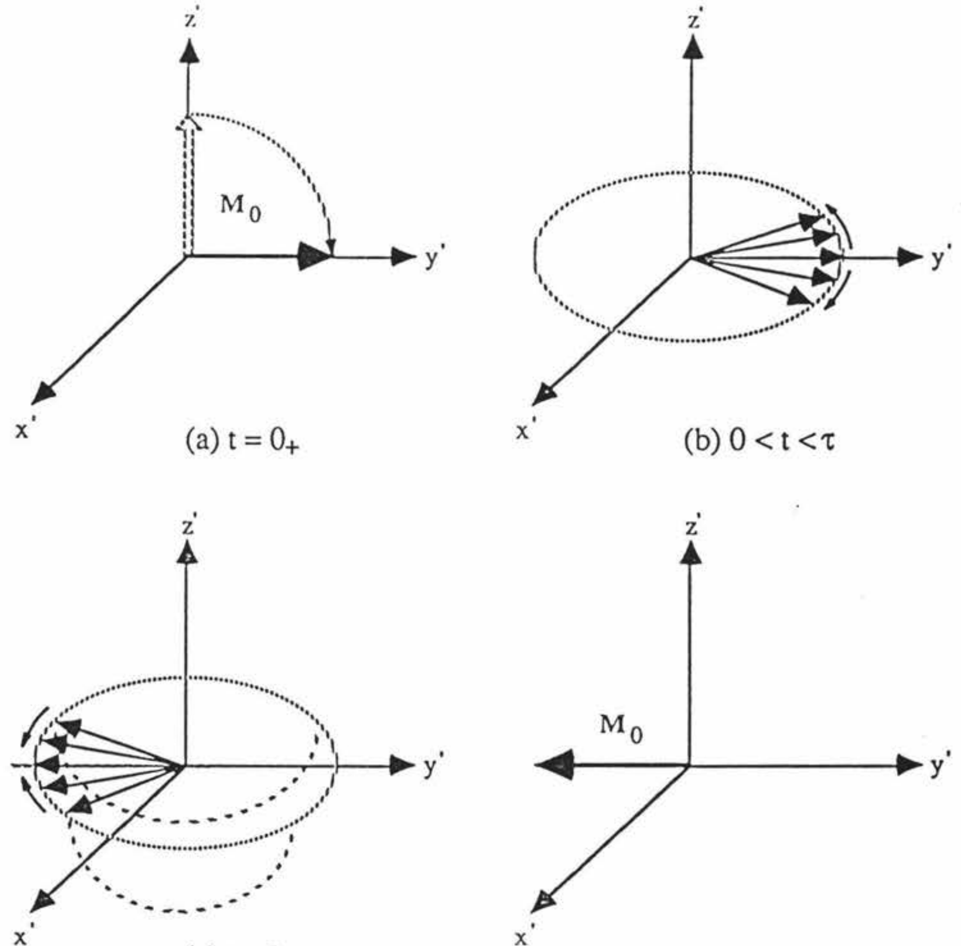

(a) $t = 0_+$

(b) $0 < t < \tau$

(c) $t = \tau_+$

(d) $t = 2\tau$

(e) Pulse Sequence and Nuclear Signal

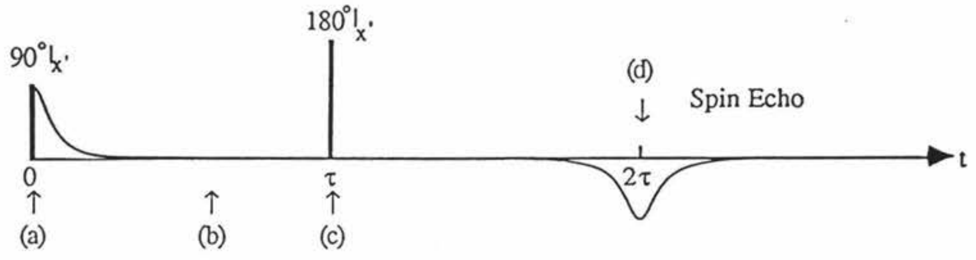

Figure 2.7 $90^\circ|_{x'} - \tau - 180^\circ|_{x'}$ Pulse Sequence and Spin Echo

2.1.4 Bloch Equation

If we assume that the two independent factors which lead to the change of the magnetization are the external magnetic fields and the relaxation processes of the nuclear spin system itself, then from Equations (2.18), (2.29) and (2.30), the equation of motion of the magnetization **M** could be written as

$$d\mathbf{M}/dt = \gamma (\mathbf{M} \times \mathbf{B}) + [-(M_x\mathbf{i} + M_y\mathbf{j})/T_2 - (M_z - M_0)\mathbf{k}/T_1] \quad (2.32)$$

This is the well known **Bloch Equation**(11). The first term is due to the precessional motion and the second term is due to the relaxation processes.

In the component form the above equation could be written as

$$dM_x/dt = \gamma (M_yB_z - M_zB_y) - M_x/T_2 \quad (2.33a)$$

$$dM_y/dt = \gamma (M_zB_x - M_xB_z) - M_y/T_2 \quad (2.33b)$$

$$dM_z/dt = \gamma (M_xB_y - M_yB_x) - (M_z - M_0)/T_1 \quad (2.33c)$$

The Bloch equation is valid for liquids and 'liquid-like' systems where the Hamiltonian is always of a simple magnetic (vector) form. The condition ' independent ' used in the derivation of the equation simplifies the calculation, but strictly speaking, the relaxation processes arise from the effects of external fields. These influences may be calculated quantum mechanically.

Now consider the evolution of **M** following a 90° rf pulse. This example is known as **Free Precession** and the signal obtained is termed the **Free Induction Decay (FID)**.

If $\mathbf{B}_1(t)$ is along the x' axis in the rotating frame, just after the 90°pulse, we will have

$$M_x(0) = M_z(0) = 0 \quad (2.34)$$

$$M_y(0) = M_0 \quad (2.35)$$

Consider the case which we are interested, namely, $B_x=B_y=0$ and $B_z=B_0$. Using Equations (2.34) and (2.35) as the initial conditions, we arrive at the solution for the Bloch equation as

$$M_x(t) = M_0\exp(-t/T_2)\sin\omega_0 t \quad (2.36a)$$

$$M_y(t) = M_0\exp(-t/T_2)\cos\omega_0 t \quad (2.36b)$$

$$M_z(t) = M_0[1 - \exp(-t/T_1)] \quad (2.36c)$$

as illustrated in Figure 2.8, Figure 2.9, and Figure 2.10.

Fourier Transformation (**FT**) will give a Lorenztian peak in the frequency domain (Figure 2.11). If the main field $\mathbf{B}_0$ is perfectly uniform, the shape of the peak is independent of the geometry of the sample, and the line-width will be $(\pi T_2)^{-1}$.

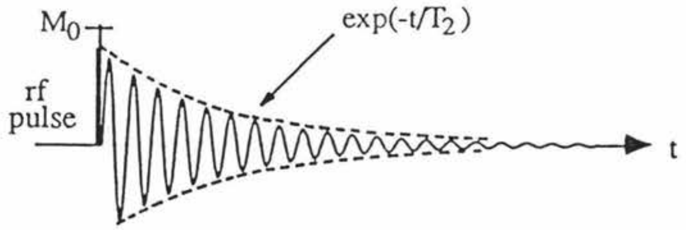

Figure 2.8 Motion of M_x (t)

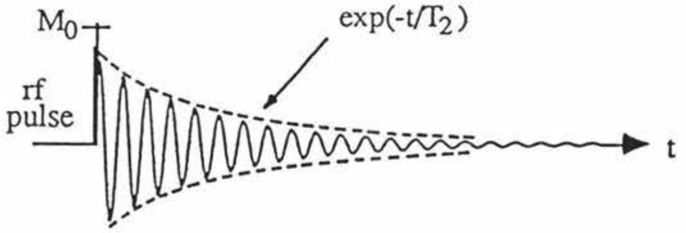

Figure 2.9 Motion of M_y (t)

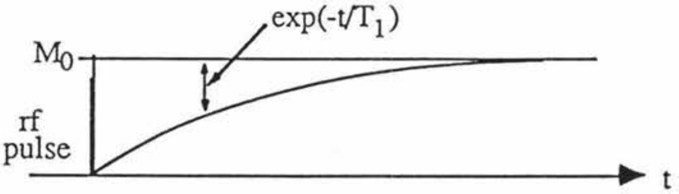

Figure 2.10 Motion of M_z (t)

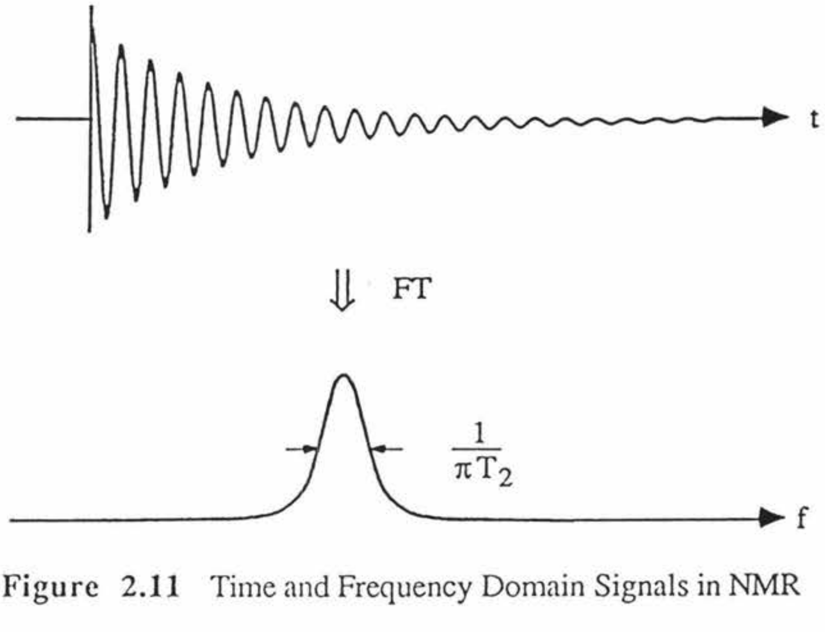

Figure 2.11 Time and Frequency Domain Signals in NMR

Another important example concerns the evolution of **M** in the presence of the rf field. This evolution determines the nature of the excitation. In the presence of $\mathbf{B}_1(t)$ (taking the clockwise component),

$$dM_x/dt = \gamma\,(M_yB_0 + M_zB_1\sin\omega t\,) - M_x/T_2 \tag{2.37a}$$

$$dM_y/dt = \gamma\,(M_zB_1\cos\omega t - M_xB_0\,) - M_y/T_2 \tag{2.37b}$$

$$dM_z/dt = \gamma\,(-M_xB_1\sin\omega t - M_yB_1\cos\omega t\,) - (M_z - M_0\,)/T_1 \tag{2.37c}$$

The solution is clearer if we transfer M_x and M_y from the laboratory frame to a rotating frame x'y'z' (Figure 2.12) in which $\mathbf{B}_1$ is stationary.

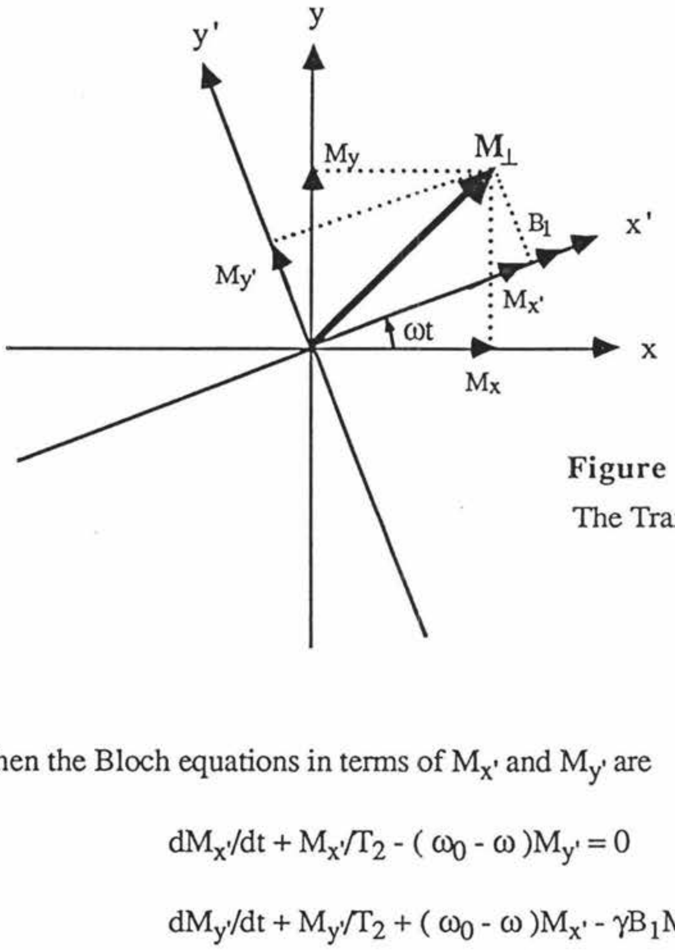

Figure 2.12

The Transverse Magnetization Vector in Two Frames

Then the Bloch equations in terms of $M_{x'}$ and $M_{y'}$ are

$$dM_{x'}/dt + M_{x'}/T_2 - (\,\omega_0 - \omega\,)M_{y'} = 0 \tag{2.38a}$$

$$dM_{y'}/dt + M_{y'}/T_2 + (\,\omega_0 - \omega\,)M_{x'} - \gamma B_1M_z = 0 \tag{2.38b}$$

$$dM_z/dt + (\,M_z - M_0\,)/T_1 + \gamma B_1M_{y'} = 0 \tag{2.38c}$$

To obtained the value of $M_{x'}$ and $M_{y'}$ at any time it is necessary to solve Equations (2.38a-c). In particular we are interested in the transverse magnetization induced by a time dependent $B_1(t)$ in the presence of a magnetic field gradient which causes a spatial distribution of ω_0 values. This is the problem of selective excitation.

2.1.5 The Signal to Noise Ratio

NMR is an insensitive technique and the available signal to noise ratio (**S/N**) is a limiting factor in many experiments. In imaging experiments it is particularly important to optimize S/N.

The signal depends primarily upon the sample, while sources of noise may be numerous. In a well designed system the probe and the rf preamplifier obviously determine the overall noise and sensitivity.

After a 90° rf pulse, a signal voltage due to the free precession of the magnetization **M** will be detected by the rf coil. The usual equation for the S/N after a 90° pulse is given by(12,13)

$$(S/N)_{rms} = K\eta M_0 \left(\frac{\mu_0 Q \omega_0 V_c}{4 F k_B T_c \Delta f} \right)^{1/2} \tag{2.39}$$

where K is a numerical factor (≈ 1) dependent on the receiving coil geometry; η is the 'filling factor', i.e., a measure of the fraction of the coil volume occupied by the sample; M_0 is the nuclear magnetization given by Equation (2.16); μ_0 is the permeability of free space; Q is the quality factor of the coil; ω_0 is the Larmor frequency; V_c is the volume of the coil; F is the noise figure of the spectrometer, T_c is the probe temperature in Kelvin; and Δf is the bandwidth (in Hertz) of the receiver.

Hoult and Richards(14) have pointed out that the interactions between the various factors in Equation (2.39) are very complicated, and therefore this equation is not 'fundamental'. By invoking the principle of reciprocity, they derived a different equation which gives a direct insight into the various factors involved and which clarifies some of the interactions inherent in the traditional relationship.

If we consider the hydrogen nucleus (j = $^1/_2$) and express the equation more conveniently in terms of the peak signal , we obtain from the Hoult and Richards expression

$$(S/N)_{peak} = \frac{V_s (B_1)_{xy} N_h \gamma \hbar^2 \omega_0^{7/4}}{6.73 k_B T_s} \left(\frac{p}{k_B T_c L F \sigma \Delta f} \right)^{1/2} \left(\frac{1}{\mu_0 \mu_r \rho_T} \right)^{1/4} \tag{2.40}$$

where V_s is the sample volume; $(B_1)_{xy}$ is the component of $\mathbf{B}_1$ perpendicular to the main field $\mathbf{B}_0$ in the volume element due to unit current flowing in the coil; N_h is the number of hydrogen nuclei per unit volume; T_s is the sample temperature in Kelvin; L is the length of the conductor; ρ_T is the resistivity of the conductor; p is the perimeter of the conductor; σ is a factor taking account of the reduction in skin depth which arises from the proximity of turns in the coil.

It is of interest to note that the signal to noise ratio depends on $(\omega_0)^{7/4}$ whereas Equation (2.39) implies (S/N) ~ $\omega_0{}^2$. The discrepancy arises because Equation (2.40) allows for the reduction in skin depth (with consequent attenuation of Q) as ω_0 increases.

2.2 Static NMR Imaging Theory

Traditionally NMR imaging involves a determination of the stationary nuclear spin distribution. Various methods(15,16) have been successfully used to produce such static NMR images. The following description employs one of the most commonly used methods, **Filtered Back Projection** Reconstruction (**FBP**).

2.2.1 The Field Gradient

Equation (2.9) shows that Larmor frequency is a measure of the external field. This means that any variation in the external field will lead the change of the Larmor frequency. We notice in the previous section (2.1.3) that the non-uniformity of the main field will yield some additional linewidth in NMR experiments. Therefore in high resolution NMR spectroscopy specific efforts are made to improve the uniformity of the field, so that each chemically identical nucleus resonates at the same frequency.

By contrast, we can imagine a system in which the field strength has been purposefully adjusted so as to vary linearly across the sample, thus producing a Larmor frequency also varying linearly across the sample(17). All the nuclei in a plane perpendicular to the field gradient will experience the same field strength and contribute to the signal amplitude at the same frequency. In other words, the spatial displacements are turned into frequency displacements. So the spectrum after Fourier transformation will take a functional form representative of the shape of the sample (Figure 2.13). This spectrum is known as the '1-D image' or 'projection profile'.

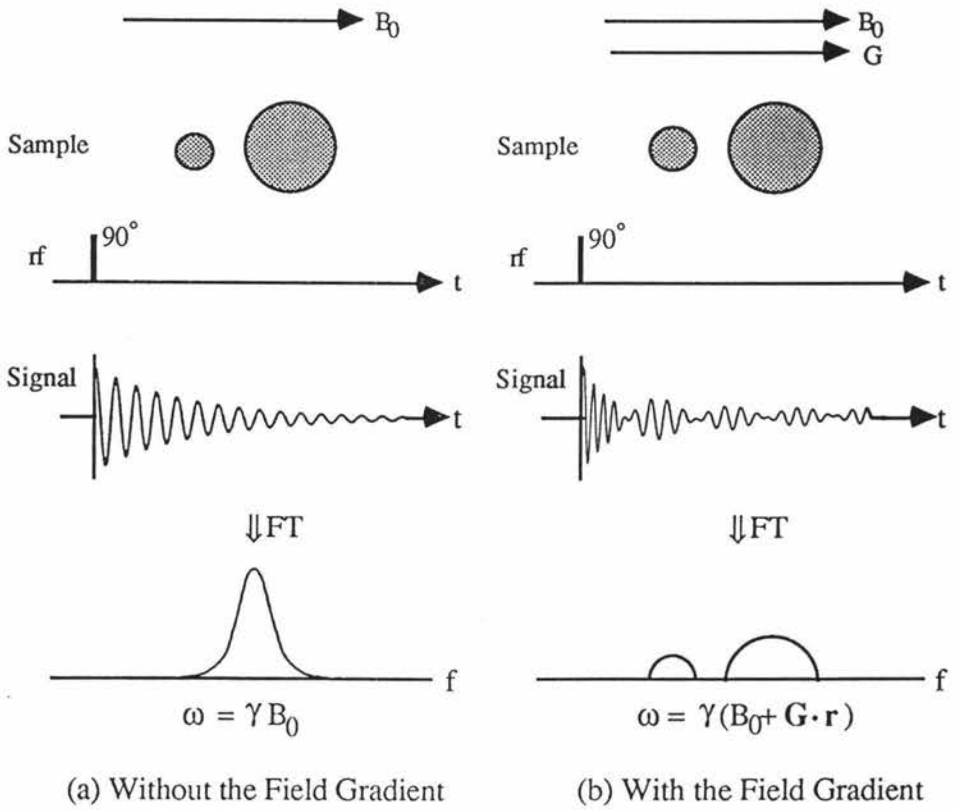

(a) Without the Field Gradient (b) With the Field Gradient

Figure 2.13 The Effect of Field Gradient in NMR

In practice, this linear field gradient is a superposition of an uniform field $\mathbf{B}_0$ and a gradient field $\mathbf{G}$. The ideal gradient $\mathbf{G}$ has three independent components, G_x, G_y, G_z, (Figure 2.14), which make all 'points' in the sample inherently distinguishable.

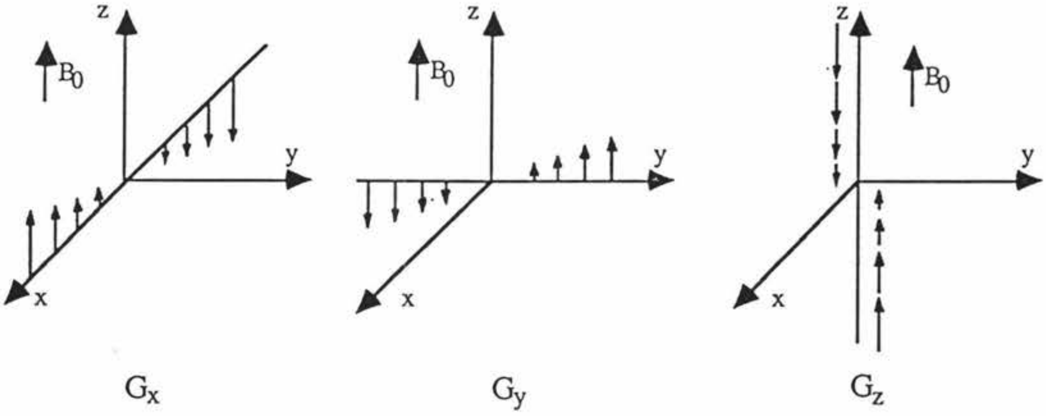

Figure 2.14 Magnetic Field Gradients (along the axes)

$\mathbf{G}$ is defined by

$$G = \nabla B_0 \tag{2.41}$$

so that the expression of the precession frequency [Equation (2.9)] will be

$$\boldsymbol{\omega}(\mathbf{r}) = -\gamma(B_0 + \mathbf{G}\cdot\mathbf{r})\mathbf{k} \tag{2.42}$$

2.2.2 Selective Excitation

NMR is inherently a three-dimensional phenomenon. The rf pulse which we have previously described (Section 2.1) tips the magnetization through the same angle at all points in our sample. Although it is possible to perform NMR imaging in three-dimensions, one of the most common strategies in NMR imaging is to generate a two-dimensional slice through the sample. This reduces the size of the data set which must be handled and is consistent with the display of the image as a two dimensional array.

It would be very nice to tip the magnetization only at points within a slice of the sample. That means we selectively and non-invasively excite a thin slice. In practice this is achieved by using simultaneously a narrow band rf pulse and a gradient field in the direction orthogonal to the slice plane (imaging plane).

To excite a rectangular slice, the rf pulse requires a complicated time dependence, which in linear response theory would correspond to sinc{ [sin(at)]/at } amplitude modulation. In fact the response of the nuclei spin system for large turn angles is highly non-linear and can only be described exactly by solving Equations (2.37) or (2.38). Eccles and Callaghan$^{(18)}$ gives an example of a numerical solution to the above equations for the sinc modulation, which is shown in Figure 2.15.

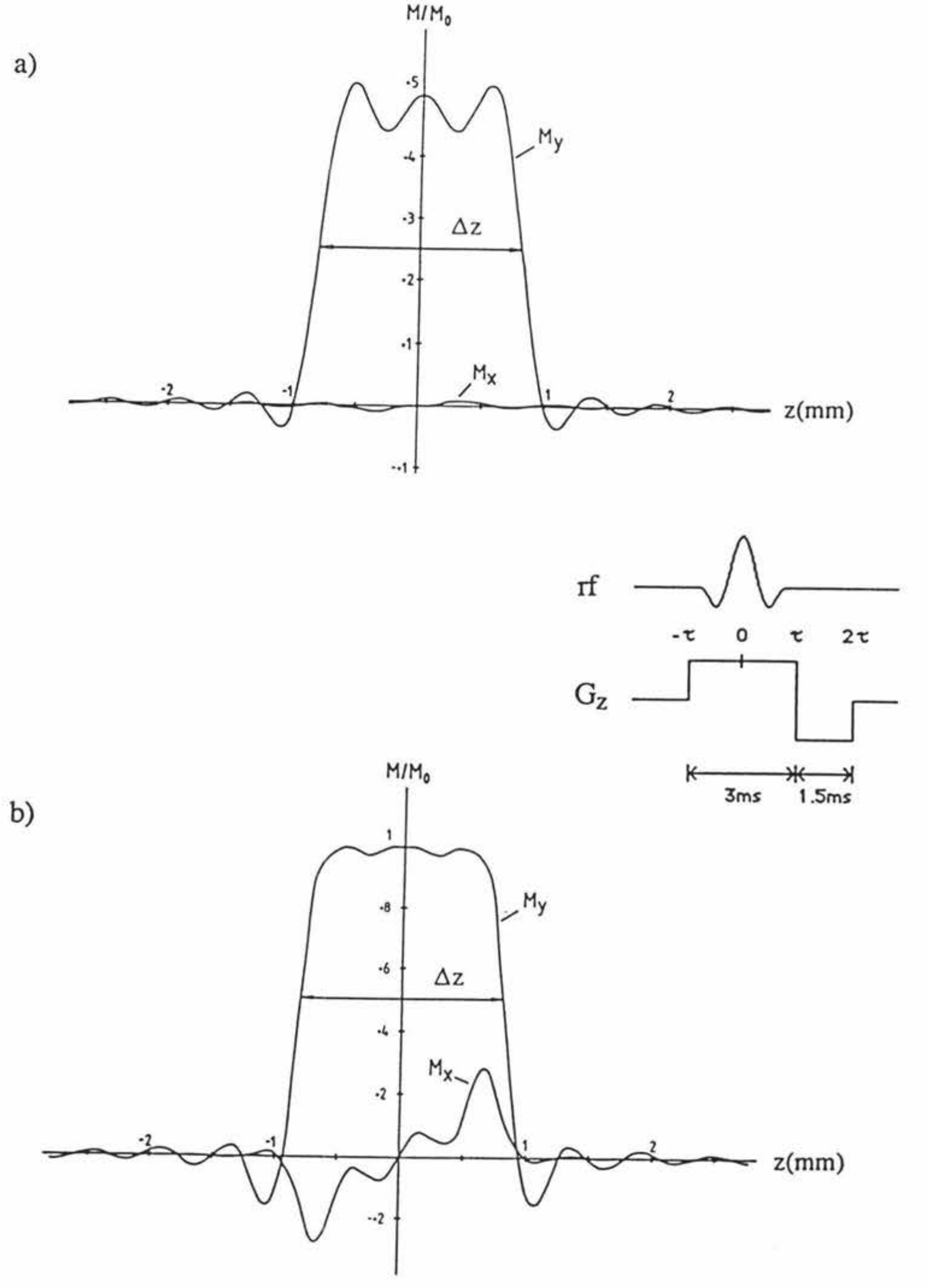

Figure 2.15 Transverse Magnetization at Time 2τ as a Function of Position due to Selective Excitation with a Sinc Modulated rf Pulse for a Tip Angle at z = 0 of, a) 30° and b) 90°.
[taken from Reference (18)]

It is noteworthy that the result for a 90° pulse is qualitatively similar to that expected for a linear response model and therefore the simpler linear description is a useful aid in understanding the selective excitation process. An example of this description has been given by Bailes and Bryant(19).

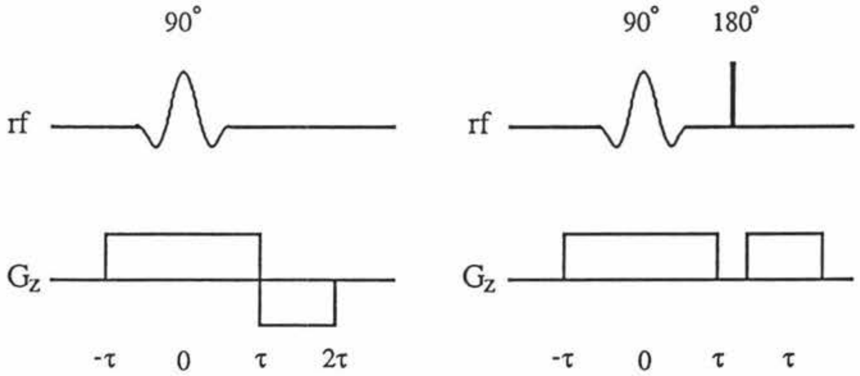

(a) A pulse sequence used to selectively excite a slice of spins along the z axis

(b) An alternative rephasing method used when G_z must remain positive

Figure 2.16 Pulse Sequences for Selective Excitation

Let's consider the effect of a pulse sequence (Figure 2.16) in the rotating frame x'y'z', where the rf amplitude, $B_1(t)$, is stationary and the Larmor frequency of the magnetization along the gradient axis z is given by Equation (2.42) as

$$\omega' = \gamma G_z z \tag{2.43}$$

Equation (2.43) shows that the Larmor frequency of **M** varies with the position. Therefore we define z = 0 as the centre plane where **M** and $B_1(t)$ precess at the same frequency ω_0. At any where away from the centre plane, **M** and $B_1(t)$ are no longer precess at the same frequency.

We rewrite Equations (2.38a-c) as

$$dM_{x'}/dt - [\ \omega(r) - \omega\ ]M_{y'} = 0 \tag{2.44a}$$

$$dM_{y'}/dt + [\ \omega(r) - \omega\ ]M_{x'} - \gamma B_1(t)M_{z'} = 0 \tag{2.44b}$$

$$dM_{z'}/dt + \gamma B_1(t)M_{y'} = 0 \tag{2.44c}$$

where $\omega(r)$ is the Larmor frequency which is now a function of the position, ω is the rf field rotating frame x'y'z' frequency. The effects of relaxation have been neglected. The difference $[\omega(r) - \omega]$ can be written as ω' (Figure 2.17).

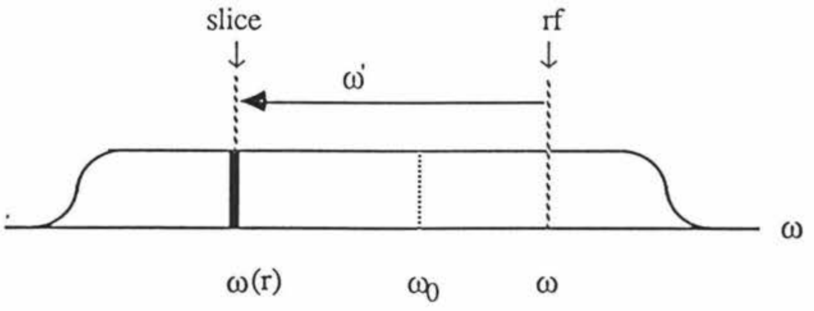

Figure 2.17 The Larmor Frequency is a Function of the Position

The analysis has been simplified by Bailes and Bryant who introduce another frame x"y"z" which rotates clockwise at the frequency displacement ω' with respect to the x'y'z' frame (Figure 2.18). The linearity assumption involves keeping $M_{z'}$ constant.

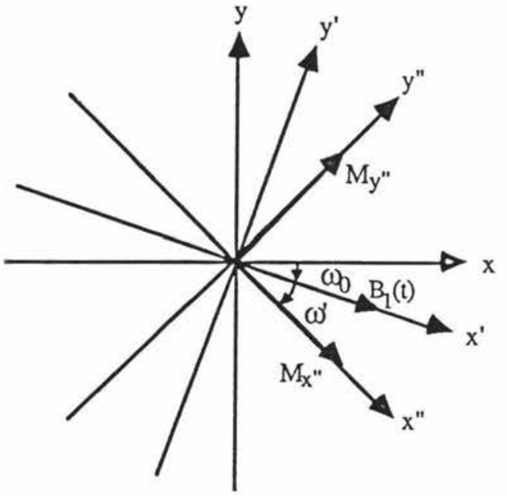

Figure 2.18
The Rotating Frames and
the Magnetization

In the x"y"z" frame **M** does not precess at ω', while $B_1(t)$ is no longer stationary but will rotate anticlockwise (Figure 2.19) with an instantaneous displacement angle $\omega'(t+\tau)$ if $B_1(t)$ is applied initially at $t = -\tau$. $B_1(t)$ can therefore be decomposed into

$$B_{x''} = B_1(t)\cos\omega'(t+\tau) \tag{2.45}$$

and

$$B_{y''} = B_1(t)\sin\omega'(t+\tau) \tag{2.46}$$

Note that only $B_{x''}$ can influence $dM_{y''}/dt$ and only $B_{y''}$ can influence $dM_{x''}/dt$, so that in the x"y"z" frame we get

$$dM_{x''}/dt + \gamma M_{z''}B_1(t)\sin[\omega'(t+\tau)] = 0 \tag{2.47a}$$

$$dM_{y''}/dt - \gamma M_{z''}B_1(t)\cos[\omega'(t+\tau)] = 0 \tag{2.47b}$$

$$dM_{z''}/dt = 0 \tag{2.47c}$$

Using the complex plane to represent $M_{\perp''}$, we have

$$dM_{\perp''}/dt = \gamma M_{z''}B_1(t)\exp[-i\omega'(t+\tau)] \tag{2.48}$$

which gives

$$M_{\perp''} = \gamma M_{z''}\exp(-i\omega'\tau)\int_{-\tau}^{\tau} B_1(t)\exp(-i\omega' t)dt \tag{2.49}$$

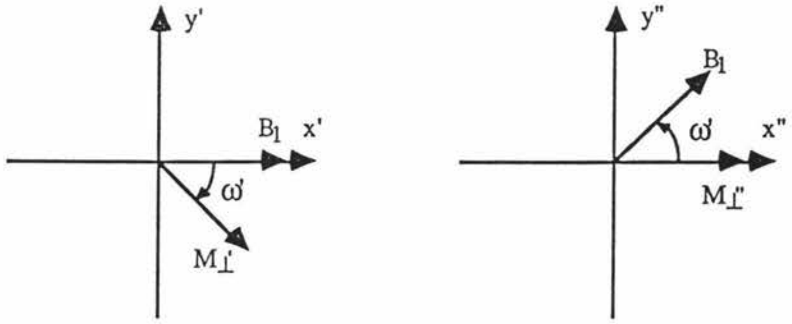

(a) In the x'y'z' Frame (b) In the x"y"z" Frame

Figure 2.19 The Transverse Component of **M** in Two Rotating Frames

Note that because of the linearity assumption, we need only integrate $B_1(t)$ not $M_{z'}B_1(t)$. This integral is just a FT of $B_1(t)$, namely, $F\{B_1(t)\}$.

Therefore

$$M_{\perp''} = \gamma M_0\exp(-i\omega'\tau)F\{B_1(t)\} \tag{2.50}$$

where we have used M_0 instead of $M_{z''}$ (and $M_{z'}$ later). Since the x"y"z" frame has rotated $\omega'2\tau$ clockwise with respect to the x'y'z' frame during the rf pulse time, one obtains

$$\begin{aligned} M_{\perp'} &= M_{\perp''}\exp(i\omega' 2\tau) \\ &= \gamma M_0 F\{B_1(t)\}\exp(i\omega'\tau) \end{aligned} \tag{2.51}$$

The extra phase shift, $\exp(i\omega'\tau)$, is a function of position in the sample and so leads to a dephasing of the signal. It can be removed by applying what is called 'rephasing gradient' which has shown in Figure 2.16. Then

$$M_{\perp'} = \gamma M_0 F\{B_1(t)\} \tag{2.52}$$

or

$$M_{y'} = \gamma M_0 \mathrm{Re}[F\{B_1(t)\}] \tag{2.53}$$

At 2τ $M_{y'}$ is proportional to the real part of the Fourier transform of the applied rf pulse. Of course(20) the rectangular function and the sinc function are the FT pair, so exciting using a sinc modulated rf pulse will yield a rectangular slice of spins.

By changing the precession frequency of $B_1(t)$, we can adjust the position of the plane where **M** and $B_1(t)$ precess at the same frequency, that means the position of the slice can be adjusted.

2.2.3 Filtered Back Projection Reconstruction

Since the selective excitation has defined a 'thin' slice, we can therefore consider our spin system in 2-D rather than 3-D. We define the nuclear spin density $\rho(x,y)$ as the contribution of each point in the transverse plane towards the detected signal S(t). For a perfect slice and perfect system, $\rho(x,y)$ is equal to $M_{y'}$, and consequently, equal to M_0 if a 90° pulse has been employed. In practice $\rho(x,y)$ is proportional to $M_{\perp'}$ precessing in the transverse plane, differed by a constant depending upon the sensitivity of the receiver and other practical factors.

The acquisition of the signal occurs in the absence of the rf field but in the presence of the applied magnetic gradients oriented in the plane of the slice. Therefore the signal is given by

$$S(t) = \int \rho(x,y) \exp[\ -i\omega_0(\mathbf{r})t\ ] d\mathbf{r} \tag{2.54}$$

where $\omega_0(\mathbf{r})$ is given by Equation (2.42).

In the heterodyne detection frame, we get

$$S(t) = \int \rho(x,y) \exp[\ -i\gamma \mathbf{G}\cdot\mathbf{r}t\ ] d\mathbf{r} \tag{2.55}$$

A reciprocal space, **k** space, is introduced to express the time domain signal S(t). By defining

$$\mathbf{k} = (2\pi)^{-1}\gamma \mathbf{G}t \tag{2.56}$$

Equation (2.55) can be expressed as

$$S(\mathbf{k}) = \int \rho(x,y) \exp[\ -i2\pi \mathbf{k}\cdot\mathbf{r}\ ] d\mathbf{r} \tag{2.57}$$

or in polar coordinates,

$$S(\mathbf{k}) = \int_0^{\pi} \int_{-\infty}^{+\infty} \rho(x,y) \exp[\ -i2\pi \mathbf{k}\cdot\mathbf{r}\ ] r dr d\phi \tag{2.58}$$

It can be shown that for a real function $\rho(\mathbf{k})$, we have the relationship

$$S^*(\mathbf{k},\phi) = S(-\mathbf{k},\phi) \tag{2.59}$$

where S^* is the complex conjugate of S.

This symmetry relation means that we need sample only two quadrants, since the real spectrum is identical in the opposite **k** direction, while the imaginary spectrum has the opposite sign in the opposite **k** direction.

Since the image space (**r** space) is conjugate to the signal space (**k** space) via the Fourier transform, a 2-D FT will yield a 2-D image which is the spatial distribution of $\rho(x,y)$

$$\rho(x,y) = \int_0^{\pi} \int_{-\infty}^{+\infty} S(\mathbf{k})\exp[\, i2\pi\mathbf{k}\cdot\mathbf{r}\,]\, |k|dkd\phi \tag{2.60}$$

Note the above equation incorporates a 1-D transform where the signal has been multiplied by a ramp $|k|$. This step is termed '**filtering**' which removes the 'star artifacts' or 'blurring' produced by the simple back projection reconstruction process(21).

In practice, after the ramp multiplication, the signal is Fourier transformed to produce the 'filtered profile'

$$P^*(x,y,\phi) = \int_{-\infty}^{+\infty} S(\mathbf{k})\exp[\, i2\pi k(\, x\cos\phi + y\sin\phi\,)\,]\, |k|dk \tag{2.61}$$

which is then projected into the image plane by summing through the **k** space

$$\rho(x,y) = \sum_{j=1}^{m} P^*(x_j,y_j,\phi_j)\Delta\phi \tag{2.62}$$

where $\Delta\phi = \pi/m$. A series of filtered profiles, each one corresponding to a different value of ϕ, is back projected and interpolated into a cartesian matrix to form a final 2-D image (Figure 2.20). If N_{acc} is the number of accumulations per projection with t_{rep} being the repetition time, then the product $mN_{acc}t_{rep}$ gives estimatly the total imaging experimental time.

Equation (2.61) plays a central role in the FBP image reconstruction. It states that a 1-D FT of the projection data at a given angle ϕ represents the 2-D FT values of the object function $\rho(x,y)$ in **k** space along the radial line, which is named the sampling line, with the given angle ϕ (Figure 2.21).

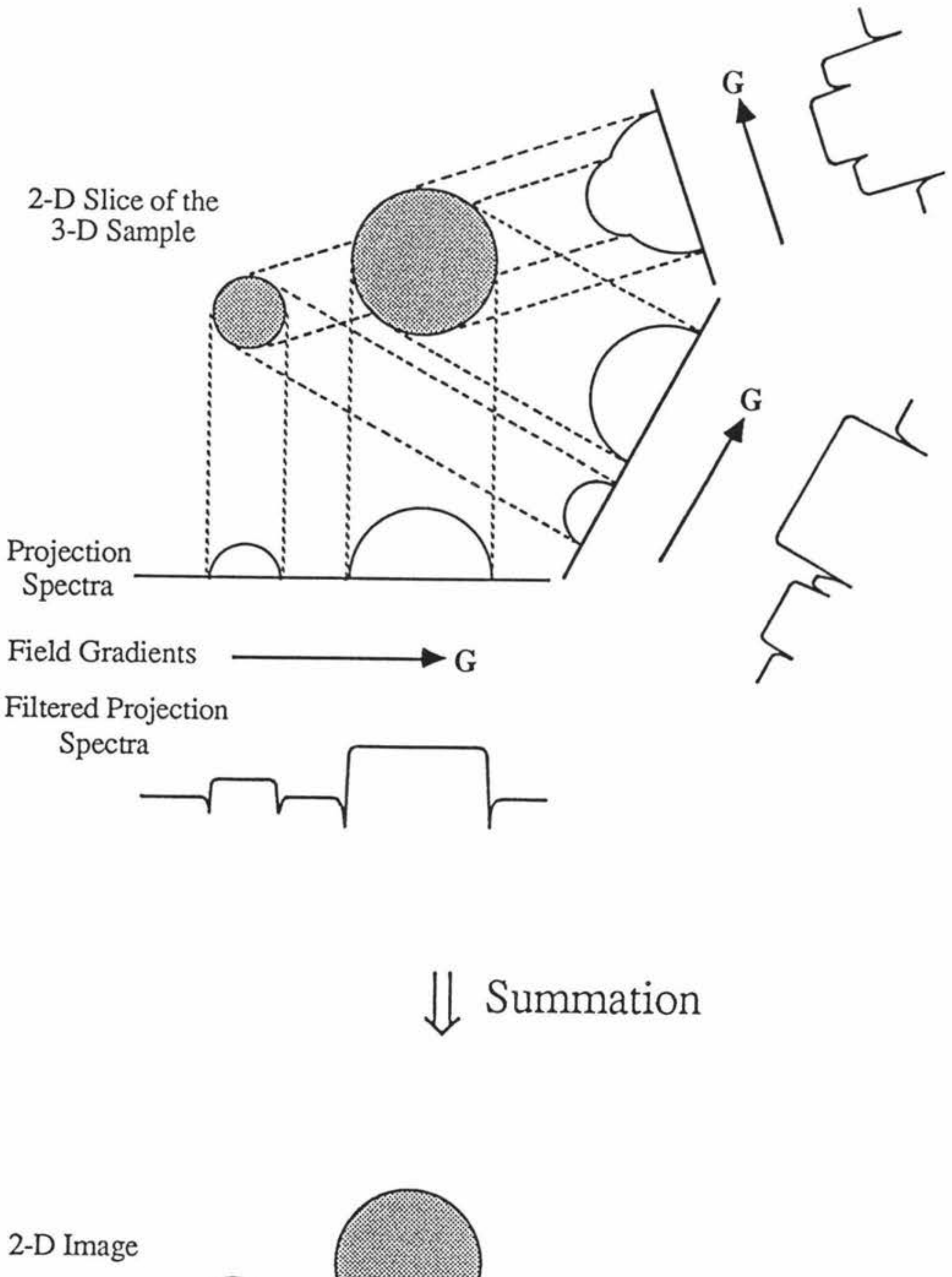

Figure 2.20 Filtered Back Projection Reconstruction

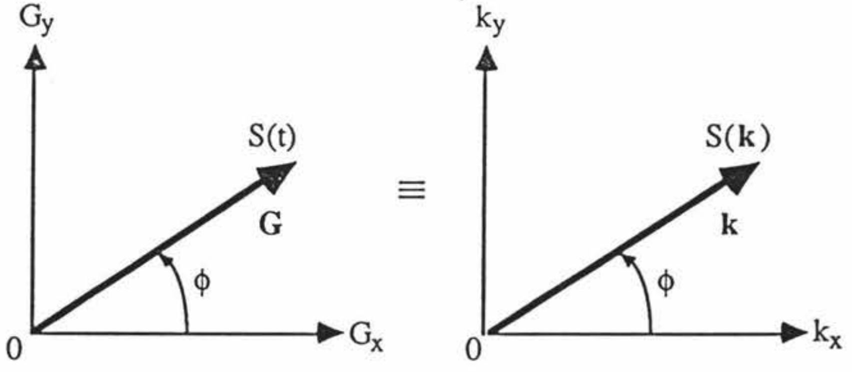

$$\phi = \tan^{-1}(G_y/G_x)$$
$$k = (2\pi)^{-1}\gamma|G|t$$

Figure 2.21 Time Domain Signal and **k** Space

It can be shown that the signal S(t) at a given time and under a given gradient corresponds to a point in **k** space. We name this a 'sampling point' [Equation (2.56)]. After the selective 90° pulse, the sampling point is at the centre of **k** space. From then on, its position is determined by the time effect of the imaging gradients. That means the sampling point can be moved through **k** space. In our system we use a radial mapping to sample **k** space. The data points form a polar grid. The FBP process described by Equation (2.61) involves a Fourier transformation in a polar coordinates, but in which the image is returned on a cartesian grid. The inevitable interpolation occurs during the back projection process as illustrated in Figure 2.22. The data acquisition and processing procedures are illustrated in Figure 2.23.

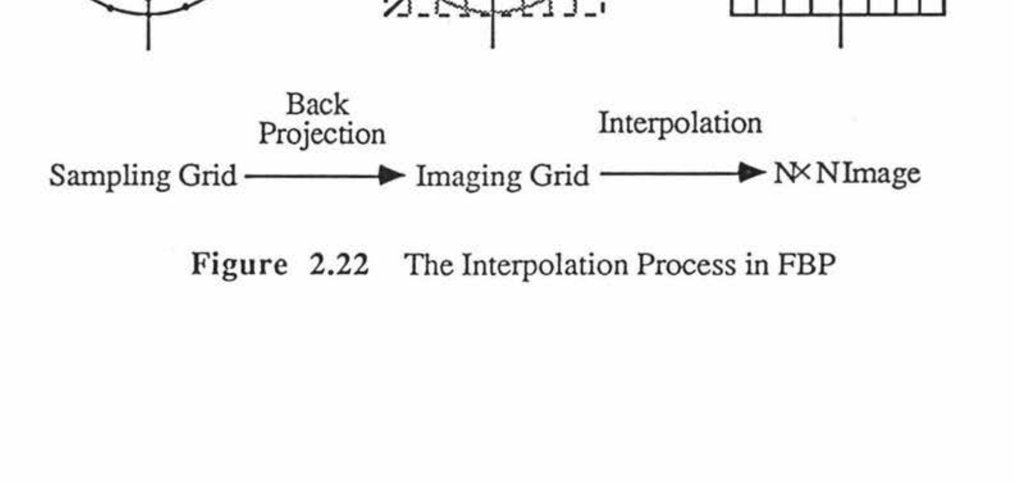

Figure 2.22 The Interpolation Process in FBP

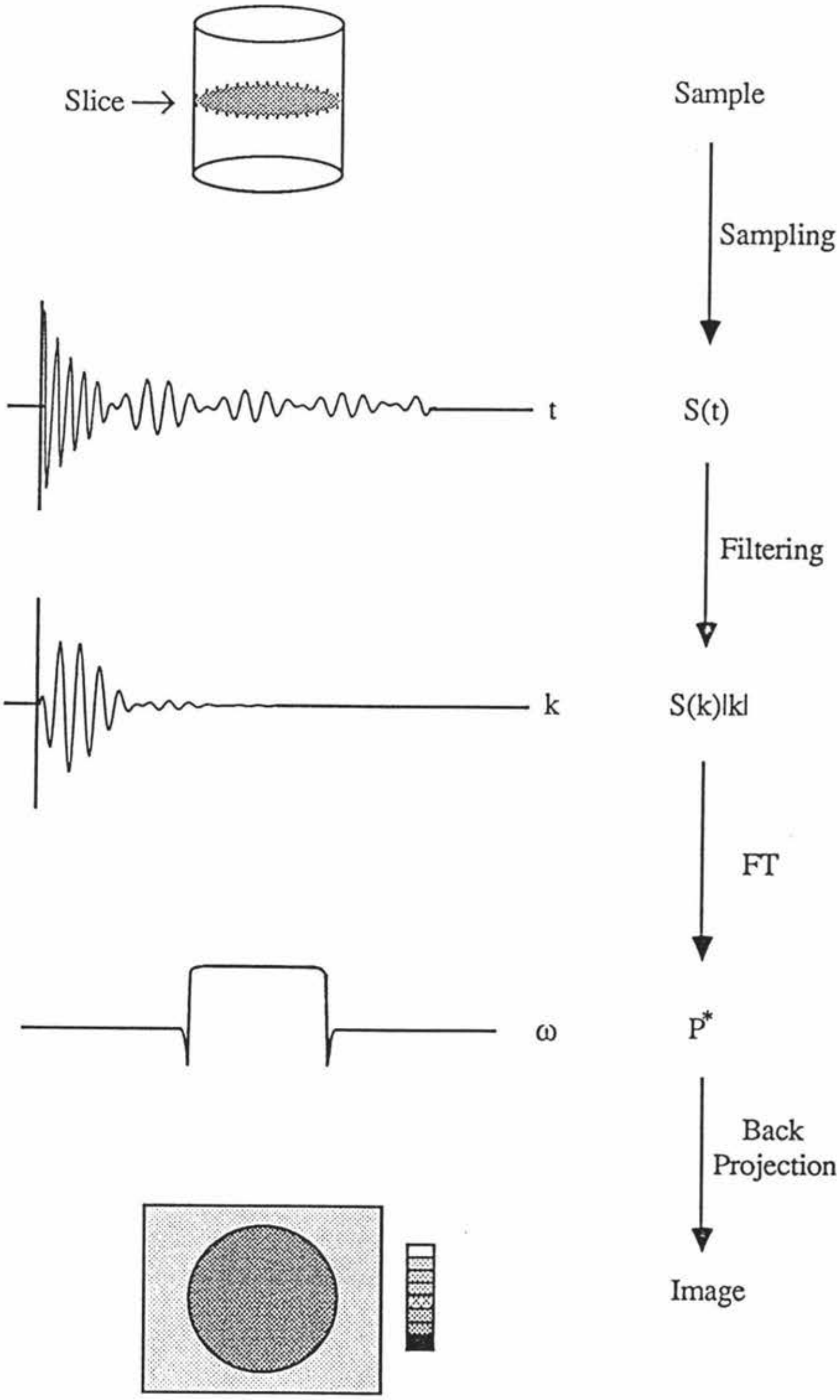

Figure 2.23 Data Processing Sequence of FBP

There are several parameters which influence NMR image contrast. By varying the conditions under which NMR data are acquired, we can vary the contributions from these different parameters, and consequently, the image will vary. For example, the nuclear spin density $\rho(x,y)$ that we obtain from an experiment quite often is not a real spin density but rather may be weighted by T_1 or T_2. T_1 varies(22) greatly between different tissues or normal and abnormal tissues, so that the image obtained by extracting T_1 information is found to be extremely useful in biological differentiation (see Sections 4.4 and 4.5). We can also emphasize T_2 effects by using appropriate pulse sequences.

2.2.4 NMR Microscopy

Although NMR imaging has been successfully performed since 1972, most effort has been involved in 'scaling up' to large samples such as humans. The current resolution for medical applications is of order 1 mm.

Recently it has been noticed(23,24,25) that very useful work can be done if the imaging apparatus 'scaled down'. This enables microscopic resolution. NMR microscopy is however inherently difficult to perform due to the smaller signal from the smaller volume element as the resolution is enhanced. In consequence the recent development of NMR microscopy, with an optimal transverse resolution around 20 μm, is focussed on water in biological systems, since these provide high proton density and therefore high sensitivity. However there are many potential applications to be made to non-biological materials. It is possible in principle to employ other nuclei but the $\gamma\omega_0{}^{7/4}$ factor in Equation (2.40) is significantly higher for protons than that for other nuclei.

Besides the inherently low sensitivity of NMR, there are many other factors which restrain NMR microscopy. To achieve high resolution requires small receiver coils and hence, small samples. One obvious problem concerns the high surface to volume ratio of small samples, and hence the time of 'freshness' of small biological samples. In many case the time needed to acquire adequate voxel S/N may prove prohibitive.

2.2.5 S/N and Resolution

We know, in general, S/N obtainable from an element of the sample will be proportional to the number of spins in this elemental volume. That means there is an inherent connection between S/N and resolution. For a minimum acceptable S/N, there will correspond to a minimum voxel resolution. Some other factors associated with the S/N and the resolution are T_2 relaxation, which gives a natural NMR linewidth in any sample; and an intrinsic limit which arises directly from the Brownian motion inherent to the sample. The latter gives a fundamental limit to the resolution, but in most of the practical situation, it is not the main restraint.

S/N for images can be calculated by considering the reference time domain S/N which has been given in Section 2.1.5, while resolution may be defined in terms of the Rayleigh criterion. In practice, with the optimal broadening, the fundamental equation which describes the S/N and the transverse resolution Δx is(26)

$$\Delta x = 16a^{1/2}({}^{S}/_{N})^{1/2}F^{1/4}\sigma^{1/4}\Delta z^{-1/2}(N_{acc}N_pT_2)^{-1/4}f^{-7/8} \qquad (2.63)$$

where a is the rf coil radius, F is the spectrometer noise figure (ideally, F=1), σ is the coil proximity factor (typically 5 for ideal solenoidal geometry), Δz is the slice thickness, N_{acc} is the number of accumulations per projection, N_p is the number of projections, and f is the spectrometer frequency. Therefore the voxel resolution is $(\Delta x^2 \Delta z)^{1/3}$.

2.3 Dynamic NMR Imaging Theory

Dynamic NMR images describe some time-dependent function of a given sample. In particular we are concerned with a nucleus initially at position $\mathbf{r}_0$ migrating to position $\mathbf{r}$ at a later time Δ. Two obvious examples of such dynamic processes are fluid flow and self-diffusion.

The purpose of this section is to investigate the possibility of visualizing the distribution of flow (**Velocity Map**) and/or self-diffusion (**Diffusion Map**). The high spatial resolution of static imaging combined with completely non-invasive measurement could give valuable information about flow and diffusion. Although still in the development phase, such flow contrast methods have been tried in medical research(27,28,29,30).

Before discussing the imaging of flow and diffusion it is appropriate to review the influence of magnetic field gradients on spin echoes in what is known as the Pulse-Gradient-Spin-Echo (**PGSE**) technique. Subsequently the superposition of PGSE and imaging will be considered.

2.3.1 Pulse Gradient Spin Echo Technique

The suggestion that it is possible to measure microscopic random flow (self-diffusion) using Spin-Echo techniques (see Section 2.1.3) was firstly given by Hahn(10), and later developed by Carr and Purcell(31). In the absence of diffusion and/or flow, and using a common $90°|_{x'}$-τ-$180°|_{y'}$ pulse sequence, we observe in the rotating frame a spin-echo with the amplitude [cf. Equation (2.36)]

$$M(t) = M_0 \exp(-2\tau/T_2) \tag{2.64}$$

which appears at 2τ (Figure 2.24).

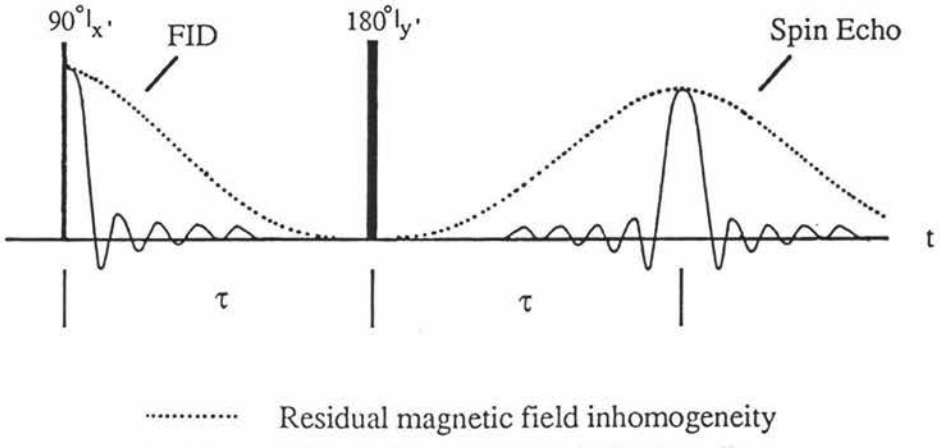

Figure 2.24 Spin Echo and Field Gradient

If diffusion and/or flow do exist, then after the 90° pulse, some nuclei will migrate to a region with different field during the time Δ, and therefore their magnetizations cannot be refocussed perfectly in the phase shifts following the 180° pulse. Diffusion in the presence of the field gradient causes an irreversible dephasing of the magnetization in addition to that caused by the relaxation. It is this additional decay that enables the measurement of self-diffusion.

For a steady gradient experiment it can be shown that

$$M(t) = M_0 \exp[\, -(2\tau/T_2 + 2\gamma^2 G^2 \tau^3 D/3)\,] \tag{2.65}$$

where D is the self-diffusion coefficient, G is the amplitude of the field gradient and M_0 is the initial amplitude of **M**.

The steady gradient experiment suffers from the need to employ a large bandwidth for excitation and detection. This problem may be circumvented by applying the gradient in the form of pulses. In the mid-sixties, following the idea(32) of using pulse gradient instead of 'constant gradient', Stejskal and Tanner demonstrated the first experiments and gave a detailed analysis(33). The basic form of PGSE technique is shown in Figure 2.25. The two rf pulses are the same as in Figure 2.6, but the dephasing and refocussing of the nuclear spins occur in two strong and identical field gradient pulses of magnitude g, duration δ and separation Δ. Note that in order to distinguish the PGSE gradient pulse amplitude for the steady gradient amplitude used for the static imaging, we use the lower case symbol.

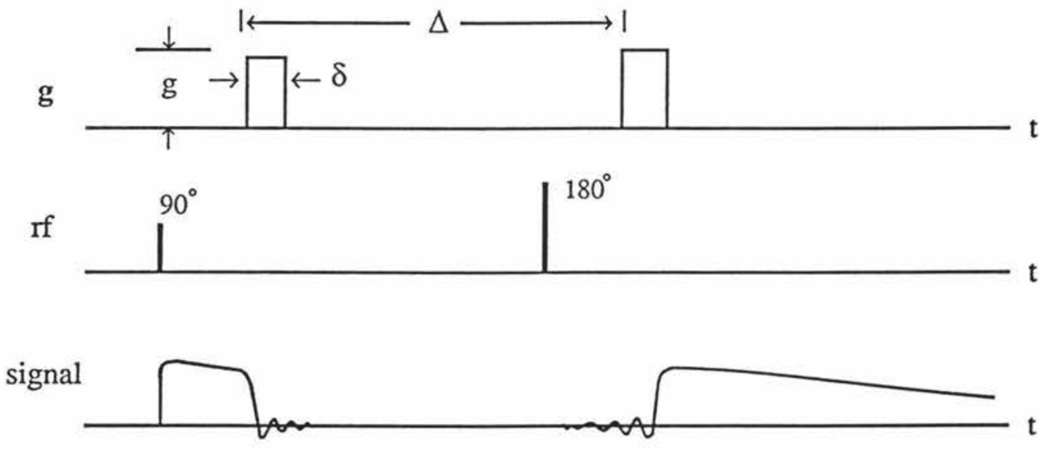

Figure 2.25 Pulse Gradient Spin Echo Technique

In the presence of the first gradient pulse, any phase shift depending upon the position of each nucleus is recorded. Between the pulses the molecules containing the nuclei keep changing their positions due to self-diffusion and/or flow. Following the second rf pulse (180°), all prior phase shifts have been inverted. Any nucleus which has not moved between the two gradient pulses will be refocused perfectly, and any motion of the nucleus will result in the incomplete refocussing. A major advantage of PGSE method is that a larger field gradient can be applied so that much slower diffusion can be measured.

An attenuation factor R is defined as

$$R(g,\delta,\Delta) = M(t)/M_0 \tag{2.66}$$

therefore Equation (2.65) can be expressed in terms of R as

$$R(g,\delta,\Delta) = \exp(\, -\gamma^2\delta^2 g^2 D\Delta \,) \tag{2.67}$$

where we have assumed that $\delta << \Delta$ (the narrow pulse approximation) and the dephasing due to T_2 is negligible compare with that due to the field gradient .

2.3.2 Stejskal Equation

The first theoretical analysis of measuring flow and diffusion using PGSE technique was given by Stejskal(34) and was based on the Bloch-Torrey Equation(35)

$$\partial \mathbf{M}/\partial t = \{\, \gamma(\, \mathbf{M} \times \mathbf{B}\,) + [\, -(\, M_x\mathbf{i} + M_y\mathbf{j}\,)/T_2 - (\, M_z - M_0\,)\mathbf{k}/T_1\,]\}$$

$$+ \{\, \nabla \cdot \mathbf{D} \cdot \nabla \mathbf{M} - \nabla \cdot \mathbf{v}\, \mathbf{M}\,\} \tag{2.68}$$

where the first half of the right hand side is the Bloch equation we had before [Equation (2.32)], and the second half is the terms related with diffusion **D** and fluid velocity **v**. In this description the magnetization is treated as a fluid.

An alternative description due to McCall, Douglass and Anderson(32) involves the use of the self-correlation function of the nuclear spin. $P_s(\mathbf{r}_0|\mathbf{r},\Delta)$ has been defined as the spatial probability distribution function that a nucleus initially at position $\mathbf{r}_0$ will have moved to position $\mathbf{r}$ at the later time Δ. The evolution of $P_s(\mathbf{r}_0|\mathbf{r},\Delta)$ is given by

$$\partial P_s/\partial t = -\nabla \cdot \mathbf{v}\, P_s + \nabla \cdot \mathbf{D} \cdot \nabla\, P_s \tag{2.69}$$

For a uniform, constant diffusion and uniform, constant flow, the above equation has the solution as

$$P_s(\mathbf{r}_0|\mathbf{r},\Delta) = (\, 64\pi^3 D^3 \Delta^3\,)^{-1/2}$$

$$\cdot \exp\{\, (\, 1/4D\,)[(\, x-x_0-S_x\,)^2 - (\, y-y_0-S_y\,)^2 - (\, z-z_0-S_z\,)^2\,]\} \tag{2.70}$$

where D is the diagonal element of the diffusion tensor **D**, and S_i is the component of the fluid displacement vector S which is given by

$$S(\Delta) = \int_0^{\Delta} v\,dt \tag{2.71}$$

Therefore under the narrow pulse approximation, the observed signal attenuation factor is given(34) by

$$R(g,\delta,\Delta) = \int_v P_s(\mathbf{r}_0|\mathbf{r},\Delta)\exp[\ -i\gamma g\cdot(\ \mathbf{r}-\mathbf{r}_0\ )\delta\ ]dv \tag{2.72}$$

By substituting Equation (2.70) into the above equation, we get

$$R(g,\delta,\Delta) = \exp(\ -\gamma^2\delta^2 g\cdot\mathbf{D}\cdot g\Delta\ -\ i\gamma\delta g\cdot\mathbf{v}\Delta\ )$$

$$= \exp(\ -\gamma^2\delta^2 g\cdot\mathbf{D}\cdot g\Delta\ )\exp(\ -\ i\gamma\delta g\cdot\mathbf{v}\Delta\ ) \tag{2.73}$$

It can be seen that the signal amplitude depends upon the diffusion (the first exponential decay term) and the signal phase depends upon the flow (the second complex oscillatory term).

For finite pulse widths the description is more complicated. An exact analysis for the special case of Brownian motion shows that Δ may be replaced by $(\Delta - \delta/3)$. However, it is easy to show that the phase shift arising from velocity $\mathbf{v}$ is given exactly by Equation (2.73) irrespective of the pulse width.

2.3.3 Combined PGSE-Imaging Experiment

Suppose that the signal acquired in the NMR imaging experiment results from a spin echo generated using a PGSE sequence. We will assume that the initial excitation is by a modulated rf pulse so that the desired slice of spins may be observed.(cf. Figure 2.15 and Figure 2.16).

Now the magnetization which exists immediately prior to the application of the imaging gradients is influenced by the factors arising from diffusion and flow as given in Equation (2.73). Furthermore, because of the delay between excitation and acquisition there will be some transverse relaxation. In consequence the spin density $\rho(x,y)$ used in Section 2.2.3 must now be multiplied by an attenuation factor

$$R(g,\delta,\Delta) = \exp[-t/T_2(x,y)]\exp[-\gamma^2\delta^2 g^2 D(x,y)\Delta]\exp[-i\gamma\delta g v(x,y)\Delta] \tag{2.74}$$

where it is presumed that diffusion and velocity are measured along the direction of the gradient. We shall not be concerned with the spatial dependence of T_2. However, the combined PGSE-imaging experiment can reveal the spatial dependence of D and v(36).

We define the 'dynamic reciprocal space' for the PGSE experiment,

$$\mathbf{q} = (2\pi)^{-1}\gamma\delta\mathbf{g} \tag{2.75}$$

$\mathbf{q}$ stands in contrast to the 'static reciprocal space' $\mathbf{k}$ of the 'normal' imaging experiment. We can express the nuclear spin density as

$$\rho(\mathbf{r},\mathbf{q}) = \rho(\mathbf{r},0)R(g,\delta,\Delta)$$

$$= \rho(\mathbf{r},0)\exp[-4\pi^2 q^2 D(\mathbf{r})\Delta]\exp[-i2\pi\mathbf{q}\cdot\mathbf{v}(\mathbf{r})\Delta] \tag{2.76}$$

or in terms of its real and imaginary spin density parts as

$$\rho_R(\mathbf{r},\mathbf{q}) = \rho(\mathbf{r},0)\exp[-4\pi^2 q^2 D(\mathbf{r})\Delta]\cos[2\pi\mathbf{q}\cdot\mathbf{v}(\mathbf{r})\Delta] \tag{2.77a}$$

and

$$\rho_I(\mathbf{r},\mathbf{q}) = -\rho(\mathbf{r},0)\exp[-4\pi^2 q^2 D(\mathbf{r})\Delta]\sin[2\pi\mathbf{q}\cdot\mathbf{v}(\mathbf{r})\Delta] \tag{2.77b}$$

When $q = 0$, which could be obtained by setting either $\delta = 0$ or $g = 0$ (in our system, it is more convenient to adjust the PGSE gradient amplitude g rather than the pulse duration δ), we have

$$\rho_R(\mathbf{r},0) = \rho(\mathbf{r}) \tag{2.78a}$$

and

$$\rho_I(\mathbf{r},0) = 0 \tag{2.78b}$$

That means $\rho_R(\mathbf{r},0)$ is just the 'real' spin density $\rho(\mathbf{r})$ we defined in Section 2.2.3 for the 'static' imaging, while the imaginary part $\rho_I(\mathbf{r},0)$ should be zero.

Therefore by comparison with Equation (2.57), the observed signal $\xi(\mathbf{k},\mathbf{q})$ in the time domain is given by

$$\xi(\mathbf{k},\mathbf{q}) = \int_0^{2\pi}\int_{-\infty}^{+\infty} \rho(\mathbf{r},\mathbf{q})\exp(-i2\pi\mathbf{k}\cdot\mathbf{r})d\mathbf{r} \tag{2.79}$$

or

$$\xi(\mathbf{k},\mathbf{q}) = \int \underbrace{\exp[-4\pi^2 q^2 D(\mathbf{r})\Delta]}_{\text{diffusion contrast}}\underbrace{\exp[-i2\pi\mathbf{q}\cdot\mathbf{v}(\mathbf{r})\Delta]}_{\text{velocity contrast}}\underbrace{\rho(\mathbf{r})\exp(-i2\pi\mathbf{k}\cdot\mathbf{r})d\mathbf{r}}_{\text{resolution}} \tag{2.80}$$

Note, because the modulation due to **q** is complex, the symmetry $S^*(\mathbf{k},\phi) = S(-\mathbf{k},\phi)$ given by Equation (2.59) no longer exists(37). Further, it is apparent that both the signal acquired and the image, which is obtained by the FT of the signal, are inherently complex. In practice this means that all the four quadrants must be sampled and both real and imaginary images must be computed.

Thus $\xi(\mathbf{k},\mathbf{q})$ is a complex Fourier transform of the image density modulated by the diffusion and flow factors, i.e., we have

$$\rho(\mathbf{r},\mathbf{q}) = \int_0^{2\pi}\int_{-\infty}^{+\infty} \xi(\mathbf{k},\mathbf{q})\exp(i2\pi\mathbf{k}\cdot\mathbf{r})|k|dkd\phi \tag{2.81}$$

By varying g, we can step through **q** space. A FT of $\rho(\mathbf{r},\mathbf{q})$ with respect to **q**, or more accurately, with respect to g, will give a gaussian peak (Figure 2.26) in **q** space, with its peak position given by the velocity **v**, and its width given by the diffusion coefficient D.

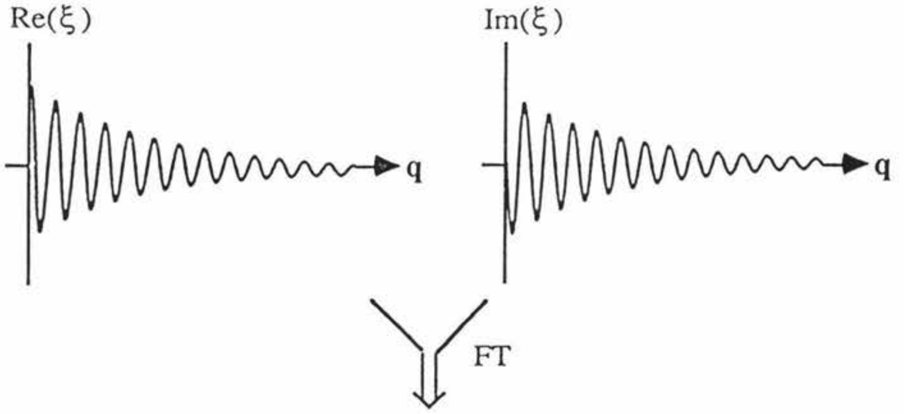

(a) Real $\mathbf{q}$ Space Signal

(b) Imaginary $\mathbf{q}$ Space Signal

(c) Dynamic Displacement Spectrum ($\mathbf{q}$ Space Transform)

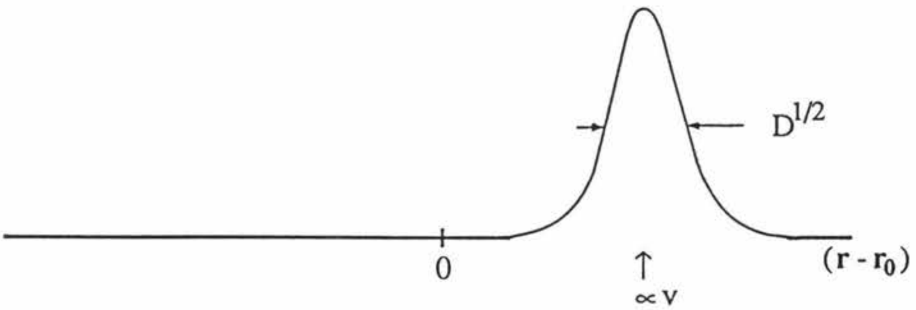

Figure 2.26 Fluid Velocity and Diffusion Measurement using the PGSE Technique

The dynamic imaging experimental procedures are as follows. For any particular value of g, we will get a real and an imaginary 2-D 'data image' by filtered back projection. As g increases, the signal is attenuated, so that a complete data image set contains equal number (n_D) of real and imaginary images, each real and imaginary image corresponding to a certain g. The first real image is the 'static' $\rho(\mathbf{r})$ image while the first imaginary image should be zero (within the accuracy of the noise). The last real image and imaginary image should effectively zero if truncation effects resulting from zero filling are to be avoided. The number of data images and the image size are determined by the computer memory size and speed.

When analyzing data, we select one pixel from exactly the same position of each real and imaginary data images. The sequence of the real data should vary as in Figure 2.26a while that of the imaginary should vary as in Figure 2.26b. A complex N digits discrete FT will yield a peak whose position gives nuclear velocity, and whose Full-Width-Half-Maximum (**FWHM**) gives the diffusion coefficient (Figure 2.26c). By going through the data images pixel by pixel we can obtain a 2-D velocity map and a 2-D diffusion map. Figure 2.27 illustrates the data acquisition and processing procedures.

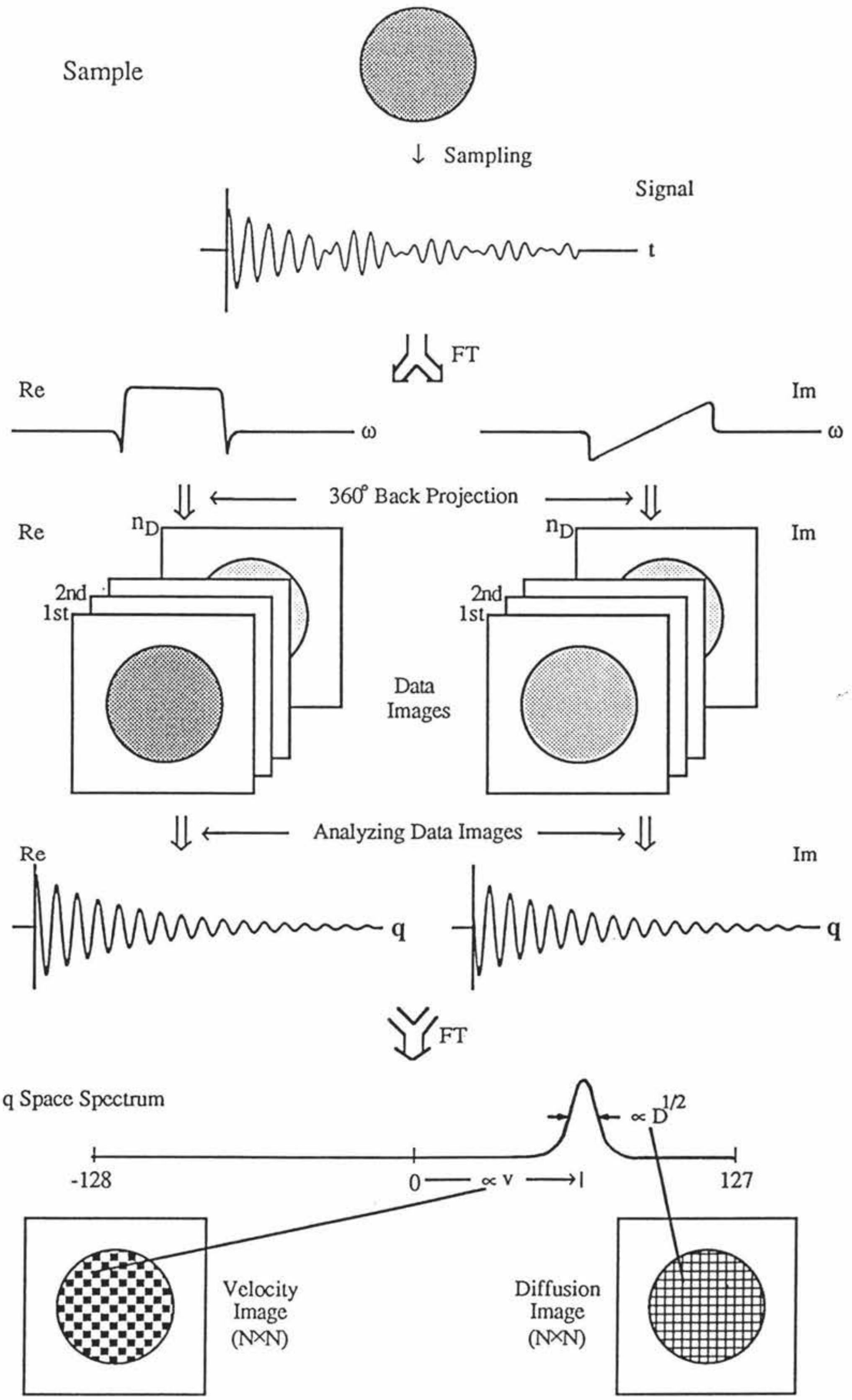

Figure 2.27 Data Processing Sequence for Dynamic Imaging

2.3.4 Interpreting the Velocity and Diffusion Digits

The last step of dynamic imaging is to interpret the digital values obtained from the discrete FT and calculate the velocity and diffusion coefficient. In the following discussion we retain the 'time' and 'frequency' domain pictures for the conjugate spaces relating to dynamic imaging simply for convenience.

Given a time domain function h(t), the Fourier integral is defined as

$$H(f) = \int_{-\infty}^{+\infty} h(t)\exp(-i2\pi ft)dt \tag{2.82}$$

where H(f) is the Fourier transform of h(t) in the frequency domain, and $i^2 = -1$.

The inverse FT is defined as

$$h(t) = \int_{-\infty}^{+\infty} H(f)\exp(i2\pi ft)df \tag{2.83}$$

If two functions h(t) and H(f) are related by Equations (2.82) and (2.83), these two functions are termed a **Fourier transform pair**. Each of these contains the same information as the other, this enables us to examine a particular relationship from an entirely different point of view.

Two relevant examples are,

$$h_1(t) = \exp(i2\pi f_0 t) \iff H_1(f) = \delta(f-f_0) \tag{2.84}$$

and

$$h_2(t) = (\alpha/\pi)^{1/2}\exp(-\alpha t^2) \iff H_2(f) = \exp(-\pi^2 f^2/\alpha) \tag{2.85}$$

The example of combined PGSE and flow and/or diffusion involves a product of $h_1(t)$ and $h_2(t)$ and hence a convolution of $H_1(f)$ and $H_2(f)$. (Figure 2.28).

When a computer is used the function must be digitized. The discrete FT, with its both time and frequency domains being represented by discrete values, is closely related to the continuous FT.

Specifically an N digit discrete FT, with time domain sampling interval T (Figure 2.29a), is expressed as

$$H(k/NT) = \sum_{n=0}^{N-1} h(nT)\exp(-i2\pi kn/N) \qquad k = 0,1,2,...,N-1 \tag{2.86}$$

where 1/NT gives the frequency domain sampling interval (Figure 2.29b) and n and k are the variables in the time and frequency domains respectively. Note sampling in the time domain results in a periodic function in the frequency domain.

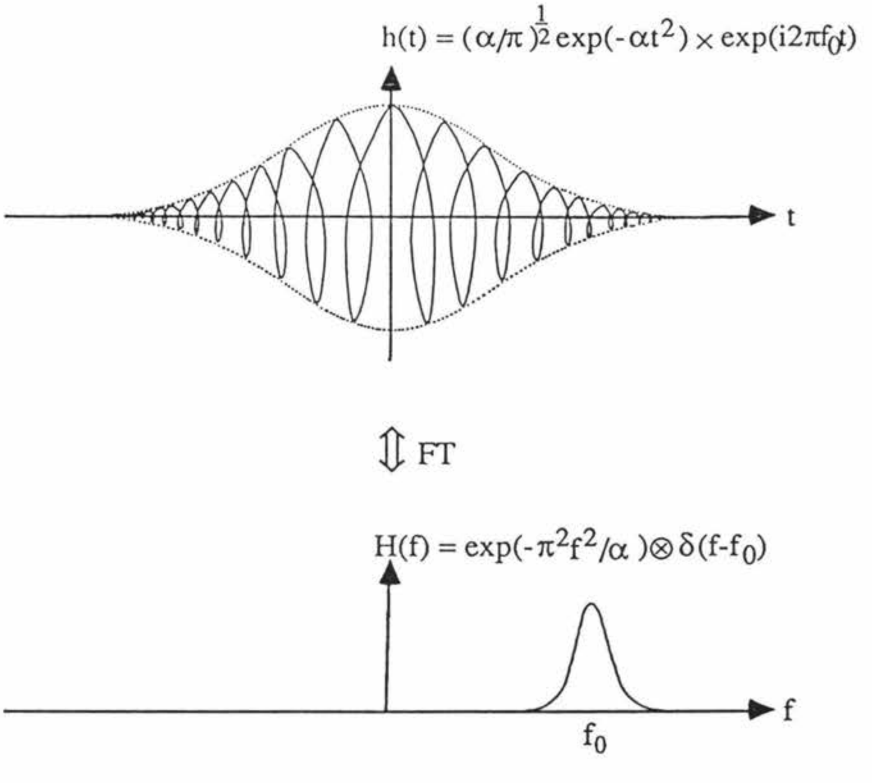

Figure 2.28 Convolution in Dynamic Imaging

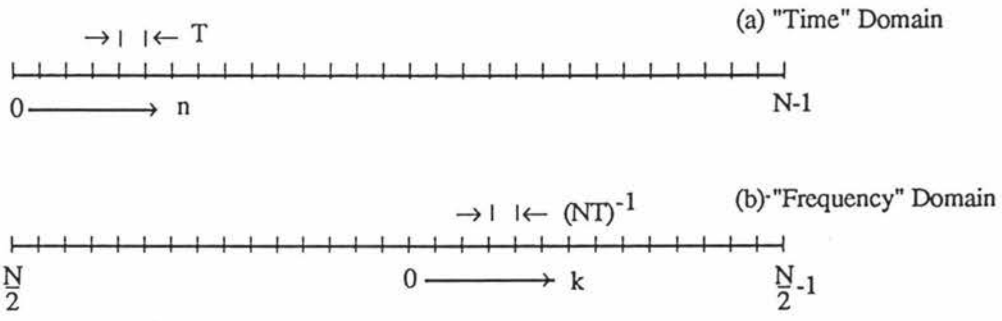

Figure 2.29 Discrete Time and Frequency Domains

The corresponding inverse discrete FT is expressed as

$$h(nT) = (1/N)\sum_{k=0}^{N-1} H(k/NT)\exp(i2\pi kn/N) \qquad n = 0,1,2,\ldots,N-1 \tag{2.87}$$

Therefore, in the discrete forms, the above examples can be written as

$$h_1(nT) = \exp(i2\pi f_0 nT) \iff H_1(k/NT) = \delta(k/NT - f_0) \tag{2.88}$$

and

$$h_2(nT) = (\alpha/\pi)^{1/2}\exp(-\alpha n^2T^2) \iff H_2(k/NT) = \exp[-\pi^2(k/NT)^2/\alpha] \tag{2.89}$$

Note that the actual digitization space is related to the fictional time domain by setting T = 1.

Now we consider the velocity effect in dynamic imaging, which has been given by the second exponential term of Equation (2.76). The discrete form of the velocity in terms of the 'time' domain variable n could be written as

$$\begin{aligned}\exp[-i2\pi vq\Delta] &= \exp\{-i2\pi v[(1/2\pi)(g_m/n_D)\gamma\delta n\Delta]\}\\ &= \exp[-i(\gamma\delta v\Delta)(g_m/n_D)n]\end{aligned} \tag{2.90}$$

where n_D is the maximum number of the discrete values which could be given by one experiment, this number being equal to the maximum number of 'data images' (see Section 3.5.1), g_m is the maximum gradient employed, and g_m/n_D is the gradient per digitization interval.

By comparison of Equation (2.90) with Equation (2.88), we know the FT of Equation (2.90) should give a function with a single peak, and we have the relationship

$$2\pi f_0 = \gamma\delta v\Delta(g_m/n_D) \tag{2.91}$$

Since in the 'frequency' domain, the variable k is given by

$$f = k/N \tag{2.92}$$

therefore the velocity peak should appear at the position

$$f = f_0 \tag{2.93}$$

We can therefore express the velocity in terms of the digital variable k as

$$v = (2\pi n_D k)/(N\gamma g_m\delta\Delta) \tag{2.94}$$

where N is the total number of digits in the 'time' domain while k is the 'digital position' of the dynamic displacement profile peak.

Note that the use of a complex transform (and hence the acquisition of quadrature images) permits positive and negative velocities to be distinguished.

The diffusion coefficient given by the first exponential term of Equation (2.76) could be written in the discrete form as

$$\begin{aligned}\exp[-4\pi^2Dq^2\Delta] &= \exp\{-4\pi^2D[(1/2\pi)(g_m/n_D)\gamma\delta n]^2\Delta\}\\ &= \exp[-\gamma^2\delta^2(g_m/n_D)^2Dn^2\Delta]\end{aligned} \tag{2.95}$$

$$= \exp[-\gamma^2\delta^2(g_m/n_D)^2Dn^2\Delta] \qquad (2.95)$$

For the gaussian function given by Equation (2.85), the half maximum amplitude arises when

$$\pi^2f^2/\alpha = 0.693 \qquad (2.96)$$

Therefore, $\text{FWHM} = 2f$

$$= 2(0.693\alpha/\pi^2)^{1/2}$$

$$= 0.53\alpha^{1/2} \qquad (2.97)$$

Combining Equations (2.95) and (2.97) yields

$$k_{FWHM}/N = 0.53[\gamma^2\delta^2(g_m/n_D)^2D\Delta]^{1/2} \qquad (2.98)$$

and hence $D = (n_D{}^2k^2)/(0.28N^2\gamma^2g_m{}^2\delta^2\Delta)$ (2.99)

In this relationship k is the FWHM of the dynamic displacement profile.

From Equations (2.94) and (2.99) we can calculate the experimental velocity and diffusion in SI units.

2.3.5 Uncertainty of Velocity and Diffusion Data

There are several possible sources which can effect the accuracy of experimental velocity and diffusion results. They could come from computer software, or the practical experimental arrangements.

The first possible source which will lead to some extra broadening is due to the method of calculating FWHM used in the software (see Section 3.5.3 for reasons). In the case where there is no pixel amplitude exactly equal to the half peak value (which would be true most of the time, Figure 2.30), the FWHM given by the computer will be larger than the real FWHM.

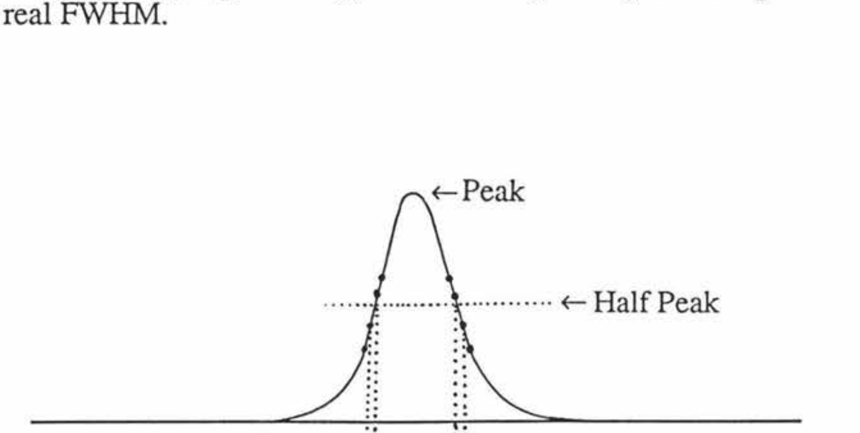

Figure 2.30 Possible Error of FWHM due to the Software

It is easy to see that the range of this error is between zero and two digits. Using Equation (2.99), the absolute error value can be calculated. It seems that no simple method can remove this error source, but by increasing the Fourier transform digit number (say from 256 to 512), one can reduce the percentage effect of this error.

The second possible error source is the effect of a finite base line. This will cause inaccuracy in calculating the FWHM. We know that the following equations are a Fourier transform pair

$$h(t) = k\delta(t) <=> H(f) = K \qquad (2.100)$$

Therefore a finite base line in the frequency domain arises from a spike at the origin of the time domain. It is possible that spikes at origin appear during an experiment

Another source of a finite base line is the dynamic experimental data itself. We know that complex Fourier transform can be mathematically considered as the sum of real cos transformation and imaginary sin transformation. That means in the discrete Fourier transform a function H can be written as

$$H = H_R + H_I \qquad (2.101)$$

in which $$H_R = F_c\{h_R\} - F_s\{h_I\} \qquad (2.102)$$

and $$H_I = F_c\{h_I\} + F_s\{h_R\} \qquad (2.103)$$

F_s and F_c in the above equations are the sin and cos transforms respectively; and the subscripts R and I indicate the real and imaginary parts of the function.

Consider a signal which is 'on resonance' with the correct phase, i.e., $h_I = 0$. Because the periodic relationship

$$h(n-N) = h(n) \qquad (2.104)$$

this means that the data set can range either from 0 to (N-1), or from -N/2 to (N/2-1), and it also can be decomposed into an even function and an odd function (Figure 2.31).

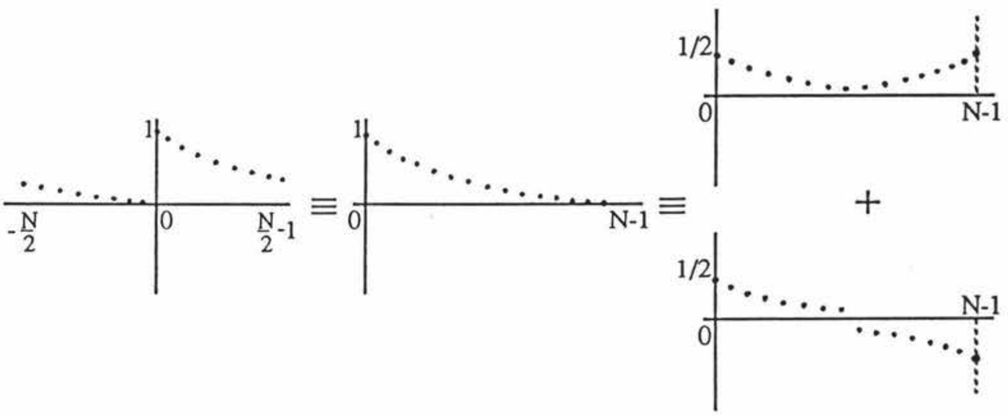

Figure 2.31 Experimental Data and its Equivalents

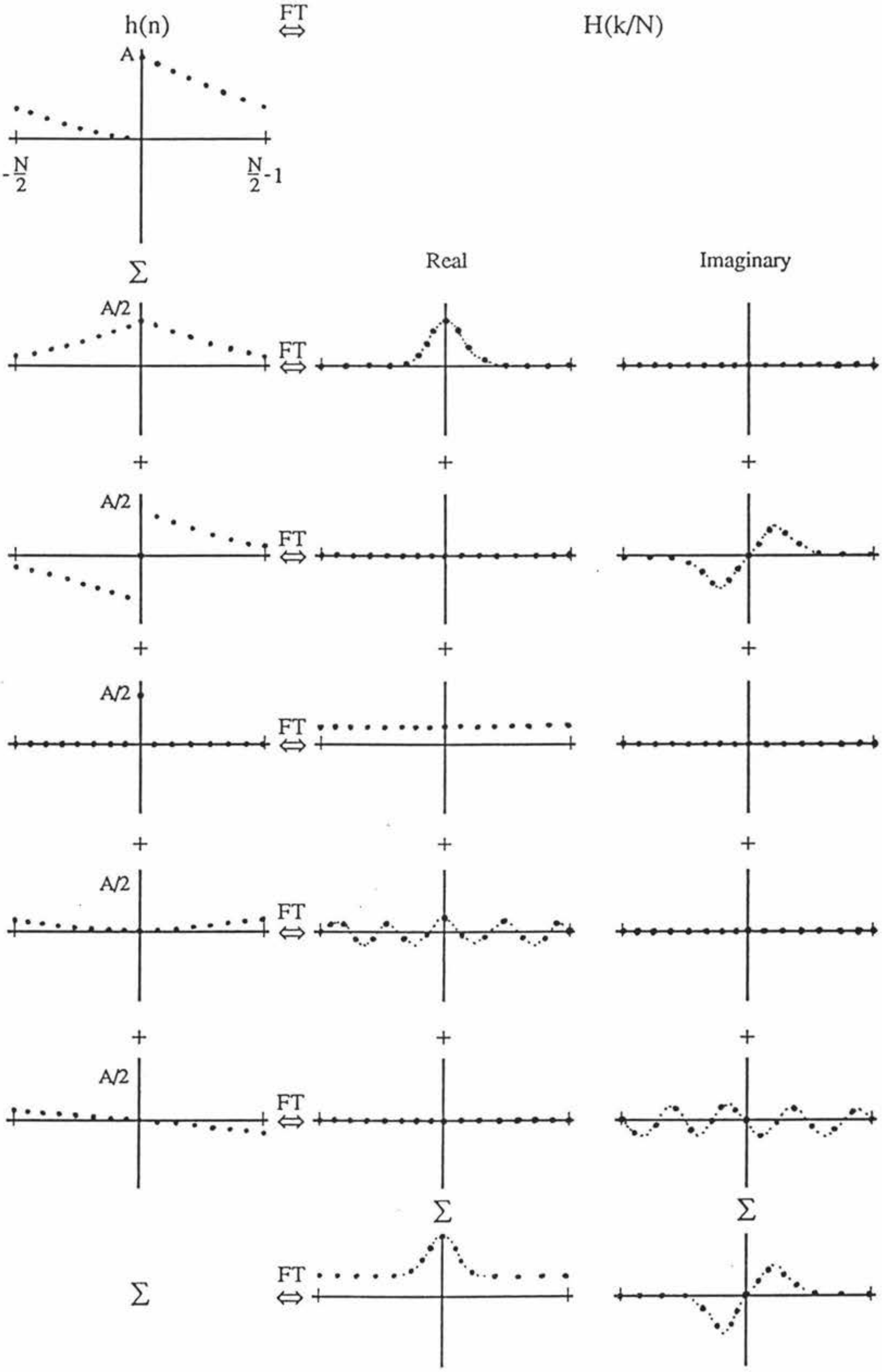

Figure 2.32 Decomposition of FT Data

Therefore any such 'on resonance' signal h(n) can be broken into the sum of symmetrical and antisymmetrical parts. The symmetrical part of h(n) gives only a real function($H_I = 0$) and the antisymmetrical part of h(n) gives only an imaginary function ($H_R = 0$). The Fourier transform pairs for such a signal are shown schematically in Figure 2.32. It is clearly that a finite base line is introduced by the data at the origin, n=0. If no base line is to appear then the amplitude of the data at n=0 should be halved. This effect has been tested using the digital FFT routine on the Hitachi computer, with a result shown in Figure 2.33.

Figure 2.33 Simulating the Effect of A_0 being Halved

(a) A_0

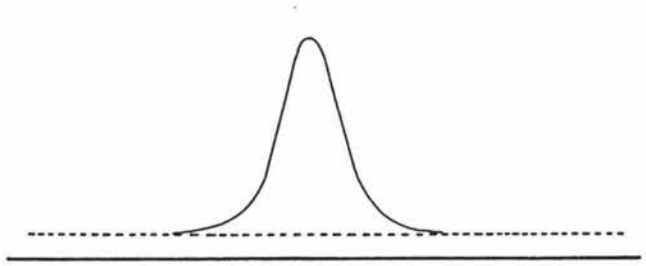

(b) $A_0/2$

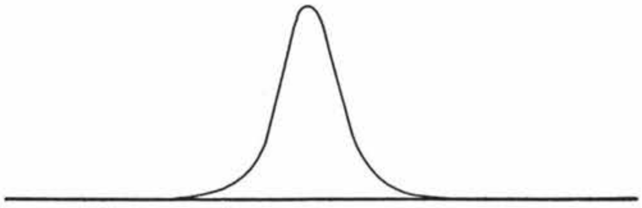

Note that the value of a base line is about $A_0/2N$, where A_0 is the original signal amplitude. This means that we can reduce the base line value by using more data digits.

Correction procedures can be incorporated in the computer program to correct for this effect (cf Section 3.5.3). The value of this effect has been simulated by computer, with a result shown in Figure 2.34. [Note the variable α in Equation (2.97) is being varied in the simulating process.]

Figure 2.34 Simulating the Effect of Finite Base Line

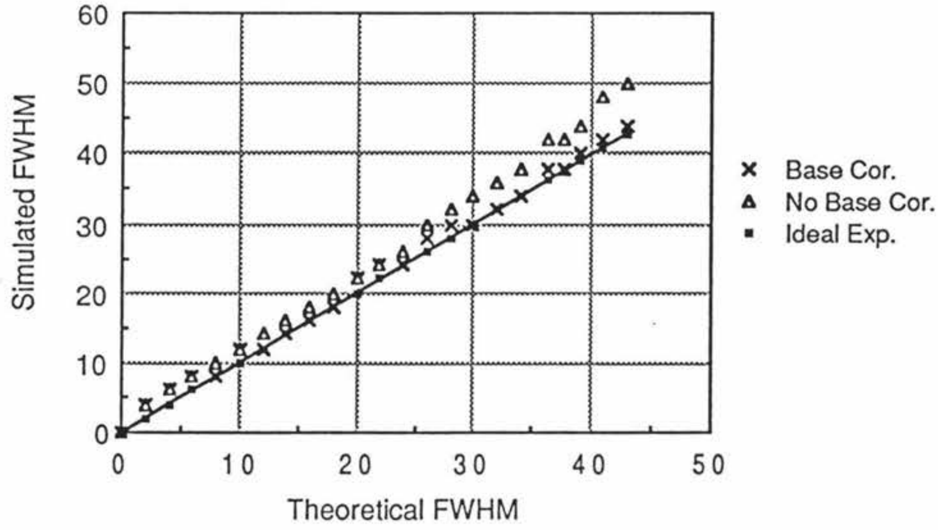

In the current dynamic imaging experiments, we use zero-filling to improve the accuracy of the final data (see Section 3.5.1 for practical reasons). This zero-filling in the time domain is actually equal to a convolution of a gaussian function and a sinc function in the frequency domain. Therefore extra broadening will be introduced due to this zero-filling procedure (Figure 2.35). The computer simulating results are shown in Figure 2.36. [α in Equation (2.97) being varied.]

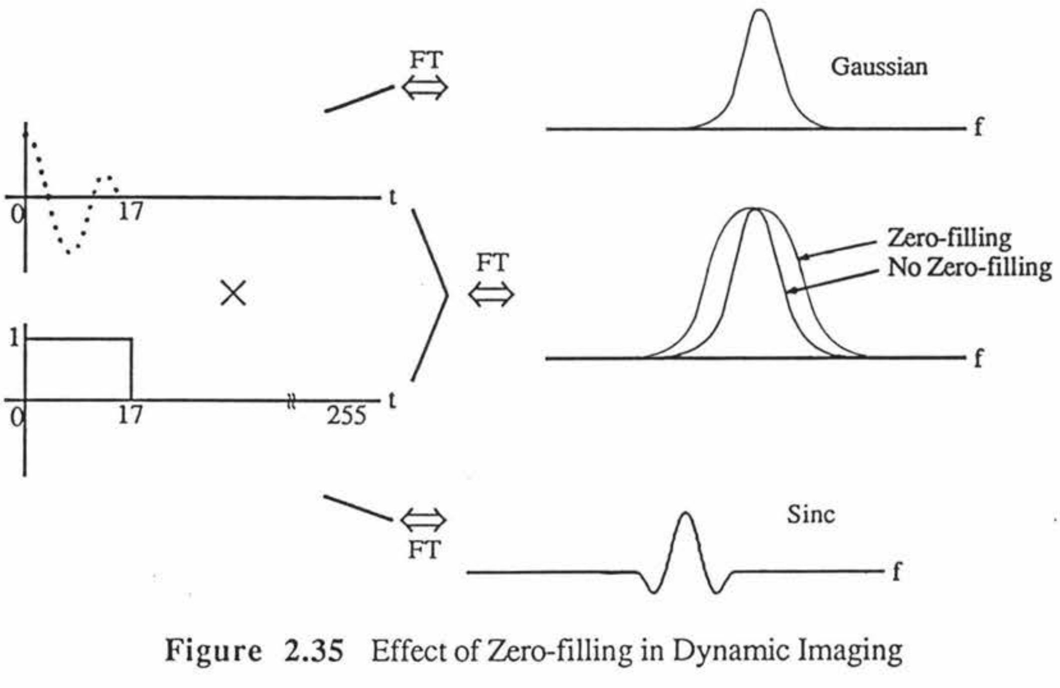

Figure 2.35 Effect of Zero-filling in Dynamic Imaging

Figure 2.36 Simulating the Effect of Zero-filling

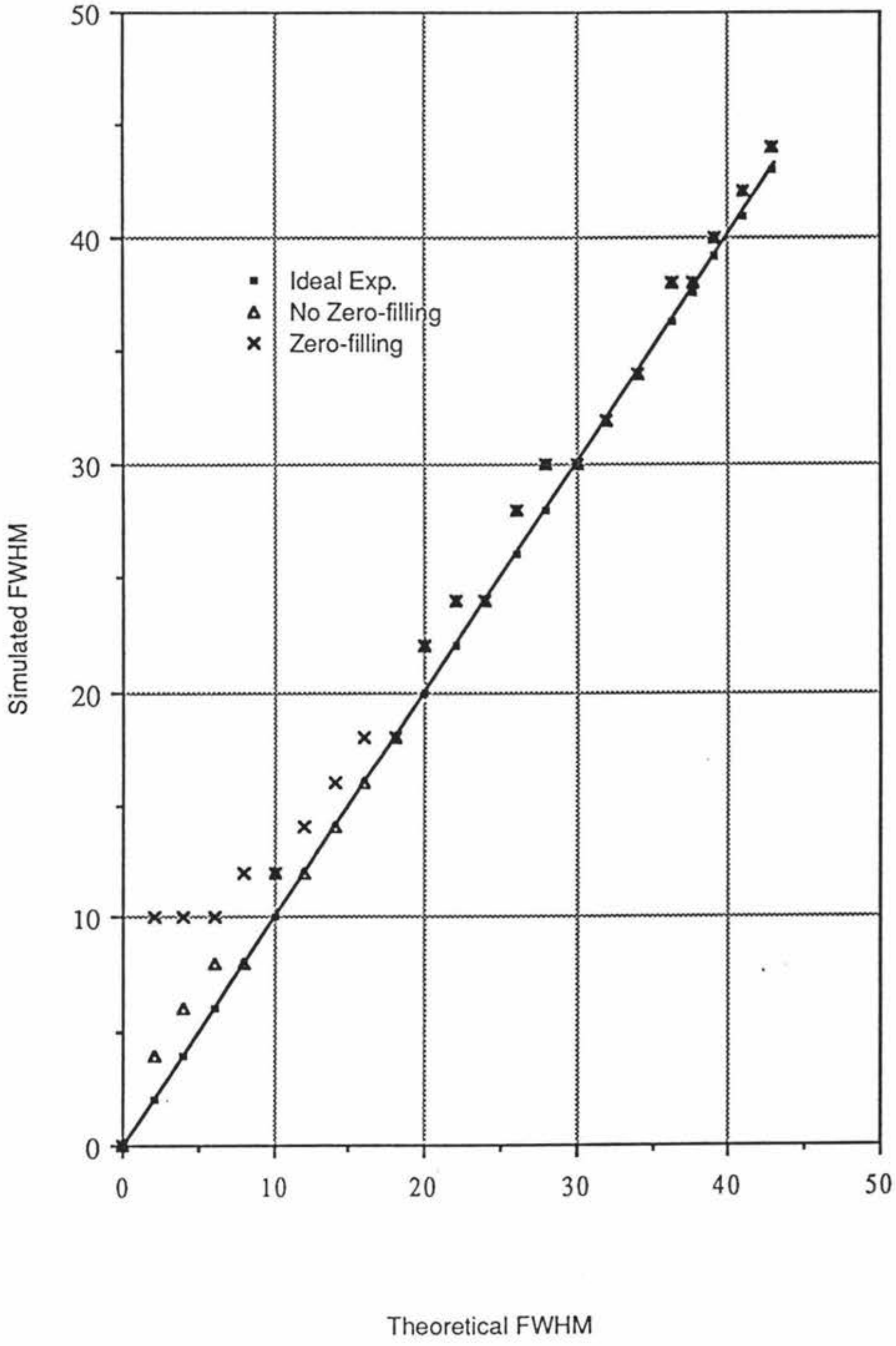

In the zero-filling procedure, if the last data is not effective zero, truncation will result. This truncation in the time domain will lead to an oscillation in the frequency domain (Figure 2.37), which may introduce some error into the FWHM calculation. See Figure 2.36 for the computer simulation results.

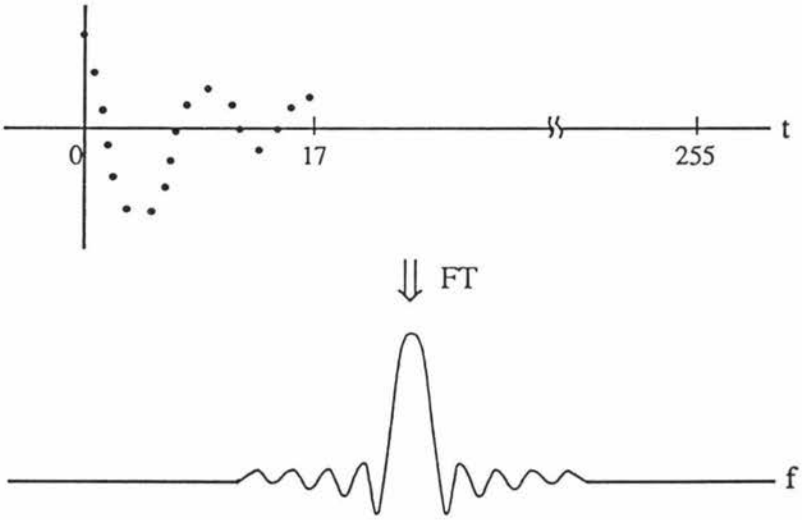

Figure 2.37 Oscillation due to Data Truncation

In fact this "truncation broadening" corresponds to normal convolution broadening. Where the data is effectively zero before zero-filling, the convolution broadening is effectively zero because of the oscillating nature of the sinc function. This unusual behavior relating to truncation is to be contrasted with exponential apodization where the additional broadening is independent of the relative signal decay rate.

In the current situation, zero-filling is necessary, so that Figure 2.36 should be used as a look-up table to get the correct diffusion coefficient.

The above analysis presumes that the profile broadening arises from diffusion. In fact there may be a broadening arising from the velocity spread. Because of velocity shear we may have a distribution of velocity across a single pixel. From Equation (2.94). we can derive a velocity spread in adjacent pixels as

$$\Delta v_{FWHM} = (2\pi n_D \Delta k_{FWHM})/(Ng\gamma\delta\Delta) \qquad (2.105)$$

Substituting the above equation into Equation (2.99), we get an extra broadening term as

$$D_e = 0.09\Delta(\Delta v)^2 \qquad (2.106)$$

The value of Δv depends on the dimensions of the shear rate and pixel size. But numerical calculations show that this extra broadening should normally be quite small (see Section 5.2.3).

Chapter 3 NMR Imaging System and Its Development

In Chapter 2 the principles of static and dynamic NMR imaging were described. Next the technical details of the NMR imaging system are discussed. Note that a discussion of the system is related to one particular NMR imaging method, in this case the FBP reconstruction method. First a general description of the existing system is given, then in Section 3.2 to 3.5, a more detailed description is given of developments undertaken as part of this work. These have enabled high gradient PGSE and velocity and/or diffusion imaging experiments.

3.1 NMR Imaging System

The NMR imaging system is shown diagrammatically in Figure 3.1. The basic rf spectrometer has some major additional items such as the pulse programmer, the gradients generating unit, the image processing and display unit, and the rf modulator. The whole system can be briefly divided into eight units:

1. Static Magnetic Field (B_0) Unit,
2. Field Gradients (**G**) Unit,
3. RF Pulse Field ($\mathbf{B_1(t)}$) Unit,
4. Experimental Controller (computer),
5. Pulse Programmer Unit,
6. RF coil and its tuning circuit,
7. Receiver Unit,
8. Image Processing and Display Unit.

The NMR imaging system in Massey, shown detailed in Figure 3.2, is built around(38) a JEOL FX60 multinuclear NMR spectrometer.

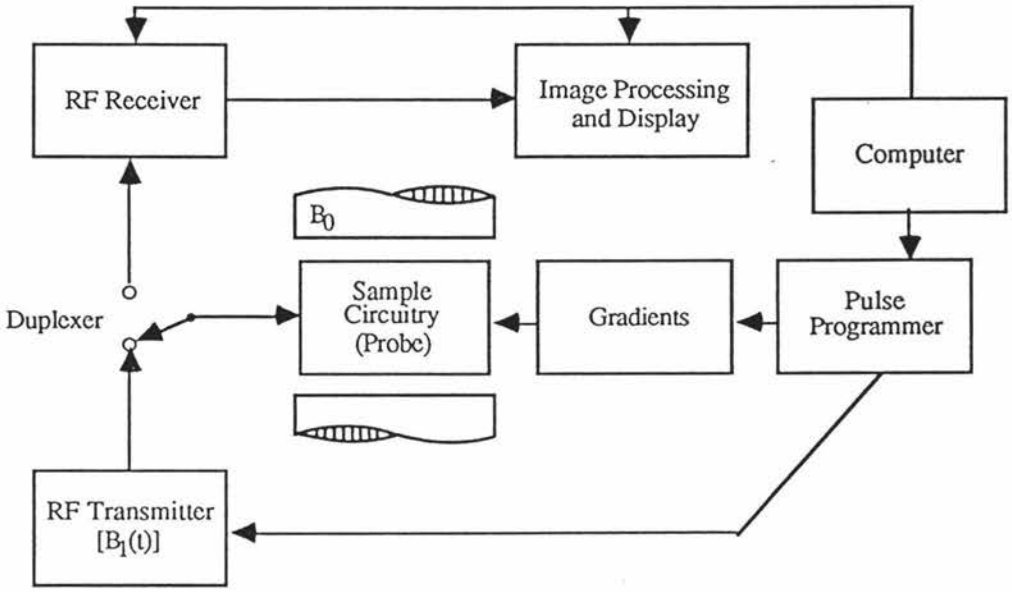

Figure 3.1 Block Diagram of an NMR Imaging System

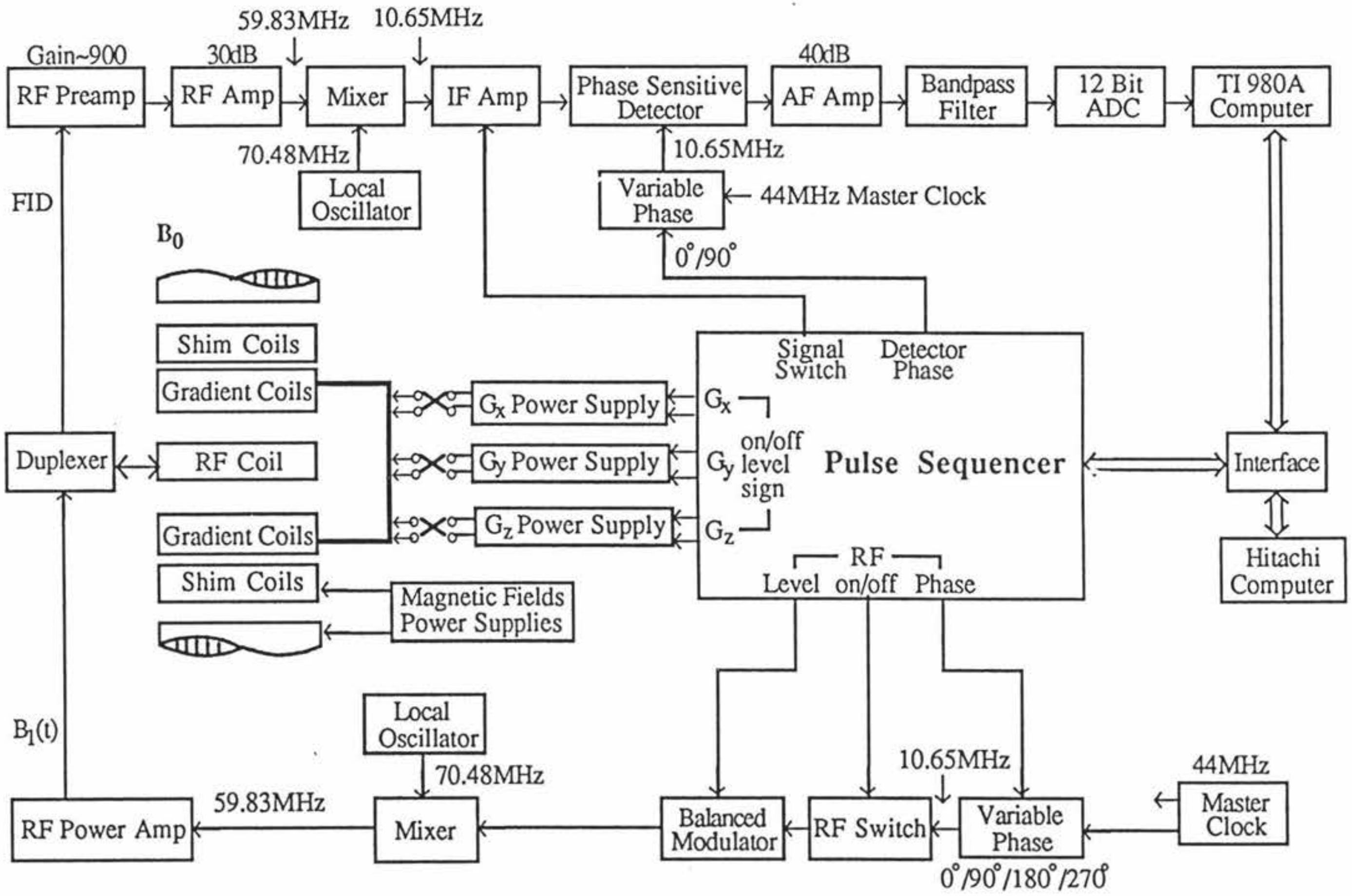

Figure 3.2 Massey NMR Imaging System

3.1.1 Static Magnetic Field Unit

The 1.4 T polarizing magnetic field ($\mathbf{B}_0$) is generated by an electromagnet, which has a 32 mm gap between the polarizing magnet pole faces, and with geometry as shown in Figure 3.3. This field, with a stability in order of ~10^{-8}, corresponds to a proton NMR frequency of 60 MHz.

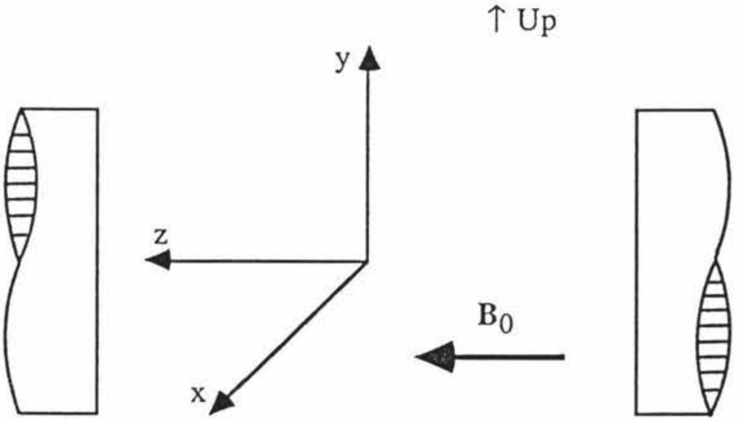

Figure 3.3 The Coordinates of the NMR Imaging System

Shim coils are used to generate small field gradients which can compensate the non-uniformity due to the main magnet or practical environments. These shim coils are mounted on the exterior-side of the side plates (silver plated fibreglass printed-circuit-board) of the probe.

The probe is effectively a solid copper box, which hosts the rf coil and its tuning circuit, the shim coils, the gradient coils and the lock detector (Figure 3.4). The lock system, which is actually a small cw NMR spectrometer with a drift-detector and feed-back loop, is used as the final stabilization part of the main field unit.

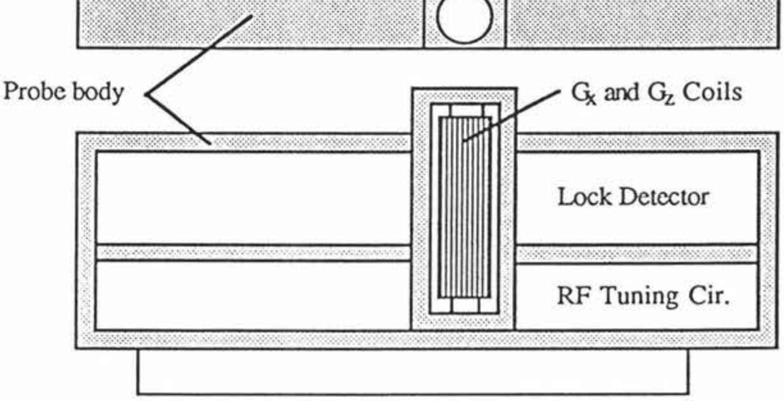

Figure 3.4 Structure of the Probe (without the side pcbs)

3.1.2 Field Gradients Unit

The gradients unit consists of the gradient coils, gradient power supplies, and gradient switches.

As discussed previously (Section 2.2.1), it is necessary to produce three orthogonal and uniform field gradients in NMR imaging experiments. The quality of the gradients is one of the most important factors in determining the distortion of the image produced. Larger gradients are required than those used in medical imaging systems. These latter systems use typically 0.01 Tm^{-1} whereas gradients of order 1 Tm^{-1} have been used in the present work. There are two reasons for using larger gradients. First, the applied gradient determines the final resolution, and to improve on the resolution used in medical imaging a proportionate increase in gradients is required (at the same bandwidth). Second,the superposition of PGSE requires much larger gradient than that used for imaging. (Henceforth we use the non-SI units of Gcm^{-1} where 100 Gcm^{-1} = 1 Tm^{-1}).

There are three basic geometries which may be used to generate the desired linear gradient. These are the Maxwell pair(39), the planar coil(40), the quadrupolar coil(41). The existing system used quadrupolar coils to generate the x gradient (21±4 $Gcm^{-1}A^{-1}$) and the z gradient (15±3 $Gcm^{-1}A^{-1}$) for imaging, and employed the shim coils mounted outside of the probe to generate the y gradient (1.6±0.1 $Gcm^{-1}A^{-1}$) for the slice selection. This latter choice was dictated by available geometry.

The gradient coils are driven by three KEPCO power supplies operating in a constant current mode. A 25V-4A power supply is used for the x gradient giving a maximum G_x = 84 Gcm^{-1}, a 25V-10A supply for the z gradient giving a maximum G_z = 150 Gcm^{-1}, and a 25V-10A supply for the y gradient giving a maximum G_y = 16 Gcm^{-1}.

Note that the existing y gradient was far too small to perform high resolution NMR microscopy, and was also far too small to perform flow and/or diffusion experiments for motion along the y axis. This axis is the longitudinal symmetry axis of the probe so that the latter constraint proved highly inconvenient.

The gradient switches are used to switch the currents between the gradient coils and the dummy load. They also provide the over-heat protection for the gradient coils in the event of a program error or other malfunction.

3.1.3 RF Pulse Field Unit

$B_1(t)$ is used to tip the magnetization vector prior to detection. Due to Equation (2.26) it is clear that to achieve short pulse times, large rf voltages are necessary to tip the nuclear spins through 90° or 180°. Such short pulse times provide a wide transmission bandwidth. The $B_1(t)$ system provides short (~ several μs) and powerful (~ 100V) pulses with short rise and fall times.

The system master clock is working at 44 MHz. This signal is fed into the frequency divider and the four-phase generator, yielding signals at 10.65 MHz with the four different phases. These signals are selected by the pulse programmer (see Section 3.1.5), controlled by an rf switch (to chop the continuous rf wave into the pulse form), envelope-modulated by a double balanced modulator to the desired pulse form (such as the sinc pulse), mixed by a mixer to produce the 59.8 MHz rf signal, and finally amplified by a broadband rf power amplifier (rf transmitter). The output pulses are supplied to the rf coil via the duplexer. The rf coil generates rf fields [$B_1(t)$] orthogonal to the direction of the main magnetic field ($\mathbf{B_0}$).

A duplexer is necessary because a single transmitter/receiver coil configuration is used in this system. The duplexer protects the delicate high gain rf preamplifier, which is used as the first stage of the signal detector, in the transmission mode; and isolates the rf transmitter from the receiver unit while the latter is amplifying the microvolt level FID signal. Usually diodes and $\lambda/4$ line are used to complete this task(42).

3.1.4 Experimental Controller

Two computers are employed in the imaging system, a Texas Instruments 980A computer and a Hitachi MB16000 personal computer.

As an original part of JEOL FX60 spectrometer, the TI 980A is a 16 bit computer with 32 kwords memory. It is supported by an extensive assembly language software package(43), which provides various functions such as controlling pulse timing and phase, collecting and averaging data, analyzing data including apodization filtering, integration and fast Fourier Transformation (FFT). A light pen is provided for interacting with the system, and an oscilloscope is used to display data in real time, or subsequent to analysis.

During imaging experiments, the TI 980A computer stores the parameter settings loaded from the Hitachi computer, and in addition enables other local parameters to be set. It also provides real time experimental control, collection of the k space data, application of filters and Fourier Transformation. The filtered profile $P^*(x,y,\phi)$ [c.f. Equation (2.61)] is then transferred to the Hitachi, via a parallel interface, for the image reconstruction, display and analysis. All these processes are under software control.

3.1.5 Pulse Programmer Unit

A versatile pulse programmer is used, which can be divided into two parts. A pulse code generator based on the Hitachi computer generates binary pulse sequence codes for a particular experiment. This code sequence is then transferred to a hardware pulse sequencer.

A pulse sequence is actually a multi-component function of time. One component for example describes the strength of the rf signal, and another three govern those of the field gradients in which the sample is immersed. Another sets the sampling time while another opens the rf receiver gate. The pulse sequencer is described in detail elsewhere(38).

The pulse sequence created for a particular experiment using the Hitachi software is then processed to generate a series of binary control codes. There are five bytes per code word. Each word contains destination (1 byte), command (1 byte) and time (3 bytes). Then the pulse sequence codes are transferred to the TI 980A computer which passes these to the 4 kbytes RAM in the pulse sequencer at the beginning of an experiment. The TI 980A computer subsequently gives the start signal to the pulse sequencer. Once the experiment is started, the pulse sequencer controls the timing of the events by sending out the commands step by step according to the pulse sequence codes stored in the sequencer memory.

3.1.6 RF Coil and Its Tuning Circuit

The rf coil (solenoid coil) is used both for applying the irradiation to the sample and detecting the NMR signal. This reception mode is critical to sensitivity. As seen in

Equation (2.63), the sensitivity will be the highest when the coil has the smallest possible size for a given sample. It is therefore necessary to have a few different diameter coils to optimize the sensitivity according to the sample examined. In transmission, the smaller the coil diameter, the more intense the rf field produced, and the shorter the 90° pulse time.

Optimizing sensitivity requires that the probe rf circuit Q be optimized. Note that in practice, the value of Q is not only dependent on the factor $\omega L/R$ for the coil, but also on capacitive loss to the surrounding conductors (such as the gradient coils), the dielectric loss in the matching capacitors, and significantly, the manner in which the coil is made and the way in which the coil and its tuning circuit is mounted. The rf tuning circuit (tank circuit) is also required to be impedance matched (50 Ω) to the transmitter.

In the existing system two coils were available with diameters as 13 mm and 5.8 mm. Each can be plugged into the probe.

3.1.7 Receiver Unit

The induced NMR signal is routed by the duplexer into the detection unit, which actually is a series of amplifiers and mixers. The amplifiers are used to amplify the microvolt level initial signal to the volt level final signal necessary for the analog-to-digital converter (**ADC**). The mixers are used to convert the high frequency (**rf**) signal to the low frequency (**af**) signal, and maintain the phase information.

The FID signal is detected in quadrature which gives M_x and M_y. As the first stage, a three-stage Plessey Amplifier is used as the rf preamplifier, with noise figure ~ 2dB and a voltage gain of the order 1000. This preamplifier provides the first critical amplification of the microvolt level signal. Further amplification is made through the main amplifiers. The signal goes through a single stage (60 MHz) rf amplifier, followed by a mixer which produced an 11 MHz intermediate frequency (**if**) signal. This mixer stage is convenient because the main amplification within the spectrometer can be carried out efficiently at one frequency, no matter what excitation frequency is used. The 11 MHz if signal is fed into a two-stage if amplifier, followed by a second mixer, this time as the Phase Sensitive Detector (**PSD**), which produces an audio frequency (af) signal. A bandpass filter which has a bandwidth equal to the observation spectrum width is used to reduce the aliasing of the noise, and a 12 Bit ADC is used to convert the signal to the digitized form, which is stored in the TI-980A computer memory temporarily, and then transferred to the Hitachi for the back projection and display.

3.1.8 Image Processing and Display Unit

The image processing and display function is performed using the Hitachi computer, which is based on the 8088 microprocessor and supported by MS-DOS. It is configured with 256 kbytes main memory and 192 kbytes graphics memory, with two 320 kbytes floppy disk drivers. A 640×400 pixels image in 8 colours or a 320×200 pixels one in 16 colours can be displayed.

After receiving the data from the TI 980A, the Hitachi performs the back projection process. The image data is stored in the upper memory as an array of maximum 256×256 pixels with 16 bits per data point, so that the maximum possible level is 16 for a pixel. The final image can be stored on the floppy disk, a 256×200 image can be stored as two 50 kbytes data files.

The image reconstruction, display and analysis programs running in the Hitachi are written in FORTRAN. But in order to speed up the processes of image reconstruction, display and analysis, various assembly language subroutines had been written(44) as functions to support the FORTRAN programs.

The final image can be displayed in either a grey scale or colour scale. The grey scale ranges from black to white, while the choice of the colours is actually arbitrary, as far as the scale can distinguish the adjoining digital levels. As part of this work a variety of colour scales has been developed (see Chapter 4 and Chapter 5).

3.2 Small RF Coil (ϕ2.1 mm) and Its Tuning Circuit

It was shown in Section 2.2.5 that the spatial resolution of an image varies as the square root of the rf coil radius. Furthermore, the smaller the coil, the more intense the rf field produced (two fold field increase for half the radius). While this more intense rf field can be useful in transmission, the principal advantage of small size in the present context is the sensitivity gained during detection. Ideally the size of the coil will match the size of the sample. Assuming 256×256 pixels near the transverse resolution limit of 10 μm, the useful transverse sample diameter is about 2.5 mm. The larger diameters of the existing rf coils are clearly not ideal. Thus the design of a smaller rf coil was considered valuable.

3.2.1 Design and Constructions

For the present geometry of the main magnet, the solenoid coil is the most convenient configuration. The design of this kind of coil has been described elsewhere(42).

The perspex coil plug construction, shown in Figure 3.5, is designed to be versatile. The coil is mounted on a perspex coil holder. The changeable coil holder together with the two-piece coil plug body make it possible to change this coil for one of a different diameter if necessary. The perspex sample holder is found very important for holding the sample tube right at the centre of the coil, and consequently, the centre of the fields. Because of the small dimensions the precise geometric destination and construction of

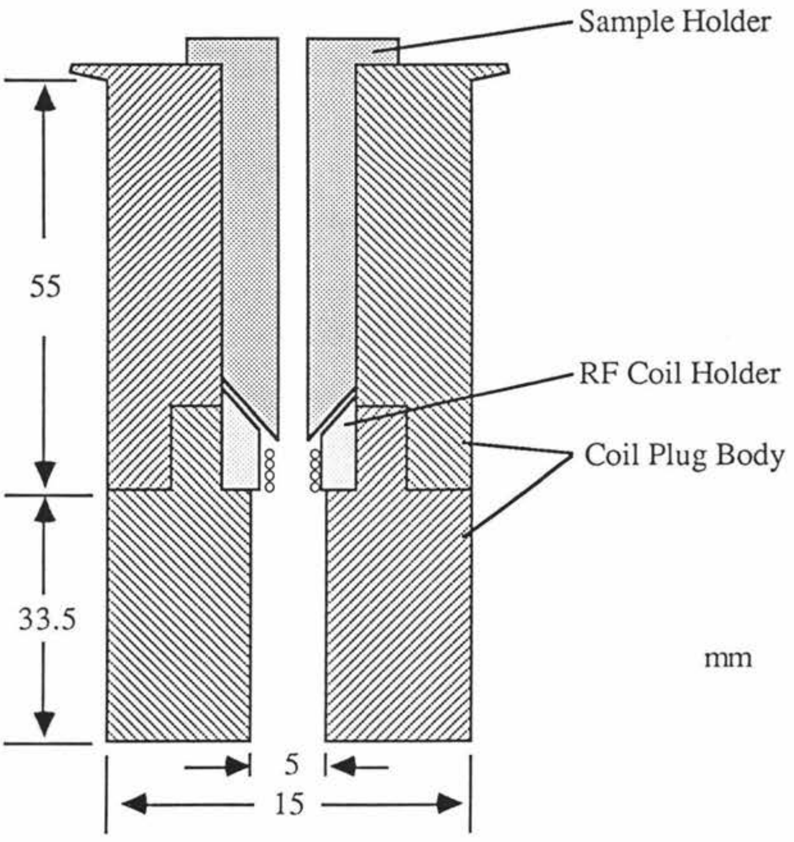

Figure 3.5 ϕ 2.1 mm RF Coil Construction
(not to scale)

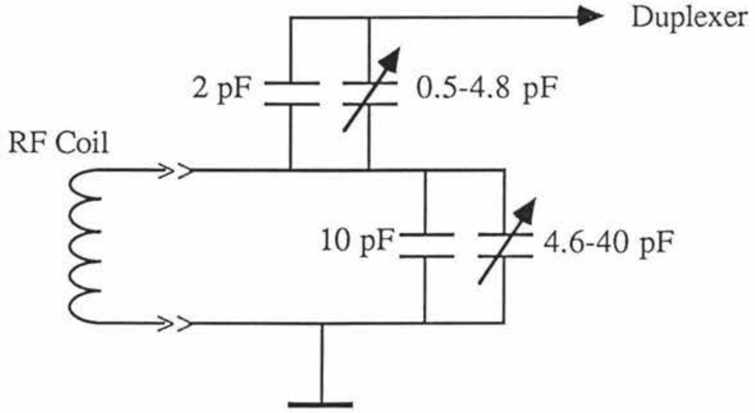

Figure 3.6 RF Tank Circuit

the rf coil, the coil holder, the coil plug and the sample holder become critical. The position of the rf coil and the sample can be checked by using a standard water sample and checking its 1-D profile position on the oscilloscope screen.

Due to the difficulty of tuning the original tank circuit for different rf coils, a modification has been made using the circuit shown in Figure 3.6, which is found very convenient for tuning to one of the three different coils. Two multiturn capacitors are used for the tuning. Careful layout is necessary in mounting the capacitors. Large distributed capacitance will lead to the difficulty in tuning. For the present work, the distributed capacitance between the tuning circuit and the probe was finally reduced to 4 pF. The tank circuit is tuned to 50 Ω using a Wheatstone bridge, in which the tank circuit is placed as one of the four arms. 60 MHz rf signal is fed in and the output is sent to a TRIO MD-85 oscilloscope. A null on the oscilloscope corresponds to a **resistive** tank circuit load of **50** Ω and so represents the correct tuning.

This new rf coil, shown in Figure 3.7, has a diameter of 2.1 mm and is named the small coil in Table 3.1:

Table 3.1 Characteristics of RF Coils

	Large Coil	**Medium Coil**	**Small Coil**
Diameter (mm)	13	5.8	2.1
Wire Dimension (mm)	0.8×3	0.76	0.376
No. of Turns	3	6	12
Inductance (μH)	0.141	0.179	0.181
Quality Factor Q	54	61	40

*Inductances are measured by using HP4192A LF Impedance Analyzer at 1 MHz frequency.

**The quality factor Q is measured when the coil has been plugged into the probe, but with the probe is outside the magnet.

Figure 3.7 RF Coils

3.2.2 Calibration of the RF Coil

The requirement for well characterized sinc modulated rf fields for selective excitation means that it is necessary to calibrate the different rf coils, because in practice, the rf transmitter and probe are highly non-linear. Most of the system non-linearity is due to the diodes in the circuits (for example, in the duplexer). Great difficulty has been experienced in the calibration of the new rf coil.

The conventional method to calibrate the system is by observing the nuclear tip angle as a function of the modulation amplitude for a fixed pulse width, as follows. First, it is necessary to find the (minimum) gain of the modulator for a narrow 180° pulse, and then to record the echo amplitude as a function of various DAC levels (0-255) by adjusting the amplitude of a 90° pulse. In this manner a function of tipping angle vs the input voltages can be obtained.

The system response curve has been obtained (Figure 3.8) and the amplitudes of the 180° pulse have been measured (Table 3.2), so that the input and output voltages can be identified from the response curve.

Table 3.2 RF Pulse Amplitudes

	Large Coil		**Medium Coil**		**Small Coil**	
	V_I(mV)	V_o(V)	V_I(mV)	V_o(V)	V_I(mV)	V_o(V)
180°, 200μs	29	6.6	18.5	1.8	15.8	0.8
90°, 1ms	17.4	1.32	13.8	0.36	12.6	0.16

In considering the operating region of the response curve, one is constrained by the need for use a standard sinc pulse duration of around 1 ms. This simplifies programming and provides a bandwidth appropriate to the slice selection gradient. It is necessary to have the sinc pulse amplitude lying in the region of the response curve (Figure 3.8) where V_0 depends on V_I. This implies that we employ the region above the "knee". In order for the 180° pulse amplitude to lie within this region, the duration of the 180° pulse must be chosen so that $V_0(180°)$ is not much bigger than $V_0(\text{sinc}_{max})$. For convenience we choose a 180° pulse duration of 100 to 200 μs which implies that $V_0(180°) \approx 5V_0(\text{sinc}_{max})$.

Figure 3.8 shows that the rf response of the new coil is unfortunately but not unexpectedly in the slowly changing part of the system response curve. This behavior is consistent with the higher sensitivity of the new coil. The lower position on the graph indicates that only a few different rf field values are available with the software control. Figure 3.9 shows the relationship of the tip angles vs the DAC levels. In obtaining these curves the modulator gain has been adjusted so that the 180° 200 μs lies within the range of DAC levels.

Figure 3.8 System RF Response Curve

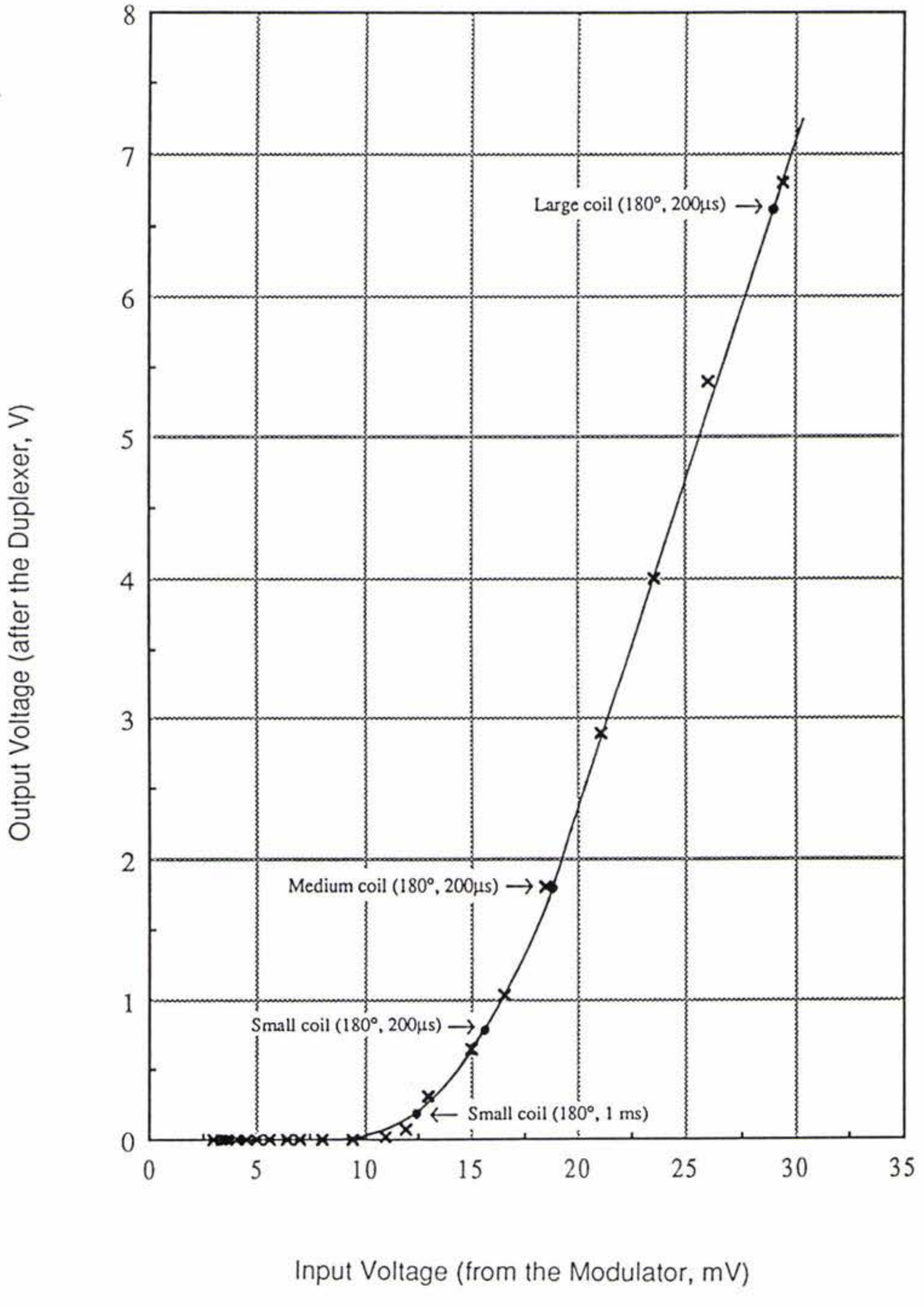

Figure 3.9 Tip Angle as a Function of DAC Level

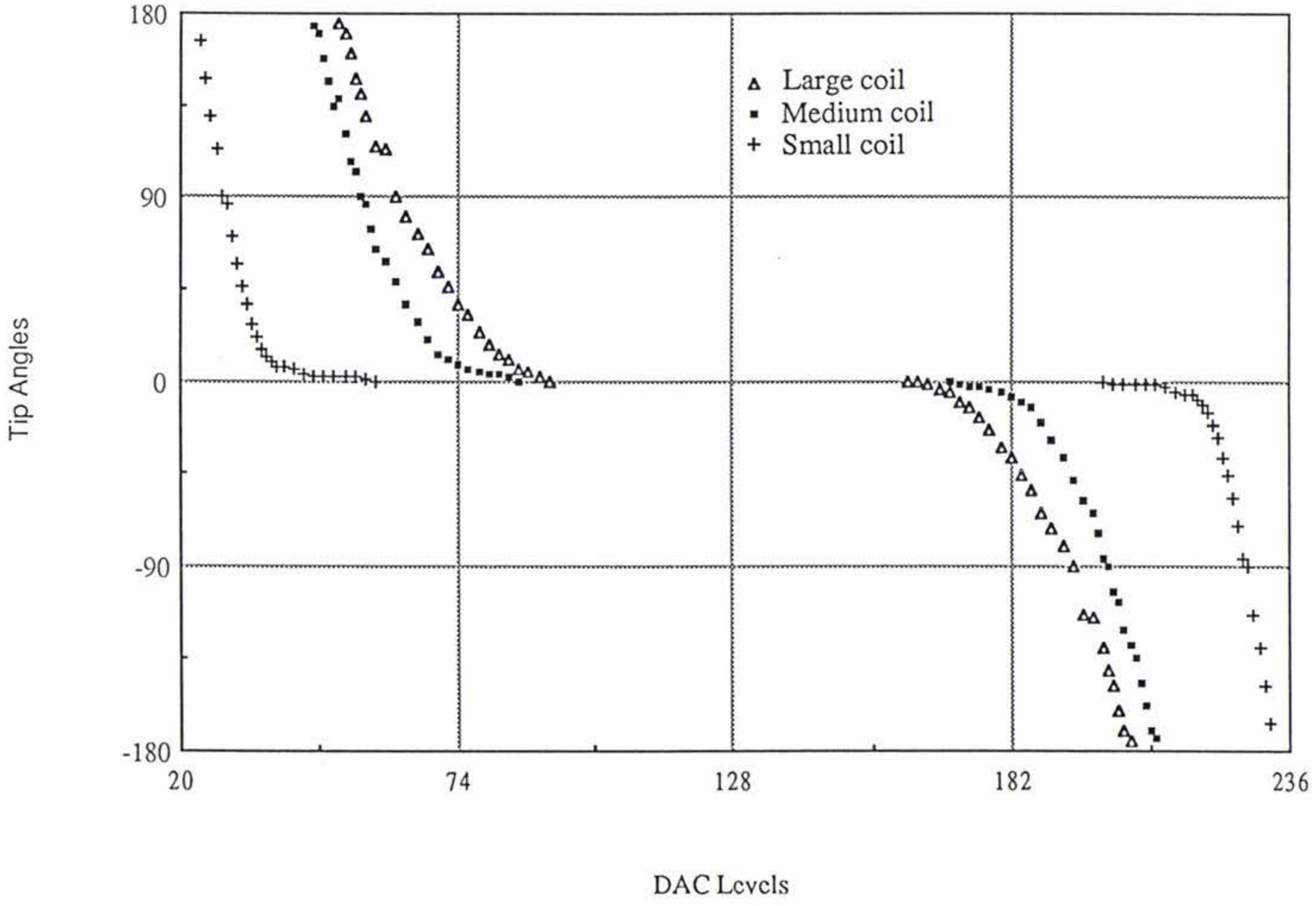

It is clear that for the small coil fewer DAC levels are available due to the new rf coil's response curve falling in the more severely non-linear region of the transmitter output.

Further examination showed that part of the system non-linearity is due to the large number of diodes used in the original JEOL system [Figure 3.10(a)]. These diodes are used to inhibit low level noise output from the transmitter. Modifications have been made by using more good quality series diodes in the duplexer box and bypassing the original diodes in the rf transmitter [Figure 3.10(b)]. The number of series diodes required is determined by the need to ensure that the residual output is insufficient to produce a transmitter output level capable of penetrating the duplexer.

(a) Original Circuit

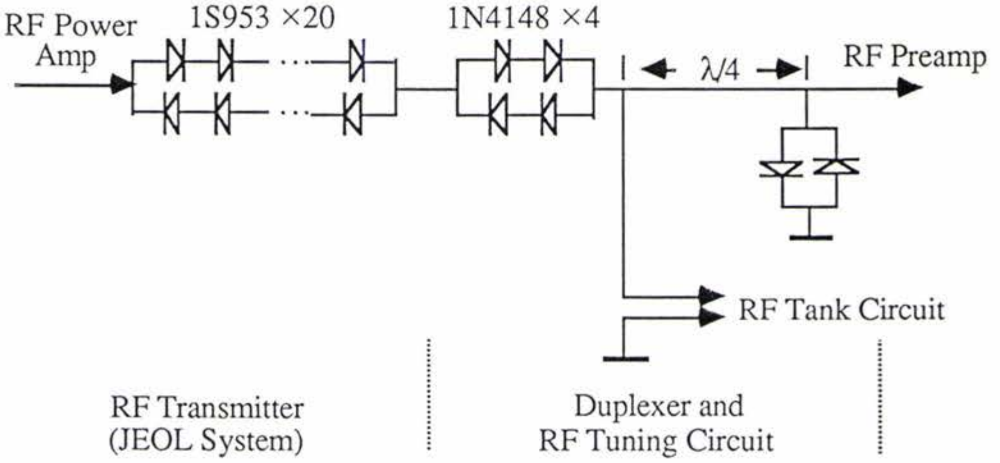

(b) After Modification

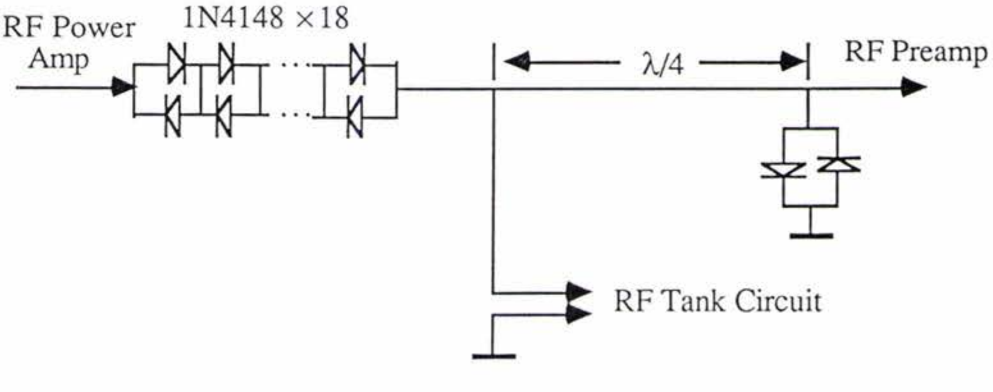

Figure 3.10 Circuit Diagrams of Duplexer

3.2.3 System Performance

Following the replacement of the series diodes it was found that some empirical modifications based on the medium coil's response curve actually gave quite good sinc pulse on the oscilloscope screen. The sensitivity measurements also give good results (Table 3.3).

Table 3.3 System Performance

	Large Coil	Medium Coil	Small Coil
Sensitivity (S/N)	108	520	2030
90° Pulse Time (μs)	11.5	3.5	1.5

* The sensitivity is measured using 1 mg Ethanol sample. The values have been renormalised in terms of 10 mg H_2O.

Note the new rf coil gives almost four times better sensitivity than that of the medium coil. The shorter 90° pulse time in a smaller coil is consistent with this improvement.

The imaging experimental results using the new rf coil are presented in Sections 4.2 and 5.2.

3.3 Y Gradient Power Supply

The previously existing system used a KEPCO JQE 25-10 power supply to drive the Y gradient coil. There are two problems with this power supply. The first is that its 10 A current is too small for the dynamic imaging experiments, and the second is that the 50 Hz ripple (hum) of the power supply is one of the main sources of the image distortion. A new KEPCO ATE 75-15M power supply was purchased to partially solve the first problem, but some modifications had to be made to solve the second problem, the ripple.

3.3.1 Effects of Ripple on Gradients

We know that the nuclear magnetization phase is determined by the field strength and the interaction time, given by Equation (2.26). In NMR imaging experiments, we can rewrite Equation (2.26) as

$$\theta(\mathbf{r}) = \gamma\int_0^\tau (\mathbf{G}\cdot\mathbf{r})\,dt \tag{3.1}$$

If there is ripple in the field gradient, we have

$$\theta(\mathbf{r}) = \gamma\int_0^\tau [\mathbf{G}_0+\mathbf{G}(\mathbf{t})]\cdot\mathbf{r}\,dt \tag{3.2}$$

Therefore for the static NMR imaging experiments, an additional time-dependent phase shift will appear due to the ripple. This leads to the image distortions. For the dynamic NMR imaging experiments, besides the image distortions, the existence of the ripple will also lead to an imperfect matching of the area under the PGSE pulses. This matching is required to be as accurate as possible. The effect of current ripple is more severe in microscopy where the small gradient coils have low inductance and minimal choking action. It is often one of the main sources of the image distortions. Any effort expended in reducing the ripple is very worthwhile.

3.3.2 KEPCO Power Supply and Its Ripple

The KEPCO ATE power supply is a programmable stabilized DC power supply. A simplified schematic diagram is shown in Figure 3.11. It can deliver either constant voltage or constant current, depending upon the magnitude of the load resistance. When it is in the constant current mode (as in this work), with the maximum 75 V and 15 A output, this power supply can operate as an 1000 Watt operational amplifier with the rms ripple and noise less than 0.03% I_{0max} given by the specification.

From Figure 3.11, we can see this power supply can be controlled internally (by the front panel) or externally (by an external control signal). It also has an overvoltage protection circuit. Figure 3.12 gives its outline and main chassis assembly.

Ripple measurements were carried out using a 3 Ω sensing resistor and a (battery supplied) operational amplifier to enhance the oscilloscope gain by 10. Measurements on the unmodified supply showed a 4.2 mA ripple, or ~0.03 % I_{0max}, in its output. This ripple was independent of the current strength. The main source of the 50 Hz

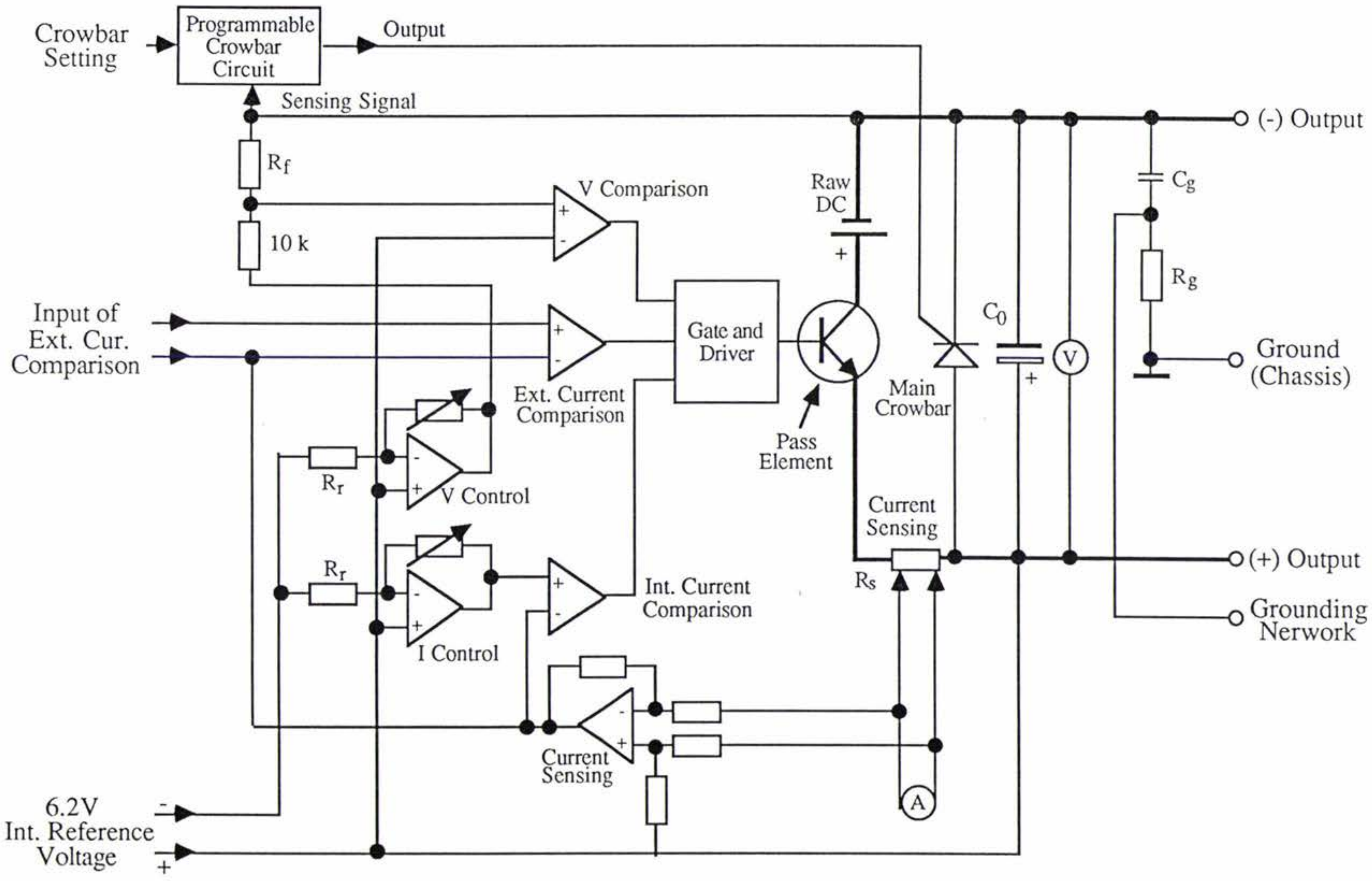

Figure 3.11 Simplified Schematic Diagram of KEPCO ATE 75-15M Power Supply

(a) KEPCO ATE 75-15M

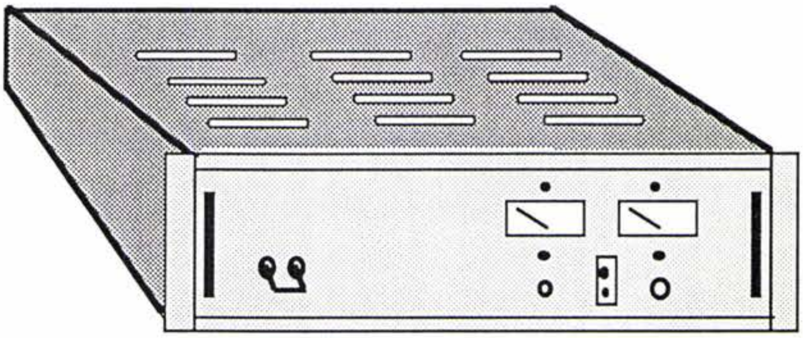

(b) Component Locations

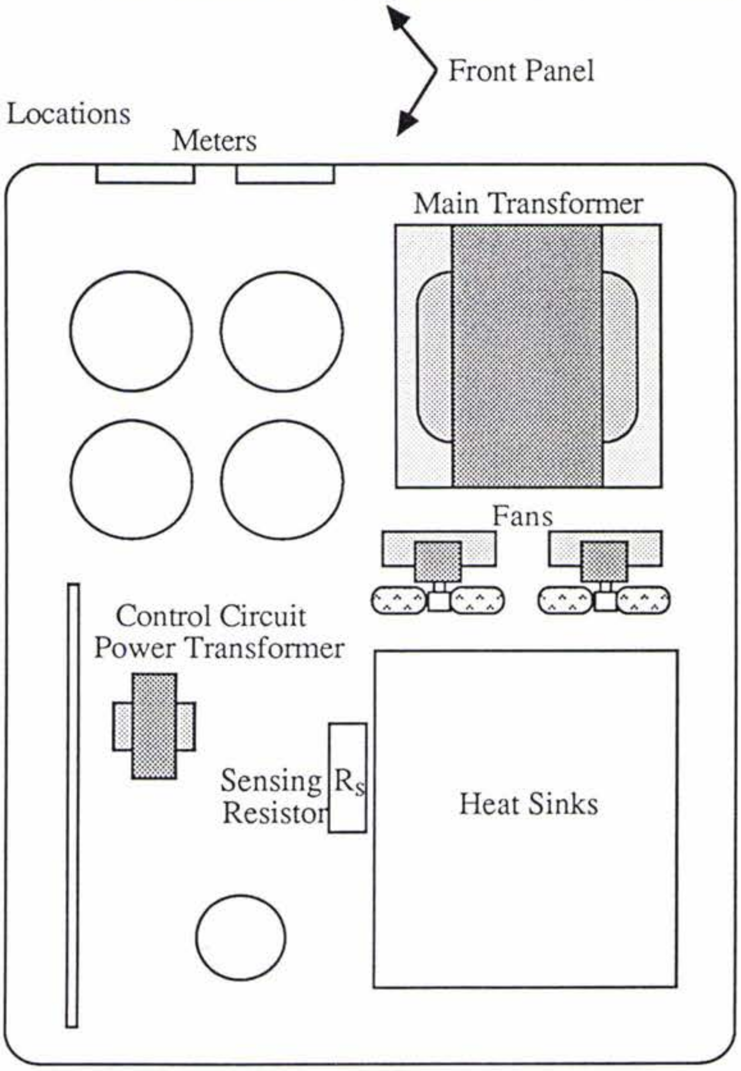

Figure 3.12 Main Chassis Assembly and Component Locations of KEPCO ATE 75-15M Power Supply

Table 3.4 The Ripple Measurements

	Ripple (mV_{pp})	Ripple (mA)	% I_{0max}
Original	12.5	4.2	~0.03
Fans OFF	5	1.2	~0.008
Fans OFF,Transformers OUT	2.5	0.83	~0.005

*The above measurements were under 2 A current.

ripple is obviously the transformers and fans. We suspected that the KEPCO sensing resistor (R_s in Figure 3.11 and Figure 3.12) was too close to the ripple sources.

By removing the fans and transformers separately we identified that these elements were indeed the ripple sources (Table 3.4).

By using car batteries to support the DC voltage (the last measurement of the above table), the ripple disappears from the oscilloscope's screen, leaving only noise. Therefore the clear conclusion was to reconstruct the power supply by moving the ripple sources away from the sensing resistor.

3.3.3 Reconstruction

The reconstructed power supply is a two-layer movable system (Figure 3.13 and Figure 3.14), with an additional LCD digital meter (using an INTERSIL 7106 chip) to give the accurate current value. The bottom chassis hosts all the AC parts, the main transformer, the circuit power transformer, the digital meter transformer, and the two

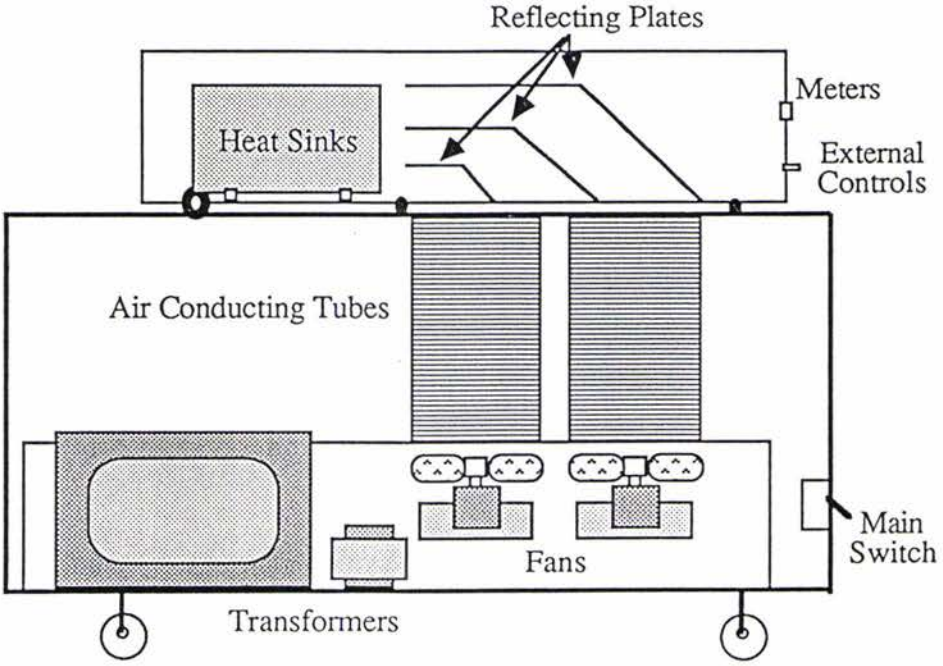

Figure 3.13 The Internal Layout of the Reconstructed KEPCO Power Supply

Figure 3.14 The Reconstructed KEPCO Power Supply

fans. The top chassis hosts the remaining DC and control parts. Two 155 mm ID plastic tubes are used to conduct the cooling air from the bottom chassis to the top chassis, and some reflecting plates are used to change the propagation direction of the air to the heat sinks.

3.3.4 Performance

The measurements show that the reconstruction of the power supply was successful (Table 3.5).

Table 3.5 Comparison of the Ripple

	Ripple		**% I_{0max}**
	(mV_{pp})	(mA)	
Before Reconstruction	12.5	4.2	~0.03
After Reconstruction	2.7	0.9	~0.006

The remaining time-dependent output is very close to 'pure' noise and no obvious ripple can be observed (Figure 3.15). Note that some spikes (f=100 Hz) can be observed, which are due to the main rectifier diodes (This has been verified in the measurement using car batteries).

The following table gives the measurements of the three gradient power supplies, in which the new reconstructed power supply is named the Y gradient power supply.

Table 3.6 Performance of the Gradient Power Supplies

	X Gradient	**Y Gradient**	**Z Gradient**
Max. Output (A)	4	15	10
Ripple (mA_{pp})	0.87	0.9	0.73
% I_{0max}	0.022	0.0060	0.0073

*The measurements are under 2 A output current.

I = 2A

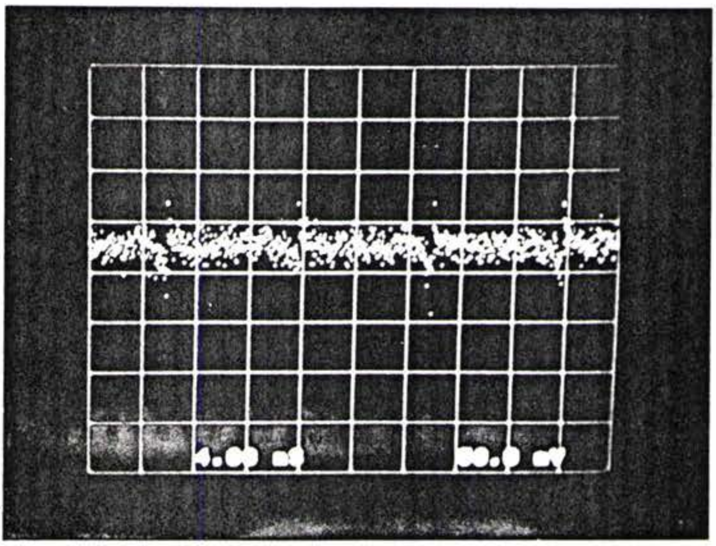

I = 10A

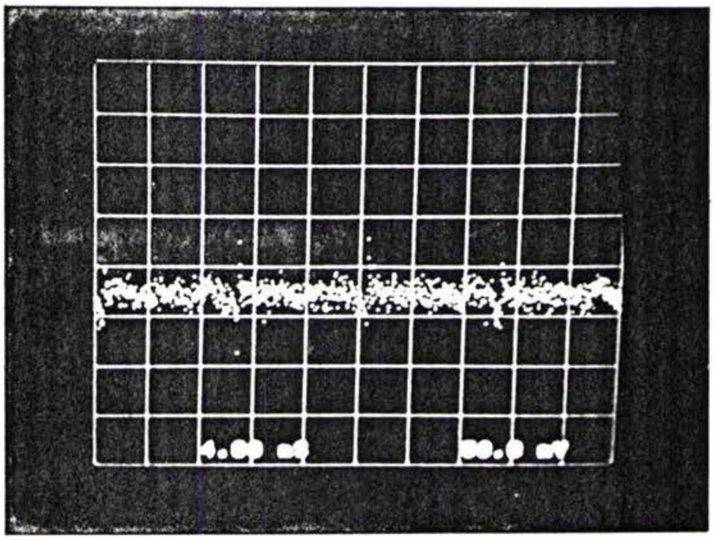

Figure 3.15 Output Waveforms of the Reconstructed KEPCO Power Supply [Timebase 4.0 ms/div.; Vertical scale 50 mV/div.]

3.4 Y Gradient Coil

In Section 3.1.2 we mentioned that the existing system utilizes the JEOL shim coil as the Y gradient coil, which gives unit gradient of only 1.6 $Gcm^{-1}A^{-1}$. Even using the new power supply, we can obtain a gradient strength of only 24 Gcm^{-1}. This is too small for PGSE and dynamic imaging experiments. This section describes the design of a new Y gradient coil, which, when incorporated with the new power supply, would generate a gradient with a magnitude of 140 Gcm^{-1}, or 1.4 Tm^{-1}.

3.4.1 Some Considerations

The available magnet geometry of the pre-existing system is shown in Figure 3.16. There is a 32 mm gap between the polarizing magnet pole faces, but the thickness of the probe is already 30 mm. So that the existing Y shim coil (mounted on the exterior-side of the 3 mm thick side pcb plates) was used to generate the Y gradient.

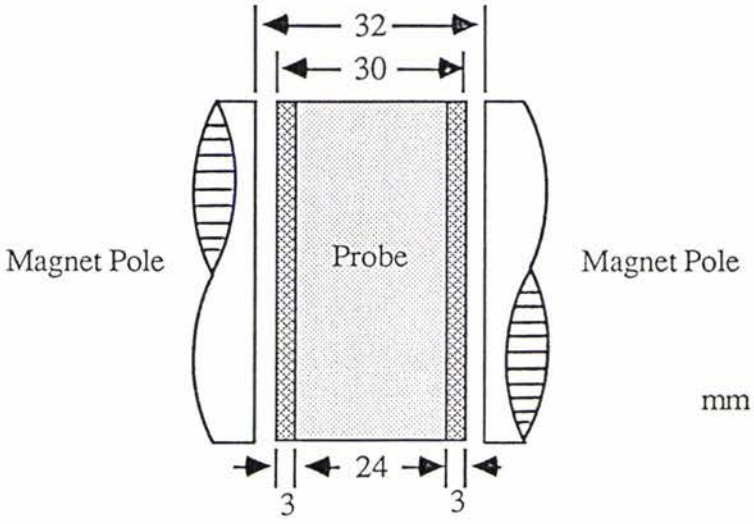

Figure 3.16 Dimensions of the Probe
(not to scale)

Because a set of quadrupolar coils had been used to generate the X and Z gradients, no space was available inside the probe. The only possible means of incorporating a new Y gradient coil was by leaving 0.5 mm gap on each side between the probe body and the pcb. Then the total thickness of the probe is 31 mm, leaving an 0.5 mm gap on each side between the probe and the main magnet poles. Due to the limited space, the planar coil geometry was the only choice. Examples of these have been well described by Anderson(40)

A set of conditions had to be considered next:

1) The total resistance of the new coil must be less than 2.5 Ω (so that is possible to use the 75V-15A power supply).

2) Due to the requirement of high gradient, (> 100 Gcm^{-1}), more turns were needed in the coil, and consequently, thicker wire was required if Condition 1 was to be satisfied.

3) Field gradient distortions (non-linearity in G_y and un-wanted G_x and G_z orthogonal gradients) must be as small as possible. A 256×256 image requires a linearity of better than 1 part in 256 if image distortions due to non-linearities are to be negligible. That means less turns and thiner wire are desirable, because the field non-linearities are closer to the minimum if the coil's wires are nearer the ideal line positions of the coil (Figure 3.17).

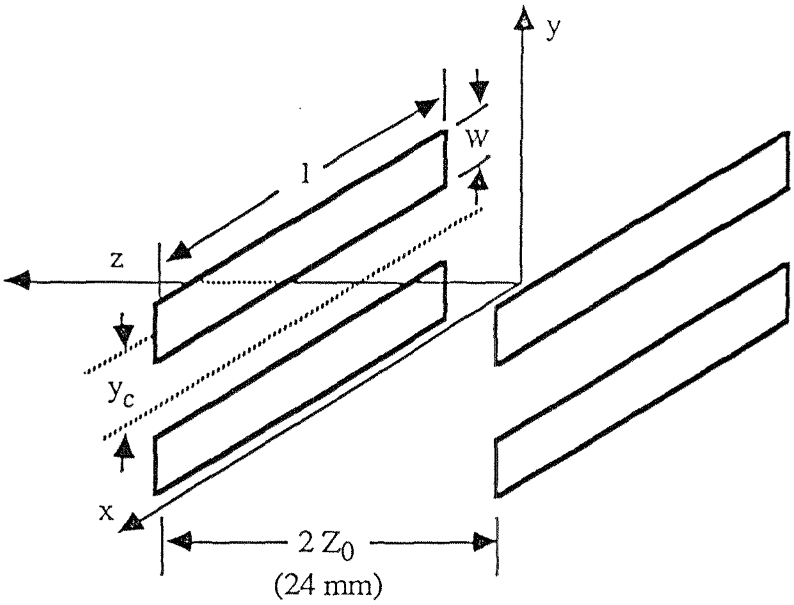

Figure 3.17 Planar Coil Geometry

It is therefore quite difficult to choose the best combination of the thickness of the wire, the number of turns, the dimensions of the coil. Anderson has pointed out that for planar coil geometry, once Z_0 is determined, then $W=1.55Z_0$ and $Y_c=1.19Z_0$ for optimal gradient uniformity. In our system, Z_0 is given by the probe body thickness, that is $Z_0=24/2=12$mm, so that $Y_c=14.3$mm and $W=18.6$mm (Here Y_c and W refer to the ideal line positions of the coil). The remaining three choices, the diameter of the wire, the number of turns and the length of the coil, are compromises to meet the above conditions.

3.4.2 Calculations of the Gradient

The gradient field strength for such a planar coil can be calculated as follows (Figure 3.18).

The field at point (x_0,y_0,z_0) due to the current I flowing through a wire element dl is given by the Biot-Savart Law as

$$dB = (\mu_0/4\pi)(Idl\times r)/r^3 \qquad (3.3)$$

where $$dl = dxi \qquad (3.4)$$

Since $$r = (x-x_0)i + (y-y_0)j + (z-z_0)k \qquad (3.5)$$

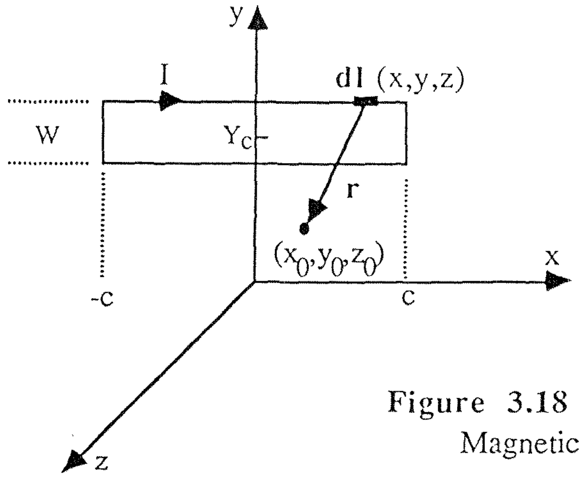

Figure 3.18
Magnetic Field Strength

so that from Equations (3.3), (3.4) and (3.5), we have

$$dB_z = d(\mathbf{B}\cdot\mathbf{k})$$

$$= (\mu_0/4\pi)[Idx(y-y_0)]/[(x-x_0)^2+(y-y_0)^2+(z-z_0)^2]^{3/2} \qquad (3.6)$$

Therefore due to the current at the source point (x,y,z), we have the field at the field point (x_0,y_0,z_0) as

$$G_{ylpoint} = \partial(dB_z)/\partial y_0$$

$$= -\frac{\mu_0 I}{4\pi}\cdot\frac{[(x-x_0)^2-2(y-y_0)^2+(z-z_0)^2]dx}{[(x-x_0)^2+(y-y_0)^2+(z-z_0)^2]^{5/2}} \qquad (3.7)$$

Integrating the above equation gives the field gradient at (x_0,y_0,z_0) due to an entire wire (-c,c) as

$$G_{ylline} = \int_{-c}^{c} G_{ylpoint}$$

$$= -\frac{\mu_0 I}{4\pi}\Big\{\int_{-c}^{c}\frac{(x-x_0)^2dx}{[(x-x_0)^2+(y-y_0)^2+(z-z_0)^2]^{5/2}} +$$

$$[-2(y-y_0)^2+(z-z_0)^2]\int_{-c}^{c}\frac{dx}{[(x-x_0)^2+(y-y_0)^2+(z-z_0)^2]^{5/2}}\Big\}$$

(3.8)

The result of Equation (3.8) can be derived as

$$
\begin{aligned}
G_y = -\frac{\mu_0 I}{4\pi}\Bigg\{ & \frac{(y-y_0)^2}{[(y-y_0)^2+(z-z_0)^2]^2}\Bigg[\frac{(c-x_0)^3}{[(c-x_0)^2+(y-y_0)^2+(z-z_0)^2]^{3/2}} + \\
& \frac{(c+x_0)^3}{[(c+x_0)^2+(y-y_0)^2+(z-z_0)^2]^{3/2}}\Bigg] + \frac{[-2(y-y_0)^2+(z-z_0)^2]}{[(y-y_0)^2+(z-z_0)^2]^2} \cdot \\
& \Bigg[\frac{(c-x_0)}{[(c-x_0)^2+(y-y_0)^2+(z-z_0)^2]^{1/2}} + \frac{(c+x_0)}{[(c+x_0)^2+(y-y_0)^2+(z-z_0)^2]^{1/2}}\Bigg]\Bigg\}
\end{aligned}
\tag{3.9}
$$

If we set c → ∞, then the above equation will be

$$G_y \rightarrow (\mu_0 I/2\pi)/(y-y_0)^2 \tag{3.10}$$

which agrees very well with the infinite long wire limit.

The effect of return wire can be calculated using Equations (3.3), (3.5) and the following equation:

$$d\mathbf{l} = dy\mathbf{j} \tag{3.11}$$

Since

$$
\begin{aligned}
dB_z &= d(\mathbf{B}\cdot\mathbf{k}) \\
&= (-\mu_0/4\pi)[Idy(x-x_0)]/[(x-x_0)^2+(y-y_0)^2+(z-z_0)^2]^{3/2}
\end{aligned}
\tag{3.12}
$$

therefore

$$
\begin{aligned}
G_{ylpoint} &= \partial(dB_z)/\partial y_0 \\
&= -\frac{3\mu_0 I}{4\pi}\cdot\frac{(x-x_0)(y-y_0)dy}{[(x-x_0)^2+(y-y_0)^2+(z-z_0)^2]^{5/2}}
\end{aligned}
\tag{3.13}
$$

So that integrating the above equation gives the field gradient at (x_0,y_0,z_0) due to an entire return wire $(Y_c-W/2,\ Y_c+W/2)$ as

$$G_{ylline} = \int_{Y_c-W/2}^{Y_c+W/2} G_{ylpoint}$$

$$= \frac{\mu_0 I}{4\pi}(x-x_0)\left\{\frac{1}{[(x-x_0)^2+(Y_c+W/2-y_0)^2+(z-z_0)^2]^{3/2}} \right.$$

$$\left. \frac{1}{[(x-x_0)^2+(Y_c-W/2-y_0)^2+(z-z_0)^2]^{3/2}}\right\} \tag{3.14}$$

Equations (3.9) and (3.14) were used to calculate the field gradient strength and the orthogonal gradients for different choices of the coil. A 15 turns planar coil with a length of 40 mm and using Gauge 32 wire were finally chosen. The computer simulating data and contour plots are shown in Table 3.7 and Figure 3.19 - Figure 3.22. The ±0.4 % (1/256) lines indicate the theoretical undistorted sample space. The computer programs used, which can be found in Appendix B, are the modified versions of that used in Reference (38).

Table 3.7 Calculations of the Unit Gradients

	G_x	G_y		G_z
		Old	New	
Desired Gradient	21±4	1.6±0.1	8.8±0.1	15±3
Orthogonal Gradients	$G_y=3\times10^{-7}$	$G_x=5\times10^{-10}$	$G_x=1\times10^{-4}$	$G_x=3\times10^{-6}$
	$G_z=0.3$	$G_z=6\times10^{-9}$	$G_z=6\times10^{-11}$	$G_y=0$

*The unit in the above table is $Gcm^{-1}A^{-1}$.

**The gradients are determined at the origin.

*** The desired gradients are the calculated values.

3.4.3 Construction and Performance

The construction of the coil was fairly difficult due to the limited space. Figure 3.23 shows the finished coil. It is wound directly on the interior-side of the probe pcb and covered with a thin layer of Araldite. Miniature sockets and plugs have been made, so that the pcb can be separated from the probe body. Copper washers have been made to provide the 0.5 mm gap.

The gradients were calibrated by using the standard pulse gradient spin echo technique to measure the doped water diffusion coefficient. Experiments show that the new coil gave an unit gradient of (9.36±0.01) $Gcm^{-1}A^{-1}$, which yielded a Y gradient of 140 Gcm^{-1} (1.4 Tm^{-1}) if the 15A power supply is used. The following table gives some characteristics of the coils and field gradients.

Table 3.8 Characteristics of the Gradients

	G_x	G_y	G_z
Resistance of the coil (Ω)	2.25	2.18	1.62
Inductance of the coil (μH)	85	54	45
Inductance* (μH)	86	58	46
Unit Gradient ($Gcm^{-1}A^{-1}$)	23.74±0.06	9.36±0.01	14.89±0.09
Gradient$_{max}$ (Gcm^{-1})	95	140	149

*Resistances and Inductances are measured by using HP4192A LF Impedance Analyzer. Frequency has been set to 1 kHz when measuring inductances.

**Inductances* are measured from the leading wires after the coils and the probe have been assembled.

*** The values of the unit gradient are the calibrated ones.

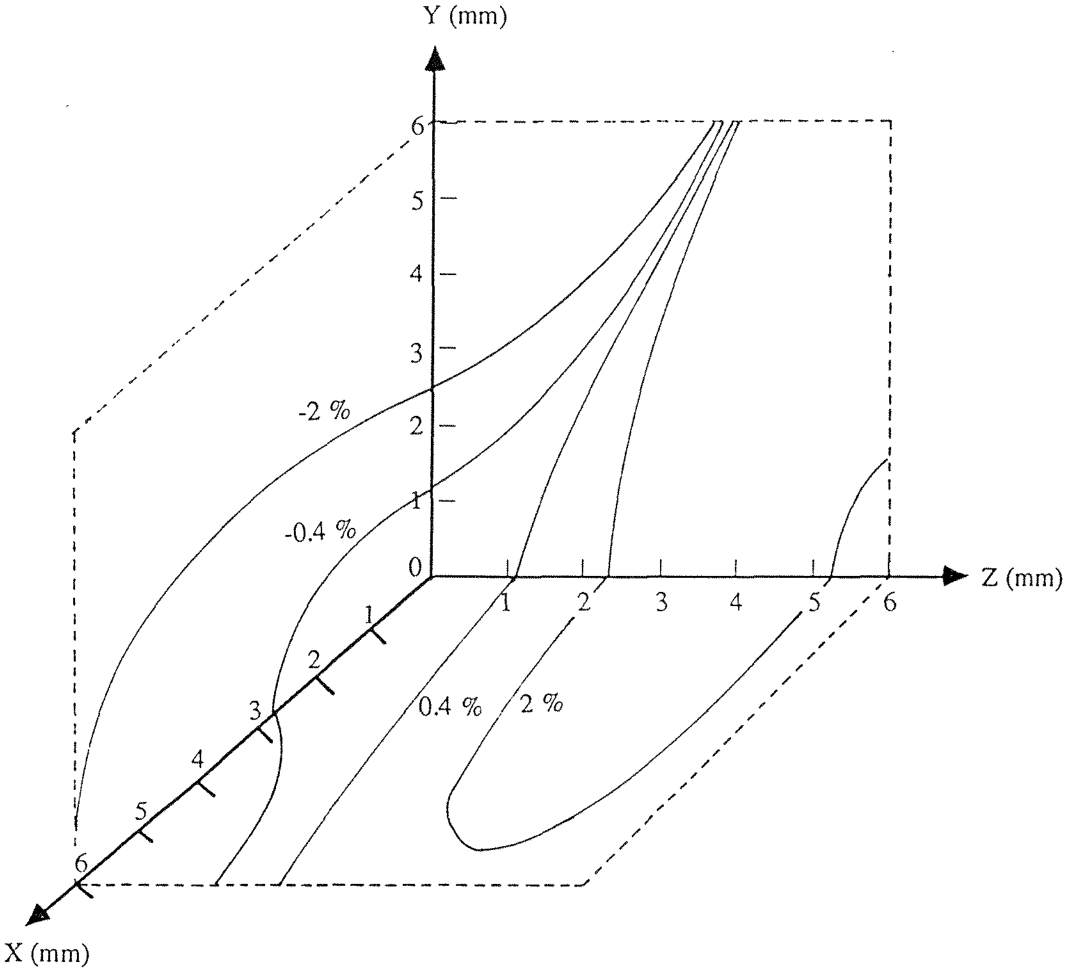

Figure 3.19 Schematic Percentage Variations in G_y Gradient

a) G_y (Y-Z Plane)

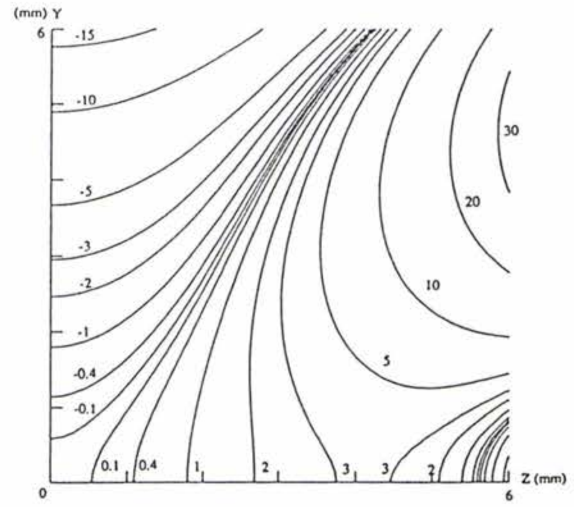

b) G_y (X-Y Plane)

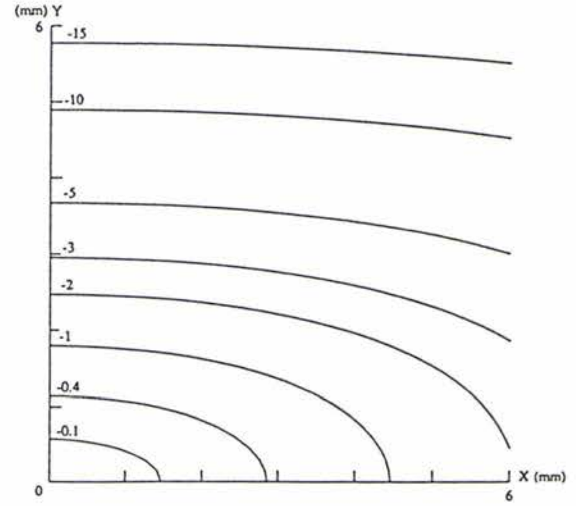

c) G_y (Z-X Plane)

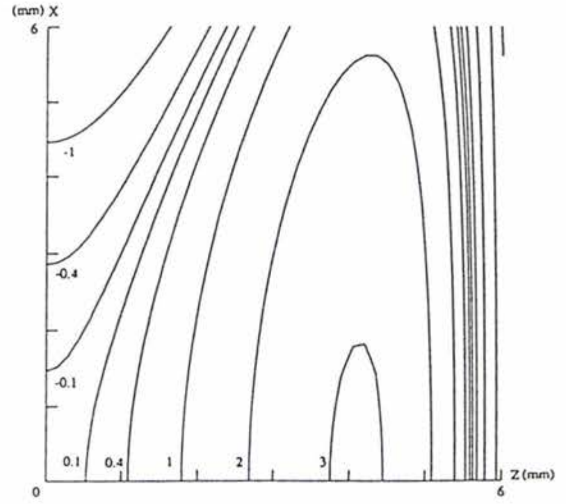

Figure 3.20 Percentage Variations in G_y Gradient

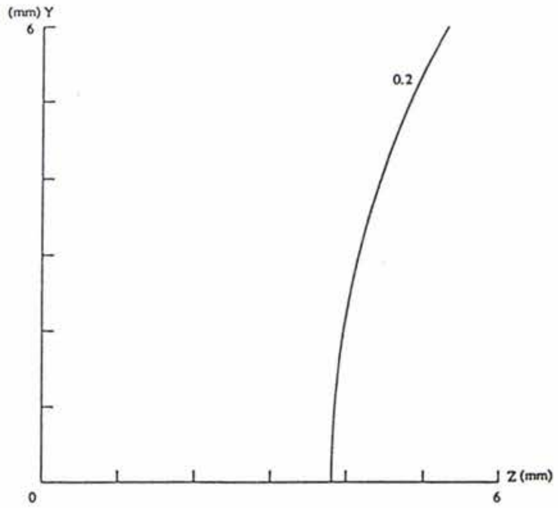

a) G_x (Y-Z Plane) / $G_y(0,0)$

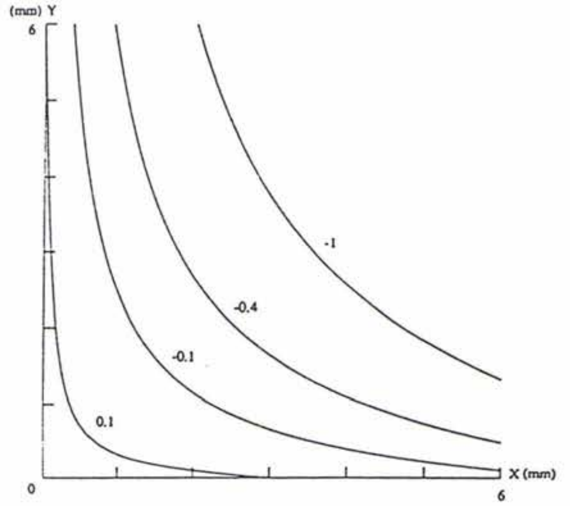

b) G_x (X-Y Plane) / $G_y(0,0)$

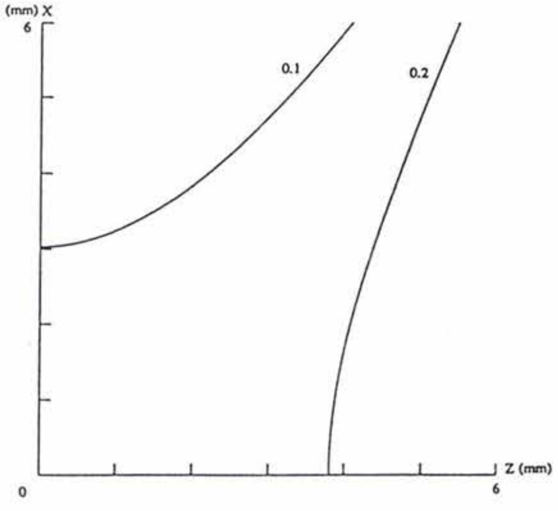

c) G_x (Z-X Plane) / $G_y(0,0)$

Figure 3.21 Percentage Variations in G_x Gradient due to G_x Orthogonal Gradient

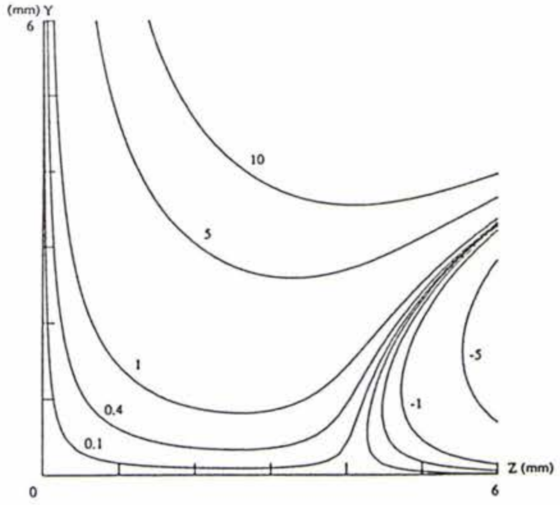

a) G_z (Y-Z Plane) / $G_y(0,0)$

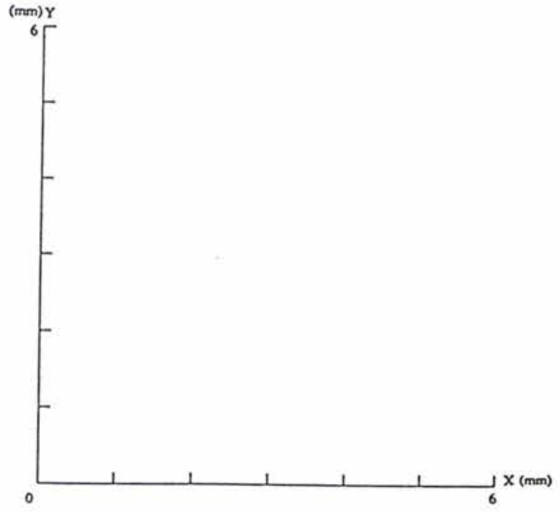

b) G_z (X-Y Plane) / $G_y(0,0)$

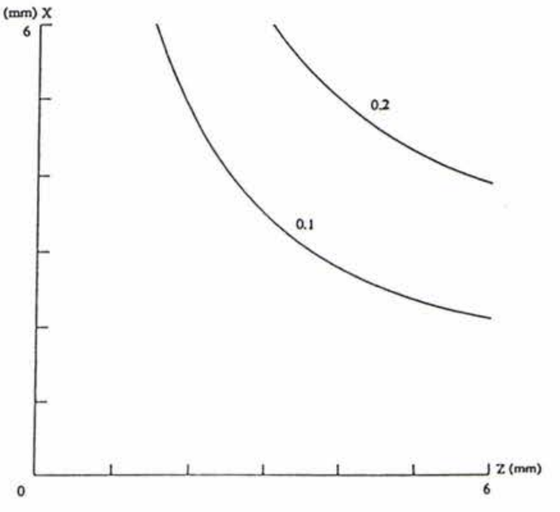

c) G_z (Z-X Plane) / $G_y(0,0)$

Figure 3.22 Percentage Variations in G_Z Gradient due to G_Z Orthogonal Gradient

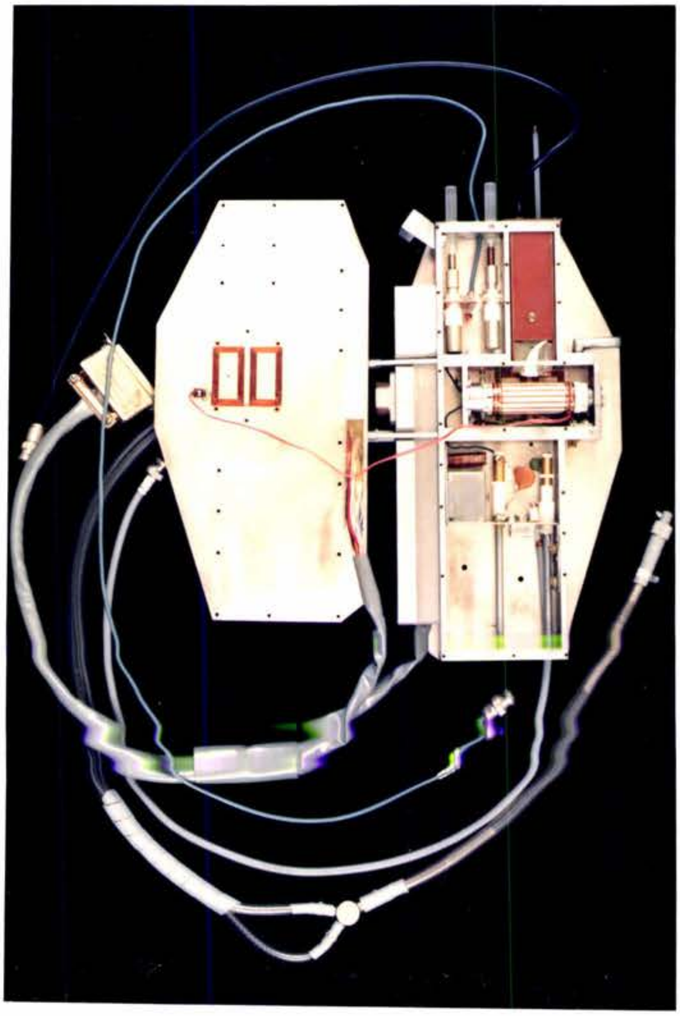

Figure 3.23 New G_y Coil and the Probe

3.5 Software Development for Dynamic Imaging Experiments

Dynamic imaging experiments have been automated under the control of two computers. Various assembly language and FORTRAN language programs were written for the dynamic experiments and the data analysis.

3.5.1 General Considerations for Dynamic Experiments

In Section 2.3.3 the data processing procedures of dynamic experiments have been presented (cf Figure 2.27). From the computer's point of view, these procedures can be shown schematically as in Figure 3.24.

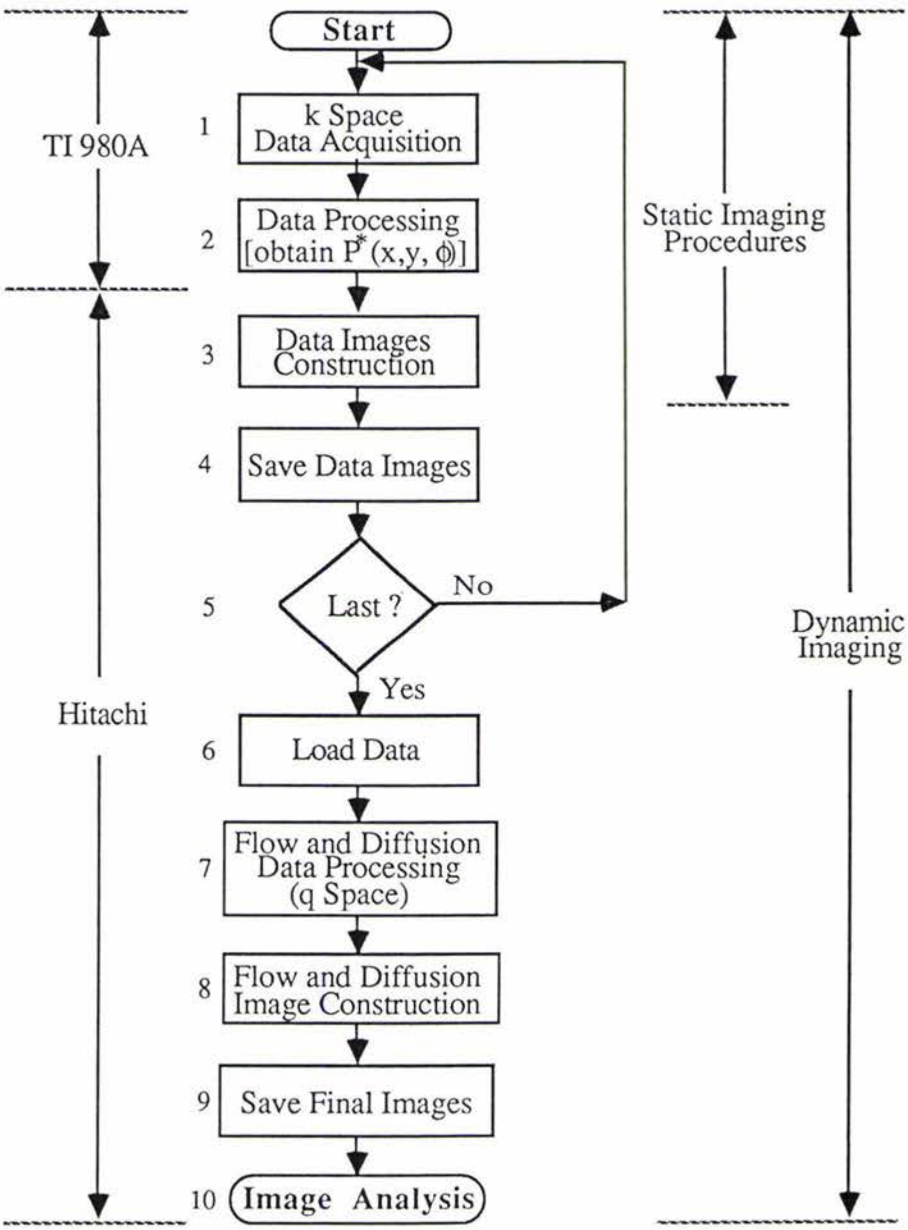

Figure 3.24 Flow Chart for Dynamic Imaging Experiments

The steps 1 to 3 are the standard static imaging experimental procedures, in which FBP reconstruction method is incorporated. Modifications to the original static imaging software are made so that the four quadrants sampling can be performed (see Appendix A.6).

The main obstacle in doing dynamic imaging experiments is the computer memory size, since for example, the data size of one 256×256 image is 128 kbytes. The Hitachi computer is configured with 256 kbytes main memory, in which the upper 128 kbytes can be used to store data. Therefore the pixel number of the dynamic images has to be reduced. But even by reducing the image pixel number to 64×64, the whole computer data memory can store only 8 sets of data images [each set contains one real image (8 kbytes) and one imaginary image (8 kbytes)]. That is not enough for the later analysis.

Another possibility is to save data images into a disk for later analysis while doing experiments. Since the computer has two 320 kbytes floppy disk drivers, we can always keep one for saving the data. Considering leaving 16 kbytes for the final velocity and diffusion images and a few kbytes for the file directory and DOS system, the remaining space can be used to store the data images. This allows a maximum of 18 sets data images (n_D=18).

If however we use only these 18 data to perform the **q** space FFT, then we will get only 18 data points in the final space, in which the peak must be searched (Velocity) and FWHM must be calculated (Diffusion). The final results are obviously not accurate if so few data points are available in the dynamic displacement domain. The trick used to improve the accuracy is zero-filling after 18 data pixels to (for example) a total domain of 256 pixels. If the last data are effectively zero, then no truncation will be introduced, and the final analysis can be done on the basis of these 256 points. The effect of zero-filling in the q-domain is therefore to provide interpolation in the conjugate domain. The influence of the truncation effect has been discussed in Section 2.3.5.

3.5.2 Programs for Disk Read/Write

From the above discussion, we know that we have to store the data images into a disk while doing experiments. After finishing all the data imaging experiments, the final velocity and diffusion analysis and image reconstruction follows. In calculating velocity and diffusion for any pixel in the final images, we need to use all the pixels with the same coordinates in the data images. This means that if the data files are stored in usual way on the disk, reconstruction of a final 64×64 velocity and diffusion images needs 2×18×64×64 disk reading operations. This is unnecessarily time consuming.

An alternative approach is to read part of the data images, say 1 kbytes per data image, from the disk, and perform data analysis for these sections alone. Such a procedure needs only 8 disk readings. This is a much better way provided that we know the exact position of each pixel of the data images on the disk. The DOS file saving and reading methods are obviously not applicable.

There are 40 tracks in one side of a 5.25 inch floppy disk. Disks are formatted into 8 sectors each track (MS-DOS 1.0). One sector can store 512 bytes information (Figure 3.25). Information exchange between the computer and the disk is done in sector units, and storage locations on the disk are defined by a number called the logical record number (LRN) which is from 0 to 639.

MS-DOS provides various BIOS and DOS interrupt calls which can be used as subroutines by the user's program. INT 25 and INT 26 are the absolute disk read and write interrupts. If the required registers of the INTEL 8088 microprocessor have been configured in the desired way, these two interrupt calls can accurately locate any sector position on a disk. Another advantage of using the interrupt calls is that they take much less time than using high level languages, so that the process of saving the data into a disk does not affect the execution of the following experiment.

An assembly language program employing INT 25 has been written, with a flow chart shown in Figure 3.26. The complete listing of the program can be found in Appendix A.1. This program can read any sector from the disk, fully dependent on the instructions given by the operator. Therefore this program can be used to read hidden files or recover a file which has been accidentally wiped.

By comparison, the program for writing data to a disk needs more features. In particular it is necessary to write a file directory, which under normal circumstances is handled by the DOS system automatically. The disk writing program has a few versions, Figure 3.27 gives a flow chart for a complete program and a full listing can be found in Appendix A.2.

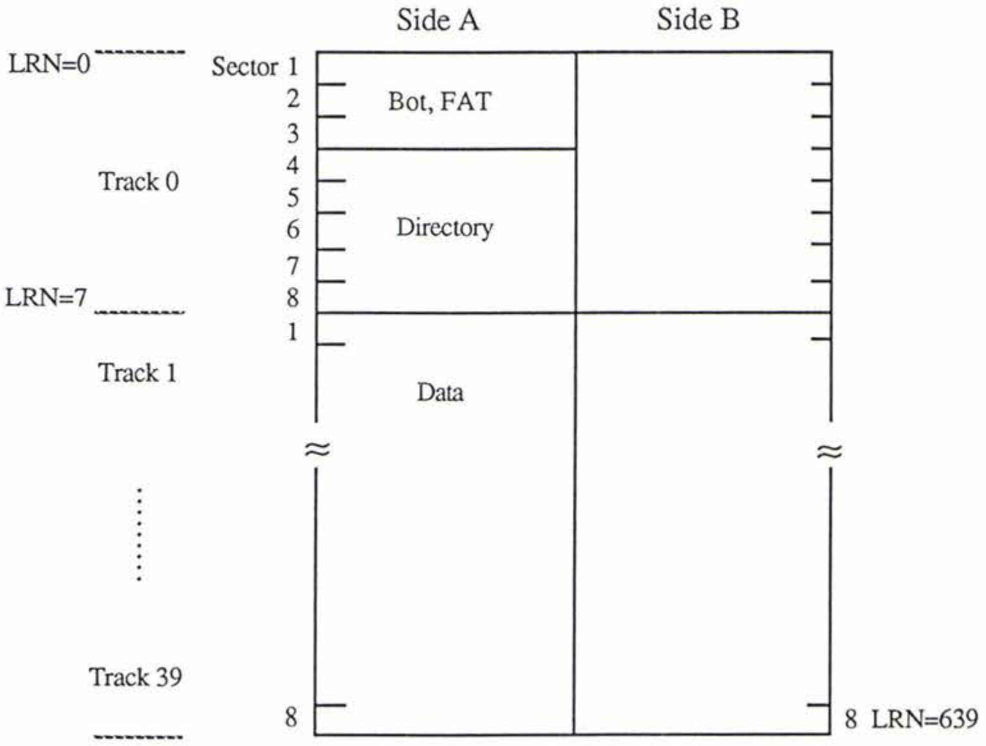

Figure 3.25 Floppy Disk Format

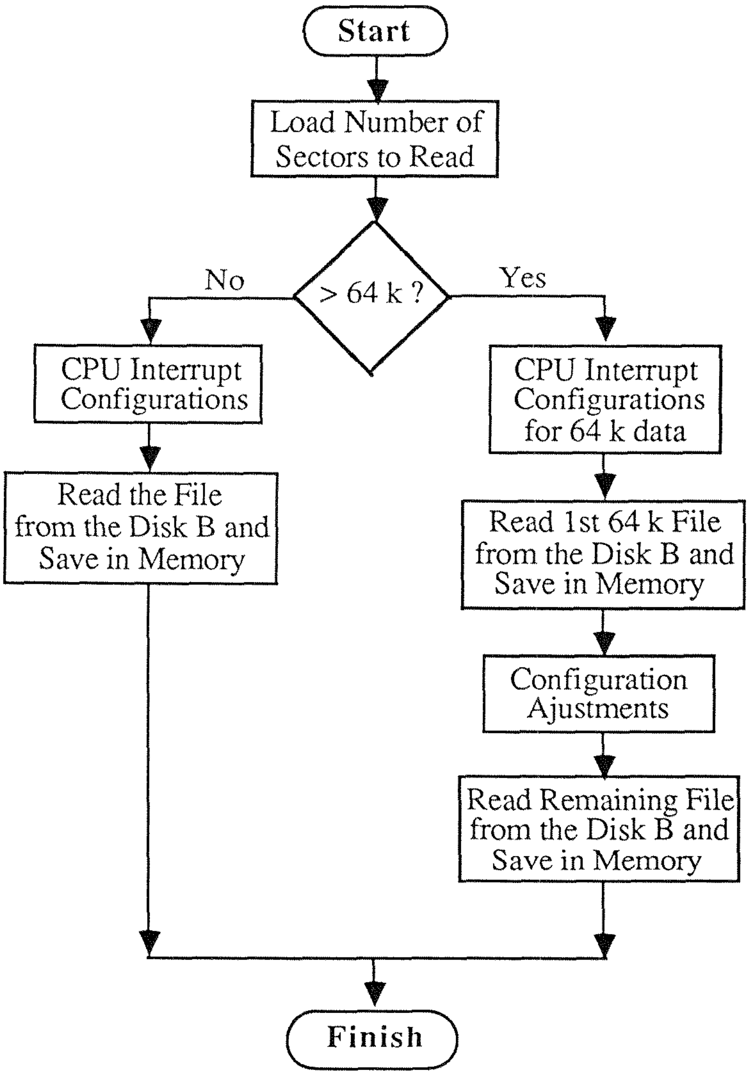

Figure 3.26 Flow Chart for Disk Reading Program

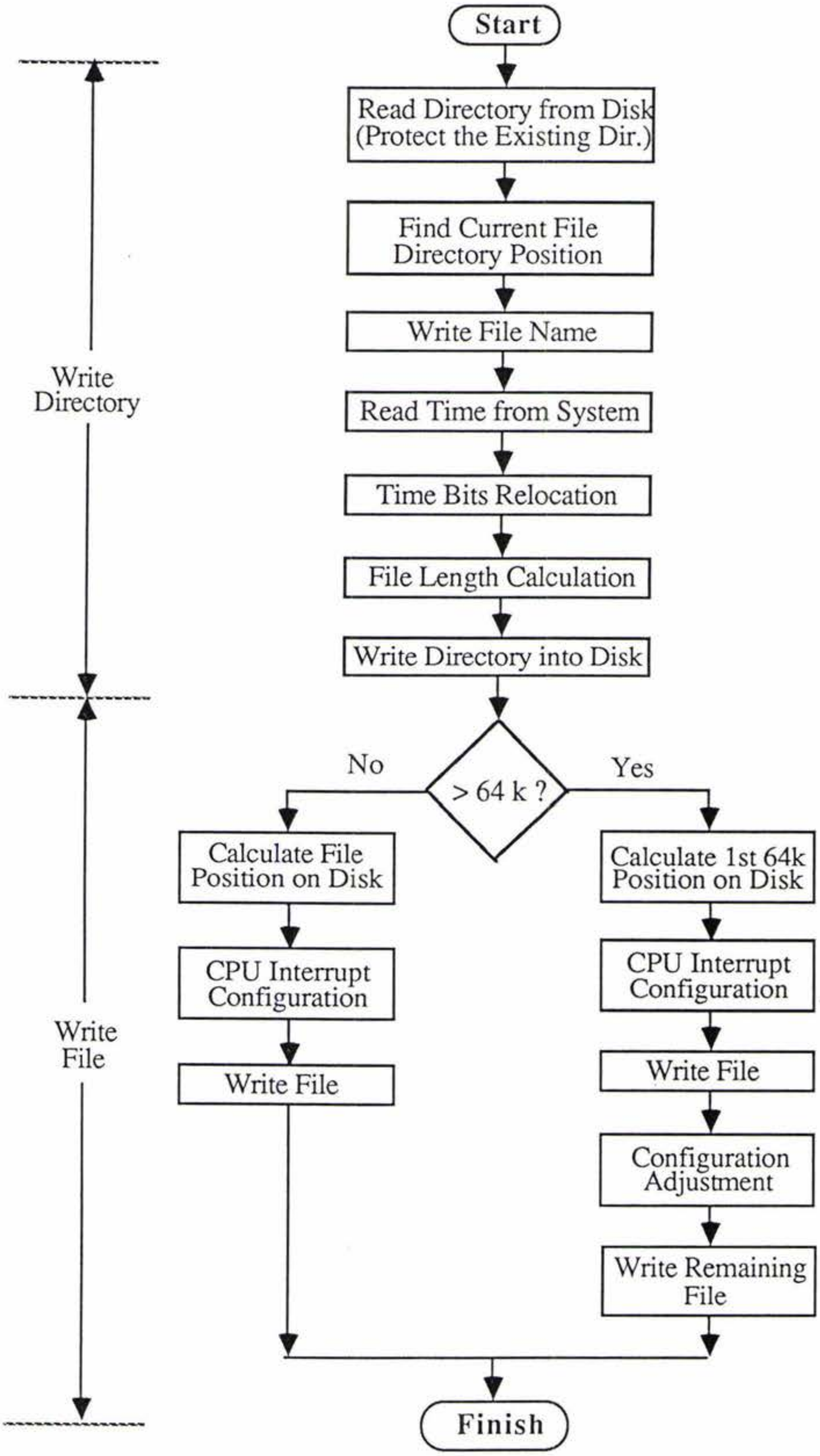

Figure 3.27 Flow Chart for Disk Writing Program

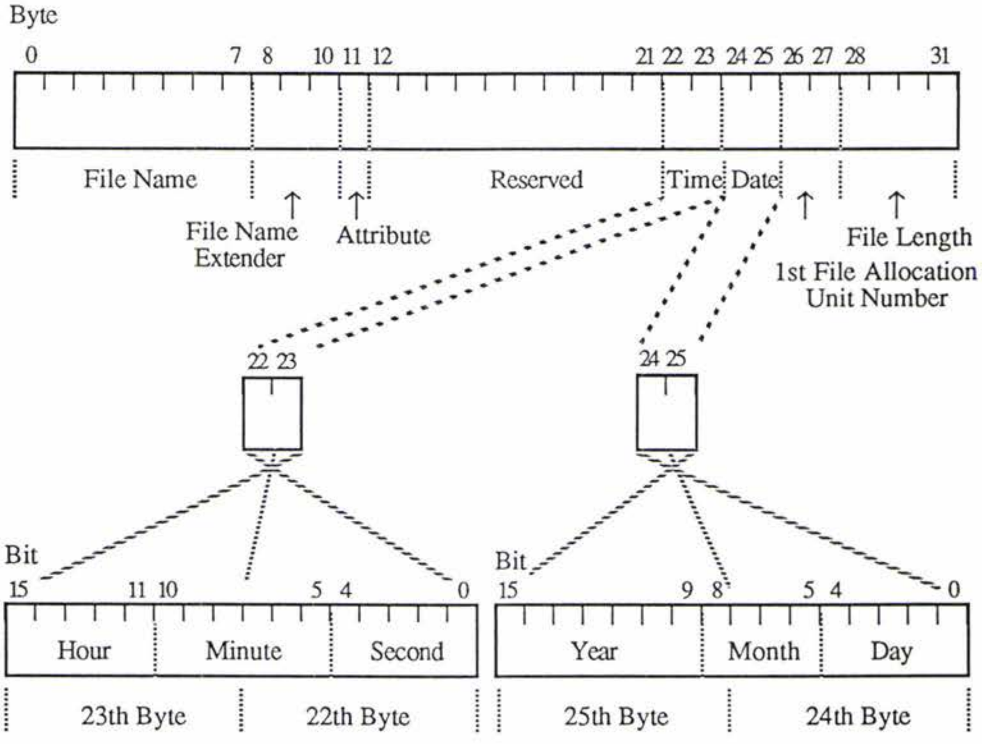

Figure 3.28 Information Position on File Directory

Writing the directory is an important part of the program, for each 32-byte long file directory contains various information, which position are shown in Figure 3.28.

3.5.3 Programs for Searching Peak and Calculating FWHM

The program for searching the displacement profile peak and calculating the FWHM is also written in assembly language. The method to search the peak is quite straightforward. The signal amplitude is computed pixel by pixel until the highest one is found.

There are two methods to calculate the FWHM. The simplest method [Figure 3.29(a)] is, having found the peak, to go on to find the half peak pixels at each side of the peak and then calculate the FWHM. But this method could introduce some systematic error (cf Section 2.3.5). An alternative method is a two-way approach, searching from both sides of the half peak pixel [Figure 3.29(b)]. The final result is obtained by averaging between FWHM pixels obtained in the two sweep directions. This method is intrinsically more accurate than the first one, if the data is perfect. But in real experiments, there are bound to be some small peaks due to noise [Figure 3.29(c)]. Therefore the latter method gives worse results in practice. The one-way approach method is used in the program.

Another factor influencing the FWHM calculation is the existence of a finite base line to FFT (Figure 3.30). It is obvious that in the case of larger base line (cf Section 2.3.5 for theoretical details), some correction has to be made in the calculation. This can be done by calculating the average amplitude of part of the 'spectrum' pixels which are outside the peak region, then using this average as the base value. Of course such a procedure presumes that we know where the peak will appear (positive or negative) and also presumes that the noise of the final 'spectrum' is small.

There are two versions of the program, one considering the base line effect and the other not. Figure 3.31 gives a flow chart of the program which allows the base line effect. A full listing of the program is shown in Appendix A.3.

(a) One Way Searching Method

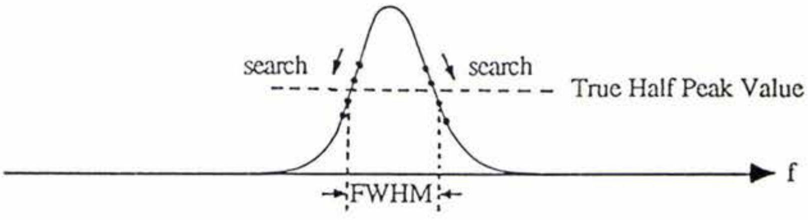

(b) Two Way Searching Method

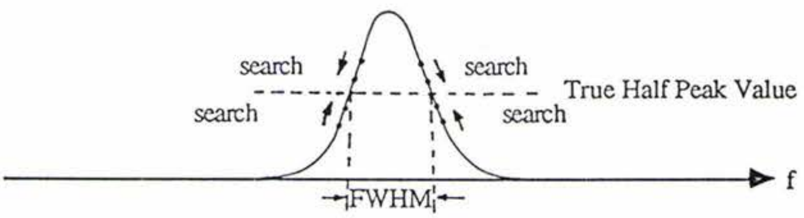

(c) Two Way Searching Method in Possible Practical Situation

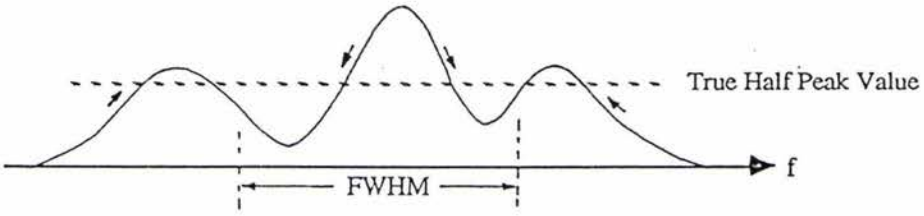

Figure 3.29 Methods for Searching Peak and Calculating FWHM

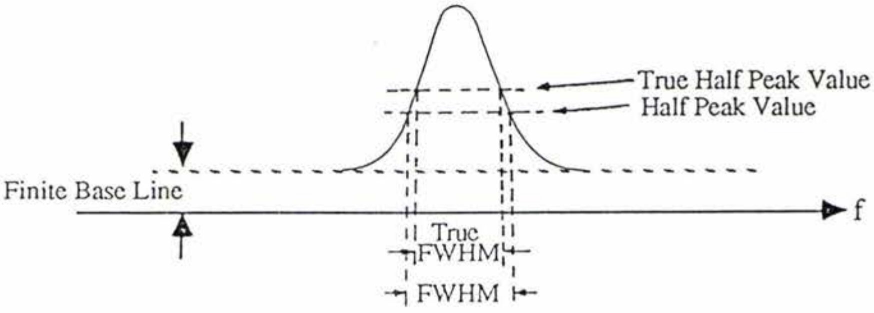

Figure 3.30 Effect of Finite Base Line

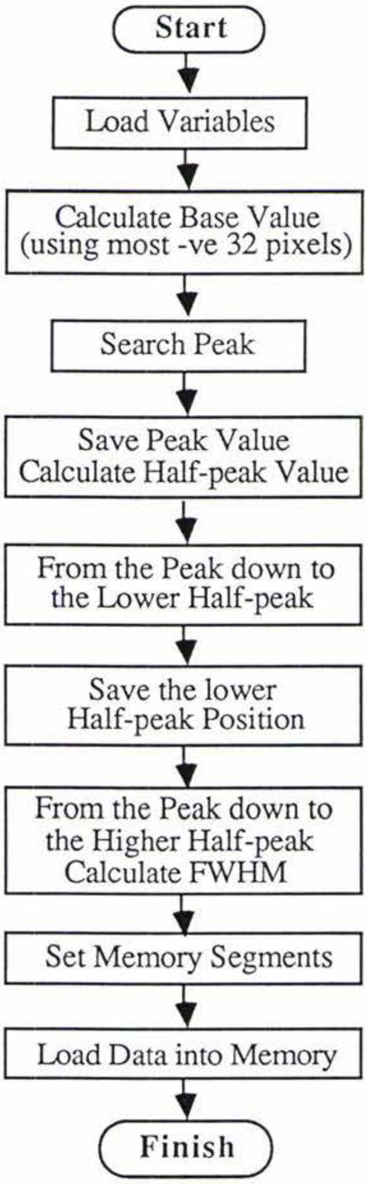

Figure 3.31 Flow Chart for the Program Searching Peak and Calculating FWHM

3.5.4 Program for Imaging Experiments and Reconstruction

Other software subroutines written as part of this work include writing an assembly language program to get the time and date from the computer system, various modifications of the existing assembly language subroutines such as those used for the display of colour scales, image reconstruction, the drawing of graphs, back projection, and printing of images. A description of the subroutine library is shown in Appendix A.4.

The main program used for the dynamic experiments is written in FORTRAN. Figure 3.24 can be used as the block flow chart of this program, named FLOW.FOR. An important consideration is the data position in the computer memory. Figure 3.32 gives the computer memory map for the flow and diffusion experiments. The complete list of the program can be found in Appendix A.5.

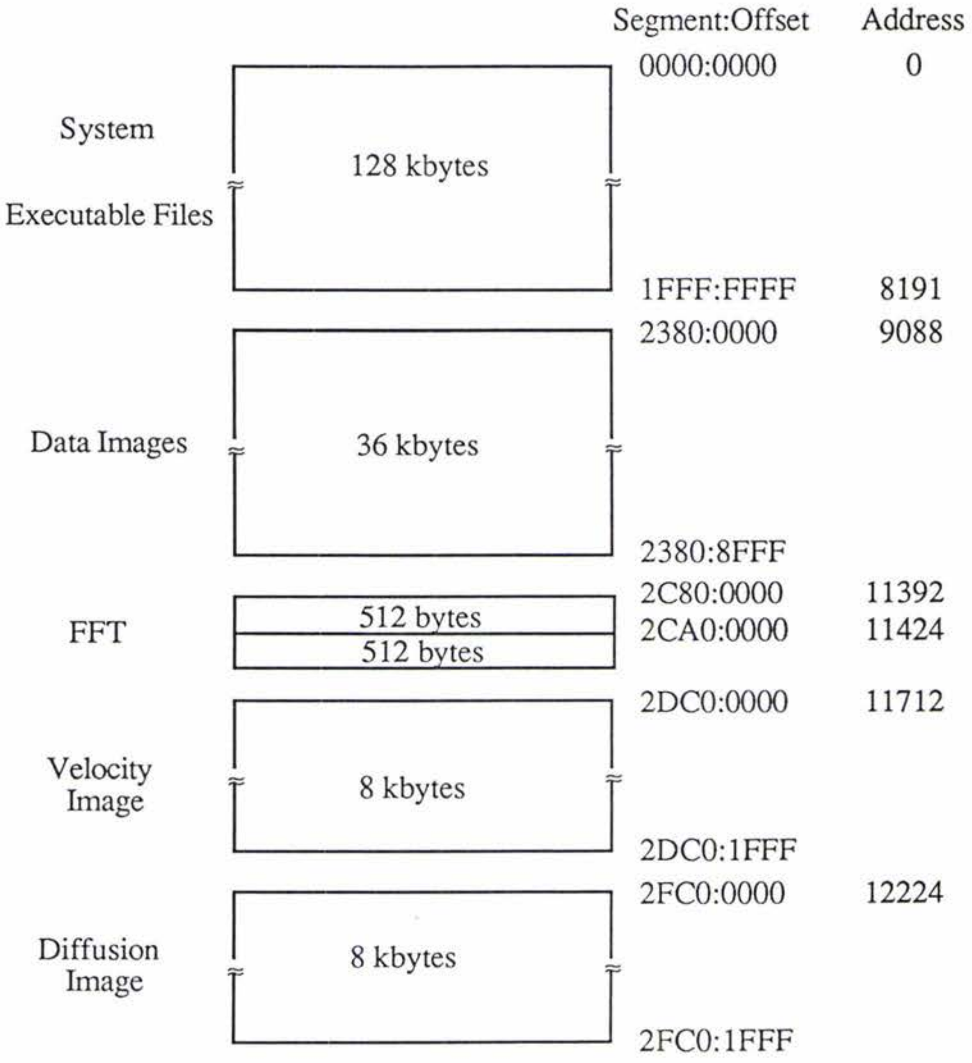

Figure 3.32 Memory Map for Dynamic Imaging Experiments

3.5.5 Modifications to TI 980A Programs

As mentioned in Section 3.1.4, the TI 980A computer is an original part of the JEOL FX60 spectrometer. This computer is supported by an extensive software package in a very poorly documented way. Various assembly language programs had been written later, which incorporate the original software, to perform static imaging experiments, PGSE experiments and others. To clearly present the complete software for TI 980A is very difficult (if not impossible). Several parts of this software relevant to imaging are given in Reference (44). Appendix A.6 gives a list of modifications to the existing programs.

Some of the modifications to the original static FBP program enable the four quadrants sampling, while the others were required by the dynamic imaging experiments.

3.5.6 Program for Dynamic Image Analysis

Using the software developed in the last few sections, it is possible to obtain the velocity image (velocity map) and diffusion image (diffusion map). It would be very worthwhile to incorporate further image analysis, such as obtaining the exact digits for velocity and diffusion, and examining the signal or noise level at any final pixel position. In addition it was considered useful to be able to carry out the **q** space FFT and display the **q** space 'spectrum' on the screen. A FORTRAN program was written to complete these tasks.

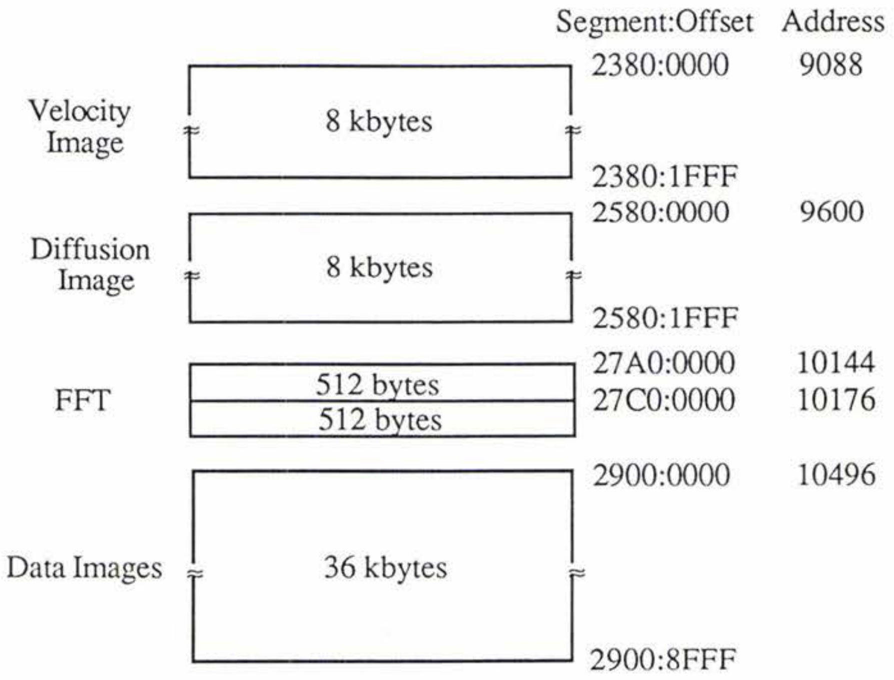

Figure 3.33 Memory Map for Dynamic Image Analyses

This program, named FLOWD.FOR with a computer memory map shown in Figure 3.33, sets up a computer screen appearance as in Figure 5.6. It can display three images, a velocity, a diffusion and the first real original image, on the same screen. A menu is supplied on the screen with various available functions. When carrying out the **q** space FFT, the program will go to the disk, read the required data, perform FFT and display the 'spectrum' on the bottom of the screen.

The flow charts for this program are shown in Figure 3.34, in which the number I indicates the function being selected. The complete program is presented in Appendix A.7.

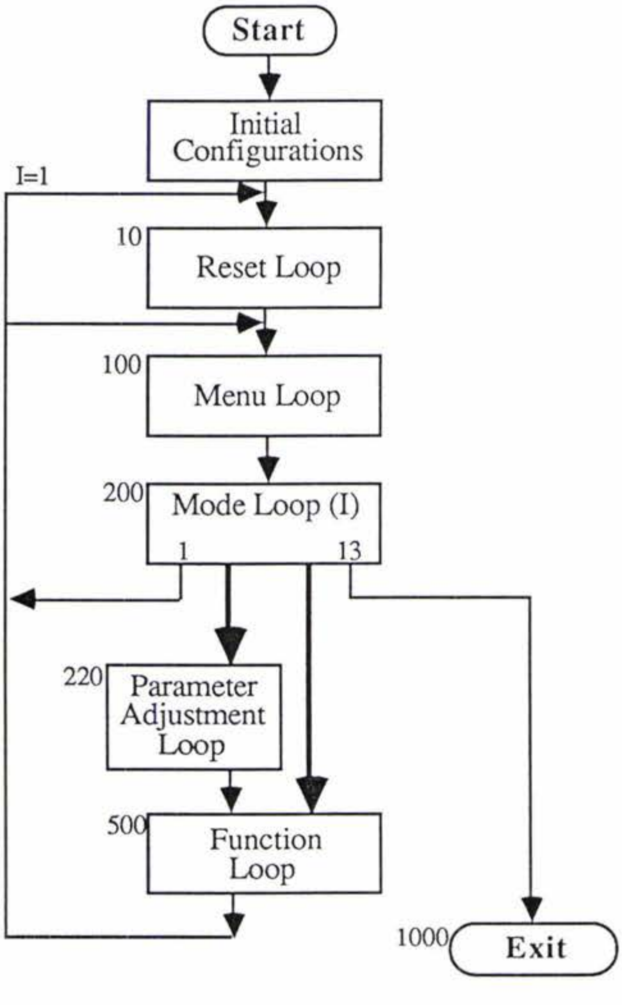

Figure 3.34 Flow Chart for the Program Analyzing Dynamic Image Data
(a) General

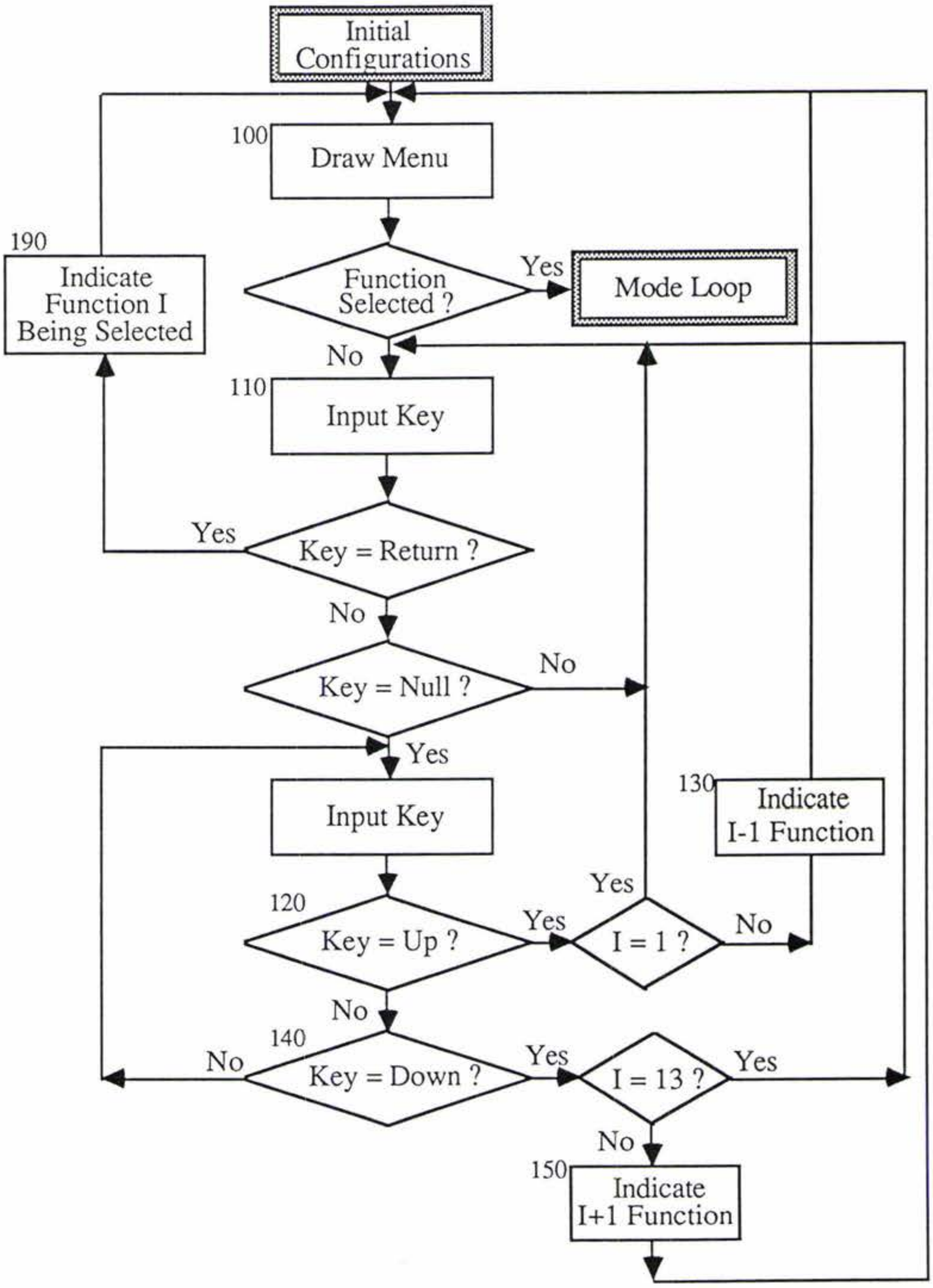

Figure 3.34 Flow Chart for the Program Analyzing Dynamic Image Data
(b) Menu Loop

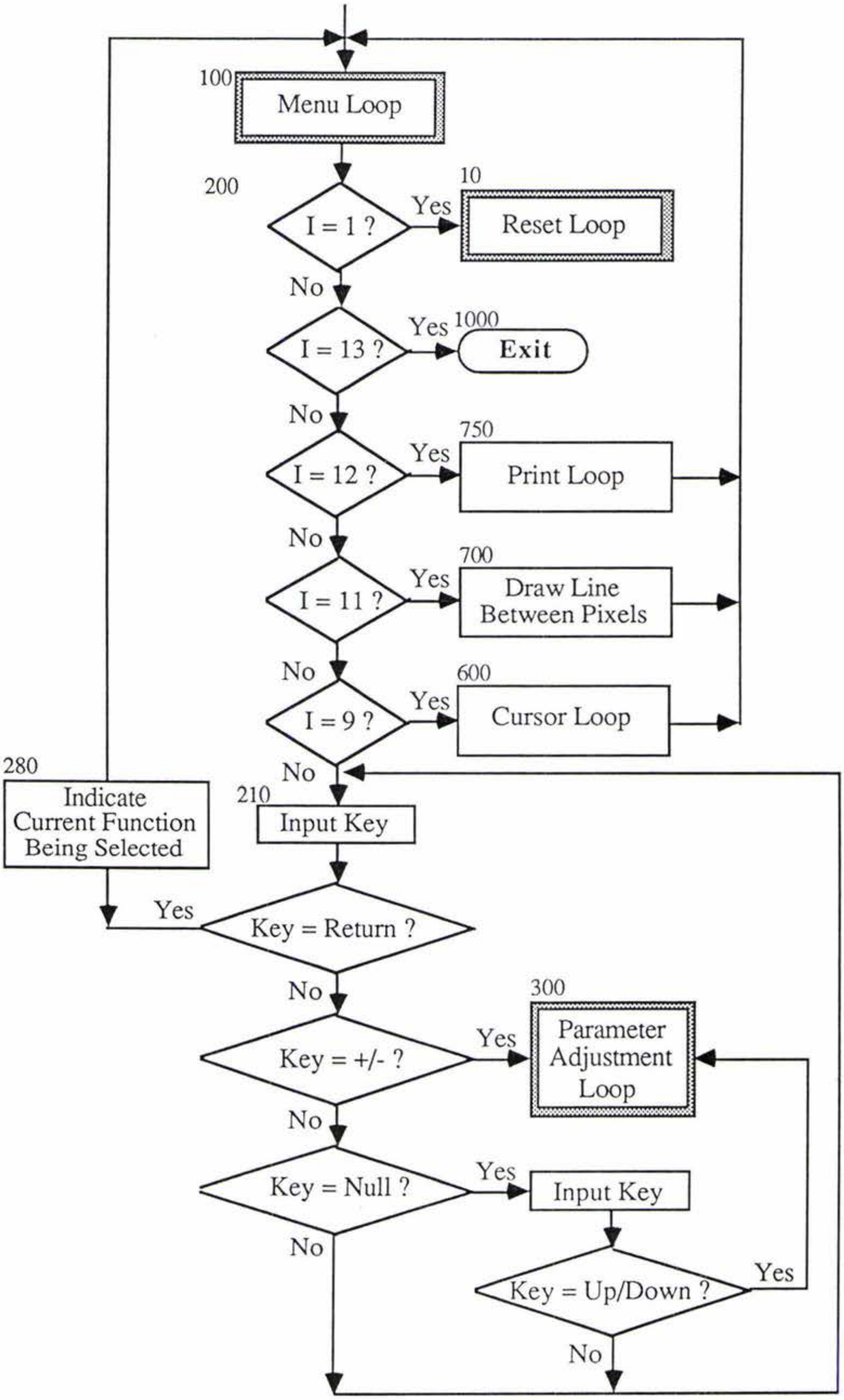

Figure 3.34 Flow Chart for the Program Analyzing Dynamic Image Data: (c) Mode Loop and Function Loop (i)

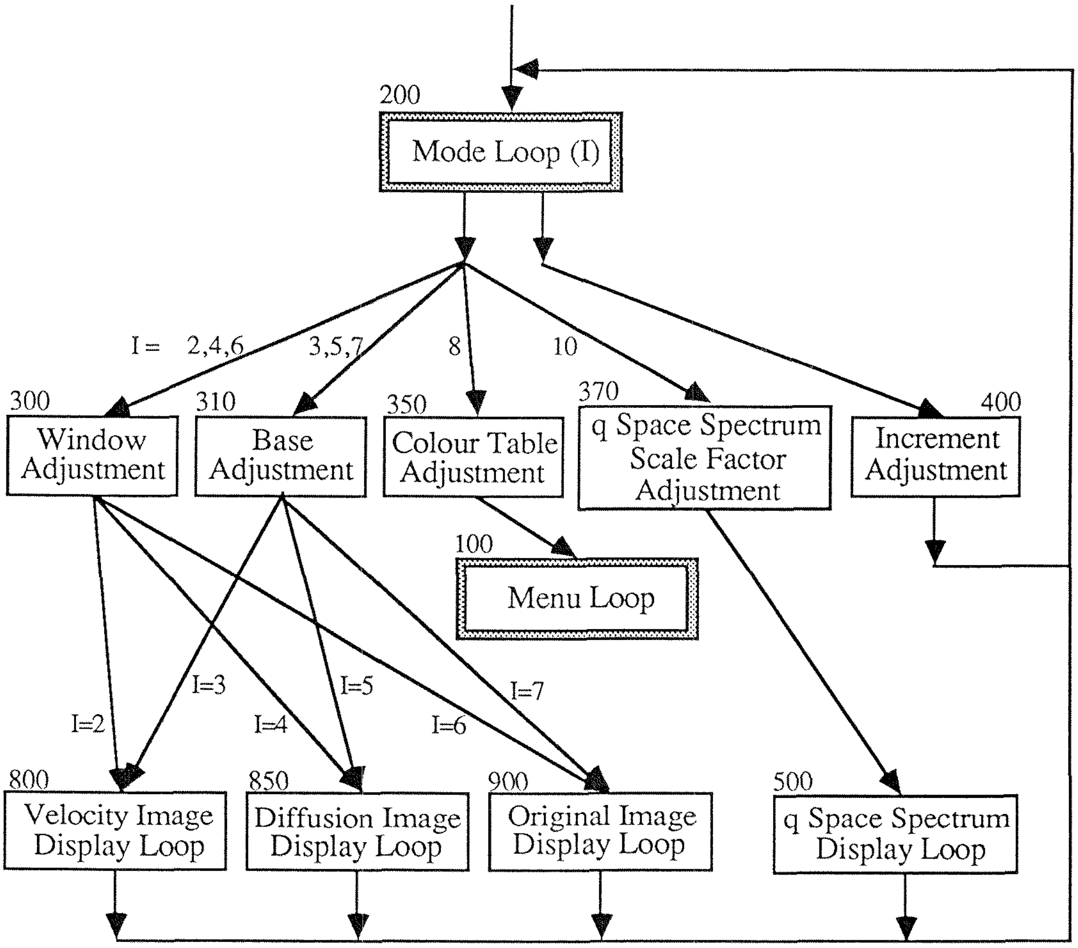

Figure 3.34 Flow Chart for the Program Analyzing Dynamic Image Data: (d) Parameter Adjustment Loop and Function Loop (ii)

Chapter 4 Static Imaging Experiments

Having considered the theory of NMR imaging and described the imaging system and its developments, we now present the imaging experimental results in the next two chapters. In this chapter, the experimental method for static imaging is given in Section 4.1, followed by the imaging results in the remaining sections.

4.1 Experimental Considerations for Static Imaging

The experimental considerations include the generation of an appropriate pulse sequence and the setting of experimental parameters.

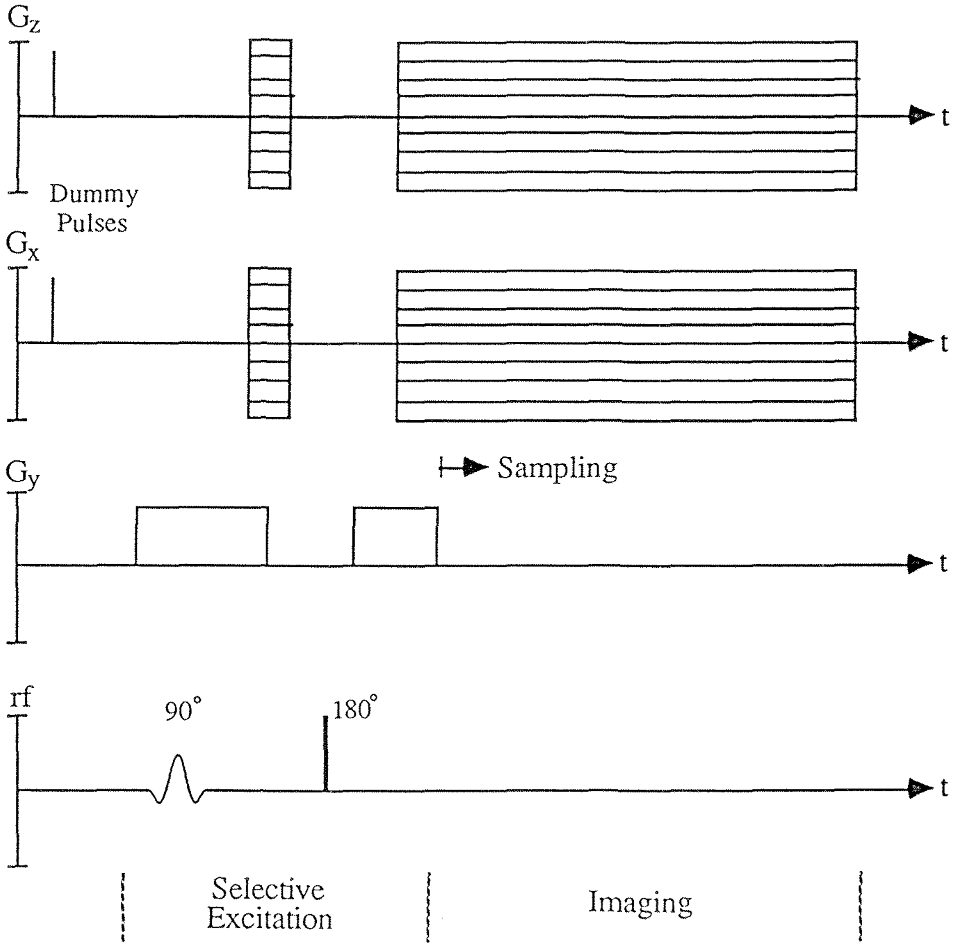

Figure 4.1 Pulse Sequence for Static Imaging Experiments

The pulse sequence using in the static imaging experiments is shown in Figure 4.1. The selective excitation part has been described in Section 2.2.2 [cf Figure 2.16(b)]. Due to the geometry of the imaging system, the x-z plane is the transverse plane and the y axis gives the longitudinal direction. Consequently the x and z gradients are used as the imaging gradients (mapping gradients), and the y gradient is used for the selective excitation together with the rf pulses. In the x and z gradients, the 2 μs prepulses are used to establish the initial gradient level and so reduce the gradient rise time. The pulse sequence shown employs a spin echo in order that the origin of **k** space does not occur during gradient pulse switching.

The pulse sequence is designed with selective rf pulses chosen to match the different rf coils. The gradient turning angle [$\Delta\phi$ in Equation (2.62)] is usually chosen as either 2 or 6 degrees, a finer turning angle can improve the resolution but increases the required experimental time. The time available is restrained by the sample lifetime and the stability of the system. The chosen values represent a compromise.

The magnitude of the y gradient determines the slice thickness of the sample. The larger the gradient, the thinner the slice. This leads to better resolution but poorer S/N.

Sampling time starts after the selective excitation at the echo centre, and lasts for a time

$$T = N/\Delta f \qquad (4.1)$$

where N is the number of the data points sampled by the spectrometer and Δf is the bandwidth of the spectrometer.

For particular G_x and G_z values, the real and imaginary time domain signals are obtained by detecting the quadrature signal. This is done by simply changing the relative phase in the phase sensitive detector. The signal is accumulated in N_{acc} repetitive co-additions to improve S/N. Then a quadrature FFT is performed to obtain the frequency domain signal. This signal can be exponentially filtered to improve S/N at the cost of poorer resolution. By multiplying the signal by a ramp before transformation, we obtain the filtered profile $P^*(x,y,\phi)$, which is sent to the Hitachi computer for the image reconstruction.

Note that the FID signal lasts about T_2 seconds, but the minimum repetition time between the accumulations is determined by T_1. Therefore if the T_2 of the sample is much less than its T_1, most of the experimental time is used just waiting for the recovery of the magnetization.

After $P^*(x,y,\phi)$ has been transferred to the Hitachi, the values of G_x and G_z gradients are updated according to the pulse sequence codes stored in the TI 980A memory. In this way the experiment is carried out until two quadrants have been sampled.

Some experimental parameter settings for the static imaging experiments in the next few sections are shown in the following table.

Table 4.1 Imaging Parameters for Static Imaging Experiments

Names	**Three-tube**	**Plant Stem**	**Rabbit Tracheas**
Sample Dimensions (mm)	ϕ 1	4×4×4	~ϕ 5
RF Coil	Small	Large	Large
Slice Thickness (mm)	1	2.5	2.5
Bandwidth (kHz)	10	20	20
Applied Broadening (Hz)	75	200	300
Repetition Time (sec)	0.2	0.2	1
Number of Accumulations	88	120	24
Turning Angle (°)	2	2	2

4.2 Three-Tube Phantom Image

To test an imaging system, phantom is the ideal sample. A three-tube phantom has been made as the imaging sample for the small rf coil.

The phantom (Figure 4.2) consists of three capillary glass tubes, with internal diameters of about 310 μm, full of doped water. The image is shown in Figure 4.3 (a dot matrix printer copy). This image gives a transverse resolution of 15 μm with a S/N of 18. It can be seen that S/N is not very good. This is the price of high resolution. The image is interpreted in a grey scale.

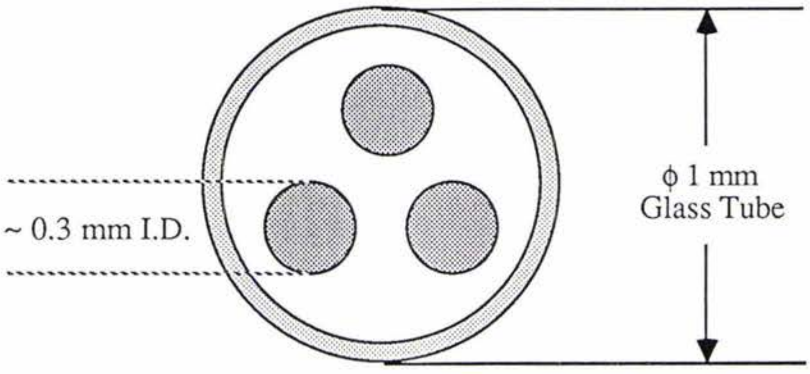

Figure 4.2 Three-Tube Phantom

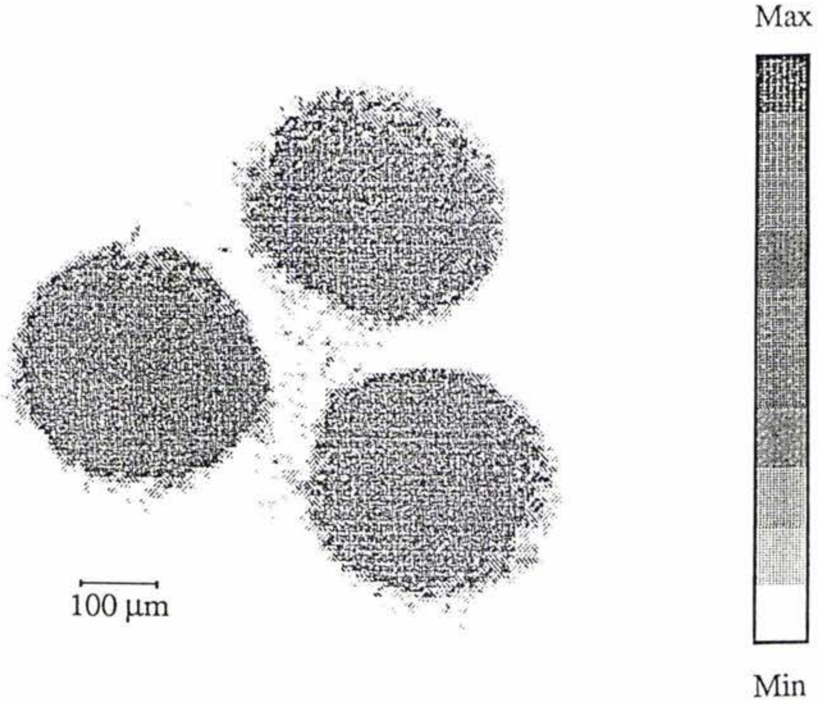

Figure 4.3 Microscopic NMR Image of the Three-Tube Phantom

4.3 Plant Stem Image

An image of the plant stem (Cyperus Eragrostis) has been obtained, which is shown in Figure 4.4. S/N of 100 has been obtained in this image with a transverse resolution of 150 μm. The colour scale indicates the proton density of the tissue, where white represents the highest free water concentration and black the least. So that the high density parts are the tissues containing the vascular bundles.

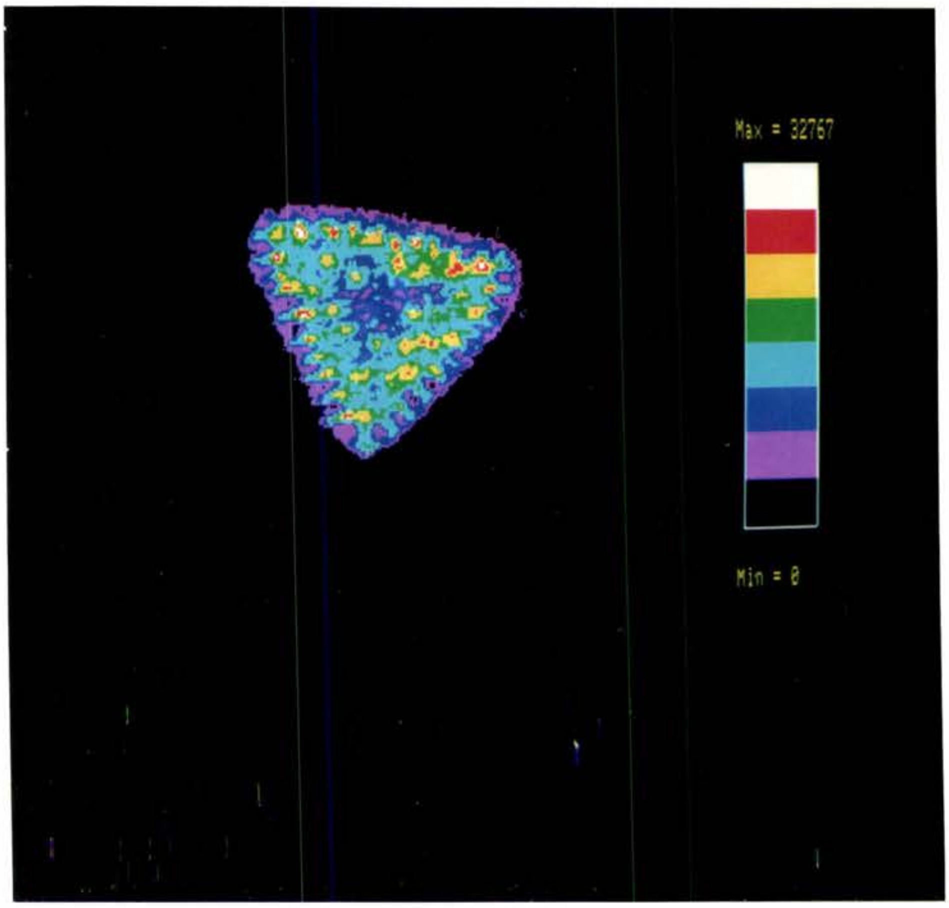

Figure 4.4 NMR Image of a Plant Stem (Cyperus Eragrostis)

4.4 Rabbit Trachea Images

One of the research activities is the Department of Physics and Biophysics concerns the modelling of pressure/flow relationships in tracheal airways(45). This work is being carried out by Dr R.K. Lambert. An important relationship in this modelling is the airway cross-sectional area. In this section, the area-transmural pressure (A-P) relationship is obtained using images of rabbit tracheal cross sections. The experimental results are the subject of a paper submitted to Journal of Applied Physiology(46). A brief description of the experiments is given here, the emphasis being on the experimental imaging arrangements and the image reconstruction.

4.4.1 Experimental Arrangement

The samples are excised and washed rabbit tracheas with outer diameters around 5 mm. A special sample holder assembly has been made for this experiment (Figure 4.5).

The glass cannula is held tightly by the teflon holder. One end of this glass cannula is connected to the pressure system and the other end is connected to the trachea. The teflon plug has a key at one end and a screw driver slit at the other end, and can be plugged and locked into the teflon socket, which has been glued in the bottom of the sample tube (ϕ 9 mm i.d. NMR tube).

The trachea is first connected with the glass cannula and the teflon plug outside the sample tube. It is then lowed into the tube. A specially made screw driver, passes through the glass cannula and the trachea to reach the teflon plug. This enables one to lock the plug into the bottom socket by turning. In this manner one end of the trachea is fixed.

The extension of the trachea can be adjusted to its 'natural' length by positioning the glass cannula. The outside of the trachea was immersed in (pH 7.3) phosphate-buffered saline (PBS) which had been made up in deuterium oxide (D_2O). The level of PBS is set 3 cm above the image plane. Figure 4.6 shows a sample and its holder assembly.

The glass cannula is connected to a pressure system (Figure 4.7). By adjusting the water pressostat, the internal pressure of the sample can be changed, indicated by a water manometer.

Prior to imaging, the sample was conditioned by slow inflation to +22 cm H_2O, slow deflation to 0 cm H_2O, and then re-inflation to +22 cm H_2O. The pressure was held constant for at least a minute at the both ends of the first inflation and first deflation.

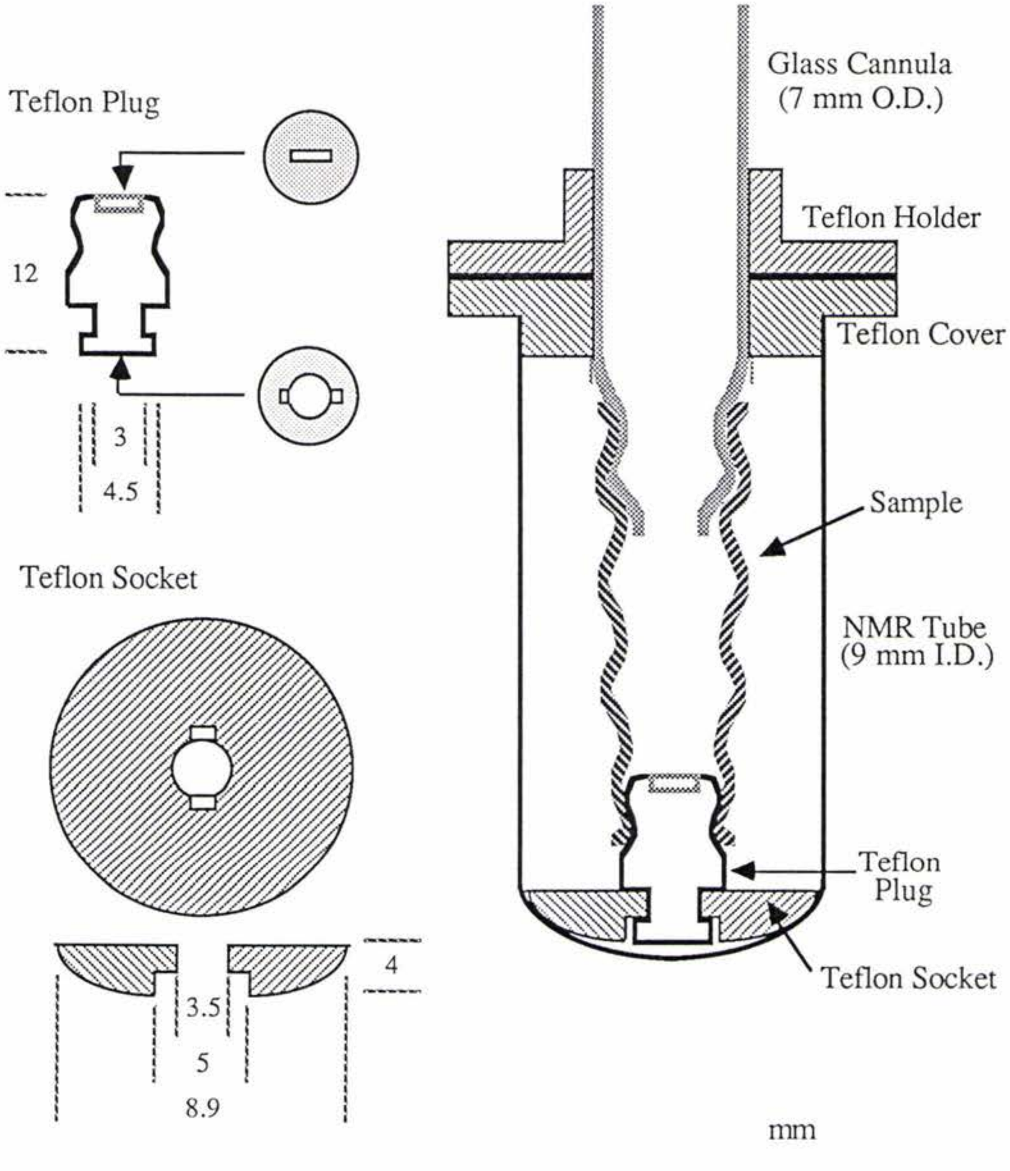

Figure 4.5 Sample Holder Assembly for Rabbit Trachea Experiment (not to scale)

Figure 4.6 Sample Assembly in Rabbit Trachea Experiment

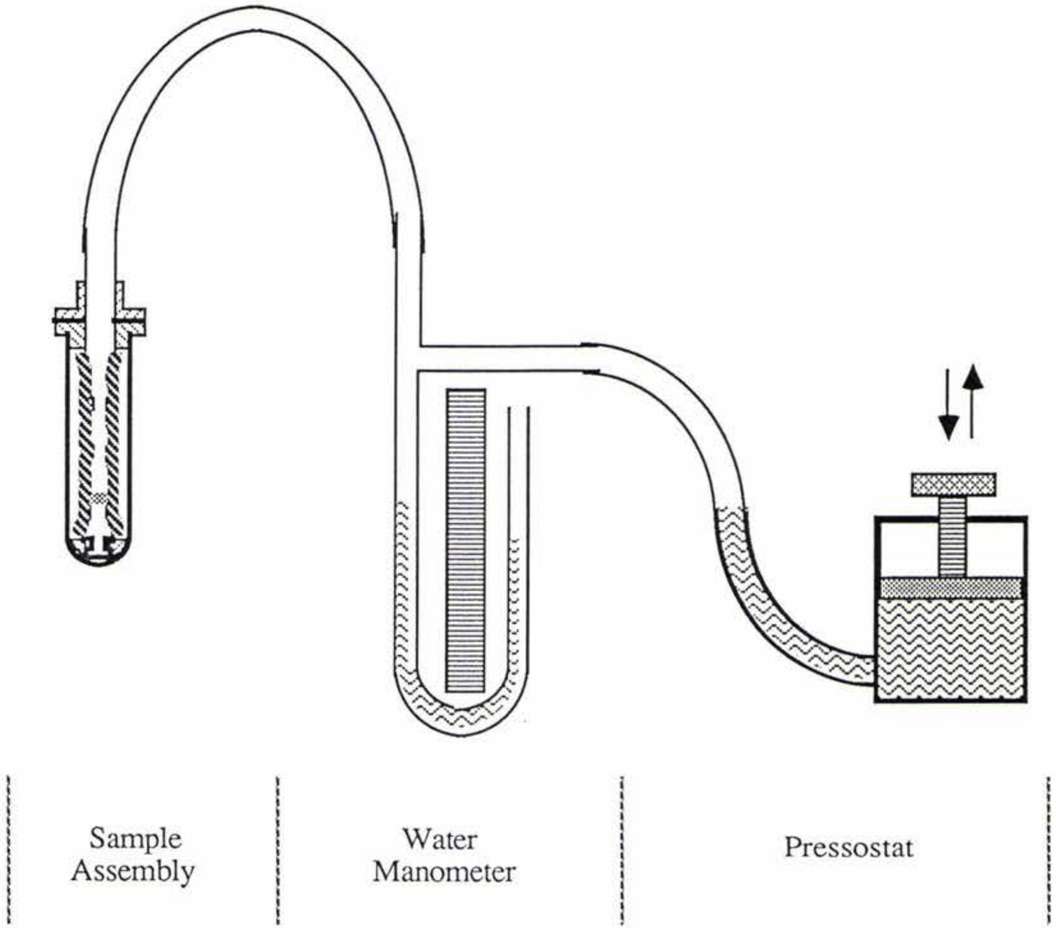

Figure 4.7 Experimental Set Up for Rabbit Trachea Experiment (not to scale)

4.4.2 Results and Discussions

Spectra of the tracheas are obtained during experiments, one from the sixth trachea being shown in Figure 4.8. A FWHM of 70 Hz is observed from the peak, which is due to various tissues of the trachea, but the tissue containing water predominates.

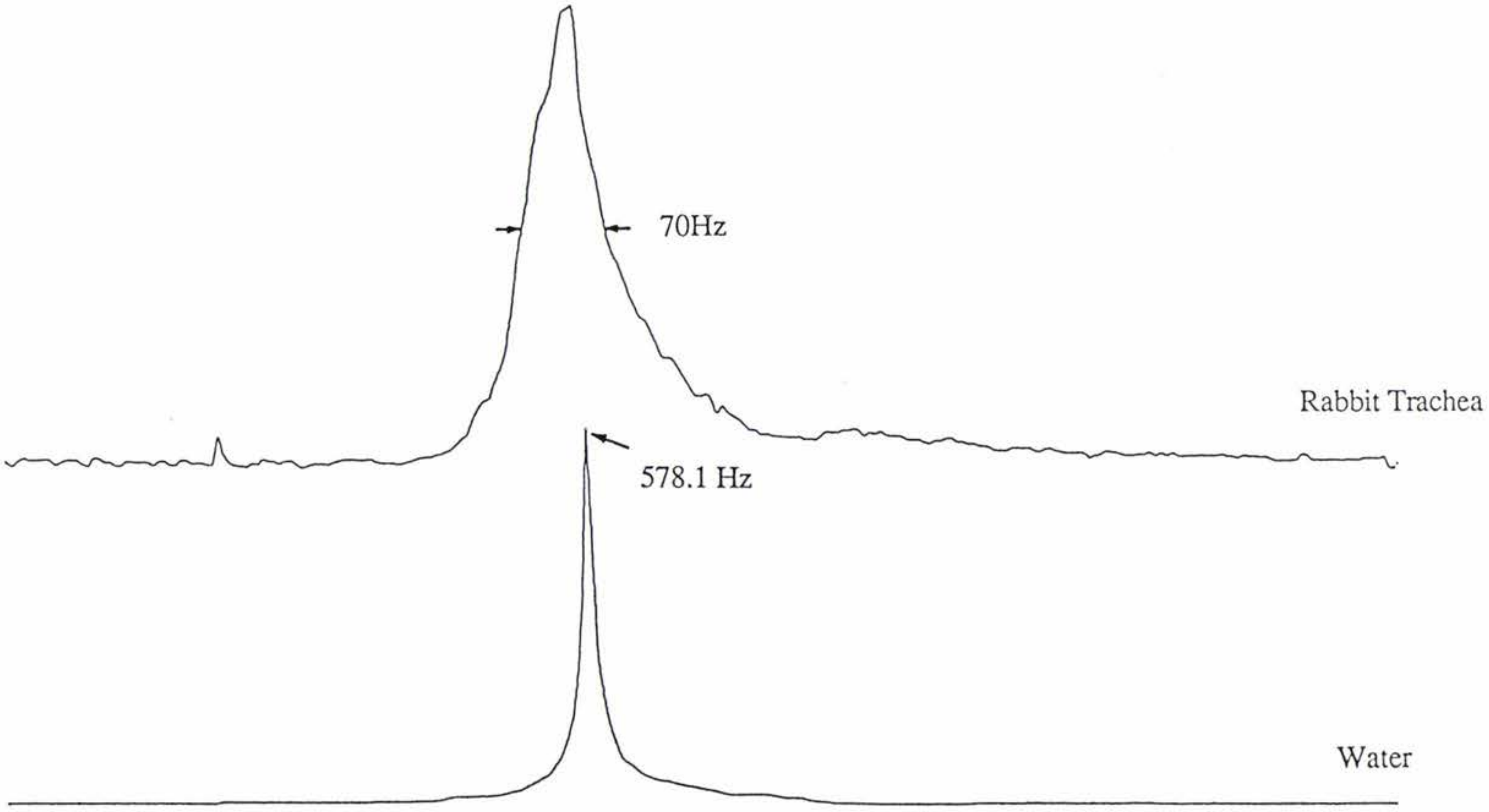

Figure 4.8 NMR Spectra in Rabbit Trachea Experiment

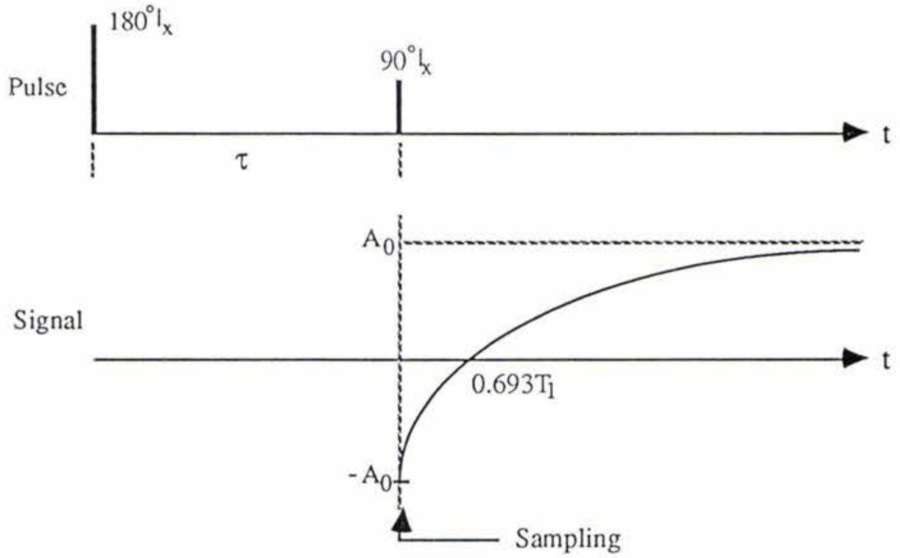

Figure 4.9 T_1 Measurement

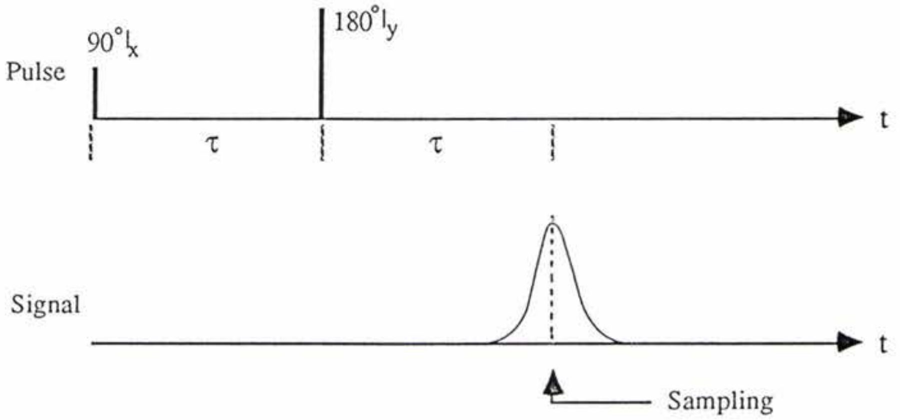

Figure 4.10 T_2 Measurement

T_1 and T_2 of the excised samples of trachealis muscle, cartilage and connective tissue are measured using the inversion-recovery method (Figure 4.9) and the spin-echo method (Figure 4.10), respectively. By varying τ, one can obtain the signal amplitude A(t) as a function of time as

$$A(t) = A(0)[1-2\exp(-t/T_1)] \tag{4.2}$$

for T_1, and

$$A(t) = A(0)\exp(-t/T_2) \tag{4.3}$$

for T_2.

The results are shown in the following table:

Table 4.2 Relaxation Times of Rabbit Trachea

Names	Muscle	Cartilage	Connective Tissue
T_1 (sec)	0.26	0.32	1.0
T_2 (sec)	0.028	0.039	0.069

A repetition time of 1.0 sec was chosen for the experiments. Six tracheas were imaged at transmural pressures of +22, +7, +2, 0, -3, -6, -8, -13, -28, -53 and -95 cm H_2O. One trachea was imaged at pressures of 0, -8, -13, -18, -23, -28, -33, -38 and -43 cm H_2O in order to obtain more detailed collapse process.

Hard-copy print of each image is produced by a dot matrix printer. Because the boundaries of intensity are not well defined by the grey scale if too many levels are used, so that a four level scale has been developed for this experiment. This scale facilitates the data analysis (Figure 4.11). These printed images are used to calculate the imaged tissue area.

A series of cross-sections obtained from one trachea during a series of step changes in transmural pressure is shown in Figure 4.12. The cartilage of the trachea has the colour which is highest on the scale and hence has the greatest content of free water. The epithelium, muscle and some other tissues of the trachea are also apparent as a thin hydrated band. Five of the six tracheas are shown similar with Figure 4.12, collapsing asymmetrically.

One trachea started to collapse symmetrically but finished up asymmetrically collapsed [Figure 4.13 a) and b)]. Trachea #6 appeared to collapse through one end of the cartilage ring passing inside the other end [Figure 4.13 c) and d)]. Figure 4.14 shows the collapsing process in detail.

Physiological and biophysical interpretations of these images are beyond the scope of this thesis and can be found in Reference (46). One obvious conclusion can be drawn. The tracheas collapse asymmetrically in the transverse plane and non-uniformly in the longitudinal direction. This behaviour differs from the symmetrical collapse described previously(47).

It is known(48) that there is a mechanism which limits expiratory flow. In the wave-speed limitation model, forced expiratory flow becomes limited when the local flow velocity reaches the local speed of wave propagations at a point in the airway known as the choke point. A mathematical model of maximal expiratory flow has been developed(45) applicable to collapsible elastic tubes (such as tracheas). In this model the following equation ('tube law') is used to predict the tube cross sectional area A at negative transmural pressures:

$$A = A_0(1-P/P_1)^{-n_1} \qquad (4.4)$$

where P is the transmural pressure difference; A_0 represents the area when P is zero; P_1 is a constant asymptotic pressure related to the choice of n_1 and other curve parameters; and n_1 is a constant.

The model has predicted(49) that flow in a uniform elastic tube can be limited by the wave-speed mechanism at negative (i.e., collapsing) transmural pressure differences only when the tube is sufficiently compliant. For values of n_1 less than 0.5, the wave-speed limitation is not possible at negative transmural pressure.

In our experiment, the n_1 values(46) of (1.2±0.4) in the inter-ring region and (20±7) in the ring plane suggest that rabbit trachea *in vitro* is sufficiently compliant for flow to be limited by the wave-speed mechanism.

a) An Image being interpreted by an eight-level scale

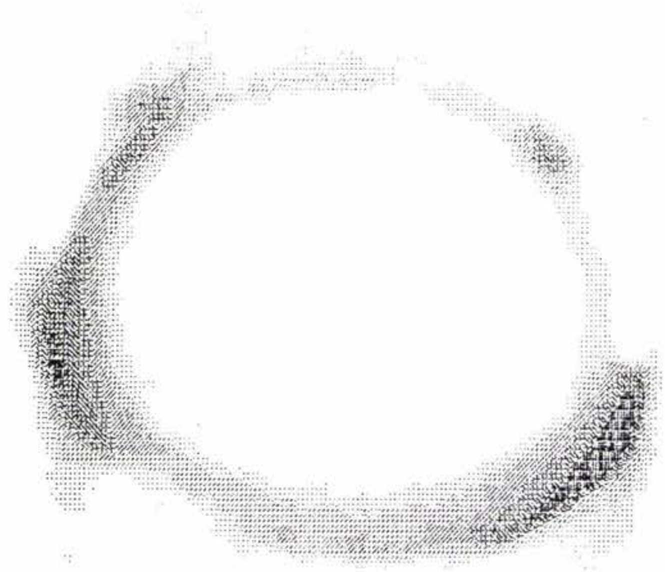

b) The same image being interpreted by a four-level scale

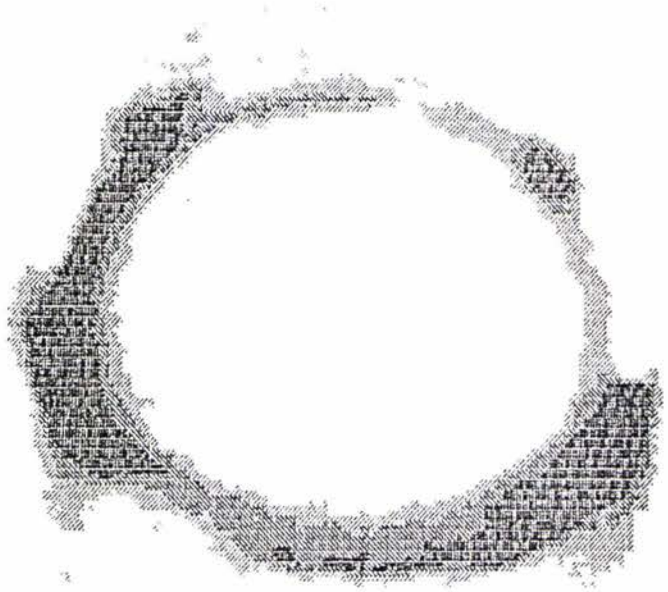

Figure 4.11 Interpretations of the Rabbit Trachea Image

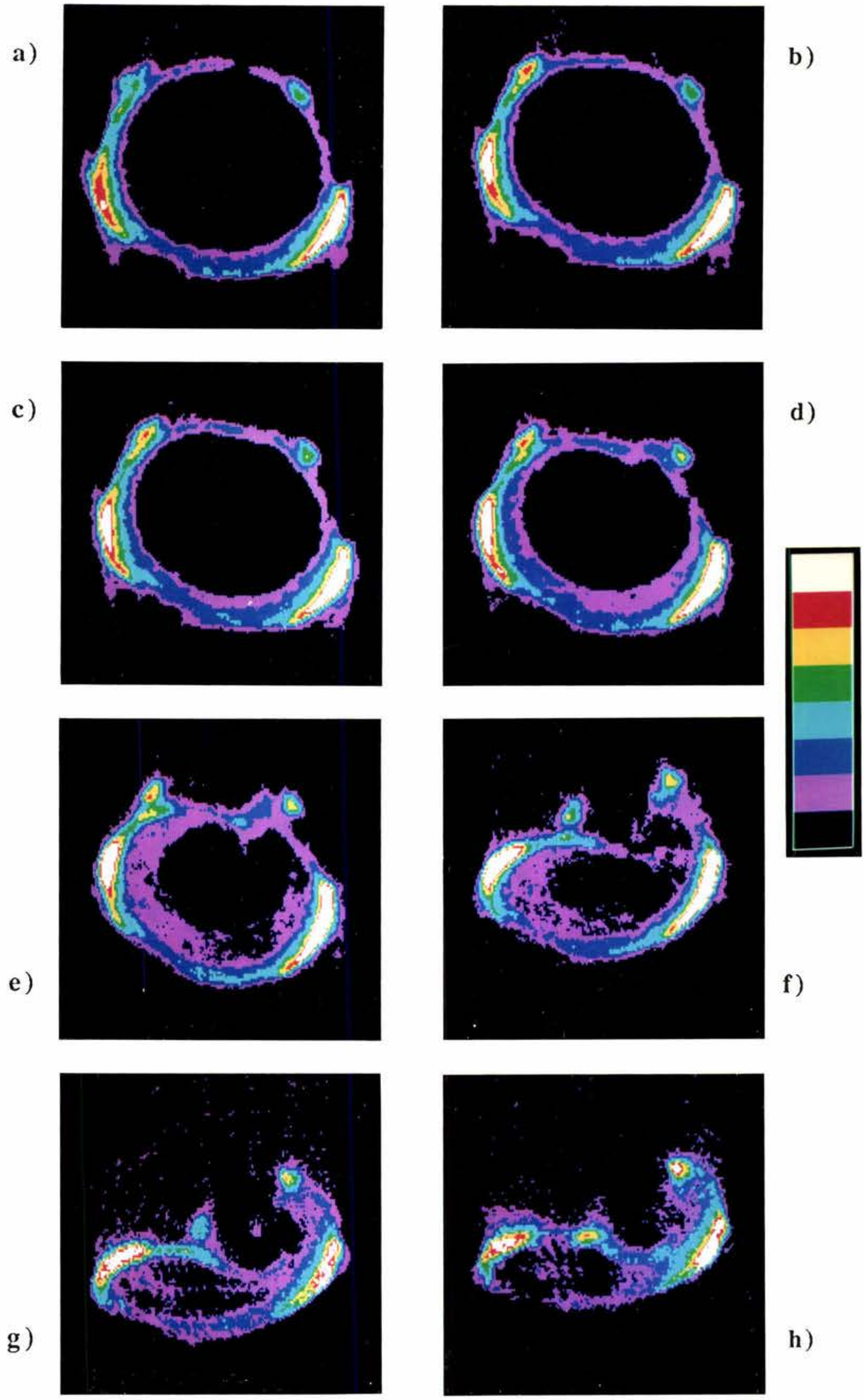

Figure 4.12 Images from the Deflation Sequence of Trachea #2. Reading from a) to h), the pressures at which the images were obtained are: 22,0,-3,-6,-13,-28,-53,-95 cm H_2O.

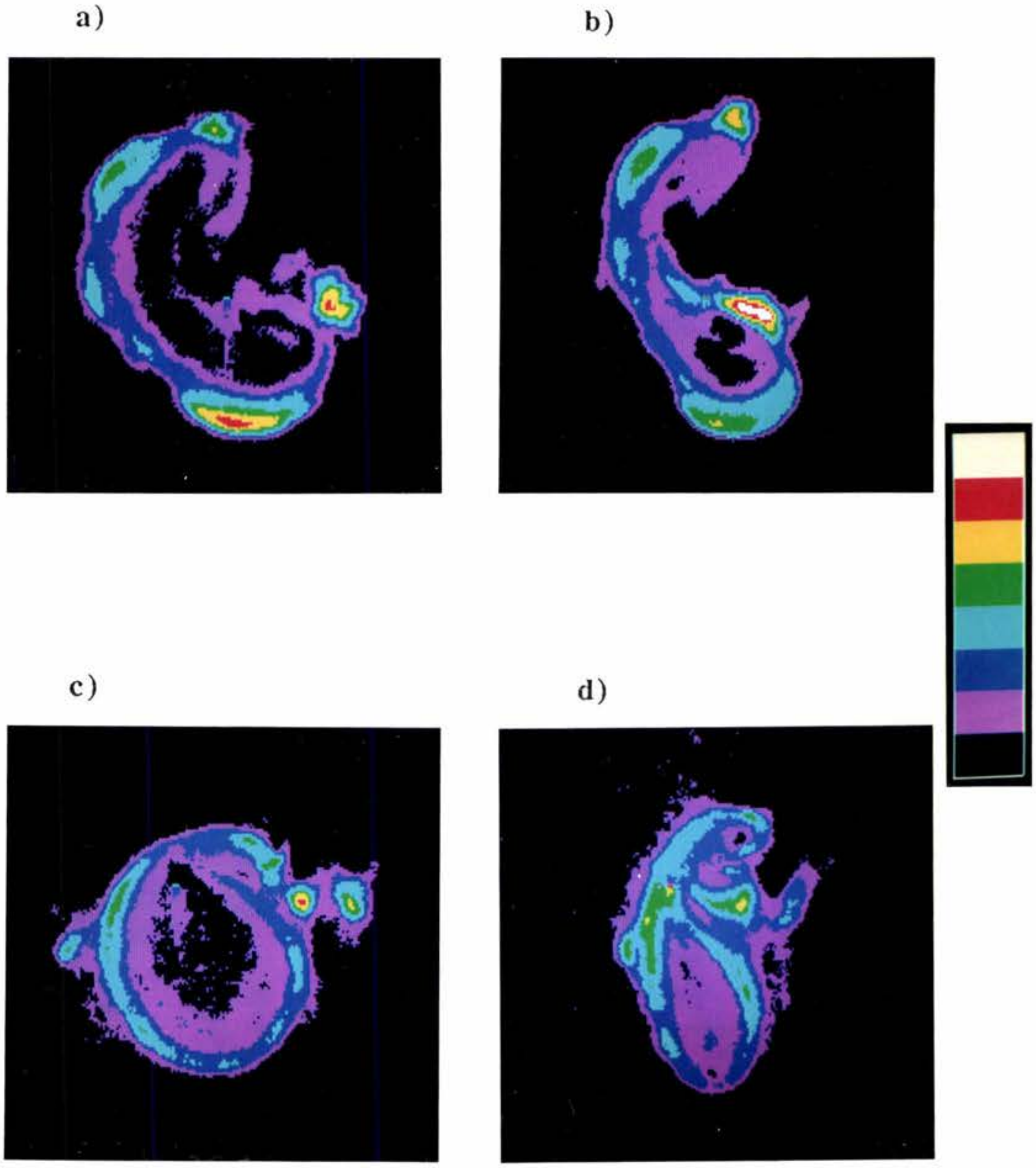

Figure 4.13 Images obtained from Tracheas #5 and #6
a) and b) are from #5, at pressures of -28 and -95 cm H_2O;
c) and d) are from #6, at pressures of -28 and -53 cm H_2O.

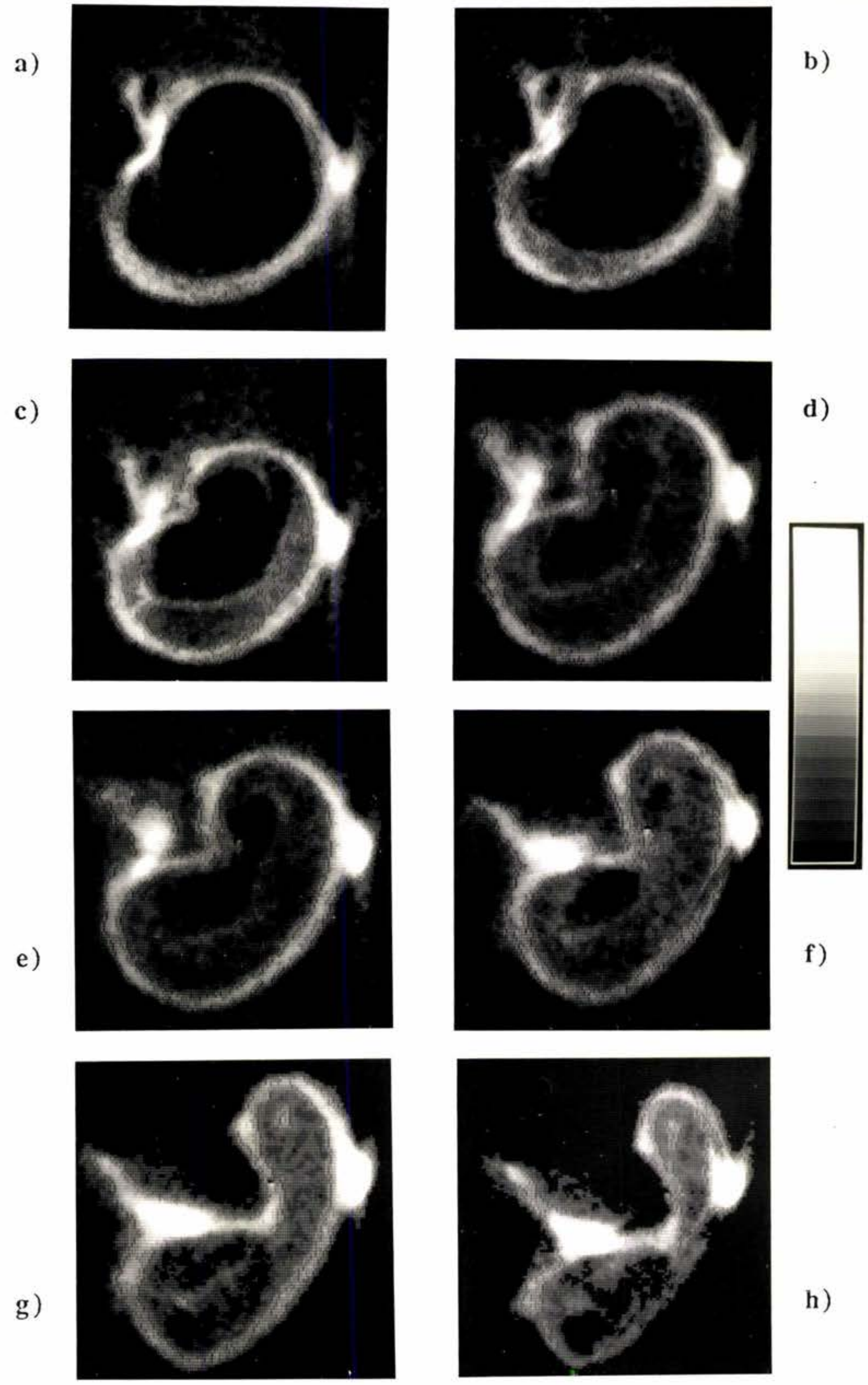

Figure 4.14 Images from Trachea #8 showing the Collapsing Process in detail Reading from a) to h), the pressures at which the images were obtained are: 0,-8,-13,-18,-23,-28,-33,-38 cm H_2O.

4.5 T_1 Contrast Imaging

In order to differentiate the tissues of rabbit trachea, a T_1 contrast experiment was performed.

In theory, if a sample has different local relaxation times, a relaxation time contrast experiment can be performed to identify regions according to T_1 or T_2. This form of identification is very useful when proton densities are not strongly differentiated.

Suppose for example, that one part of the sample has a T_1 of 3 seconds and an other has T_1 of 1 second. By using the pulse sequence shown in Figure 4.15, one can get a different image by varying the time τ. A τ value of 2.1 seconds (0.693×3) will give an image in which "crossover" nulls the signal from the region 1 leaving a signal only from the region 2. If τ equals 0.69 second then the image will contain a contribution only from the region 1.

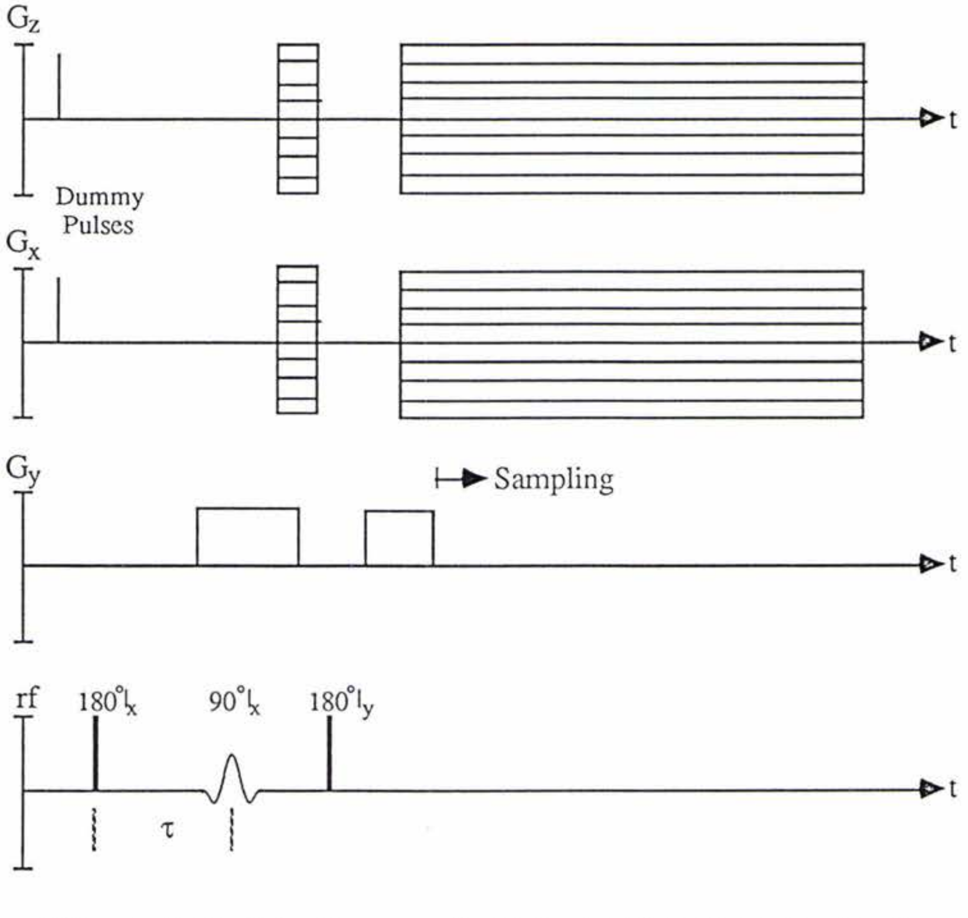

Figure 4.15 Pulse Sequence for T_1 Contrast Imaging Experiment

The T_1 contrast pulse sequence shown in Figure 4.15 is almost identical with that shown in Figure 4.1 except that a 180° rf pulse is preceded just after the start of the experiment.

To differentiate the tissues of rabbit trachea, τ is chosen as 0.2 second, so that the signals from the muscle and cartilage are effectively suppressed. Figure 4.16 shows the proton signal arising from a line of the image in which the region of cartilage and muscle can be clearly identified. The upper trace shows that a line through the normal image using the pulse in Figure 4.1 whereas the lower trace shows that the line in the same position through the T_1 contrast image using the pulse in Figure 4.15. the relatively higher intensity of the signal within the ring identifies it as arising from connective tissue.

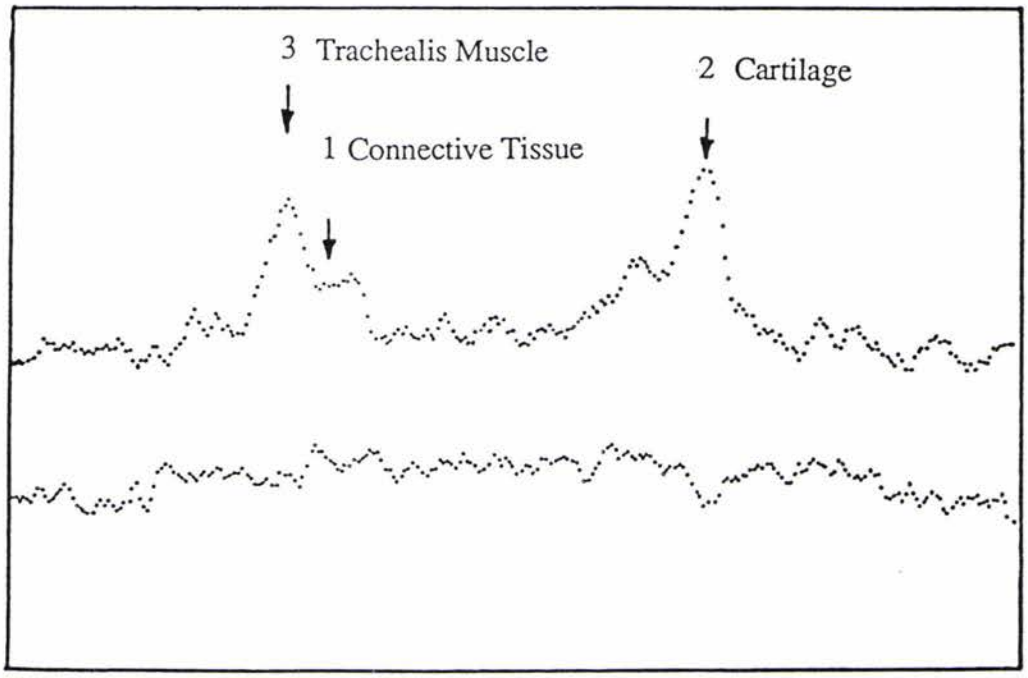

Figure 4.16 Proton Signals through a Line of T_1 Contrast Images
Note that the lower profile has been "phased" to give a positive signal for region 1.

Chapter 5 Dynamic Imaging Experiments

Experimental results of dynamic NMR imaging are presented in this chapter. Some parameter values for the dynamic imaging experiments are given first. Images of velocity and diffusion obtained simultaneously in a 0.7 mm capillary tube at microscopic resolution are described in the second section. The last section gives the distribution 'maps' of velocity and diffusion within a single wheat grain.

5.1 Experimental Considerations for Dynamic Imaging

The choices of δ, Δ, and **g** depend on the relative magnitudes of velocity and diffusion to be measured. In other respects the choice of experimental parameters follows the same guideline as appropriate for a static imaging experiment.

Note that dynamic imaging requires all four quadrants to be sampled and both real and imaginary signals to be stored. In practice less image distortion can be expected from a dynamic imaging experiment if the gradient turning angle is the same as that in a static imaging experiment because of the four quadrant sampling.

The following table gives some parameters for the dynamic experiments which will be described latter.

Table 5.1 Imaging Parameters for Dynamic Imaging Experiments

Names	Poiseuille Flow	Wheat Grain
Sample Dimensions (mm)	ϕ 0.7, ID	~ϕ 4, OD
RF Coil	Small	Medium
Slice Thickness (mm)	2.0	1.5
Bandwidth (kHz)	10	10
Applied Broadening (Hz)	120	120
Repetition Time (sec)	0.3	0.5
Number of Accumulations	32	120
Turning Angle (°)	6	6
δ (ms)	2	0.8
Δ (ms)	5	291
Maximum g (Tm^{-1})	0.996	0.996

5.2 Poiseuille Flow Images

A constant water flow system with a 0.7 mm ID capillary is set up as the imaging object. The velocity map obtained in this experiment agrees well with the Poiseuille velocity distributions.

5.2.1 Experimental Arrangement

The pulse sequence used in the Poiseuille flow imaging experiments is shown schematically in Figure 5.1. Note the similarity with Figure 4.1 in which no PGSE gradient is employed.

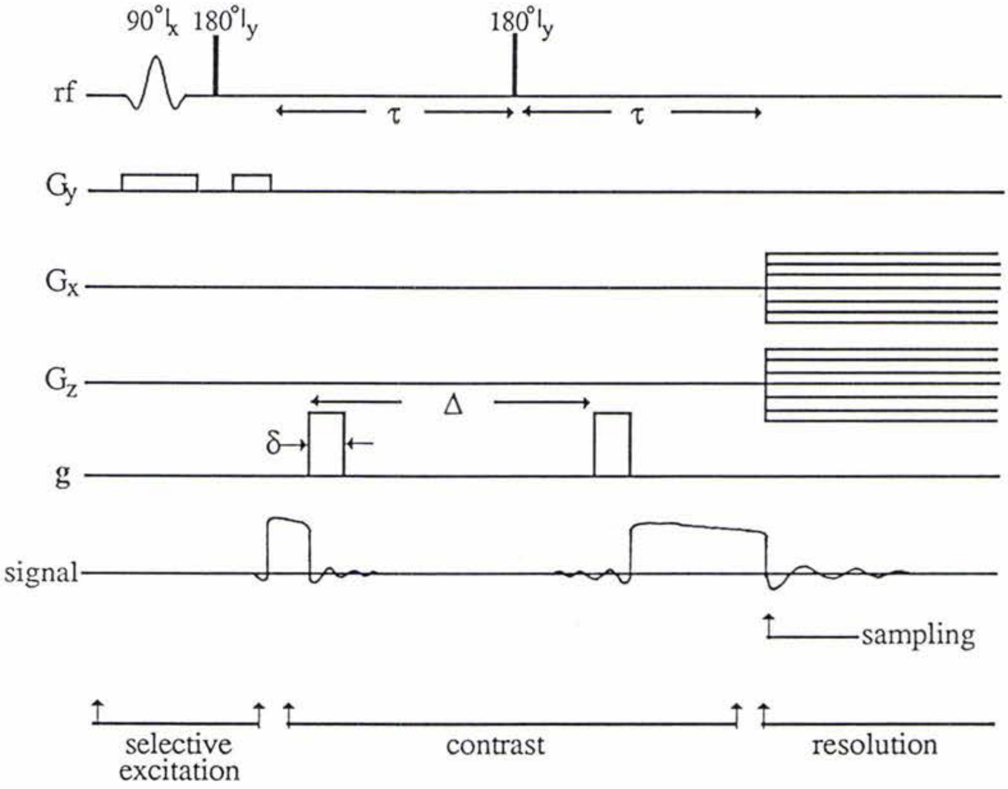

Figure 5.1 Pulse Sequence for the Poiseuille Flow Imaging

The sample system is shown in Figure 5.2. The water (doped with $CuSO_4$ to reduce T_1) is passed through a 0.7 mm ID teflon capillary. The flow can be adjusted by the tap and by the height difference Δh to a rate sufficiently small to keep excited spins inside the rf coil during the entire rf excitation and acquisition period. The existence of invisible tiny air bubbles inside the water is a problem because, during the experiment, these bubbles will stick to the wall of the capillary and accumulate there as the water passes through it, resulting in a decrease of the flow rate. To avoid this effect the water is pretreated in an ultrasonic oscillator for about twenty minutes to drive out the air bubbles. Even then, it is difficult to obtain the calculated average Poiseuille flow rate if there is a low pressure head.

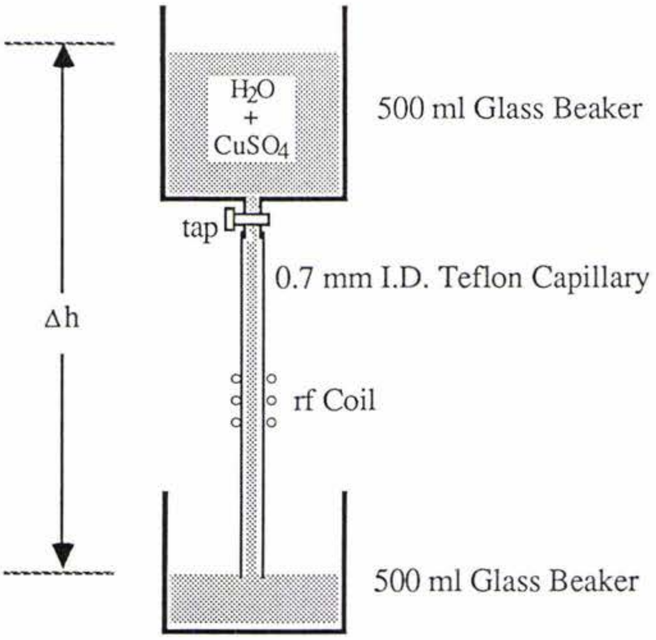

Figure 5.2 Sample System for Poiseuille Flow Experiment

The sample system has been "calibrated" by two methods. The first is the theoretical calculation, as follows.

By considering incompressible fluid with constant viscosity, the Navier-Stokes Equation(50) in cylindrical coordinates can be written as

$$\partial \mathbf{v}/\partial t = -\rho^{-1}\nabla P + \nu\nabla^2\mathbf{v} \tag{5.1}$$

where ρ is the density of the fluid, ∇P is the pressure gradient and ν is the kinematic viscosity of the fluid.

For a steady flow, we have

$$\partial \mathbf{v}/\partial t = 0 \tag{5.2}$$

and

$$\nabla P = -\Delta P/l \tag{5.3}$$

where ΔP is the pressure decrement after the length l of the pipe.

So that from Equation (5.1), the velocity distribution function for a long thin pipe (Figure 5.3) can be derived as

$$v(r) = \Delta P(R^2 - r^2)/4\eta l \tag{5.4}$$

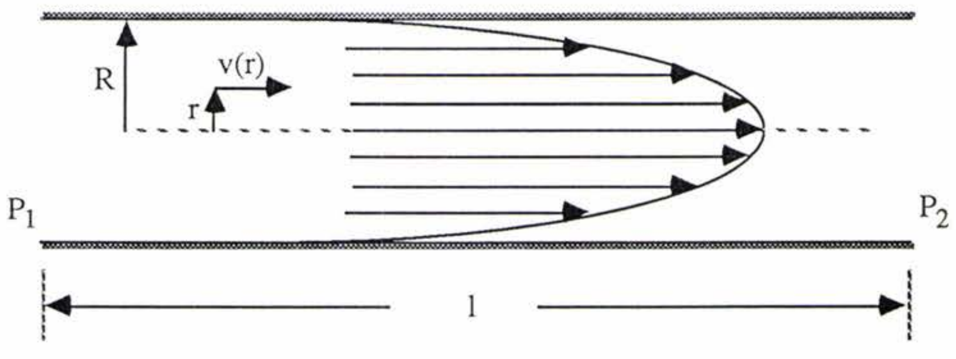

Figure 5.3 Fluid Flow in a Pipe

where η is the dynamic viscosity of the fluid and $\eta = \rho v$, g is equal to 9.8 ms^{-2}, and ΔP can be defined by the height difference Δh as

$$\Delta P = \rho g \Delta h \tag{5.5}$$

Therefore the volume amount of the fluid passing through the pipe in unit time is given by the following expression

$$\begin{aligned} Q &= \int v(r) ds \\ &= \pi R^4 \Delta P / 8 \eta l \end{aligned} \tag{5.6}$$

which gives the average velocity for such a cylindrical pipe as

$$\begin{aligned} v &= Q/\pi R^2 \\ &= R^2 \Delta P / 8 \eta l \\ &= R^2 \rho g \Delta h / 8 \eta l \end{aligned} \tag{5.7}$$

Knowing the length l and the radius R of the pipe, the average velocity is just a function of the height difference Δh.

The second method is by collecting the water in a certain time t and weighting it using Mettler AE 100 electronic balance, so that the average velocity can be calculated by

$$v = (w/\rho)/\pi R^2 t \tag{5.8}$$

The results of these two methods are shown in Figure 5.4, where they agreed well. In the imaging experiment, Δh is set to about 80 mm, thus giving an expected average flow rate of 4.0 mms^{-1}.

Note that the data in Figure 5.4 were obtained over a few minutes after sonication during which bubbles were absent. The dynamic imaging experiment, however, requires a much longer time period during which bubbles were observed to form.

Figure 5.4 Calibration of the Poiseuille Flow System

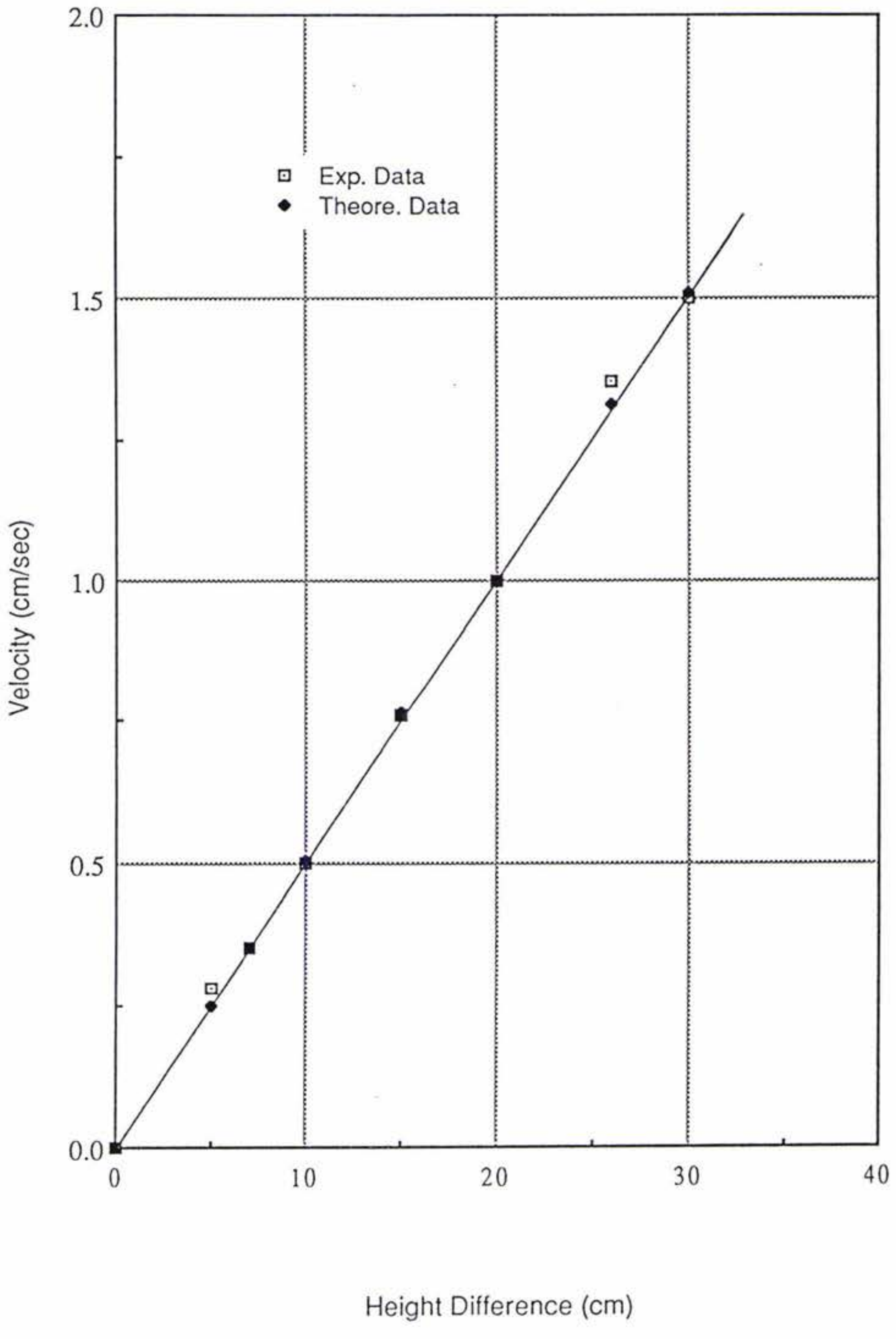

The magnitude of the PGSE gradient g has to be calibrated so that it gives an equal magnitude increment during each data image. The calibrated results are stored in TI 980A memory (cf Appendix A.6) so that the experiment is fully automatic. The maximum g used was 0.996 Tm^{-1}, which corresponds to a maximum current of 10 A.

5.2.2 Results and Images

Figure 5.5 shows the 18 successive real and imaginary images obtained as $\mathbf{q}$ is increased by stepping the PGSE gradients in 18 intervals. Note that a special colour scale is used so that both positive and negative values can be interpreted. These images clearly exhibit alternating phase rings which grow progressively more closely spaced as the PGSE gradient is increased. These rings arise because of the distribution in molecular velocity from zero at the capillary wall to a maximum at the center. A 90° phase difference can be seen from the real images and their corresponding imaginary images. Note that the the phase has to be set correctly at the spectrometer before starting the experiments.

As predicted before, the first real image is exactly as an ordinary static image, and the first imaginary is effective nothing. As g is increased, signal attenuation increases because of diffusive motion. Signals from the last real and imaginary images are effective zero, which avoids the truncation of $\mathbf{q}$ space data when zero filling.

Maps of diffusion coefficients and velocity are shown in Figure 5.6, along with a typical dynamic displacement profile from within the image. Figure 5.7 shows stacked profile plots for velocity and diffusion images. It is immediately apparent that the diffusion image is essentially uniform while the velocity image exhibits a cylindrical symmetric variation consistent with Poiseuille flow.

By using Equation (2.94) and (2.99), the velocities and diffusion coefficients of the image can be calculated. For example, the velocity at one coordinate given by Figure 5.6 is (4.30 ± 0.09) mms^{-1}, and the diffusion coefficient of that is 6.0×10^{-9} m^2s^{-1}. Note that to obtain the better diffusion coefficient, Figure 2.36 has been incorporated.

5.2.3 Discussions and Conclusions

From the above results, it can be seen that the dynamic NMR imaging technique works well. While other workers have employed diffusion and flow contrast methods, there are three novel aspects in the present results. They are, the measurement of a Poiseuille velocity distribution inside such a small (0.7 mm) capillary, the simultaneous measurement of velocity and diffusion distribution, and the application of dynamic contrast with microscopic resolution in NMR imaging.

A comparison of the experiment velocity with the Poiseuille distribution (Figure 5.8 and Table 5.2) shows excellent agreement although the absolute velocity is less than that calculated on the basis of Equation (2.94) because of the air bubble problem.

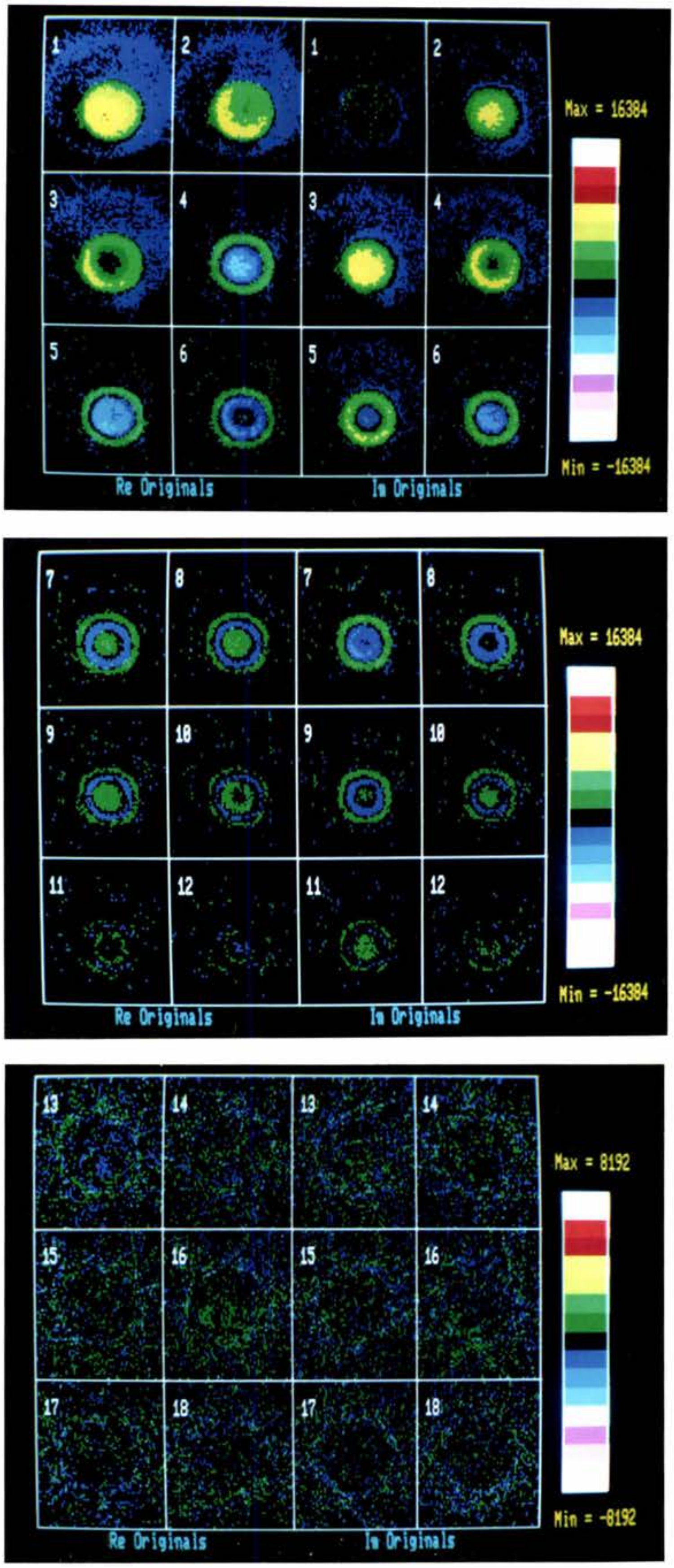

Figure 5.5 Data Images of the Poiseuille Flow Experiment

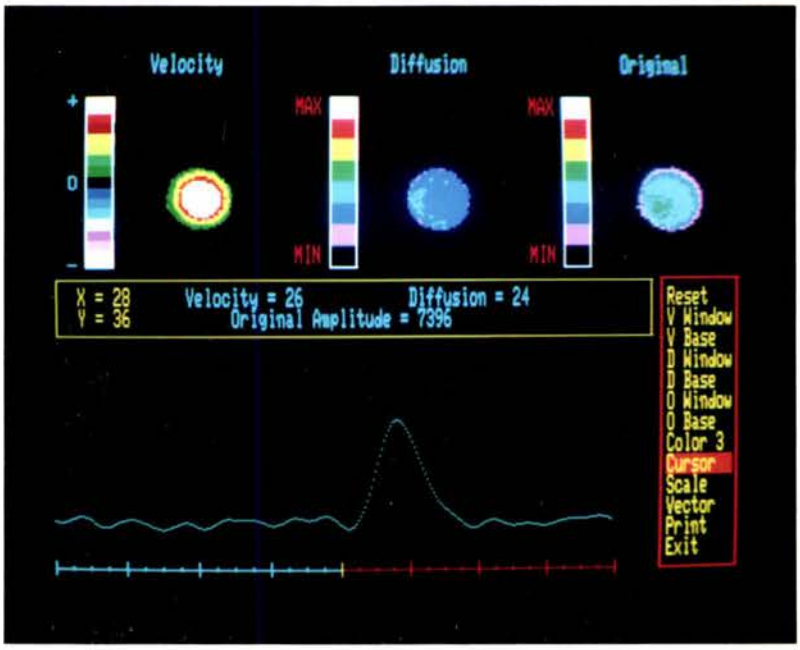

X = 28
Y = 36
Velocity = 26
Diffusion = 24
Original Amplitude = 7396

Figure 5.6 Velocity and Diffusion Images of Poiseuille Flow

a) The Velocity Image

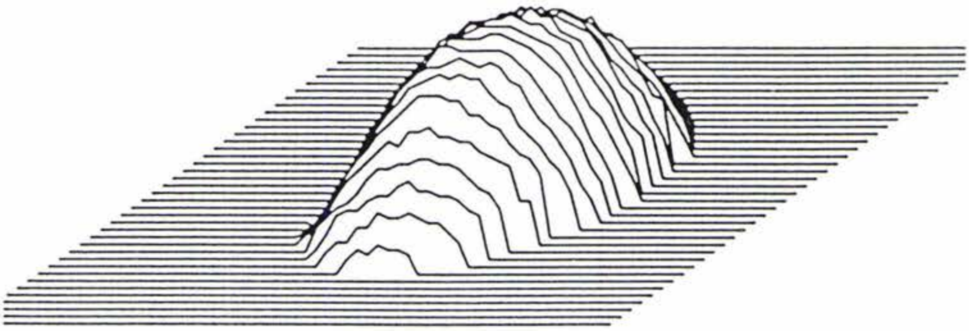

b) The Diffusion Image

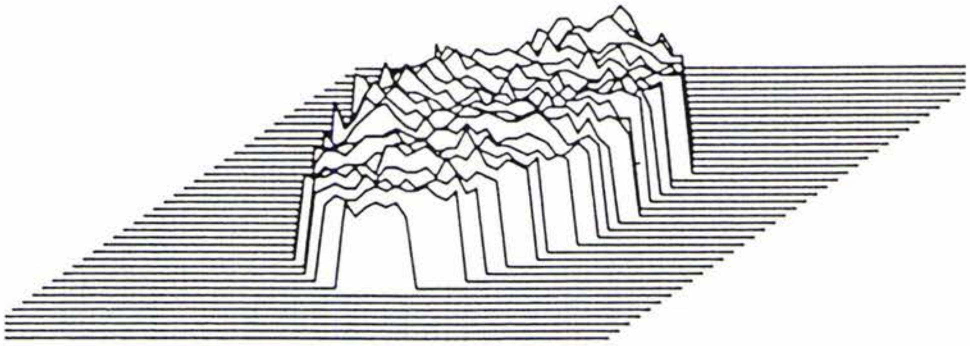

Figure 5.7 Stacked Plots of the Poiseuille Flow Image

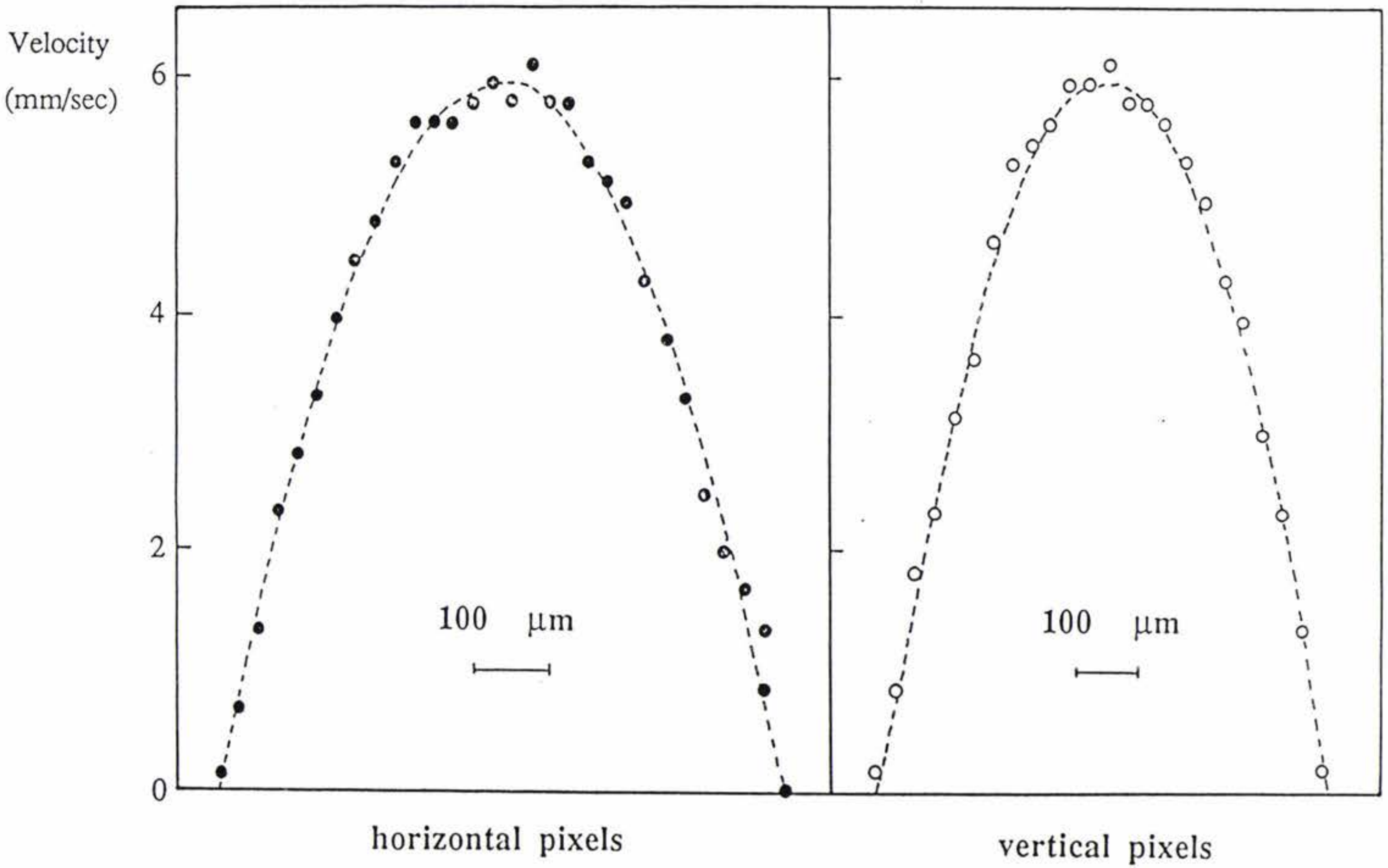

Figure 5.8 Velocity Profiles of the Poiseuille Distribution

Table 5.2 Velocity Rate

	r = 0	r = R/2
Experimental Data (ms^{-1})	$(6.1\pm0.1)\times10^{-3}$	$(4.50\pm0.09)\times10^{-3}$
Theoretical Data (ms^{-1})	$(7.7\pm0.6)\times10^{-3}$	$(5.8\pm0.5)\times10^{-3}$

* The experimental data is calculated using Equation (2.94), where $N = 256$, $n_D = 18$, $g = 0.996\ Tm^{-1}$, $\gamma = 2.68\times10^8 radT^{-1}s^{-1}$, $\delta = 2\times10^{-3}$ s, $\Delta = 5\times10^{-3}$ s.

** The theoretical ones are calculated using Equations (5.4) and (5.5), where $\rho = 1\times10^3\ kgm^{-3}$, $g = 9.8\ kgm^{-2}$, $\Delta h = 80\times10^{-3}$ m, $l = 3.73$ m, $\eta = 0.833\times10^{-3}$ (28°C), and $R = 0.35\times10^{-3}$ m

In the current dynamic imaging experiment we use the FWHM to calculate the diffusion coefficient D. This is actually based on an assumption that the peak after the FFT in the dynamic displacement space is a **gaussian**. To test this assumption we can analyze the data in the original **q** space domain, for which the dependence of signal amplitude on **q** is also gaussian. The test involves taking the modulus of the local signal (to remove the oscillatory effects of velocity) and plotting $\ln[|S(n)|/|S(0)|]$ vs g^2. For a gaussian the result should be a straight line where the slope yields the diffusion coefficient.

We know however that during an experiment the appearance of noise is unavoidable. Therefore the complex peak function S(n) is the superposition of the 'pure' gaussian h(n) and noise $\sigma(n)$, as

$$S(n) = [\ h_R(n) + ih_I(n)\ ] + [\ \sigma_R + i\sigma_I\ ] \tag{5.9}$$

so that

$$|S(n)| = [\ (h_R{}^2 + h_I{}^2) + 2(\ h_R\sigma_R + h_I\sigma_I\ ) + (\ \sigma_R{}^2 + \sigma_I{}^2\ )\ ]^{1/2} \tag{5.10}$$

Therefore the signal modulus before FFT consists of three parts. The first part is the 'pure' gaussian function; the second part is a fluctuating noise term, which will have bigger proportional effect as h(n) becomes smaller; and the third part is a constant. This constant can be easily identified and subtracted before plotting the data in semi-logarithm form as in Figure 5.9.

"Corrected signal modulus" from one of the central pixels from each of the Poiseuille flow data images was plotted in Figure 5.9.It is obvious that the data didn't fit a straight line, which it should do if it is a gaussian. Figure 5.9 b) and c) used fewer data in different ranges, which gave diffusion coefficients of $10.5\times10^{-9}\ m^2s^{-1}$ and $3.5\times10^{-9}\ m^2s^{-1}$ respectively. It is clear that the value calculated from the FWHM in the conjugate domain ($6.0\times10^{-9}\ m^2s^{-1}$) is just a compromise.That is probably the reason why we obtained an anomalous diffusion value. In other words, using FWHM to fit the gaussian peak and calculate the diffusion is dangerous unless we can certain that the data is indeed gaussian. In the present instance the non-gaussian behaviour of the data is curious and will be the subject of future work.

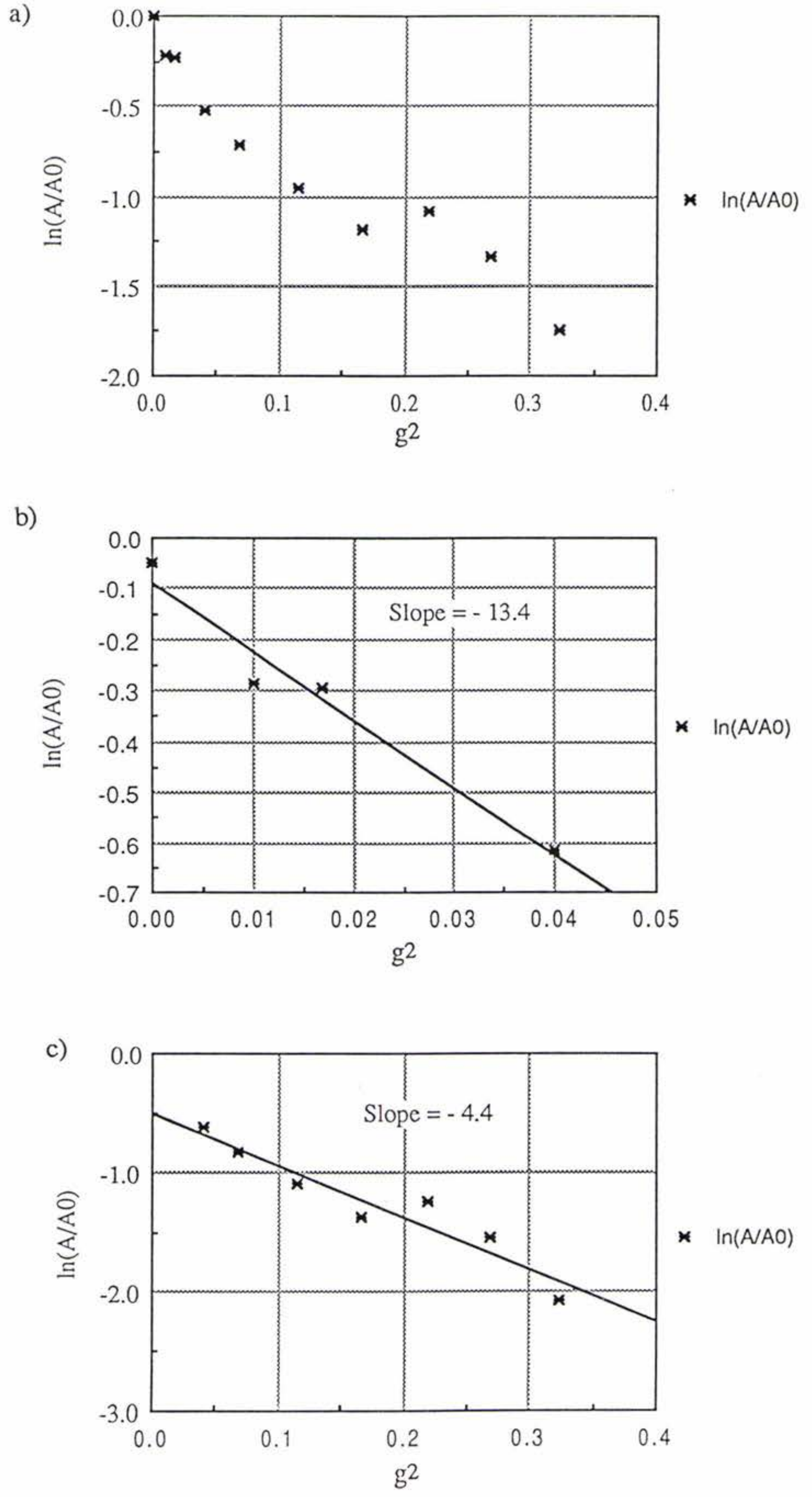

Figure 5.9 Noise Effect in Diffusion Calculation

A possible cause of this effect is finite velocity spread. In Section 2.3.5 we discussed the extra broadening due to velocity spread. A numerical calculation is given as follows.

The image is 0.7 mm across 30 pixels, so that the pixel size Δx is 2.3×10^{-5} m. The maximum shear rate appears at the edge of the capillary, so that the maximum velocity spread between the pixels is

$$\begin{aligned}\Delta v_{max} &= v_{pixel2} - v_{pixel1} \\ &= v_{pixel2} \\ &= \Delta p(R^2-r^2)/4\eta l \qquad (5.11)\end{aligned}$$

where r is equal to $(R-\Delta x) = 3.27\times10^{-4}$ m, and $\Delta p = 80\times10^{-3}\times100\times10^3/10$ Pa.

This yields $\Delta v_{max} = 1\times10^{-3}$ ms^{-1}. Substituting this value into Equation (2.106), we get an extra broadening due to the velocity spread equal to 4.5×10^{-10} m^{2}s, which is practically negligible. It does not provide an explanation of the curious diffusive motion observed here.

5.3 Wheat Grain Images

The purpose of this experiment was to investigate quantitatively the water translocation process within a single wheat grain. The experiment was motivated by a desire to learn more about nutrient transport. It is believed that movement of water and transport of solutes in biological systems are closely interrelated(51). No *in vivo* measurement of localized water movement has been previously performed on the submillimeter scale. In our experiment, *in vivo* **velocity and diffusion maps** are obtained successfully. Although detailed physiological interpretations of the data are still not quite clear at the moment, the obtained images are consistent with some models of grain physiology.

5.3.1 Experimental Arrangement

A wheat ear is shown schematically in Figure 5.10. Samples were obtained from a greenhouse at the Plant Physiology Division, DSIR. The wheat ears used for imaging were selected about 14 days after anthesis when they were approximately half way through the grain filling stage of development. We found during the experiments that the age of the wheat is extremely important. No obvious flow can be observed when the sample is only a few days older.

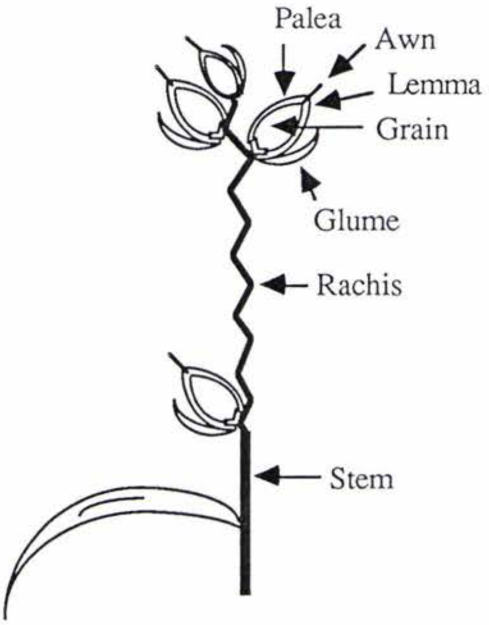

Figure 5.10 Schematic Diagram of a Wheat Ear

The wheat grain used for imaging is selected from the second to forth spikelet from the top of the ear. Then the spikelets below and above the selected one have to be removed very carefully, and the rachis above the selected spikelet also has to be cut off. The next step is to cut off the awns and remove the glumes of the selected one, but keep its palea and lemma. There are two grains at each spikelet. One of these can be used to test for signal strength, some pairs having more free water than others. If the signal is good enough to produce a reasonable image, the companion grain is used as the imaging object.

A thin layer of moist cotton fibre was then wrapped around the exposed rachis and a 'stop' mark was to taped to locate the imaging plane of the grain (Figure 5.11). Figure 5.12 shows a sample and the experimental arrangements.

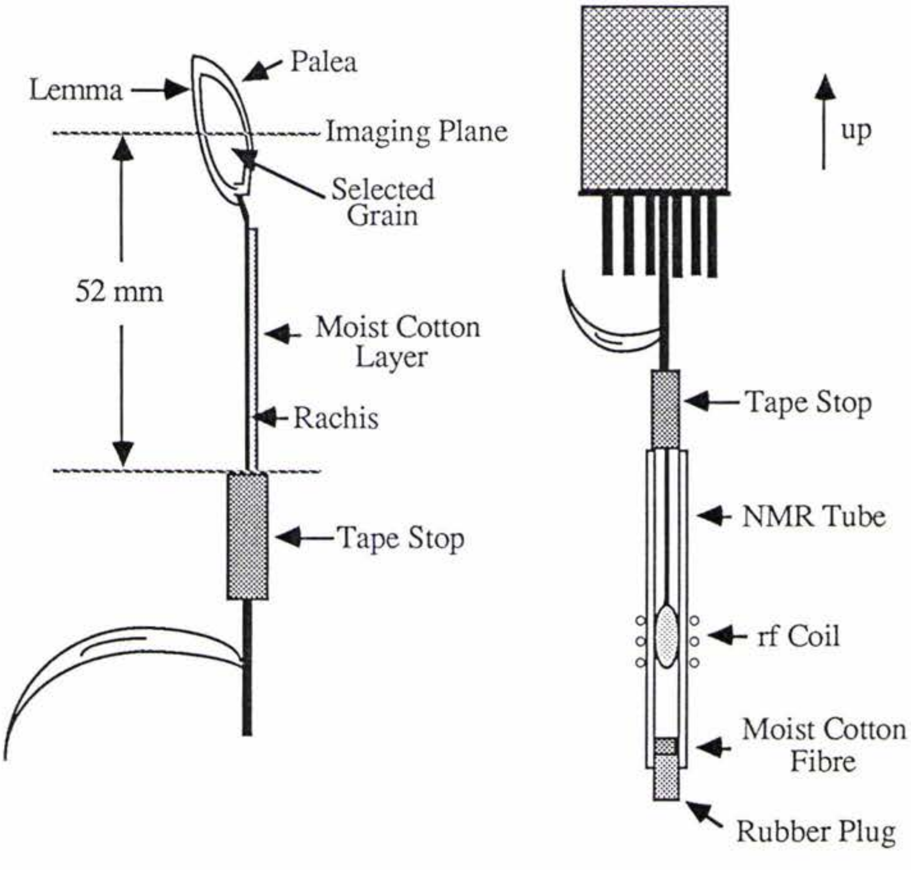

(a) Sample Parperation (b) Experimental Arrangement

Figure 5.11 Experimental Parperation for Wheat Grain Imaging

The cross-section of a wheat grain is shown schematically in Figure 5.13. It has been estimated that there are about 40 sieve tubes(52) in the vascular bundles running along the furrow midway along the length of the grain, with an average internal radius of 1.4 $\mu m^{(53)}$, giving a total cross-section area of sieve tubes 0.25×10^{-3} mm^2. The average velocity over the vascular bundle area has been estimated(54) by ^{14}C measurement to be of order 200 μms^{-1}. This rate is low in comparison with the Poiseuille experiment and therefore the Δ of the pulse sequence has to be stretched to sense this tiny velocity.

However the average T_2 for the grain has been measured at around 34 ms, so that increasing Δ as required leads to a catastrophic loss of signal. This loss due to transverse relaxation can be avoided by the use of the stimulated echo sequence shown in Figure 5.14. This sequence protects the signal from T_2 relaxation between the "store" and "recall" pulses by tipping the magnetization to the longitudinal axis, although it will be subject to T_1 relaxation during this period. T_1 is measured as 0.3 s

a) A wheat grain sample

b) Sample and NMR imaging system

Figure 5.12 Experimental Arrangement for the Wheat Grain Imaging

and the observation period is chosen as a suitable compromise of 291 ms. Due to the weak signal, more accumulations have to be used to improve the S/N. So that it takes about 100 minutes to reconstruct one data image set.

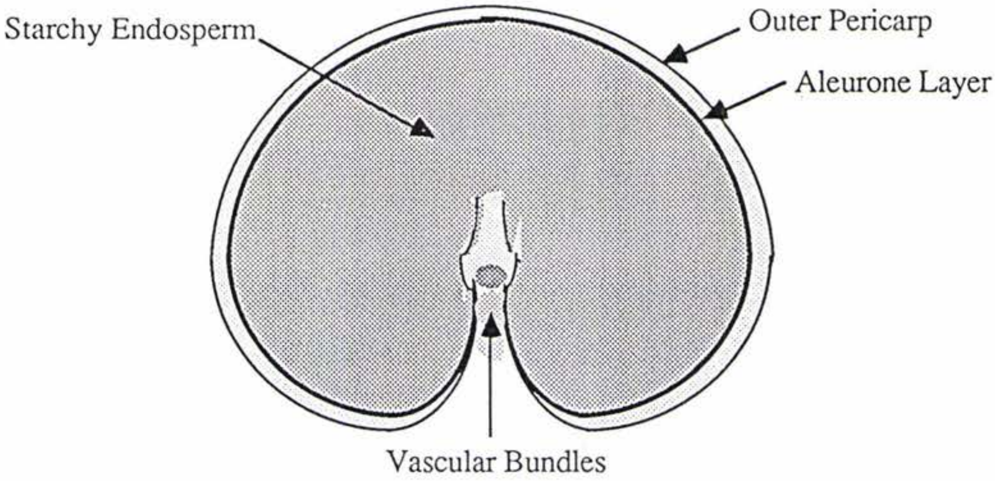

Figure 5.13 Transection of a Wheat Grain

5.3.2 Results and Images

Velocity and diffusion maps of a single wheat grain have been obtained successfully from three pots of wheat. A typical *in vivo* image is shown in Figure 5.15(a). it can be seen that there is a bright spot right in the centre of the grain, which is the place of vascular bundles. After the *in vivo* imaging experiment, the same wheat grain has been detached and imaged again under the same conditions. The *in vitro* image is shown in Figure 5.15(b), where the flow stopped of course. The more detailed data about the central region can be found in Figure 5.16 and Figure 5.17. From these results, an average velocity over pixels in the vascular bundle area can be calculated as about (78±2) μms^{-1} while the diffusion is about $8.3 \times 10^{-10}\ m^2s^{-1}$.

It should be noted that when this average velocity is attributed to the much smaller vascular bundle area of $0.25 \times 10^{-3}\ mm^2$, a sieve tube water velocity much higher than that observed for ^{14}C labeled solute flow is indicated. This suggests that water flow occurs through semi-permeable barriers which impede the free flow of solutes. It should also be noted that some reversed flow is apparent in the endosperm tissue, suggesting that water is circulating within the grain.

Figure 5.18 gives the stacked plots for the images shown in Figure 5.15. The difference of the *in vivo* and the *in vitro* velocity images is obvious. Note that there is not much difference between the *in vivo* and the *in vitro* diffusion images.

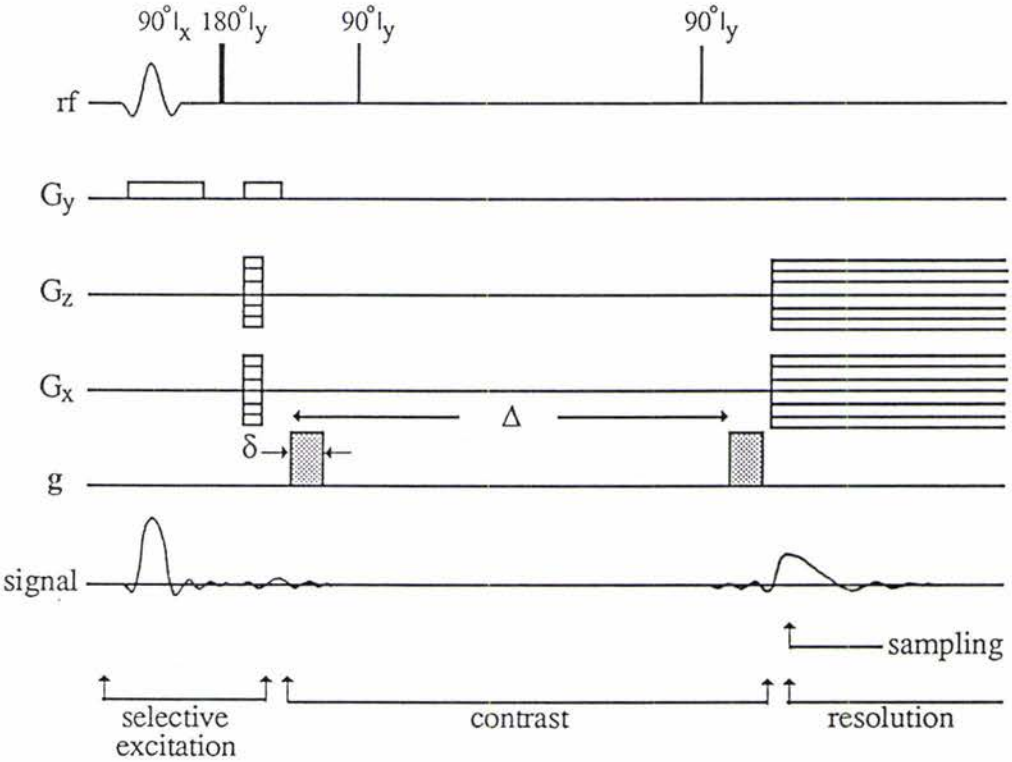

Figure 5.14 Pulse Sequence for the Wheat Grain Imaging

a) *In vivo* Images

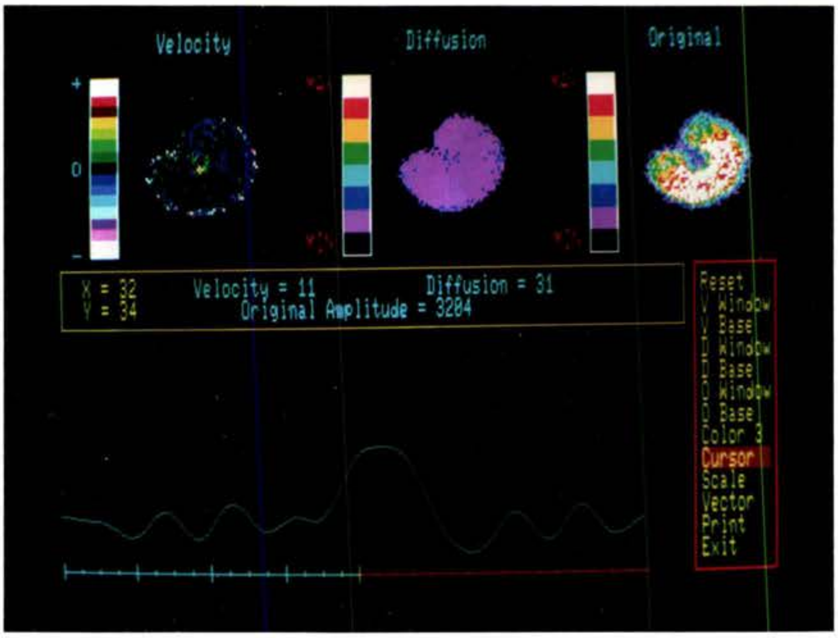

X = 32 Velocity = 11 Diffusion = 31
Y = 34 Original Amplitude = 3204

b) *In vitro* Images

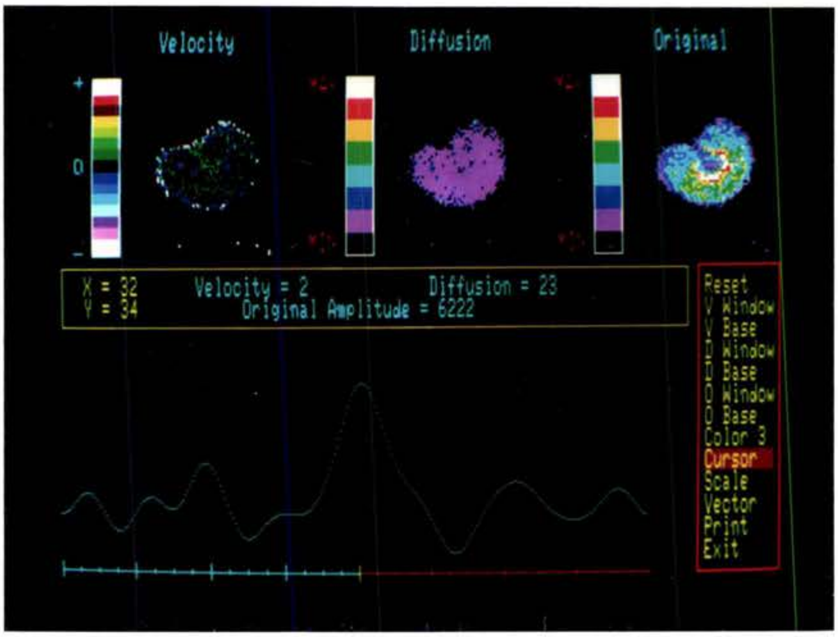

X = 32 Velocity = 2 Diffusion = 23
Y = 34 Original Amplitude = 6222

Figure 5.15 Velocity and Diffusion Maps of a Wheat Grain

x	29	30	31	32	33	34	35	36
y								
29								
30			1	1	0	2	2	
31		2	1	1	-2	-3	2	2
32	-2	-1	3	3	-3	-1	2	2
33	-3	1	-5	15	-3	6	2	2
34	-3	0	14	11	15	8	2	0
35	-2	3	1	15	5	1	2	-1
36		-2	3	-1	-2	-2	-1	

(a) Central Region of the *in vivo* Velocity Image

x	29	30	31	32	33	34	35	36
y								
29								
30		1	5	1	1	2	-2	
31	-2	0	-1	4	1	3	2	-1
32	0	-1	0	3	4	-1	1	-1
33	-1	-3	-2	3	7	2	4	5
34	-4	0	1	2	-2	0	-3	1
35	-4	-1	0	-1	1	0	1	0
36		-1	-2	0	0	1	1	

(b) Central Region of the *in vitro* Velocity Image

Figure 5.16 Central Regions of the Wheat Grain Velocity Images

x	29	30	31	32	33	34	35	36
y								
29								
30			19	20	20	36	21	
31		33	24	26	37	21	22	24
32	21	19	22	24	24	18	32	20
33	18	17	33	21	18	29	23	26
34	19	16	27	31	16	28	22	23
35	16	35	28	31	30	20	28	23
36		22	25	25	25	26	27	

(a) Central Region of the *in vivo* Diffusion Image

x	29	30	31	32	33	34	35	36
y								
29								
30		16	25	27	23	16	17	
31	17	18	28	17	18	17	20	17
32	18	22	21	15	22	23	20	21
33	20	21	20	16	17	21	24	17
34	21	20	19	23	23	16	20	13
35	25	23	18	18	17	15	15	25
36		24	20	20	21	22	19	

(b) Central Region of the *in vitro* Diffusion Image

Figure 5.17 Central Regions of the Wheat Grain Diffusion Images

a) *In vivo* Diffusion Image

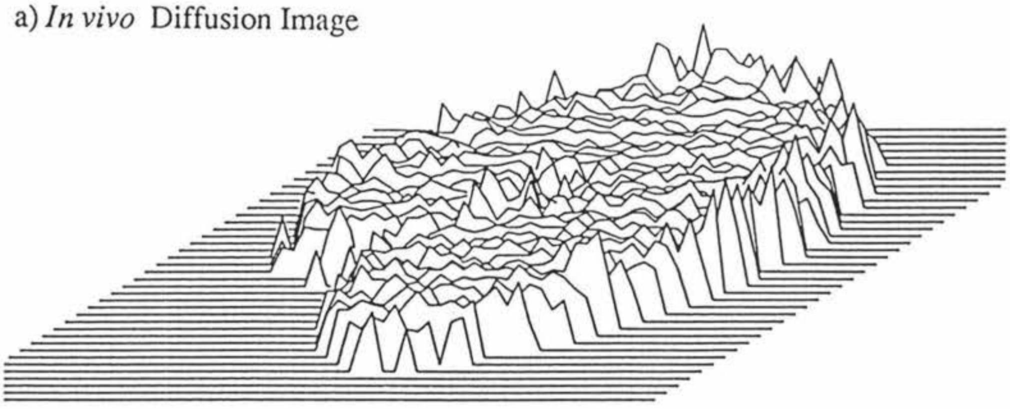

b) *In vivo* Velocity Image

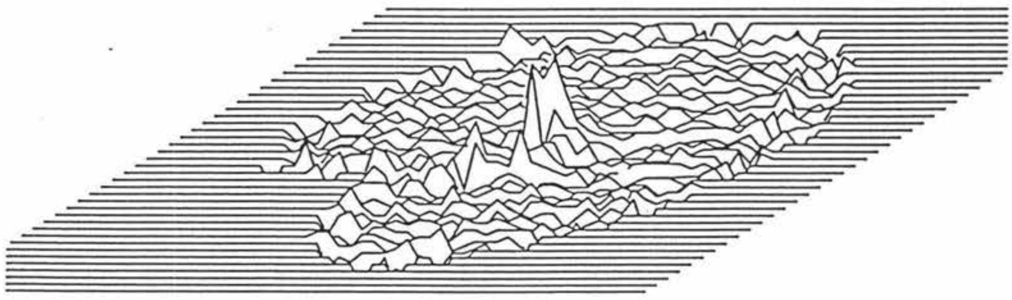

c) *In vitro* Velocity Image

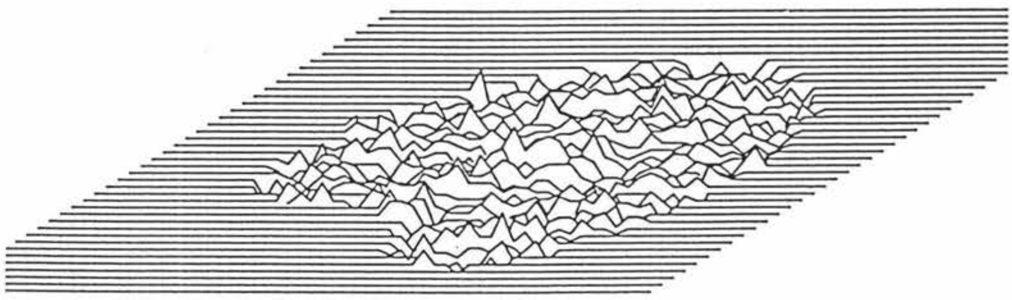

Figure 5.18 Stacked Plots of the Wheat Grain Images

5.3.3 Discussion

The above velocity map is consistent with the following model.

The nutrient substances (such as sucrose) carried by the water translocate to the growing grain via the vascular bundles (the phloem), along the length of the furrow of the grain(55). The nutrients are accumulated inside the endosperm of the grain, with the water flowing back. The high positive velocity in the vascular bundles area and the slightly negative velocity over the rest of grain support this model. Note that the velocity image is consistent with flow in a closed system where there is net zero flow over the whole wheat grain cross section. The experimental mass flow rate in the vascular bundle area is 6.2×10^{-3} mm^3s^{-1}, much higher than previously believed (see Section 5.3.1, where it is about 0.06×10^{-3} mm^3s^{-1}).

A useful further investigation could be to correlate velocity rates with the age of the grain. For example the growth of the developing grain is slow for the first two or three days after the pollination and very quick from the fourth to the eighth or ninth day(56). Clearly there must be some relationship between the velocity rate and the grain age and this has already been implied strongly in our experiment.

Chapter 6 Summary and Future Work

This work sets out to investigate the potential of NMR microscopy in the imaging of both static and dynamic distributions.

By various modifications to and development of the existing static imaging system, this work has established an imaging system which is capable both of dynamic imaging and of improved static imaging.

Some interesting and unexpected physiological phenomena have been discovered during the rabbit trachea experiments. The Poiseuille flow and wheat grain *in vivo* experiments have shown the great potential of dynamic imaging.

Various dynamic experiments can now be carried out using this system. These might include the accurate flow and diffusion distribution functions of various shaped tubes as well as the non-invasive investigation of the shear dependent fluid properties at the microscopic level.

While the apparatus has obvious applications it does suffer from two major drawbacks. First, there is the computer system with its limited memory. In particular we are unable to include more than 18 64×64 **q**-space images in the dynamic reconstruction. Second, the apparatus suffers from the low sensitivity associated with the low $\mathbf{B}_0$ field of the electromagnet. The NMR laboratory has recently acquired a 6.3 T superconductor magnet and 270 MHz spectrometer. Its incorporation in the imaging system will greatly enhance the potential resolution of the NMR microscope.

Appendix A Software for Flow and Diffusion Experiments

Appendix A.1 DREAD.ASM

```
;***********************************************************************
;                               DREAD.ASM                              *
; This program can READ data from any specific positions of the Disk.  *
;***********************************************************************


FRAME   STRUC
SAVEBP  DW      ?
SAVERET DD      ?
MSEG    DD      ?                       ;Beginning memory add. to write data
NSR     DD      ?                       ;Number of sectors to read
LR      DD      ?                       ;Beginning Logical Record Number (LRN)
FRAME   ENDS

DATA    SEGMENT
BPBAK   DW      ?
BANK1   DW      ?
BANK2   DW      ?
BANK3   DW      ?
DATA    ENDS

CODE    SEGMENT 'CODE'
DGROUP  GROUP   DATA
        ASSUME  CS:CODE,DS:DGROUP,ES:DGROUP,SS:DGROUP

DREAD   PROC    FAR
        PUBLIC  DREAD
        PUSH    BP                      ;Save caller's BP
        MOV     BP,SP                   ;Set frame base
        PUSH    DS

        MOV     AX,DATA
        MOV     DS,AX

        MOV     BPBAK,BP

;Read the contents of the file

        LES     BX,[BP]+NSR
        MOV     CX,ES:[BX]              ;Number of sectors to read
        MOV     BANK2,CX
        CMP     CX,128                  ;Larger than 64 k?
        JG      LOOP                    ;If yes, go to LOOP

        LES     BX,[BP]+LR              ;No,
        MOV     DX,ES:[BX]              ; load beginning LRN
```

```
        LES     BX,[BP]+MSEG      ;Load beginning memory segment
        MOV     AX,ES:[BX]        ;        to store the file
        MOV     DS,AX

        MOV     AH,0
        MOV     AL,1              ;Drive B
        MOV     BX,0
        INT     25H               ;Call DOS interrupt routine
        INC     SP
        INC     SP                ;Restore the stack (back normal control)
        JMP     FIN

LOOP:   MOV     CX,128            ;Read first 64 k file

        LES     BX,[BP]+LR        ;Load beginning LRN
        MOV     DX,ES:[BX]
        MOV     BANK3,DX

        LES     BX,[BP]+MSEG      ;Load beginning memory segment
        MOV     AX,ES:[BX]
        MOV     BANK1,AX
        PUSH    DS
        MOV     DS,AX

        MOV     AH,0
        MOV     AL,1              ;Drive B
        MOV     BX,0
        INT     25H               ;Call DOS interrupt routine
        ADD     SP,2
        POP     DS
        MOV     BP,BPBAK

        MOV     DX,BANK3          ;Adjust beginning LRN
        ADD     DX,128

        MOV     CX,BANK2          ;Calculate the remaining file length
        SUB     CX,128

        MOV     AX,BANK1          ;Adjust memory segment
        ADD     AX,1000H
        MOV     DS,AX

        MOV     AH,0
        MOV     AL,1              ;Drive B
        MOV     BX,0
        INT     25H               ;Call interrupt routine
        INC     SP
        INC     SP

FIN:    POP     DS
        POP     BP

        RET     12
```

```
DREAD   ENDP

CODE    ENDS
        END
```

Appendix A.2   DWRITE.ASM

```
;*********************************************************************
;                               DWRITE.ASM                           *
; This program can WRITE data to any specific positions of the Disk. *
;    (This version is used to write files having the same length)    *
;*********************************************************************


FRAME    STRUC
SAVEBP   DW       ?
SAVERET  DD       ?
MSEG     DD       ?                  ;Beginning memory address to read data
FL       DD       ?                  ;File length (kbytes)
SN       DD       ?                  ;Current File Series No. on Disk B
FNAME    DD       ?                  ;Filename
FRAME    ENDS

DATA     SEGMENT
TEMP     DW       1024 DUP (0)       ;2k temporary file directory store
BPBAK    DW       ?
SNBAK    DW       ?                  ;Save series number
BANK1    DW       ?                  ;Save Year and Month, MSEG
BANK2    DW       ?                  ;Save Date and Hour, FL
BANK3    DW       ?                  ;Save Minute and Second
DATA     ENDS

CODE     SEGMENT 'CODE'
DGROUP   GROUP    DATA
         ASSUME   CS:CODE,DS:DGROUP,ES:DGROUP,SS:DGROUP

DWRITE   PROC     FAR
         PUBLIC   DWRITE
         PUSH     BP                          ;Save caller's BP
         MOV      BP,SP                       ;Set frame base
         PUSH     DS

         MOV      AX,DATA
         MOV      DS,AX

         MOV      BPBAK,BP                    ;Save current BP

;Write the directory

         MOV      BX,OFFSET TEMP
         MOV      CX,4                        ;Read 4 directory sectors (2k)
         MOV      DX,3                        ;Start from first Dir. sector
         MOV      AH,0
         MOV      AL,1                        ;Disk B
         INT      25H                         ;Read directory from Disk B and
         INC      SP                          ;       store in memory DS:[BX].
         INC      SP
         MOV      BP,BPBAK
```

```
        LES     BX,[BP]+SN
        MOV     AX,ES:[BX]
        MOV     SNBAK,AX                ;Load and save Series No.
        MOV     CX,32
        MUL     CX                      ;32xSN (32 Bytes/per file dir.)
        MOV     CX,OFFSET TEMP
        MOV     DI,CX
        ADD     DI,AX                   ;DI=OFFSET TEMP + 32xSN
        SUB     DI,32
        MOV     DX,DI                   ;Find Bytes No. already in dir.

        ADD     DX,12                   ;12 Bytes/file name & attribute
        LES     BX,[BP]+FNAME
NAME:   MOV     AX,ES:[BX]
        MOV     DS:[DI],AX
        ADD     DI,2                    ;DI is Directory Store Counter
        ADD     BX,2                    ;BX is Offset for TEMP Store
        CMP     DI,DX
        JNZ     NAME                    ;Load file name and attribute

        ADD     DI,0AH
        ADD     BX,0AH                  ;Jump over 10 reserved bytes

        MOV     SI,BX                   ;Save Offset

        MOV     AH,80H
        INT     1AH                     ;Get time from the system

        MOV     BANK1,BX
        MOV     BANK2,CX
        MOV     BANK3,DX                ;Save the time

        MOV     BX,SI

        MOV     AX,BANK2
        MOV     AH,0
        MOV     CL,11
        SHL     AX,CL                   ;Relocate position of Hour
        MOV     DX,BANK3                ;        in binary
        MOV     DL,0
        MOV     CL,3
        SHR     DX,CL
        OR      AX,DX                   ;Relocate position of Minute
        MOV     DX,BANK3                ;        in binary
        MOV     DH,0
        SHR     DX,1
        OR      AX,DX                   ;Relocate position of Second
        MOV     DS:[DI],AX              ;        in binary
        INC     DI
        INC     DI
        ADD     BX,2                    ;Load Hour,Minute and Second

        MOV     AX,BANK1
        MOV     AL,0
        ADD     AH,20
```

```
        MOV     CL,1
        SHL     AX,CL                    ;Relocate position of Year
        MOV     DX,BANK1                 ;         in binary
        MOV     DH,0
        MOV     CL,5
        SHL     DX,CL
        OR      AX,DX                    ;Relocate position of Month
        MOV     DX,BANK2                 ;         in binary
        MOV     DL,DH
        MOV     DH,0
        OR      AX,DX                    ;Relocate position of Date
        MOV     DS:[DI],AX               ;         in binary
        INC     DI
        INC     DI
        ADD     BX,2                     ;Load Year, Month and Date

        MOV     AX,2
        MOV     DS:[DI],AX
        ADD     DI,2
        ADD     BX,2                     ;Load beginning sector of file

        MOV     SI,BX

        LES     BX,[BP]+FL
        MOV     AX,ES:[BX]
        MOV     BANK2,AX
        CMP     AX,64                    ;File size more than 64k ?
        JL      SIZE3                    ;If not,go to Size3
        MOV     DX,0                     ;Yes
SIZE1:  SUB     AX,64
        ADD     DX,1
        CMP     AX,64                    ;File size more than 128k ..?
        JL      SIZE2                    ;If not,go to Size2
        JMP     SIZE1
SIZE2:  MOV     CL,10
        SHL     AX,CL                    ;1024xSize (1k = 1024 Bytes)
        MOV     DS:[DI],AX
        ADD     DI,2
        ADD     BX,2                     ;Load low-order part of size
        MOV     AX,DX
        MOV     DS:[DI],AX
        ADD     DI,2
        ADD     BX,2                     ;Load high-order part of size
        JMP     DIR
SIZE3:  MOV     CL,10
        SHL     AX,CL                    ;Calculate size when <= 64k
        MOV     DS:[DI],AX
        ADD     DI,2
        ADD     BX,2
        MOV     AX,0
        MOV     DS:[DI],AX
        ADD     DI,2
        ADD     BX,2                     ;Load the file size

DIR:    MOV     AX,SNBAK
```

```
        MOV     CX,32
        MUL     CX                      ;Find total length of directory
        SUB     DI,AX                   ;Restore directory countor
        MOV     BX,DI
        MOV     AH,0
        MOV     AL,1                    ;Drive B
        MOV     CX,4                    ;Write 4 sectors dir. (2k)
        MOV     DX,3                    ;Start from first dir. Sector
        PUSH    DS
        INT     26H
        INC     SP
        INC     SP
        POP     DS
        MOV     BP,BPBAK

;Write the contents of the file

        MOV     CX,BANK2
        CMP     CX,64                   ;File size more than 64k ?
        JG      LOOPL                   ;If yes, go to LoopL
        SHL     CX,1                    ;Not, 2xFL=Sectors need to write

        MOV     AX,0
        MOV     DX,SNBAK
LOOPS:  CMP     DX,1                    ;First file ?
        JE      LOOP1                   ;If yes, go to Loop1
        ADD     AX,CX                   ;Not
        SUB     DX,1
        JMP     LOOPS

LOOP1:  MOV     DX,8                    ;Beginning Logical Record No.
        ADD     DX,AX

        LES     BX,[BP]+MSEG
        MOV     AX,ES:[BX]
        MOV     DS,AX                   ;Beginning memory segment to rea


        MOV     AH,0
        MOV     AL,1                    ;Drive B
        MOV     BX,0                    ;DS:[BX] is data Add.in computer
        INT     26H
        INC     SP
        INC     SP                      ;Finish write data into Disk B
        JMP     FIN                     ;     when file length <= 64k.

LOOPL:  MOV     CX,128                  ;128 Sectors X 512 bytes = 64k

        MOV     AX,0
        MOV     DX,SNBAK
        MOV     BX,BANK2
        SHL     BX,1                    ;Total sectors need to write
LOOP2:  CMP     DX,1                    ;First file ?
        JE      LOOPW                   ;If yes,go to LOOPW
        ADD     AX,BX                   ;Not
        SUB     DX,1
```

```
        JMP     LOOP2

LOOPW:  MOV     DX,8                    ;Beginning Logical Record No.
        ADD     DX,AX
        MOV     BANK3,DX

        LES     BX,[BP]+MSEG
        MOV     AX,ES:[BX]
        MOV     BANK1,AX
        PUSH    DS
        MOV     DS,AX                   ;Beginning memory segment

        MOV     AH,0
        MOV     AL,1                    ;Drive B
        MOV     BX,0
        INT     26H
        INC     SP
        INC     SP                      ;Write the first 64k data
        POP     DS
        MOV     BP,BPBAK

        MOV     DX,BANK3
        ADD     DX,128                  ;Next starting sector position

        MOV     CX,BANK2
        SHL     CX,1
        SUB     CX,128                  ;Remaining sectors

        MOV     AX,BANK1
        ADD     AX,1000H
        MOV     DS,AX                   ;Computer Add. to read

        MOV     AH,0
        MOV     AL,1
        MOV     BX,0
        INT     26H
        INC     SP
        INC     SP


FIN:    POP     DS
        POP     BP

        RET     16

DWRITE  ENDP

CODE    ENDS
        END
```

Appendix A.3   VD.ASM

```
;**********************************************************************
;*                              VD.ASM                                *
;* This program is for searching Peak (Velocity) and                  *
;*             calculating FWHM (Diffusion) from the peak position.   *
;* (This version can remove the finite base line effect for the FWHM) *
;**********************************************************************

FRAME   STRUC
SAVEBP  DW                      ; Storage for base pointer
SAVERT  DD                      ; Storage for return address
BSEG    DD      ?               ; Segment for returning base value
SQ      DD      ?               ; Sequence number of final data
N       DD      ?               ; Number of data words to be analyzed
DSEG    DD      ?               ; Segment for final Diffusion image
VSEG    DD      ?               ; Segment for final Velocity image
FSEG    DD      ?               ; Data segment where FFT performed
FRAME   ENDS

DATA    SEGMENT
TEMPF   DW      ?               ;FWHM frequency temp store
FWHM    DW      ?               ;Full-width-half-max
NUM     DW      ?               ;No. of data bytes
BV      DW      ?               ;Base value
DATA    ENDS

CODE    SEGMENT 'CODE'
DGROUP  GROUP   DATA
        ASSUME  CS:CODE,ES:DGROUP,DS:DGROUP,SS:DGROUP

VD      PROC    FAR
        PUBLIC  VD
        PUSH    BP
        MOV     BP,SP
        PUSH    DS

        MOV     AX,DATA
        MOV     DS,AX           ; Data base segment

;Load the variables

        MOV     DI,0            ;Initialize data counter

        LES     BX,[BP]+N
        MOV     AX,ES:[BX]
        SHL     AX,1
        MOV     NUM,AX          ;Number of bytes to be analyzed

        LES     BX,[BP]+FSEG
        MOV     AX,ES:[BX]
        MOV     ES,AX           ;Define data segment

;Calculate the base line value
```

```
        MOV     BX,32           ;Use 32 pixels to average the base
        SHL     BX,1            ;32 pixels = 64 bytes long
        MOV     DX,0

BV32:   MOV     AX,0
        MOV     CX,8            ;First average loop counter (4 pixels)

BV4:    ADD     AX,ES:[DI]      ;Load the data
        INC     DI
        INC     DI              ;Increase the total counter
        DEC     CX
        DEC     CX              ;Decrease the 4 pixel counter
        CMP     CX,0            ;Already 4 pixels?
        JG      BV4             ;If not, continue
        SAR     AX,1            ;Yes,
        SAR     AX,1            ;AX/4=Average of four pixels
        ADD     DX,AX
        CMP     DI,BX           ;Already 32 pixels?
        JL      BV32            ;If not, continue

        MOV     CL,3            ;Yes
        SAR     DX,CL
        MOV     BV,DX           ;Save the base value
        MOV     DI,0            ;Clear the counter

;Search for peak frequency and half-peak frequencies

        MOV     DX,-32768       ;Set initial comparison level

LOOP:   MOV     AX,ES:[DI]
        CMP     AX,DX           ;Is it larger than the previous one ?
        JLE     LOOP1           ;If not, try next one
        MOV     DX,AX           ;Yes, set this as the comparison level
        MOV     CX,DI           ;Save current frequency
LOOP1:  INC     DI
        INC     DI              ;Increase the counter
        CMP     DI,NUM          ;The last one ?
        JL      LOOP            ;Not,go on

        SUB     DX,BV           ;Base line correction
        SAR     DX,1            ;Real half Peak-Amplitude
        ADD     DX,BV           ;Half peak comparison level

        MOV     DI,CX           ;From the peak frequency down to
LEFT:   DEC     DI              ;        the lower half-peak frequency
        DEC     DI
        MOV     AX,ES:[DI]
        CMP     AX,DX           ;Is this the half-peak point?
        JG      LEFT            ;If not, go on
        MOV     TEMPF,DI        ;Yes, save the lower half-peak freq.

        MOV     DI,CX           ;From the peak frequency down to
RIGHT:  INC     DI              ;         the higher half-peak frequency
        INC     DI
```

```
        MOV     AX,ES:[DI]
        CMP     AX,DX               ;Is this the half-peak frequency?
        JG      RIGHT               ;If not, go on
        MOV     AX,DI               ;Yes, save the higher half-peak freq.

        MOV     BX,TEMPF
        SUB     AX,BX               ;Calculate Full-width-half-maximum
        MOV     FWHM,AX

        LES     BX,[BP]+SQ
        MOV     DI,ES:[BX]

        LES     BX,[BP]+VSEG
        MOV     AX,ES:[BX]
        MOV     ES,AX               ;Define Velocity Image Segment
        MOV     BX,NUM
        SAR     BX,1
        SAR     BX,1                ;BX/4=Middle of the real data
        SAR     CX,1                ;CX/2=Velocity in words
        SUB     CX,BX               ;Start from the zero
        MOV     ES:[DI],CX          ;Load velocity into memory VSEG:SQ

        LES     BX,[BP]+DSEG
        MOV     AX,ES:[BX]
        MOV     ES,AX               ;Define Diffusion Image Segment
        MOV     AX,FWHM
        SHR     AX,1                ;AX/2=Diffusion^1/2 in word
        MOV     ES:[DI],AX          ;Load diffusion into memory DSEG:SQ

        LES     BX,[BP]+BSEG
        MOV     AX,ES:[BX]
        MOV     ES,AX               ;Define Segment for Return Base
        MOV     AX,BV
        MOV     ES:0,AX             ;Load Base Value into BSEG:0

FIN:    POP     DS
        POP     BP

        RET     24                  ; Return to calling program

VD      ENDP

CODE    ENDS
        END
```

Appendix A.4 Description of NMR.LIB

```
**********************************************************************
*  NMR.LIB is an assembly language subroutine library which can be  *
*                                    called by FORTRAN programs.     *
**********************************************************************
```

APHASE.ASM

CALL APHASE(PR,SLICE,SEGM,NUM)

Program to generate R*sin(PO) + I*cos(PO) with input and output data segments declared and autophase returning the optimum phase angle and the phased data.

PR : Autophase value returned to calling program (degrees)
SLICE : Segment for Original data
SEGM : Segment for autophase data
NUM : Number of data points in each phase of spectrum

BAKPRJ.ASM

CALL BAKPRJ(THETA)

Back projects filted profile data to form a 256*256 point image. (Image in up memory from segment=8192, 180 degree projection)

THETA : Projection angle

BP64.ASM

CALL BP64(DSEG,ISEG,THETA)

Back projects filted profile data to form a 64*64 point image. (Image in up memory from DSEG:0000, 360 degree projection)

DSEG : Data segment for filtered profile
ISEG : Data segment for image
THETA : Projection angle

CLS.ASM

CALL CLS(MODE)

Clear the screen

MODE=0 : Clear both screens

MODE=1 : Clear graphics screen
MODE=2 : Clear text screen

COLORA.ASM

CALL COLORA(X,Y,H,W,CLR)

Draws a colour scale in any length, width and positions on the screen.

X : X coordinate of the top left hand corner of the scale (0-639)
Y : Y coordinate of the top left hand corner of the scale (0-399)
H : Height of the scale (in lines)
W : Width of the scale (in 8 dots)
CLR : Colour scale table (1=mono, 2=4 clr, 3=8 clr, 4=16 clr, 5=+/-)

COLORS.ASM

CALL COLORS(CLR)

Draws a colour scale in the fixed size and positions on the screen.

CLR : Desired colour scale (1=mono, 2=4 clr, 3=8 clr, 4=16 clr)

CROSS.ASM

CALL CROSS(X,Y,COL)

Draw a small cross on the screen at the coordinates (X,Y) in colour COL.

CURPOS.ASM

CALL CURPOS(Y,X)

Position the cursor at text screen coordinates (X,Y)

CURSOR.ASM

CALL CURSOR(PARAMETER)

PARAMETER=1 Cursor off
PARAMETER=2 Cursor on

DRCUR.ASM

CALL DRCUR(X,Y,CLR,KEY)

Draw a 20*20 cursor at coordinates (X,Y) and in colour CLR. Using the arrow keys the cursor may be moved to any position on the screen. The + and - keys may be used to set the step size to 16 or 1 respectively. After pressing a key, the cursor is removed and (X,Y) position is updated. The key pressed is also returned.

DRLINE.ASM

CALL DRLINE(X1,Y1,X2,Y2,CLR)

Draw a line from coordinates (X1,Y1) to (X2,Y2) in colour CLR.

DREAD.ASM

CALL DREAD(LR,NSR,MSEG)

Read data from any positions of Disk B using the following parameters:

LR : Logical record number on disk.
NSR : Number of sectors to be read (1 sector = 512 bytes).
MSEG : Computer memory segment where data is going to be stored.

DWRITA.ASM

CALL DWRITA(LR,NSW,MSEG)

Write data to any positions of Disk B using the following parameters:

LR : Logical record number on disk.
NSR : Number of sectors to be written (1 sector = 512 bytes).
MSEG : Computer memory segment where data is to be read.

DWRITE.ASM

CALL DWRITE(FNAME,SN,FL,MSEG)

Used to store a series of images on disk (as used in flow imaging).

FNAME : Filename of current image.
SN : Series number (determines where images will be stored).
FL : Length of each data file in kbytes.
MSEG : Computer memory segment where the image is stored

FFT.ASM

CALL FFT(SEG,LOG2(N),N,NGAIN)

Perform an N point fast fourier transform on the data stored at SEG:0000

Real data is stored from SEG:0000 to SEG:(N-1). Imaginary data is stored from SEG:(N) to SEG:(2N-1). After the transformation, the real and imaginary data is reversed.

The FFT uses a radix 2 algorithm.

SEG : Segment where data is stored.
LOG2(N) : Log to the base 2 of N.
N : Number of data points (must be a power of 2).
NGAIN : Number of times data has been divided by 2.

FFT2D.FOR

CALL FFT2D(DIR,SCAL,FSEG,ISEG)

Perform a 2-D 128*128 point Fourier transform on the data stored from ISEG:0000. Real data is stored at offset 32256+512*Y+(X+64)*2 and imaginary data at 32512+512*Y+(X+64)*2, where -64<X, Y<63.

DIR : Forward (0) or reverse (1) transform.
SCAL : Total number of times data has been divided by 2 (returned).
FSEG : Segment where FFTs are to be performed.
ISEG : Image data segment.

FFTINT.FOR

CALL FFTINT(N,SEG)

Write a N point sine look up table in memory at decimal address SEG:4096

Must be called before performing an N point FFT. SEG is the same as that used in FFT.ASM.

GRAPH.ASM

CALL GRAPH(SEG,ADSI,ADSF,XZERO,YZERO,SPC,COL,SCALE,YMIN,YMAX)

Plot data in memory address SEG:ADSI to SEG:ADSF on the screen.

SEG : Memory segment where data is to be found.
ADSI : Initial data address.
ADSF : Final data address.
XZERO : X coordinate of zero data values.
YZERO : Y coordinate of zero data values.

SPC : Number of spaces between pixel plotted.
COL : Colour of pixels plotted (0-7).
SCALE : Power of two by which data is to be scaled before displayed.
YMIN : Minimum Y coordinate of data to be displayed.
YMAX : Maximum Y coordinate of data to be displayed.

IMAGEA.ASM

CALL IMAGEA(SEG,ADRS,N,X,Y,SCALE,OFFSET,CLR)

Draw an N*N image on the screen using data stored at SEG:ADRS
(Colour scale 1 to 4 can only interpret positive numbers.)

SEG : Start segment of image data.
ADRS : Start address of image data.
N : Number of data points horizontally and vertically.
X : X screen coordinate of top left hand corner of image.
Y : Y screen coordinate of top left hand corner of image.
SCALE : Power of two by which data is to be scaled before displayed.
OFFSET : An offset subtracted from the image data before being scaled.
CLR : Colour table (1=mono, 2=4 clr, 3=8 clr, 4=16 clr, 5=+/- clr).

IMAGEB.ASM

CALL IMAGEB(SEG,ADRS,N,X,Y,SCALE,OFFSET,CLR)

Draw an N*N image on the screen using data stored at SEG:ADRS
(Able to interpret both positive and negative numbers in all scales.)

IMAGEC.ASM

CALL IMAGEC(SEG,ADRS,N,X,Y,SCALE,OFFSET,CLR)

Draw an N*N image on the screen using data stored at SEG:ADRS
(Color scale 1 can only interpret negative numbers.)

INTFAC.AM

CALL INTFAC(DATSEG,NUM)

Read data from the the 980A and load it into memory via the Centronics parallel interface.

DATSEG : Data is read into DATSEG:0000
NUM : Number of words to be transfered (16 bit)

INPUT.ASM

CALL INPUT(CODE)

Wait for a key to be pressed and then return the ASCII code of the key pressed to the calling program {or char. if code is type character*1}.

CODE : ASCII code of key pressed.

MOVE.ASM

CALL MOVE(SADS,TADS,SSEG,TSEG,DS,DT,N)

Move data (in word form) from one part of memory to another.

SADS : Address of source data.
TADS : Address of target data.
SSEG : Souce data segment.
TSEG : Target data segment.
DS : Number of bytes between source words.
TS : Number of bytes between target words.
N : Number bytes to be transfered.

OUTPUT.ASM

CALL OUTPUT(HP,VP,COL,ATR,CODE,DATA,CODE,DATA,.....,N)

Output character or numeric data to the screen.

HP : Horizontal position of data on screen (0-79).
VP : Vertical position of data on screen (0-24).
COL : Colour of data to be displayed (0-15).
ATR : Attribute of displayed data (0=normal 16=blink 32=underline)
CODE : 0=ASCII data. 255=numeric data.
DATA : Numeric or string data. Numeric data must be integer.
N : Number of parameters-1.

PEEK.ASM

CALL PEEK(DATA,SEG,OFFSET)

Read word at location SEG:OFFSET and return in DATA.

PEEKB.ASM

CALL PEEKB(DATA,SEG,OFFSET)

Read byte at location SEG:OFFSET and return in DATA.

PHASE.ASM

CALL PHASE(THETA)

Generates R*sin(THETA)+I*cos(THETA) for the program FFT.FOR where I and R are the real and imaginary domains in a 512 FFT.

THETA : First order phase correction.

POKE.ASM

CALL POKE(DATA,SEG,OFFSET)

Store DATA at location SEG:OFFSET.

PRINTN.ASM

CALL PRINTN(SCALE,OFFSET)

This program produces an image of the data displayed using the subroutine IMAGE on a dot matrix printer. The image is displayed using a 10 level grey scale with a resolution of 640 dots horizontally.

SCALE : Power of two by which data is to be scaled before printed.
OFFSET : An offset subtracted from the image data before being scaled.

PRINTW.ASM

CALL PRINTW(SCALE,OFFSET)

This program produces an image of the data displayed using the subroutine IMAGE on a dot matrix printer. The image is displayed using a 10 level grey scale with a resolution of 720 dots horizontally.

SCALE : Power of two by which data is to be scaled before printed.
OFFSET : An offset subtracted from the image data before being scaled.

PSET.ASM

CALL PSET(X,Y,COL)

Eight pixel at screen coordinates (X,Y) in colour COL.

RESET.ASM

CALL RESET

Set up the Centronics parallel interface for output.

SCALE.ASM

CALL SCALE(SADS,SSEG,NUMDIV,NUMB,P2)

Scale data in specified locations by 2^P2

SADS : Start address
SSEG : Start segment
NUMDIV : Number of words to be divided
NUMB : Number of bytes between each word of interest
P2 : Power of two by which data is to be divided

SCMD.ASM

CALL SCMD(MODE)

Set screen mode.

MODE : See BIOS calls for mode values (Tech. material p. 48 MODE=AL)

SDUMP3.ASM

CALL SDUMP3

Dumps the screen image onto the printer.

SERIAL.ASM

CALL SERIAL(SEG,ADRS,NUM)

Tranfers data in upper memory to the 980A along a serial line.

SEG : Data segment.
ADRS : Data address.
NUM : Number of words to be transfered.

SWAP.ASM

CALL SWAP(SADRS,TADRS,SSEG,TSEG,NBS,NBT,NUM)

Swap the contents of two memory blocks.

SADRS : Address of source data block.
TADRS : Address of target data block.
SSEG : Segment of source data block.
TSEG : Segment of target data block.
NBS : No. of bytes between data in source block.
NBT : No. of bytes between data in target block.
NUM : Number of words (16 bits) to be moved.

TIMER.ASM

CALL TIMER(HOUR,MINUTE,SECOND,DAY,MONTH,YEAR)

Read time and date from the system clock.

VD.ASM

CALL VD(FSEG,VSEG,DSEG,N,SQ)

Search for maximum peak in a spectrum and determine the FWHM. Store this information in VSEG (peak position) and DSEG (FWHM).

FSEG : Segment where FFT is performed.
VSEG : Segment where the peak (velocity) data is stored.
DSEG : Segment where the FWHM (diffusion) data is stored.
N : Number of dat words to be analyzed.
SQ : Sequence number giving data position as VSEG:SQ and DSEG:SQ.

VD2.ASM

CALL VD2(FSEG,VSEG,DSEG,N,SQ,BSEG)

Search for maximum peak in a spectrum and determine the FWHM. Store this information in VSEG (peak position) and DSEG (FWHM). Using the average of the first 32 pixel amplitudes as the base line and return the base value in BSEG.

FSEG : Segment where FFT is performed.
VSEG : Segment where the peak (velocity) data is stored.
DSEG : Segment where the FWHM (diffusion) data is stored.
N : Number of dat words to be analyzed.
SQ : Sequence number giving data position as VSEG:SQ and DSEG:SQ.
BSEG : Segment where the base value is returned (BSEG:0)

ZERO.ASM

`CALL ZERO(IADS,FADS,SEG)`

Fill specified region of memory with zeros.

```
IADS     : Initial word address.
FADS     : Number of words to be zeroed (0 to 32767)
SEG      : Segment
```

Appendix A.5 FLOW.FOR

```
***********************************************************************
*                              FLOW.FOR                               *
* This program accepts filtered profile data (64X64) from spectrometer.*
* The data is then back-projected to produce one set of data image.   *
* Store the data image into Disk B then go on to do next .....        *
* Finally analyze and produce a flow image and a diffusion image.     *
***********************************************************************

$STORAGE:2

        PROGRAM FLOW

        INTEGER*2 AMP,SF,THETA,INC,U,V,W,X,Y,Z,DSEG,CSC,FNAME(6),RESP,NF
        INTEGER*2 NI,TH,LR,MSEG,NGAIN,HOUR,MINUTE,SECOND,DATE,MONTH,YEAR
        REAL AMPR

        DATA FNAME/6*0/

        DSEG=16000
        CSC=5

c Set screen mode 640*400

        CALL SCMD(183)
        CALL RESET
        CALL SETCOL(0,14,0,0)

c Generate Trig table for FFT

        CALL FFTINT(256,11392)

**************************** Input data *******************************

        WRITE (*,1)
1       FORMAT( ' Insert Data Disk into Drive B Before Start !!! ' )
        WRITE (*,2)
2       FORMAT( '                                                ' )

        WRITE(*,15)
15      FORMAT( ' Enter scale factor (XXX)')
        READ (*,20) SF
20      FORMAT( I3)

        WRITE (*,25)
25      FORMAT( ' Enter angle increment (XX) ')
        READ (*,30) INC
30      FORMAT( I2)

        WRITE (*,35)
35      FORMAT( ' Enter number of images (XX) ')
        READ (*,30) NI
```

```
*************** FILTER BACK PROJECTED DATA IMAGES LOOP *****************

c Remove cursor

        CALL CURSOR(1)

        DO 100 X=1,NI

           CALL CLS(0)
           CALL OUTPUT(24,1,11,0,0,'Data Image ',1,X,8)

           DO 90 THETA=0,360-INC,INC

c Obtain data from spectrometer

              CALL INTFAC(DSEG,128)

c Clear screen and then write angle and display data

              CALL CLS(0)
              CALL OUTPUT(24,1,11,0,0,'Data Image ',1,X,8)
              CALL OUTPUT(66,2,14,0,0,'Theta = ',1,THETA,0,'x',10)
              CALL GRAPH(DSEG,0,64,100,150,4,11,8,50,200)
              CALL OUTPUT(60,9,14,0,0,'Re ',6)
              CALL GRAPH(DSEG,64,128,100,300,4,12,8,200,350)
              CALL OUTPUT(60,18,14,0,0,'Im ',6)

c Divide data by the number of projections to prevent overflow

              DO 80 W=0,127
                 CALL PEEK(AMP,DSEG,W*2)
                 AMPR=REAL(AMP)/REAL(SF)
                 CALL POKE(NINT(AMPR),DSEG,W*2)
80            CONTINUE

c Perform back projection

              CALL BP64(DSEG,9088,THETA)
              CALL BP64(DSEG+8,9088+512,THETA)

c Display data images

              CALL CLS(0)
              CALL OUTPUT(24,1,11,0,0,'Data Image ',1,X,8)
              CALL OUTPUT(66,2,14,0,0,'Theta = ',1,THETA,0,'x',10)
              CALL OUTPUT(67,4,14,0,0,' SF = ',1,SF,8)

              CALL COLORA(560,112,8,6,CSC)
              CALL DRLINE(560,112,560,368,7)
              CALL DRLINE(608,112,608,368,7)
              CALL DRLINE(560,112,608,112,7)
              CALL DRLINE(560,368,608,368,7)

              CALL IMAGEA(9088,0,64,64,96,11,0,CSC)
              CALL DRLINE(64,96,192,96,7)
```

```
              CALL DRLINE(64,224,192,224,7)
              CALL DRLINE(64,96,64,224,7)
              CALL DRLINE(192,96,192,224,7)
              CALL OUTPUT(15,16,14,0,0,'Re',6)

              CALL IMAGEA(9088+512,0,64,288,96,11,0,CSC)
              CALL DRLINE(288,96,416,96,7)
              CALL DRLINE(288,224,416,224,7)
              CALL DRLINE(288,96,288,224,7)
              CALL DRLINE(416,96,416,224,7)
              CALL OUTPUT(43,16,14,0,0,'Im',6)

90         CONTINUE

           FNAME(1)=25938
           NF=48+X
           IF (NF .LT. 58) THEN
                FNAME(2)=NF
           ELSE
                NF=12337+(X-10)*256
                FNAME(2)=NF
           ENDIF
           CALL DWRITE(FNAME,X*2-1,8,9088)

           FNAME(1)=27977
           NF=48+X
           IF (NF .LT. 58) THEN
                FNAME(2)=NF
           ELSE
                NF=12337+(X-10)*256
                FNAME(2)=NF
           ENDIF
           CALL DWRITE(FNAME,X*2,8,9088+512)

           CALL ZERO(0,8192,9088)

100     CONTINUE

*********************** ANALYSIS DATA LOOP *****************************

        CALL CLS(0)

        WRITE (*,105)
105     FORMAT( ' Do you wish to analyze data now ? (Y=1 N=0)')
        READ (*,110) RESP
110     FORMAT( I1)

        IF(RESP .EQ. 0) THEN

        WRITE (*,115)
115     FORMAT( ' Experiments Finished, Thanks! ')

        GOTO 300

        ENDIF
```

```
        CALL CLS(0)

        WRITE (*,120)
120     FORMAT( ' Analyzing Data ' )
        WRITE (*,121)
121     FORMAT( '                                              ' )

        WRITE (*,125)
125     FORMAT( ' Enter Threshold of data images (XXXXX) ')
        READ (*,130) TH
130     FORMAT( I5)

c Clear 16K Bytes for final Velocity and Diffusion images

        CALL ZERO(0,8192,11712)

        DO 200 X=1,8

c Clear 36K data memory

           CALL ZERO(0,18432,9088)

c Read 1024 Bytes from each of real and imaginary data images

           DO 140 W=1,NI*2
              LR=8+(W-1)*16+(X-1)*2
              MSEG=9088+(W-1)*64
              CALL DREAD(LR,2,MSEG)
140        CONTINUE

c Test signal level (Skip if less than Threshold ~ Noise)

           DO 180 Y=0,511

              CALL TIMER(HOUR,MINUTE,SECOND,DATE,MONTH,YEAR)
                U=Y/64+(X-1)*8
                V=MOD(Y,64)
              CALL OUTPUT(10,1,11,0,1,U,0,',',1,V,10)
              CALL OUTPUT(60,1,11,0,1,HOUR,0,':',1,MINUTE,0,':',1,SECOND
     2                    ,0,'-',1,DATE,0,':',1,MONTH,0,':',1,YEAR,26)
              CALL PEEK(Z,9088,Y*2)
                IF(Z .LT. TH) GOTO 180

c Clear 1K Bytes for FFT data (256w Re and 256w Im)

              CALL ZERO(0,512,11392)

c Perform FFT then search for Velocity and Diffusion

              CALL MOVE(Y*2,0,9088,11392,2048,2,36)
              CALL MOVE(1024+Y*2,0,9088,11424,2048,2,36)

              CALL CLS(0)
              CALL OUTPUT(10,1,11,0,1,U,0,',',1,V,10)
```

```
            CALL OUTPUT(60,1,11,0,1,HOUR,0,':',1,MINUTE,0,':',1,SECOND
     2                 ,0,'-',1,DATE,0,':',1,MONTH,0,':',1,YEAR,26)
            CALL GRAPH(11392,0,512,0,100,1,3,9,0,200)
            CALL FFT(11392,8,256,NGAIN)
            CALL SWAP(512,512+256,11392,11392,2,2,128)
            CALL VD(11424,11712,12224,256,Y*2+(X-1)*1024)
            CALL GRAPH(11392,0,512,0,300,1,3,9,200,399)
            CALL PEEK(U,11712,Y*2+(X-1)*1024)
            CALL PEEK(V,12224,Y*2+(X-1)*1024)
            CALL OUTPUT(10,12,11,0,1,U,0,',',1,V,10)

180         CONTINUE

200       CONTINUE

c Save the final Velocity and Diffusion Images into Disk B

          FNAME(1)=25942
          FNAME(2)=28524
          FNAME(3)=26979
          FNAME(4)=31092
          CALL DWRITE(FNAME,NI*2+1,8,11712)

          FNAME(1)=26948
          FNAME(2)=26214
          FNAME(3)=29557
          FNAME(4)=8238
          CALL DWRITE(FNAME,NI*2+2,8,12224)

******************** DISPLAY FINAL IMAGES LOOP *************************

c Clear screen and 41K data memory

          CALL CLS(0)
          CALL ZERO(0,20992,9088)

c Display

          CALL DREAD(8,32,9088)

          CALL IMAGEA(9088,0,64,96,32,11,0,CSC)
          CALL OUTPUT(16,10,14,0,0,' Re (G=0) ',6)
          CALL COLORA(56,32,4,3,CSC)
          CALL DRLINE(56,32,56,160,7)
          CALL DRLINE(80,32,80,161,7)
          CALL DRLINE(56,32,80,32,7)
          CALL DRLINE(56,160,80,160,7)

          CALL IMAGEA(9088+512,0,64,352,32,11,0,CSC)
          CALL OUTPUT(48,10,14,0,0,' Im (G=0) ',6)
          CALL COLORA(496,32,4,3,CSC)
          CALL DRLINE(496,32,496,160,7)
          CALL DRLINE(520,32,520,161,7)
          CALL DRLINE(496,32,520,32,7)
          CALL DRLINE(496,160,520,160,7)
```

```
          CALL IMAGEA(11712,0,64,96,192,1,0,5)
          CALL OUTPUT(15,22,14,0,0,'Velocity',6)
          CALL COLORA(56,192,4,3,5)
          CALL DRLINE(56,192,56,320,7)
          CALL DRLINE(80,192,80,321,7)
          CALL DRLINE(56,192,80,192,7)
          CALL DRLINE(56,320,80,320,7)

          CALL IMAGEA(12224,0,64,352,192,3,0,CSC)
          CALL OUTPUT(47,22,14,0,0,'Diffusion',6)
          CALL COLORA(496,192,4,3,CSC)
          CALL DRLINE(496,192,496,320,7)
          CALL DRLINE(520,192,520,321,7)
          CALL DRLINE(496,192,520,192,7)
          CALL DRLINE(496,320,520,320,7)

300       END
```

Appendix A.6 TI 980A Software Modifications

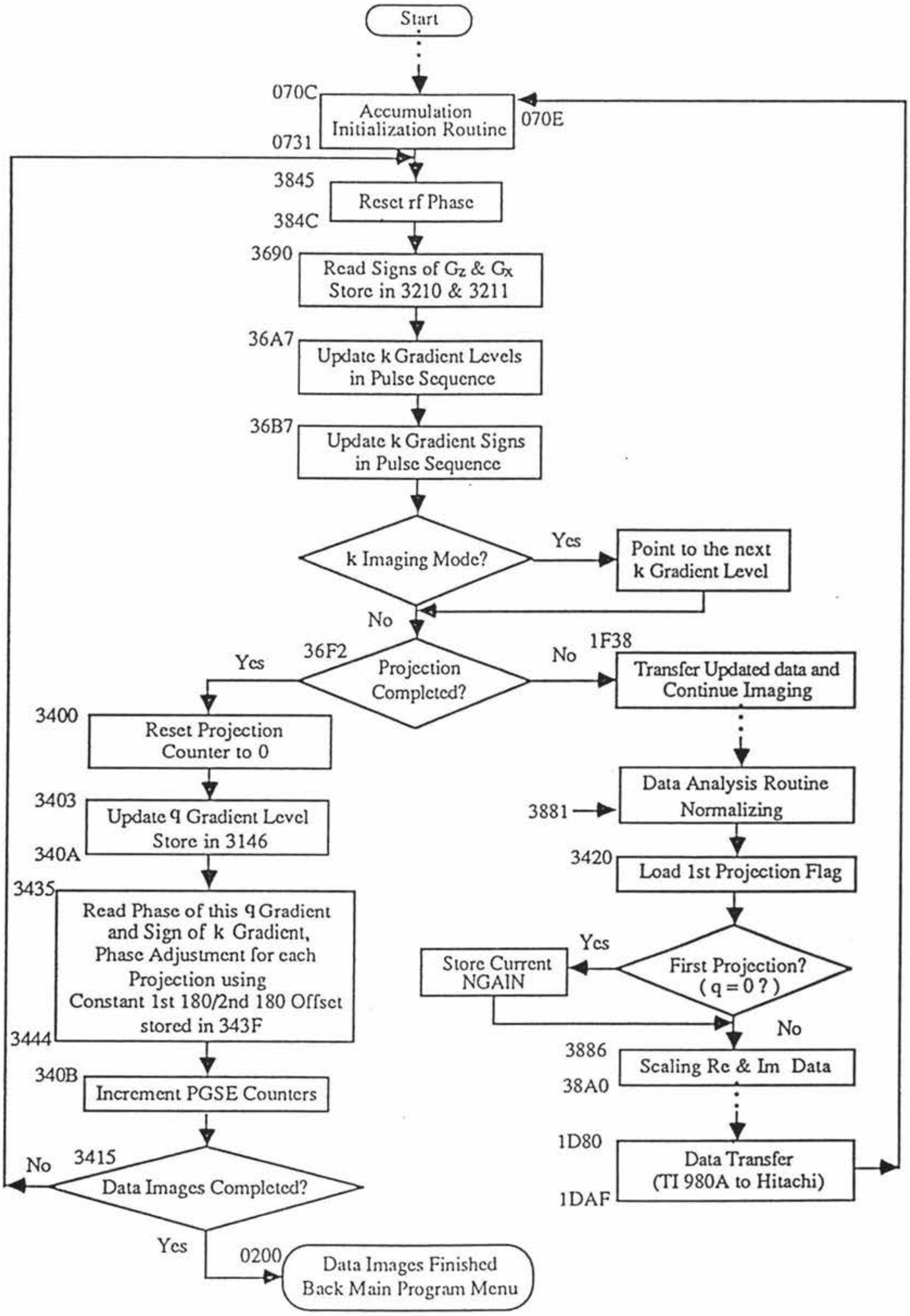

Figure A.1 Flow Chart for the TI 980A Modifications

Modification to the end of the Accumultion Initialization Routine

```
0730  7C00   BRU  (731)
0731  3845   DATA               ;Go to update parameters
```

Modification to the end of the Coherent Noise Cancellation Routine

```
3845  0000   LDA  (3846)
3846  3200   DATA               ;Load CNC update add. 3220
3847  C506   RMO  A,B
3848  0503   LDA  (((B)+3))     ;Load current rf phase
3849  DB5D   SABO  D            ;Set it to 0 and
384A  8503   STA  (((B)+3))     ;        store in 3203
384B  7C00   BRU  (384C)
384C  3690   DATA               ;Go to update k gradients
```

Update the **k** Imaging Gradients Routine*

```
3690  0700   LDA  0
3691  8400   STA  ((3692))      ;Reset gradient counter
3692  321F   DATA               ;        (321F) to zero
3693  0400   LDA  ((3694))      ;Load projection number
3694  3200   DATA               ;        Np
3695  9C00   MPY  ((3696))
3696  321F   DATA               ;(A)=Np x (321F)
3697  C510   RMO  E,A
3698  2000   ADD  (3699)        ;(A)=Np x (321F) +
3699  3220   DATA               ;    grad. data base add.
369A  2400   ADD  ((369B))      ;(A)=(A) +
369B  321E   DATA               ;        projection counter
369C  C501   RMO  A,E           ;Point to new sign word
369D  0000   LDA  (369E)
369E  3210   DATA               ;(A)=3210+(321F),
369F  2400   ADD  ((36A0))      ;        add. of temp.
36A0  321F   DATA               ;        sign storage
36A1  C504   RMO  A,S
36A2  C516   RMO  E,B
36A3  0100   LDA  ((B)+0)       ;Load new grad. sign
36A4  C546   RMO  S,B           ;Store in 3210+(321F)
36A5  8100   STA  ((B)+0)       ;        (Gz 3210, Gx 3211)
36A6  C311   RIN  E,E           ;Set pointer to new level
36A7  0400   LDA  ((36A8))
36A8  321F   DATA
36A9  2000   ADD  (36AA)        ;Load add. of gad. level
36AA  3201   DATA               ;        to be updated
36AB  C504   RMO  A,S           ;Save this address
36AC  C516   RMO  E,B
36AD  0100   LDA  ((B)+0)       ;Load gradient level
36AE  C546   RMO  S,B           ;Store in pulse sequence
36AF  8500   STA  (((B)+0))     ;        list
36B0  5400   IMO  ((36B1))      ;Increment gradient counter
36B1  321F   DATA               ;        (Gz to Gx)
36B2  0400   LDA  ((36B3))
36B3  321F   DATA               ;Both Gz and Gx
```

```
36B4  6702   CPL   2          ;       considered?
36B5  CD20   SEQ              ;Yes, go to 36B7
36B6  78DC   BRU   3693       ;No, go to 3693

36B7  0000   LDA   (36B8)
36B8  3000   DATA             ;Load pulse sequencer add.
36B9  C506   RMO   A,B        ; and save in base register
36BA  0100   LDA   ((B)+0)    ;Load p.s. register value
36BB  6704   CPL   4          ;'04' register?
36BC  CDA0   SNE              ;No, go to 36BE
36BD  7807   BRU   36C5       ;Yes, go to 36C5
36BE  6700   CPL   0          ;'00' register?
36BF  CDA0   SNE              ;No, go to 36C1
36C0  781F   BRU   36E0       ;Yes, go to 36E0
36C1  C560   RMO   B,A        ;Point to next register
36C2  2705   ADD   5          ; value in p.s. by
36C3  C506   RMO   A,B        ; increment add. by 5
36C4  78F5   BRU   36BA       ;Repeat above operations
36C5  C366   RIN   B,B        ;Point to register level
36C6  0400   LDA   ((36C7))
36C7  3210   DATA             ;Load Gz sign
36C8  6701   CPL   1          ;Negative?
36C9  CDA0   SNE              ;Go to 36CB if Gz -ve
36CA  7804   BRU   36CF       ;Go to 36CF if Gz +ve
36CB  0100   LDA   ((B)+0)    ;Load register level and
36CC  DB5F   SABO  F          ; set bit 0 to 1 if Gz -ve
36CD  8100   STA   ((B)+0)    ; and store sign
36CE  7803   BRU   36D2       ;Go to 36D2
36CF  0100   LDA   ((B)+0)    ;Load register level and
36D0  DB4F   SABZ  F          ; set bit 0 to 0 if Gz +ve
36D1  8100   STA   ((B)+0)    ; and store sign
36D2  0400   LDA   ((36D3))
36D3  3211   DATA             ;Load Gx sign
36D4  6701   CPL   1          ;Negative?
36D5  CDA0   SNE              ;Go to 36D7 if Gx -ve
36D6  7804   BRU   36DB       ;Go to 36DB if Gx +ve
36D7  0100   LDA   ((B)+0)    ;Load register level and
36D8  DB58   SABO  8          ; set bit 7 to 1 if Gx -ve
36D9  8100   STA   ((B)+0)    ; and store sign
36DA  7803   BRU   36DE       ;Go to 36DE
36DB  0100   LDA   ((B)+0)    ;Load register level and
36DC  DB48   SABZ  8          ; set bit 7 to 0 if Gx +ve
36DD  8100   STA   ((B)+0)    ; and store sign
36DE  C766   RDE   B,B        ;Restore address pointer
36DF  78E1   BRU   36C1       ;Go to 36C1 for next '04'
36E0  0400   LDA   ((36E1))
36E1  384F   DATA             ;Load mode
36E2  6701   CPL   1          ;Imaging mode?
36E3  CD20   SEQ              ;Yes, go to 36E5
36E4  7804   BRU   36E9       ;No, go to 36E9
36E5  5400   IMO   ((36E6))
36E6  321E   DATA             ;Point to next grad. level
36E7  5400   IMO   ((36E8))   ; by increment projection
36E8  321E   DATA             ; counter by 2
36E9  0400   LDA   ((36EA))
36EA  3200   DATA             ;(A) = Np x 2
36EB  6400   CPL   ((36EC))
36EC  321E   DATA             ;Last projection?
```

```
36ED  CD40   SGT              ;Yes, go to 36EF
36EE  7802   BRU   36F1       ;No, go to 36C8
36EF  7C00   BRU   (36F0)
36F0  3400   DATA             ;Go to update q parameters
36F1  7C00   BRU   (36F2)
36F2  1F38   DATA             ;Transfer data to p.s.
*This routine was written by Dr C.D. Eccles.
```

Update the **q** Parameters Routine

```
3400  0700   LDA   0
3401  8400   STA   ((3402))
3402  321E   DATA             ;Set projection counter = 0
3403  0400   LDA   ((3404))   ;Load (341F), next q
3404  341F   DATA             ; gradient level address
3405  C506   RMO   A,B
3406  0100   LDA   ((B)+0)    ;Load q grad. level data
3407  8400   STA   ((3408))   ;Store next level
3408  3146   DATA             ; address in p.s.
3409  7C00   BRU   (340A)
340A  3435   DATA             ; Go to 3435, continue

3435  0400   LDA   ((3436))
3436  341F   DATA             ;Load level add. in 341F
3437  2720   ADD   20         ;(A)=Phase address
3438  C506   RMO   A,B
3439  0900   LDE   ((B)+0)    ;Load phase value
343A  0400   LDA   ((343B))
343B  3210   DATA             ;Load Gz sign
343C  CC80   SNZ              ;If Gz is -ve, to to 343E
343D  7803   BRU   3441       ;If Gz is +ve, go to 3441
343E  C510   RMO   E,A
343F  2700   ADD   0          ;Add phase offset (here 0)
3440  C501   RMO   A,E
3441  8C00   STE   ((3442))   ;(0245) contains correct
3442  0245   DATA             ; phase value (ZPO)
3443  7C00   BRU   (3444)
3444  340B   DATA             ;Go to 340B, continue

340B  5012   IMO   (341E)     ;Increase current q counter
340C  5012   IMO   (341F)     ;Increase next q level add.
340D  0400   LDA   ((340E))   ;Load q counter
340E  341E   DATA             ; (No. of data images)
340F  6000   CPL   (3410)     ;Last one (18) ?
3410  0011   DATA
3411  CDC0   SLE
3412  7802   BRU   3415       ;Not, go to 3415
3413  7C00   BRU   (3414)     ;Yes, data images finished
3414  0200   DATA             ; back main program
3415  7C00   BRU   (3416)
3416  3845   DATA             ;Go to 3845 (imaging)
```

Modification to the Data Analysis Routine (Normalizing)

```
3881  7C00   BRU  (3882)
3882  3420   DATA                 ;Go to get scaling factor
```

Normalizing Routine

```
3420  00FC   LDA  (341D)
3421  6700   CPL  0               ;Load 1st projection flag
3422  CD20   SEQ                  ;First projection?
3423  7804   BRU  3428            ;If not first, go to 3428
3424  0701   LDA  1               ;Yes, set flag = 1
3425  80F7   STA  (341D)          ; and store it
3426  7C00   BRU  (3427)
3427  3886   DATA                 ;Store current NGAIN
3428  7C00   BRU  (3429)          ;Not first, using previous
3429  388A   DATA                 ; NGAIN to scale

3886  0116   LDA  ((B)+16)
3887  8400   STA  ((3888))
3888  321D   DATA
3889  7810   BRU  389A
388A  0116   LDA  ((B)+16)
388B  2C00   SUB  ((388C))
388C  321D   DATA
388D  C501   RMO  A,E
388E  0400   LDA  ((388F))
388F  0203   DATA
3890  C8C1   LLA  1
3891  8400   STA  ((3892))
3892  0203   DATA
3893  C510   RMO  E,A
3894  75C1   BRL  ((B)+C1)
3895  0400   LDA  ((3896))
3896  0203   DATA
3897  C841   LRA  1
3898  8400   STA  ((3899))
3899  0203   DATA
389A  0400   LDA  ((389B))
389B  0203   DATA
389C  C501   RMO  A,E
389D  7400   BRL  (389E)
389E  1564   DATA
389F  7C00   BRU  (38A0)          ;Scaling both real 64 and
38A0  1D80   DATA                 ; imaginary 64 data
*Part of this routine was used by Prof. P.T. Callaghan.
```

Modification to the Data Transfer Routine (TI 980A to Hitachi)

```
1DAB  0000   LDA  (1DAC)
1DAC  0200   DATA
1DAD  C506   RMO  A,B
1DAE  7C00   BRU  (1DAF)          ;Go to data display routine
1DAF  070E   DATA                 ; waiting for interrupt
```

q Parameter Counters

```
341D  0001     DATA                ;First projection flag
341E  000D     DATA                ;Current data image counter
341F  350E     DATA                ;Next q level address
```

q Gradient Level Locations

```
3500  00FF     DATA                ;Maximum q gradient level
3501  00F0     DATA
3502  00E3     DATA
3503  00D0     DATA
3504  00C2     DATA
3505  00B4     DATA
3506  00A6     DATA
3507  0098     DATA
3508  008A     DATA
3509  007D     DATA
350A  006E     DATA
350B  005E     DATA
350C  0050     DATA
350D  003F     DATA
350E  0031     DATA
350F  0025     DATA
3510  0014     DATA
3511  0000     DATA                ;Minimum q gradient level
```

q Gradient Phase Locations

```
3520  0087     DATA                ;Phase (ZPO) for Max. q
3521  0081     DATA
3522  007E     DATA
3523  0075     DATA
3524  006E     DATA
3525  006B     DATA
3526  0068     DATA
3527  0064     DATA
3528  0060     DATA
3529  005D     DATA
352A  005B     DATA
352B  0059     DATA
352C  0057     DATA
352D  0055     DATA
352E  0054     DATA
352F  0053     DATA
3530  0052     DATA
3531  0051     DATA                ;Phase (ZPO) for Min. q
```

Reset Routine (in Imaging Mode)

```
1CA0   0700    LDA   0
1CA1   8400    STA   ((1CA2))
1CA2   321F    DATA               ;Reset gradient counter
1CA3   8400    STA   ((1CA4))
1CA4   321E    DATA               ;Reset proj. counter
1CA5   8400    STA   ((1CA6))
1CA6   341E    DATA               ;Reset data image counter
1CA7   8400    STA   ((1CA8))
1CA8   341D    DATA               ;Reset first proj. flag
1CA9   0000    LDA   (1CAA)
1CAA   3501    DATA
1CAB   8400    STA   ((1CAC))     ;Reset q gradient add.
1CAC   341F    DATA               ; for 2nd data image
1CAD   7C00    BRU   (1CAE)
1CAE   342A    DATA               ;Go to 342A, continue

342A   07FF    LDA   FF
342B   8400    STA   ((342C))     ;Load 1st q grad. level
342C   3146    DATA               ; (FF) into 3146
342D   7C00    BRU   (342E)
342E   1C30    DATA               ;Go to 1C30, (imaging)
```

CNC Update

```
3805   0400    LDA   ((3806))
3806   0231    DATA               ;Load CNC flag
3807   6700    CPL   0            ;CNC required?
3808   CDA0    SNE                ;Yes, go to 380A
3809   780A    BRU   3814         ;No, go to 3814
380A   0000    LDA   (380B)
380B   3200    DATA               ;Load CNC update add.
380C   C506    RMO   A,B
380D   0503    LDA   (((B)+3))    ;Load current rf phase
380E   DB1D    TABO   D           ;Current 180 ?
380F   7802    BRU   3812         ;No, go to 3812
3810   DB4D    SABZ   D           ;Yes, set to zero
3811   7801    BRU   3813         ;Go to 3813
3812   DB5D    SABO   D           ;Set to 180
3813   8503    STA   (((B)+3))    ;Store rf phase in 3203
3814   7C00    BRU   (3815)
3815   1F38    DATA               ;Go to data transfer
```

Other Modifications

```
1569   6173    CPL   ((B)+73)     ;64 data points
156A   CDC0    SLE
156B   0173    LDA   ((B)+73)     ;64 data points


1DA4   0080    LDA   (1D25)       ;Transfer 64+64 data points
```

Appendix A.7 FLOWD.FOR

```
************************************************************************
*                               FLOWD.FOR                              *
*    This program Displays and analyzes Flow and Diffusion Images.    *
************************************************************************

$STORAGE:2

        PROGRAM FLOWD

c Data types

        INTEGER*4 DW,OW,OAMP,MAXO,MINO,XW,XB
        INTEGER*2 BC(13),NGAIN,LR,MSEG,X,Y,Z,U,V,W,MODE,IKEY,CX,CY,MC
        INTEGER*2 SCALEV,SCALED,SCALEO,SCALEG,DB,OB,TABPNT,FIRST,VC
        INTEGER*2 MAXV,MINV,VAMP,MAXD,MIND,DAMP,VW,VB,X1,Y1,Y2,NI
        CHARACTER KEY,RETRN,ESC,NULL,UP,DOWN,PLUS,MINUS

c Character constants

        RETRN=CHAR(13)
        ESC=CHAR(27)
        NULL=CHAR(0)
        PLUS=CHAR(43)
        MINUS=CHAR(45)
        UP=CHAR(72)
        DOWN=CHAR(80)

c Set screen mode

        CALL SCMD(183)

c Clear 22K + 8K Bytes memory for images

        CALL ZERO(0,11264,9088)
        CALL ZERO(0,4096,12800)

c Generate Trig table for FFT

        CALL FFTINT(256,10144)

c Input data, then remove cursor and clear screen

        WRITE (*,1)
1       FORMAT ( ' Enter No. of Data Images [XX] ' )
        READ (*,2) NI
2       FORMAT ( I2)

        CALL CURSOR(1)
        CALL CLS(0)

c Read Velocity and Diffusion images from Disk B and save them
```

```
        CALL DREAD(8+NI*2*16,32,9088)

c Read the Original image ( G = 0 ) from Disk B and save it

        CALL DREAD(8,16,12800)

**************************** RESET LOOP ********************************

c Wipe the previous displays

10      CALL CLS(0)
        CALL ZERO(0,512,10144)

c Initialize variables

        BC(1)=64
        BC(2)=0
        BC(3)=0
        BC(4)=0
        BC(5)=0
        BC(6)=0
        BC(7)=0
        BC(8)=0
        BC(9)=0
        BC(10)=0
        BC(11)=0
        BC(12)=0
        BC(13)=0
        MODE=1
        CX=126
        CY=94
        I=1
        INC=2
        SCALEV=2
        SCALED=4
        SCALEO=10
        SCALEG=8
        VB=0
        VW=64
        DB=0
        DW=256
        OB=0
        OW=16384
        TABPNT=3
        RET=0
        VC=5
        MC=0

c Display the Velocity image and the colour scale

20      CALL OUTPUT(11,0,11,0,0,'Velocity',6)
        CALL IMAGEA(9088,0,64,64,32,SCALEV,VB,VC)
        CALL COLORA(32,32,4,3,VC)
        CALL DRLINE(32,32,32,160,7)
        CALL DRLINE(56,32,56,161,7)
```

```
        CALL DRLINE(32,32,56,32,7)
        CALL DRLINE(32,160,56,160,7)

c Draw ' + 0 - ' OR ' MAX MIN ' for the Velocity scale

        IF (VC .EQ. 5) THEN

           CALL DRLINE(16,34,24,34,11)
           CALL DRLINE(20,30,20,38,11)

           CALL DRLINE(18,91,22,91,11)
           CALL DRLINE(18,100,22,100,11)
           CALL DRLINE(17,92,17,100,11)
           CALL DRLINE(23,92,23,100,11)

           CALL DRLINE(16,158,24,158,11)

        ELSEIF (VC .EQ. 1) THEN

           CALL OUTPUT(0,2,12,0,0,'MAX',6)
           CALL OUTPUT(0,9,12,0,0,'MIN',6)

        ENDIF

c Display the Diffusion image and the colour scale

        CALL OUTPUT(38,0,11,0,0,'Diffusion',6)
        CALL IMAGEA(9600,0,64,280,32,SCALED,DB,TABPNT)
        CALL COLORA(248,32,4,3,TABPNT)
        CALL DRLINE(248,32,248,160,7)
        CALL DRLINE(272,32,272,161,7)
        CALL DRLINE(248,32,272,32,7)
        CALL DRLINE(248,160,272,160,7)
        CALL OUTPUT(27,2,12,0,0,'MAX',6)
        CALL OUTPUT(27,9,12,0,0,'MIN',6)

c Display the Original image and the colour scale

        CALL OUTPUT(65,0,11,0,0,'Original',6)
        CALL IMAGEA(12800,0,64,496,32,SCALED,DB,TABPNT)
        CALL COLORA(464,32,4,3,TABPNT)
        CALL DRLINE(464,32,464,160,7)
        CALL DRLINE(488,32,488,161,7)
        CALL DRLINE(464,32,488,32,7)
        CALL DRLINE(464,160,488,160,7)
        CALL OUTPUT(54,2,12,0,0,'MAX',6)
        CALL OUTPUT(54,9,12,0,0,'MIN',6)

c Draw the boxes and the scale for the graph

        CALL DRLINE(0,390,256,390,11)
        CALL DRLINE(256,390,512,390,12)

        DO 30 X=0,256-16,16
           CALL DRLINE(X,388,X,392,11)
```

```
30      CONTINUE

        DO 40 X=0,256-64,64
           CALL DRLINE(X,384,X,396,11)
40      CONTINUE

        CALL DRLINE(256,384,256,396,6)

        DO 50 X=256+16,512,16
           CALL DRLINE(X,388,X,392,12)
50      CONTINUE

        DO 60 X=256+64,512,64
           CALL DRLINE(X,384,X,396,12)
60      CONTINUE

        DO 70 Y=0,1
           CALL DRLINE(554,168+Y,628,168+Y,4)
           CALL DRLINE(554,390+Y,628,390+Y,4)
70      CONTINUE

        DO 80 X=0,1
           CALL DRLINE(554+X,168,554+X,390,4)
           CALL DRLINE(628+X,168,628+X,391,4)
80      CONTINUE

        CALL DRLINE(5,170,545,170,6)
        CALL DRLINE(5,213,545,213,6)

        CALL DRLINE(5,170,5,213,6)
        CALL DRLINE(545,170,545,214,6)

90      IF (TABPNT .NE. 1) THEN
           MAXV=VW/2+VB-1
           MINV=-1*VW/2+VB
           CALL OUTPUT(2,11,14,0,0,'V +MAX = ',1,MAXV,8)
           CALL OUTPUT(4,12,14,0,0,'-MAX = ',1,MINV,8)
        ELSE
           MAXV=VW+VB
           MINV=VB
           CALL OUTPUT(2,11,14,0,0,'V MAX = ',1,MAXV,8)
           CALL OUTPUT(4,12,14,0,0,'MIN = ',1,MINV,8)
        ENDIF

        MAXD=DB+DW
        MIND=DB
        CALL OUTPUT(19,11,14,0,0,'D MAX = ',1,MAXD,8)
        CALL OUTPUT(21,12,14,0,0,'MIN = ',1,MIND,8)

        MAXO=OB+OW
        MINO=OB
        CALL OUTPUT(35,11,14,0,0,'O MAX = ',1,MAXO,8)
        CALL OUTPUT(37,12,14,0,0,'MIN = ',1,MINO,8)

****************************** MENU LOOP *********************************
```

```
c Draw the menu

100     CALL OUTPUT(70,11,14+BC(1),0,0,'Reset   ',6)
        CALL OUTPUT(70,12,14+BC(2),0,0,'V Window',6)
        CALL OUTPUT(70,13,14+BC(3),0,0,'V Base  ',6)
        CALL OUTPUT(70,14,14+BC(4),0,0,'D Window',6)
        CALL OUTPUT(70,15,14+BC(5),0,0,'D Base  ',6)
        CALL OUTPUT(70,16,14+BC(6),0,0,'O Window',6)
        CALL OUTPUT(70,17,14+BC(7),0,0,'O Base  ',6)
        CALL OUTPUT(70,18,14+BC(8),0,0,'Color ',1,TABPNT,0,'  ',10)
        CALL OUTPUT(70,19,14+BC(9),0,0,'Cursor  ',6)
        CALL OUTPUT(70,20,14+BC(10),0,0,'Scale   ',6)
        CALL OUTPUT(70,21,14+BC(11),0,0,'Vector  ',6)
        CALL OUTPUT(70,22,14+BC(12),0,0,'Print   ',6)
        CALL OUTPUT(70,23,14+BC(13),0,0,'Exit    ',6)

        FIRST=1

        IF(RET .EQ. 1) GOTO 200

110     CALL INPUT(KEY)
        IF (KEY .EQ. RETRN) THEN
        GOTO (190,160,160,170,170,180,180,190,190,190,190,190,190) I
        ENDIF

        IF (KEY .NE. NULL) GOTO 110

        CALL INPUT(KEY)
        IKEY=ICHAR(KEY)
        MODE=IKEY-70
        GOTO (110,120,110,110,110,110,110,110,110,140) MODE
        GOTO 110

c Move cursor up if UP arrow pressed

120     IF (I .EQ. 1) GOTO 110
        IF (I .NE. 9) GOTO 130

        CALL OUTPUT(2,11,14,0,0,'                                 ',6)
        CALL OUTPUT(35,11,14,0,0,'                                ',6)
        CALL OUTPUT(2,12,14,0,0,'                                 ',6)
        CALL OUTPUT(35,12,14,0,0,'                                ',6)
        CALL OUTPUT(1,15,14,0,0,'             ',6)
        BC(I)=0
        I=I-1
        BC(I)=64
        GOTO 90

130     BC(I)=0
        I=I-1
        BC(I)=64
        GOTO 100

c Move cursor down if DOWN arrow pressed
```

```
140     IF (I .EQ. 13) GOTO 110
        IF (I .NE. 7) GOTO 150

        CALL OUTPUT(52,11,14,0,0,'                              ',6)
        CALL OUTPUT(52,12,14,0,0,'                              ',6)

150     BC(I)=0
        I=I+1
        BC(I)=64
        GOTO 100

c Return detection

160     IF (TABPNT .NE. 1) THEN
           MAXV=VW/2+VB-1
           MINV=-1*VW/2+VB
           CALL OUTPUT(2,11,14,0,0,'V +MAX = ',1,MAXV,8)
           CALL OUTPUT(4,12,14,0,0,'-MAX = ',1,MINV,8)
        ELSE
           MAXV=VW+VB
           MINV=VB
           CALL OUTPUT(2,11,14,0,0,'V MAX = ',1,MAXV,8)
           CALL OUTPUT(4,12,14,0,0,'MIN = ',1,MINV,8)
        ENDIF

        GOTO 190

170     MAXD=DB+DW
        MIND=DB
        CALL OUTPUT(19,11,14,0,0,'D MAX = ',1,MAXD,8)
        CALL OUTPUT(21,12,14,0,0,'MIN = ',1,MIND,8)
        GOTO 190

180     MAXO=OB+OW
        MINO=OB
        CALL OUTPUT(35,11,14,0,0,'O MAX = ',1,MAXO,8)
        CALL OUTPUT(37,12,14,0,0,'MIN = ',1,MINO,8)

190     RET=1
        BC(I)=32
        GOTO 100

****************************** MODE LOOP ******************************

c Select modes

200     RET=0

        GOTO (250,210,210,210,210,210,210,210,250,210,700,750,1000) I

210     CALL INPUT(KEY)
        IF (KEY .EQ. RETRN .AND. MC .EQ. 1 .AND. TABPNT .NE. 1) GOTO 10
        IF (KEY .EQ. RETRN .AND. I .EQ. 8 .AND. TABPNT .EQ. 1) GOTO 550
        IF (KEY .EQ. RETRN) GOTO 280
```

```
        IF (KEY .EQ. PLUS) GOTO 400
        IF (KEY .EQ. MINUS) GOTO 410

        IF (KEY .NE. NULL) GOTO 210

        CALL INPUT(KEY)
        IKEY=ICHAR(KEY)
        MODE=IKEY-70
        GOTO (210,220,210,210,210,210,210,210,210,220) MODE
        GOTO 210

c ' Up ' or ' Down ' key has been pressed

220     GOTO (210,240,240,240,240,240,240,350,210,370,210,210,210) I

c Wipe the previous displays

240     CALL OUTPUT(52,11,14,0,0,'                 ',6)
        CALL OUTPUT(52,12,14,0,0,'                 ',6)

        GOTO (210,300,310,300,310,300,310,210,210,210,210,210,210) I

250     CALL GRAPH(10176,0,255,0,360,2,0,SCALEG,220,380)

        DO 260 X1=0,510,2
           CALL PEEK(Z,10176,X1)
           Y1=(360-Z/(2**SCALEG))
           IF (Y1 .GT. 380) Y1=380
           IF (Y1 .LT. 220) Y1=220
           IF (X1 .EQ. 0) THEN
                CALL PSET(X1,Y1,0)
           ELSE
                CALL DRLINE(X1-2,Y2,X1,Y1,0)
           ENDIF

           Y2=Y1

260     CONTINUE

        GOTO (10,210,210,210,210,210,210,210,600,390,700,750,1000) I

c Return key has been pressed

280     GOTO (290,290,290,290,290,290,290,850,290,290,290,290,290) I

290     BC(I)=64
        GOTO 100

************************ ADJUST PARAMETERS LOOP ************************

c Calculate Window

300     IF (I .EQ. 2) XW=VW
        IF (I .EQ. 4) XW=DW
```

```
        IF (I .EQ. 6) XW=OW

        IF (KEY .EQ. UP) THEN
           XW=XW*2
           IF (I .EQ. 2 .AND. XW .GE. 512) XW=512
           IF (I .EQ. 4 .AND. XW .GE. 512) XW=512
           IF (I .EQ. 6 .AND. XW .GE. 32767) XW=32767

        ELSEIF (KEY .EQ. DOWN) THEN
           XW=XW/2
           IF (XW .LT. 16) XW=16
           IF (I .EQ. 6 .AND. XW .EQ. 16383) XW=16384

        ENDIF

        CALL OUTPUT(52,11,10,0,0,'Window = ',1,XW,8)

        IF (I .EQ. 2) VW=XW
        IF (I .EQ. 4) DW=XW
        IF (I .EQ. 6) OW=XW

        GOTO (100,800,800,850,850,900,900,100,100,100,100,100,100) I

c Calculate Base

310     IF (I .EQ. 3) XB=VB
        IF (I .EQ. 5) XB=DB
        IF (I .EQ. 7) XB=OB

        IF (I .EQ. 3 .OR. I .EQ. 5) INC=1
        IF (I .EQ. 7) INC=512
        CALL OUTPUT(55,12,14,32,0,'INC = ',1,INC,8)

        IF (KEY .EQ. UP) THEN
           XB=XB+INC
           IF (I .EQ. 3 .AND. XB .GT. 511) XB=510
           IF (I .EQ. 5 .AND. XB .GT. 511) XB=510
           IF (I .EQ. 7 .AND. XB .GT. 32767) XB=32767

        ELSEIF (KEY .EQ. DOWN) THEN
           XB=XB-INC
           IF (I .EQ. 3 .AND. XB .LT. -511) XB=-511
           IF (I .EQ. 5 .AND. XB .LT. 0) XB=0
           IF (I .EQ. 7 .AND. XB .LT. -32767) XB=-32767

        ENDIF

        CALL OUTPUT(52,11,10,0,0,'Base = ',1,XB,8)

        IF (I .EQ. 3) VB=XB
        IF (I .EQ. 5) DB=XB
        IF (I .EQ. 7) OB=XB

        GOTO (100,800,800,850,850,900,900,100,100,100,100,100,100) I
```

```
c Calculate colour table pointer

350     IF (KEY .EQ. UP) TABPNT=TABPNT+1
            IF (TABPNT .GT. 5) TABPNT=1
        IF (KEY .EQ. DOWN) TABPNT=TABPNT-1
            IF (TABPNT .EQ. 0) TABPNT=5

        RET=1
        GOTO 100

c Calculate scale for the dynamic graph

370     CALL OUTPUT(1,15,14,0,0,'Scale = ',1,SCALEG,8)
        CALL GRAPH(10176,0,255,0,360,2,0,SCALEG,220,380)

        IF (FIRST .EQ. 1) GOTO 250

390     IF (KEY .EQ. DOWN) THEN
           SCALEG=SCALEG+1
        ELSEIF (KEY .EQ. UP) THEN
           SCALEG=SCALEG-1
           IF (SCALEG .LT. 0) SCALEG=0
        ENDIF

        GOTO 500

c ' Plus ' key has been pressed

400     IF (INC .GE. 16384) GOTO 420
        INC=INC*2
        GOTO 420

c ' Minus ' key has been pressed

410     IF (INC .EQ. 1) GOTO 420
        INC=INC/2
        GOTO 420

c Display INC

420     CALL OUTPUT(52,12,14,0,0,'                              ',6)
        CALL OUTPUT(55,12,14,32,0,'INC = ',1,INC,8)
        GOTO 200

************************ DISPLAY GRAPH LOOP ****************************

500     CALL OUTPUT(1,15,14,0,0,'                  ',6)

        CALL OUTPUT(1,15,14,0,0,'Scale = ',1,SCALEG,8)
        CALL GRAPH(10176,0,255,0,360,2,3,SCALEG,220,380)

        FIRST=0
        GOTO 200

********************** MONOCHROME DISPLAY LOOP ************************
```

```
550     VC=1
        CALL CLS(0)
        MC=1
        BC(I)=64
        GOTO 20

**************************** CURSOR LOOP ******************************

600     CALL DRCUR(CX,CY,7,KEY)

        IF (CX .GT. 63 .AND. CX .LT. 192) THEN
           X=(CX-62)/2
        ELSEIF (CX .GT. 279 .AND. CX .LT. 408) THEN
           X=(CX-278)/2
        ELSEIF (CX .GT. 495 .AND. CX .LT. 624) THEN
           X=(CX-494)/2
        ENDIF

        IF (CX .LT. 64) GOTO 660
        IF (CX .GE. 192 .AND. CX .LT. 280) GOTO 660
        IF (CX .GE. 408 .AND. CX .LT. 496) GOTO 660
        IF (CX .GE. 624) GOTO 660

        IF (CY .GT. 31 .AND. CY .LT. 160) THEN
           Y=(CY-30)/2
        ENDIF

        IF (CY .LT. 32) GOTO 660
        IF (CY .GE. 160) GOTO 660

c Display the coordinates and data values

        U=(Y-1)*64+(X-1)
        CALL PEEK(VAMP,9088,U*2)
        CALL PEEK(DAMP,9600,U*2)
        CALL PEEK(OAMP,12800,U*2)

        CALL OUTPUT(2,11,14,0,0,'                                                     ',6)
        CALL OUTPUT(35,11,14,0,0,'                                                    ',6)
        CALL OUTPUT(2,12,14,0,0,'                                                     ',6)
        CALL OUTPUT(35,12,14,0,0,'                                                    ',6)
        CALL OUTPUT(3,11,14,0,0,'X = ',1,X,8)
        CALL OUTPUT(3,12,14,0,0,'Y = ',1,Y,8)
        CALL OUTPUT(15,11,11,0,0,'Velocity = ',1,VAMP,8)
        CALL OUTPUT(40,11,11,0,0,'Diffusion = ',1,DAMP,8)
        CALL OUTPUT(20,12,11,0,0,'Original Amplitude = ',1,OAMP,8)

        IF (KEY .EQ. ESC) GOTO 650
        IF (KEY .NE. RETRN) GOTO 600

c Calculate the cursor positions, read from the disk, FFT ...

        CALL ZERO(0,512,10144)
```

```
        DO 630 W=1, NI*2
            LR=8+(W-1)*16+((Y-1)/8)*2
            MSEG=10496+(W-1)*64
           CALL DREAD(LR,2,MSEG)
630     CONTINUE

        V=MOD(Y-1,8)
        W=64*V+X-1
        CALL MOVE(W*2,0,10496,10144,2048,2,36)
        CALL MOVE(1024+W*2,0,10496,10176,2048,2,36)
        CALL FFT(10144,8,256,NGAIN)
        CALL SWAP(512,512+256,10144,10144,2,2,128)
        CALL GRAPH(10176,0,255,0,360,2,3,SCALEG,220,380)

        GOTO (640,640,640,640,640,640,640,650,650,650,640,640,640) I

640     CALL OUTPUT(2,11,14,0,0,'                              ',6)
        CALL OUTPUT(35,11,14,0,0,'                              ',6)
        CALL OUTPUT(2,12,14,0,0,'                              ',6)
        CALL OUTPUT(35,12,14,0,0,'                              ',6)
650     BC(I)=64
        GOTO 100

660     CALL OUTPUT(2,11,14,0,0,'                              ',6)
        CALL OUTPUT(35,11,14,0,0,'                              ',6)
        CALL OUTPUT(2,12,14,0,0,'                              ',6)
        CALL OUTPUT(35,12,14,0,0,'                              ',6)
        CALL OUTPUT(5,11,14,0,0,'Current Cursor Position out of',6)
        CALL OUTPUT(36,11,14,0,0,'the images !',6)
        GOTO 600

**************************** VECTOR LOOP *******************************

c Draw lines between the dots of the dynamic graph

700     DO 710 X1=0,510,2
           CALL PEEK(Z,10176,X1)
           Y1=(360-Z/(2**SCALEG))
           IF (Y1 .GT. 380) Y1=380
           IF (Y1 .LT. 220) Y1=220
           IF (X1 .EQ. 0) THEN
                CALL PSET(X1,Y1,3)
           ELSE
                CALL DRLINE(X1-2,Y2,X1,Y1,3)
           ENDIF

           Y2=Y1

710     CONTINUE

        BC(I)=64
        GOTO 100

**************************** PRINT LOOP ********************************
```

```
750     CALL SDUMP3

        BC(I)=64
        GOTO 100

************************* Display Images Loop *************************

c Display the Velocity Image

800     MAXV=VW/2+VB-1
        MINV=-1*VW/2+VB

        SCALEV=NINT(3.3219281*ALOG10(REAL(VW)/16.0))

        CALL IMAGEA(9088,0,64,64,32,SCALEV,VB,VC)

        IF (TABPNT .NE. 1) THEN
           CALL OUTPUT(2,11,14,0,0,'                       ',6)
           CALL OUTPUT(2,12,14,0,0,'                       ',6)
           CALL OUTPUT(2,11,14,0,0,'V +MAX = ',1,MAXV,8)
           CALL OUTPUT(4,12,14,0,0,'-MAX = ',1,MINV,8)
        ELSE
           MAXV=VW+VB
           MINV=VB
           CALL OUTPUT(2,11,14,0,0,'                       ',6)
           CALL OUTPUT(2,12,14,0,0,'                       ',6)
           CALL OUTPUT(2,11,14,0,0,'V MAX = ',1,MAXV,8)
           CALL OUTPUT(4,12,14,0,0,'MIN = ',1,MINV,8)
        ENDIF

        GOTO 200

c Display the Diffusion Image

850     MAXD=DB+DW
        MIND=DB

        SCALED=NINT(3.3219281*ALOG10(REAL(DW)/16.0))

        CALL COLORA(248,32,4,3,TABPNT)
        CALL DRLINE(248,32,248,160,7)
        CALL DRLINE(272,32,272,161,7)
        CALL DRLINE(248,32,272,32,7)
        CALL DRLINE(248,160,272,160,7)

        CALL IMAGEA(9600,0,64,280,32,SCALED,DB,TABPNT)

        CALL OUTPUT(19,11,14,0,0,'                       ',6)
        CALL OUTPUT(19,12,14,0,0,'                       ',6)
        CALL OUTPUT(19,11,14,0,0,'D MAX = ',1,MAXD,8)
        CALL OUTPUT(21,12,14,0,0,'MIN = ',1,MIND,8)

        GOTO (200,200,200,200,200,200,200,900,200,200,200,200,200) I

c Display the Original Image
```

```
900     MAXO=OB+OW
        MINO=OB

        SCALEO=NINT(3.3219281*ALOG10(REAL(OW)/16.0))

        CALL COLORA(464,32,4,3,TABPNT)
        CALL DRLINE(464,32,464,160,7)
        CALL DRLINE(488,32,488,161,7)
        CALL DRLINE(464,32,488,32,7)
        CALL DRLINE(464,160,488,160,7)

        CALL IMAGEA(12800,0,64,496,32,SCALEO,OB,TABPNT)

        CALL OUTPUT(35,11,14,0,0,'                ',6)
        CALL OUTPUT(35,12,14,0,0,'                ',6)
        CALL OUTPUT(35,11,14,0,0,'O MAX = ',1,MAXO,8)
        CALL OUTPUT(37,12,14,0,0,'MIN = ',1,MINO,8)

        BC(I)=64
        GOTO (200,200,200,200,200,200,200,910,200,200,200,200,200) I

910     IF (TABPNT .NE. 1) THEN
           CALL OUTPUT(2,11,14,0,0,'V +MAX = ',1,MAXV,8)
           CALL OUTPUT(4,12,14,0,0,'-MAX = ',1,MINV,8)
        ELSE
           CALL OUTPUT(2,11,14,0,0,'V MAX = ',1,MAXV,8)
           CALL OUTPUT(4,12,14,0,0,'MIN = ',1,MINV,8)
        ENDIF

        GOTO 100

1000    CALL CLS(0)
        CALL CURSOR(2)

        END
```

Appendix B Software for Simulating the G_y Field Gradient Uniformity

Appendix B.1 Program to Calculate G_y (Z-X Plane)

```
100 '***********************************************************************
101 '*                    Program to calculate Gy (Z-X PLANE)              *
102 '***********************************************************************
120 '
130 DIM I(16),UI(25,16),WI(16),WJ(16),VJ(25,16),EI(25,16),CI(25,16),GRADY(6,6)
140 '
150 ' Read in constants
160 ;
170 M=6
180 DJ=.02    :WT=.32   :NT=15
190 PI=3.1415927£
200 MU=4*PI*.0000001
210 GOSUB 720 :'Read in arrays
220 X1=0:Y1=0:Z1=0
230 '
240 ' Main program
250 '
260 FOR X1=0 TO .0060001 STEP .001
270   FOR Z1=0 TO .0060001 STEP .001
280       GY=0
285    FOR P=1 TO NT
290       FOR N=1 TO 16
300 '
310 ' Return wires
320 '
330   AI2=(UI(P,N)-X1)^2+(WI(N)-Z1)^2
340   TERM1=1/SQR((CI(P,N)-Y1)^2+AI2)
350   TERM2=1/SQR((Y1-EI(P,N))^2+AI2)
360   TERM3=1/((CI(P,N)-Y1)^2+AI2)^1.5
370   TERM4=1/((Y1-EI(P,N))^2+AI2)^1.5
380   GY=GY-I(N)*((Y1-EI(P,N))^2*TERM4-(CI(P,N)-Y1)^2*TERM3)*(UI(P,N)-X1)/AI2
390   GY=GY+I(N)*(TERM2-TERM1)*(UI(P,N)-X1)/AI2
400 '
410 ' Main coil
420 '
430   AJ2=(VJ(P,N)-Y1)^2+(WJ(N)-Z1)^2
440   TERM1=(DJ-X1)/SQR((DJ-X1)^2+AJ2)
450   TERM2=(DJ+X1)/SQR((DJ+X1)^2+AJ2)
460   TERM3=(DJ-X1)/((DJ-X1)^2+AJ2)^1.5
470   TERM4=(DJ+X1)/((DJ+X1)^2+AJ2)^1.5
480   GY=GY+2*I(N)*(TERM1+TERM2)*(1/(2*AJ2)-(Y1-VJ(P,N))^2/AJ2^2)
490   GY=GY-I(N)*(TERM3+TERM4)*(Y1-VJ(P,N))^2/AJ2
500       NEXT N
505     NEXT P
510       GY=GY*MU/(4*PI)
515     LPRINT GY
520       IF X1=0 AND Z1=0 THEN GY0=GY
530       CORDX=INT(X1*600/.6+.5)
540       CORDZ=INT(Z1*600/.6+.5)
550       GRADY(CORDZ,CORDX)=(GY-GY0)*100/GY0
560      LPRINT "(";CORDZ;",";CORDX;")",
570      LPRINT USING "££.£££";GRADY(CORDZ,CORDX);
580      LPRINT "%"
590    NEXT Z1
600 NEXT X1
```

```
610 OPEN "b:grad.dat" FOR OUTPUT AS £1
620 FOR CORDX=0 TO M
630   FOR CORDZ=0 TO M
640      PRINT£1,GRADY(CORDZ,CORDX)
650    NEXT CORDZ
660 NEXT CORDX
670 CLOSE £1
680 END
690 '
700 ' Read in current and wire position arrays
710 '
720 RESTORE 1030
730 FOR N=1 TO 16
740    READ A
745    FOR P=1 TO NT
750    UI(P,N)=(A+WT*(P-NT/2-.5))*.001
755    NEXT P
760 NEXT N
770 RESTORE 1040
780 FOR N=1 TO 16
790   READ WI(N)
800   WI(N)=WI(N)*.001
810   WJ(N)=WI(N)
820 NEXT N
830 RESTORE 1050
840 FOR N=1 TO 16
850   READ A
855   FOR P=1 TO NT
860   VJ(P,N)=(A+WT*(P-NT/2-.5))*.001
865   NEXT P
870 NEXT N
880 RESTORE 1060
890 FOR N=1 TO 16
900    READ A
905    FOR P=1 TO NT
910    EI(P,N)=(A+WT*(P-NT/2-.5))*.001
915    NEXT P
920 NEXT N
930 RESTORE 1070
940 FOR N=1 TO 16
950    READ A
955    FOR P=1 TO NT
960    CI(P,N)=(A+WT*(P-NT/2-.5))*.001
965    NEXT P
970 NEXT N
980 RESTORE 1080
990 FOR N=1 TO 16
1000   READ I(N)
1010 NEXT N
1020 RETURN
1030 DATA -20,-20,-20,-20,20,20,20,20,-20,-20,-20,-20,20,20,20,20
1040 DATA -12,12,-12,12,-12,12,-12,12,-19.8,19.8,-19.8,19.8,-19.8,19.8,-19.8,19.
8
1050 DATA 23.6,23.6,5,5,-5,-5,-23.6,-23.6,23.6,23.6,5,5,-5,-5,-23.6,-23.6
1060 DATA 5,5,-23.6,-23.6,5,5,-23.6,-23.6,5,5,-23.6,-23.6,5,5,-23.6,-23.6
1070 DATA 23.6,23.6,-5,-5,23.6,23.6,-5,-5,23.6,23.6,-5,-5,23.6,23.6,-5,-5
1080 DATA -1,-1,1,1,1,1,-1,-1,-1,-1,1,1,1,1,-1,-1
```

Appendix B.2 Program to Calculate G_x (Z-X Plane)

```
100 '*************************************************************************
101 '*                      Program to calculate Gx (Z-X PLANE)               *
102 '*************************************************************************
120 '
130 DIM I(16),UI(25,16),WI(16),WJ(16),VJ(25,16),EI(25,16),CI(25,16),GRADX(40,40)
140 '
150 ' Read in constants
160 '
170 M=40
175 GY0=8.799132E-02
180 DJ=.02    :WT=.32    :NT=15
190 PI=3.1415927£
200 MU=4*PI*.0000001
210 GOSUB 720 :'Read in arrays
220 X1=0:Y1=0:Z1=0
230 '
240 ' Main program
250 '
260 FOR X1=0 TO .0060001 STEP .00015
270   FOR Z1=0 TO .0060001 STEP .00015
280       GX=0
285    FOR P=1 TO NT
290       FOR N=1 TO 16
300 '
310 ' Return wires
320 '
330   AI2=(UI(P,N)-X1)^2+(WI(N)-Z1)^2
340   TERM1=1/SQR((CI(P,N)-Y1)^2+AI2)
350   TERM2=1/SQR((Y1-EI(P,N))^2+AI2)
360   TERM3=1/((CI(P,N)-Y1)^2+AI2)^1.5
370   TERM4=1/((Y1-EI(P,N))^2+AI2)^1.5
380   GX=GX+I(N)*(2*(UI(P,N)-X1)^2/AI2^2-1/AI2)*((Y1-EI(P,N))*TERM2+(CI(P,N)-Y1)
*TERM1)
390   GX=GX+I(N)*(UI(P,N)-X1)^2/AI2*((CI(P,N)-Y1)*TERM3+(Y1-EI(P,N))*TERM4)
400 '
410 ' Main coil
420 '
430   AJ2=(VJ(P,N)-Y1)^2+(WJ(N)-Z1)^2
440   TERM1=1/SQR((DJ-X1)^2+AJ2)
450   TERM2=1/SQR((DJ+X1)^2+AJ2)
460   TERM3=1/((DJ-X1)^2+AJ2)^1.5
470   TERM4=1/((DJ+X1)^2+AJ2)^1.5
490   GX=GX+I(N)*((DJ-X1)^2*TERM3-(DJ+X1)^2*TERM4)*(Y1-VJ(P,N))/(AJ2)
500       NEXT N
505     NEXT P
510       GX=GX*MU/(4*PI)
520  '    IF X1=0 AND Z1=0 THEN GX0=GX
530       CORDX=INT(X1*4000/.6+.5)
540       CORDZ=INT(Z1*4000/.6+.5)
550       GRADX(CORDZ,CORDX)=GX*100/GY0
560       PRINT "(";CORDZ;",";CORDX;")",
570       PRINT USING "££.£££";GRADX(CORDZ,CORDX);
580       PRINT "%"
590    NEXT Z1
600 NEXT X1
```

```
610 OPEN "b:gradxZX.dat" FOR OUTPUT AS £1
620 FOR CORDX=0 TO M
630   FOR CORDZ=0 TO M
640      PRINT£1,GRADX(CORDZ,CORDX)
650    NEXT CORDZ
660 NEXT CORDX
670 CLOSE £1
680 END
690 '
700 ' Read in current and wire position arrays
710 '
720 RESTORE 1030
730 FOR N=1 TO 16
740    READ A
745    FOR P=1 TO NT
750    UI(P,N)=(A+WT*(P-NT/2-.5))*.001
755    NEXT P
760 NEXT N
770 RESTORE 1040
780 FOR N=1 TO 16
790   READ WI(N)
800   WI(N)=WI(N)*.001
810   WJ(N)=WI(N)
820 NEXT N
830 RESTORE 1050
840 FOR N=1 TO 16
850   READ A
855   FOR P=1 TO NT
860   VJ(P,N)=(A+WT*(P-NT/2-.5))*.001
865   NEXT P
870 NEXT N
880 RESTORE 1060
890 FOR N=1 TO 16
900    READ A
905    FOR P=1 TO NT
910    EI(P,N)=(A+WT*(P-NT/2-.5))*.001
915    NEXT P
920 NEXT N
930 RESTORE 1070
940 FOR N=1 TO 16
950    READ A
955    FOR P=1 TO NT
960    CI(P,N)=(A+WT*(P-NT/2-.5))*.001
965    NEXT P
970 NEXT N
980 RESTORE 1080
990 FOR N=1 TO 16
1000   READ I(N)
1010 NEXT N
1020 RETURN
1030 DATA -20,-20,-20,-20,20,20,20,20,-20,-20,-20,-20,20,20,20,20
1040 DATA -12,12,-12,12,-12,12,-12,12,-19.8,19.8,-19.8,19.8,-19.8,19.8,-19.8,19.
8
1050 DATA 23.6,23.6,5,5,-5,-5,-23.6,-23.6,23.6,23.6,5,5,-5,-5,-23.6,-23.6
1060 DATA 5,5,-23.6,-23.6,5,5,-23.6,-23.6,5,5,-23.6,-23.6,5,5,-23.6,-23.6
1070 DATA 23.6,23.6,-5,-5,23.6,23.6,-5,-5,23.6,23.6,-5,-5,23.6,23.6,-5,-5
1080 DATA -1,-1,1,1,1,1,-1,-1,-1,-1,1,1,1,1,-1,-1
```

Appendix **B.3** Program to Calculate G_Z (Z-X Plane)

```
100 '*******************************************************************************
101 '*                   Program to calculate Gz  (Z-Y PLANE)                     *
102 '*******************************************************************************
120 '
130 DIM I(16),UI(25,16),WI(16),WJ(16),VJ(25,16),EI(25,16),CI(25,16),GRADZ(40,40)
140 '
150 ' Read in constants
160 '
170 M=40
175 GY0=8.799132E-02
180 DJ=.02    :WT=.32    :NT=15
190 PI=3.1415927£
200 MU=4*PI*.0000001
210 GOSUB 720 :'Read in arrays
220 X1=0:Y1=0:Z1=0
230 '
240 ' Main program
250 '
260 FOR Y1=0  TO .0060001 STEP .00015
270   FOR Z1=0  TO .0060001 STEP .00015
280       GZ=0
285    FOR P=1 TO NT
290       FOR N=1 TO 16
300 '
310 ' Return wires
320 '
330   AI2=(UI(P,N)-X1)^2+(WI(N)-Z1)^2
340   TERM1=1/SQR((CI(P,N)-Y1)^2+AI2)
350   TERM2=1/SQR((Y1-EI(P,N))^2+AI2)
360   TERM3=1/((CI(P,N)-Y1)^2+AI2)^1.5
370   TERM4=1/((Y1-EI(P,N))^2+AI2)^1.5
380   GZ=GZ+I(N)*2*(UI(P,N)-X1)*(WI(N)-Z1)/(AI2^2)*((Y1-EI(P,N))*TERM2+(CI(P,N)-
Y1)*TERM1)
390   GZ=GZ+I(N)*(UI(P,N)-X1)*(WI(N)-Z1)/(AI2)*((CI(P,N)-Y1)*TERM3+(Y1-EI(P,N))*
TERM4)
400 '
410 ' Main coil
420 '
430   AJ2=(VJ(P,N)-Y1)^2+(WJ(N)-Z1)^2
440   TERM1=(DJ-X1)/SQR((DJ-X1)^2+AJ2)
450   TERM2=(DJ+X1)/SQR((DJ+X1)^2+AJ2)
460   TERM3=(DJ-X1)/((DJ-X1)^2+AJ2)^1.5
470   TERM4=(DJ+X1)/((DJ+X1)^2+AJ2)^1.5
480   GZ=GZ+2*I(N)*(TERM1+TERM2)*((Y1-VJ(P,N))*(WJ(N)-Z1)/(AJ2^2))
490   GZ=GZ+I(N)*(TERM3+TERM4)*(Y1-VJ(P,N))*(WI(N)-Z1)/(AJ2)
500       NEXT N
505     NEXT P
510       GZ=GZ*MU/(4*PI)
520 '     IF Y1=0 AND Z1=0 THEN GZ0=GZ
530       CORDY=INT(Y1*4000/.6+.5)
540       CORDZ=INT(Z1*4000/.6+.5)
550       GRADZ(CORDZ,CORDY)=GZ*100/GY0
560       PRINT "(";CORDZ;",";CORDY;")",
570       PRINT USING "££.£££";GRADZ(CORDZ,CORDY);
580       PRINT "%"
590    NEXT Z1
600 NEXT Y1
```

```
610 OPEN "b:gradzZY.dat" FOR OUTPUT AS £1
620 FOR CORDY=0 TO M
630   FOR CORDZ=0 TO M
640      PRINT£1,GRADZ(CORDZ,CORDY)
650    NEXT CORDZ
660 NEXT CORDY
670 CLOSE £1
680 END
690 '
700 ' Read in current and wire position arrays
710 '
720 RESTORE 1030
730 FOR N=1 TO 16
740    READ A
745    FOR P=1 TO NT
750    UI(P,N)=(A+WT*(P-NT/2-.5))*.001
755    NEXT P
760 NEXT N
770 RESTORE 1040
780 FOR N=1 TO 16
790   READ WI(N)
800   WI(N)=WI(N)*.001
810   WJ(N)=WI(N)
820 NEXT N
830 RESTORE 1050
840 FOR N=1 TO 16
850   READ A
855   FOR P=1 TO NT
860   VJ(P,N)=(A+WT*(P-NT/2-.5))*.001
865   NEXT P
870 NEXT N
880 RESTORE 1060
890 FOR N=1 TO 16
900    READ A
905    FOR P=1 TO NT
910    EI(P,N)=(A+WT*(P-NT/2-.5))*.001
915    NEXT P
920 NEXT N
930 RESTORE 1070
940 FOR N=1 TO 16
950    READ A
955    FOR P=1 TO NT
960    CI(P,N)=(A+WT*(P-NT/2-.5))*.001
965    NEXT P
970 NEXT N
980 RESTORE 1080
990 FOR N=1 TO 16
1000   READ I(N)
1010 NEXT N
1020 RETURN
1030 DATA -20,-20,-20,-20,20,20,20,20,-20,-20,-20,-20,20,20,20,20
1040 DATA -12,12,-12,12,-12,12,-12,12,-19.8,19.8,-19.8,19.8,-19.8,19.8,-19.8,19.
8
1050 DATA 23.6,23.6,5,5,-5,-5,-23.6,-23.6,23.6,23.6,5,5,-5,-5,-23.6,-23.6
1060 DATA 5,5,-23.6,-23.6,5,5,-23.6,-23.6,5,5,-23.6,-23.6,5,5,-23.6,-23.6
1070 DATA 23.6,23.6,-5,-5,23.6,23.6,-5,-5,23.6,23.6,-5,-5,23.6,23.6,-5,-5
1080 DATA -1,-1,1,1,1,1,-1,-1,-1,-1,1,1,1,1,-1,-1
```

Appendix C Publications

1. **R.K. Lambert, R.J. Pack, Y. Xia, C.D. Eccles** and **P.T. Callaghan**
   "*In vitro* Tracheal Mechanics by Nuclear Magnetic Resonance Imaging"
   J Appl. Physiol. (1988) in press.

2. **P.T. Callaghan, C.D. Eccles** and **Y. Xia**
   "NMR Microscopy of dynamic displacements: **k**-space and **q**-space imaging"
   J Phys. E (1988) in press.

3. **C.F. Jenner, Y. Xia, C.D. Eccles** and **P.T. Callaghan**
   "Circulation of Water within the Wheat Grain Revealed by NMR Micro-Imaging Methods"
   Nature (1988), submitted.

Bibliography

1. **P.C. Lauterbur,** *Bull. Am. Phys. Soc.* **18**, 86(1972)
2. **P.C. Lauterbur,** *Nature* **242**, 190(1973)
3. **P. Mansfield** and **P.G. Morris,** *NMR Imaging in Biomedicine*, Academic Press, New York(1982)
4. **P.A. Bottomley,** *Rev. Sci. Instrum.* **53**, (9), pp1319-1337(1982)
5. **V. Ralph McCready, M. Leach** and **P.J. Ell,** *Functional Studies Using NMR*, Springer-Verlag(1987)
6. **R.R. Ernst, G. Bodenhausen** and **A. Wokaun,** *Principles of Nuclear Magnetic Resonance in One and Two Dimensions*, pp560-563, Clarendon, Oxford(1987)
7. **A. Abragam,** *The Principles of Nuclear Magnetism*, Clarendon, Oxford(1960)
8. **D. Shaw,** *Fourier Transform NMR Spectroscopy*, Elsevier, Amsterdam(1976)
9. **K. Blum,** *Density Matrix Theory and Applications*, Plenum, New York(1981)
10. **E.L. Hahn,** *Phys. Rev.* **80**, 580(1950)
11. **F. Bloch,** *Phys. Rev.* **70**, 460(1946)
12. Reference 7, pp 82-83
13. **H.D.W. Hill** and **R.E. Richards,** *J Phys. E.* Ser. 2, **1**, 977(1968)
14. **D.I. Hoult** and **R.E. Richards,** *J Mag. Res.* **24**, 71(1976)
15. **P.A. Bottomley,** *Rev. Sci. Instrum.* **53**, (9), 1319(1982)
16. **R.R. Ernst,** *Quarterly Rev. Biophys.* **19**, 3/4, pp183-220(1987)
17. **R. Gabillard,** *Phys. Rev.* **85**, 694(1952)
18. **C.D. Eccles** and **P.T. Callaghan,** *JEOL News* **23A**, (1), pp10-15(1987)
19. **D.R. Balies** and **D.J. Bryant,** *Contemp. Phys.* **25**, (5), pp441-475(1984)
20. **E.O. Brigham,** *The Fast Fourier Transform* pp16-18, Prentice-Hall, New Jersey(1974)
21. **R.A. Brooks** and **G. Di Chiro,** *Phys. Med. Biol.* **21**, (5), pp689-732(1976)
22. Reference 3, pp15-30
23. **C.D. Eccles** and **P.T. Callaghan,** *J Mag. Res.* **68**, pp393-398(1986)
24. **G.A. Johnson, M.B. Thompson, S.L. Gewalt** and **C.E. Hayes,** *J Mag. Res.* **68**, pp129-137(1986)

25. **J.B. Aguayo, S.J. Blackband, J. Schoeniger, M.A. Mattingly** and **M. Hintermann,** *Nature* **322**, (10), pp190-191(1986)

26. **P.T. Callaghan** and **C.D. Eccles,** *J Mag. Res.* **71**, pp426-445(1987)

27. **W.A. Edelstein, J.M.S. Hutchinson, G. Johnson** and **T.W. Redpath,** *Phys. Med. Biol.* **25**, 751(1980)

28. **L. Kaufman, L.E. Crooks** and **A.R. Margulis,** Eds. *Nuclear Magnetic Resonance Imaging in Medicine*, Igaku-Shoiu Medical Pub., New York(1981)

29. **M. O'Donnell,** *Med. Phys.* **12**, 59(1985)

30. **J.P. Ridgway** and **M.A. Smith,** *British J. Radiology* **59**, 603(1986)

31. **H. Y. Carr** and **E. M. Purcell,** *Phys. Rev.* **94**, 630(1954)

32. **D.W. McCall, D.C. Douglass** and **E.W. Anderson,** *Ber. Bunsenges. Phys. Chem.* **67**, 336(1963)

33. **E.O. Stejskal** and **J.E. Tanner,** *J Chem. Phys.* **42**, 288(1965)

34. **E.O. Stejskal,** *J Chem. Phys.* **43**, 3597(1965)

35. **H.C. Torrey,** *Phys. Rev.* **104**, 563(1956)

36. **P. T. Callaghan,** *Aust. J Phys.* **37**, pp359-387(1984)

37. **P.T. Callaghan,** Private Communication(1987)

38. **C.D. Eccles,** *Microscopic NMR Imaging*, Chapter 7 and Chapter 8, PhD Thesis, Massey University(1987)

39. **P.A. Bottomley,** *J Phys. E* **14**, 1052(1981)

40. **W. Anderson,** *Rev. Sci. Instrum.* **32**, (3), pp241-250(1961)

41. **D.S. Webster** and **K.H. Marsden,** *Rev. Sci. Instrum.* **45**, (10), pp1232-1234(1974)

42. **D.I. Hoult,** *Progress in NMR Spectroscopy* **12**, pp41-77(1978)

43. **JEOL FX 60** Software, JEOL Ltd, Japan(1974)

44. Reference 38, V2

45. **R.K. Lambert, T.A. Wilson, R.E. Hyatt** and **J.R. Rodarte,** *J Appl. Physiol.* **52**, (1), pp44-52(1982)

46. **R.K. Lambert, R.J. Pack, Y. Xia, C.D. Eccles** and **P.T. Callaghan,** *J Appl. Physiol.* (1988), in press.

47. **J.G. Jones, R.B. Fraser** and **J.A. Nadel,** *J Appl. Physiol.* **38**, (6), pp1002-1011(1975)

48. **S.V. Dawson** and **E.A. Elliott,** *J Appl. Physiol.* **43**, (3), pp498-515(1977)

49. **R. K. Lambert,** *J Appl. Physiol.* **62**, (6), pp2426-2435(1987)

50. See for example, **D.J. Tritton,** *Physical Fluid Dynamics*, Van Nostrand Reinhold, New York(1977)

51. See for example, **C.F. Jenner,** *Aust. J Plant Physiol.* **9**, pp69-82(1982)

52. **S.E. Lingle** and **P. Chevalier**, Crop Science **25**, pp123-128(1985)

53. **T.P. O'Brien, M.E. Sammut, J.W. Lee** and **M.G. Smart,** *Aust. J Plant Physiol.* **12**, pp487-511(1985)

54. **I.F. Wardlaw,** *Aust. J Biol. Sci.* **18**, pp269-281(1965)

55. **J.C. Frazier** and **B. Appalanaidu,** *Amer. J Bot.* **52**, pp193-198(1965)

56. **G.E. Scott, E.G. Heyne** and **K.F. Finney,** *Agron. J* **49**, pp509-513(1957)